



**FUNCTIONALISED GOLD NANOPARTICLE
DELIVERY FOR *c-MYC* siRNA in CANCER GENE
THERAPY**

BY

ALISCIA NICOLE DANIELS

Submitted in fulfilment of the academic requirements for the degree of

DOCTOR OF PHILOSOPHY

In the School of Life Sciences,

University of KwaZulu-Natal, Westville Campus

January 2018

As the candidate's supervisor and co-supervisor, we have approved submission of this thesis.

Supervisor: Professor M. Singh

Signed: _____

Date: _____

Co-Supervisor: Dr. S. Singh

Signed: _____

Date: _____

ABSTRACT

RNA interference (RNAi), which can be induced by chemically synthesized small interfering RNA (siRNA), has emerged as a powerful tool in molecular biology for the treatment of genetic disorders. However, due to the challenges that exist in delivery of these siRNA molecules, which include poor cellular uptake and instability, an efficient, stable and non-toxic delivery vehicle needs to be designed and developed for the introduction of siRNA to target cells. Due to the rapid progress achieved in the field of nanotechnology for drug and gene delivery, gold nanoparticles (AuNPs) have presented themselves as potential candidates for the therapeutic delivery of siRNA.

In this study, five cationic AuNP-based delivery systems were formulated, their cellular uptake efficiency assessed in four different mammalian cell lines *in vitro* and their ability to introduce the *c-MYC* oncogene targeted siRNA for gene silencing in a cancer cell culture model was investigated. AuNPs were synthesized using the modified Turckevich-Frens citrate reduction method and were functionalised with the natural cationic polymer, chitosan. The AuNP formulations were further modified with 0 – 5 % (^{w/w}) of either polyethylene-glycol 400 (PEG₄₀₀) or polyethylene-glycol 2000 (PEG₂₀₀₀), which afforded sterically stabilized AuNP formulations. The shape, size and zeta potential of the functionalised AuNPs (FAuNPs) and their corresponding nanocomplexes with siRNA were evaluated by transmission electron microscopy (TEM) and nanoparticle tracking analysis (NTA), with synthesis and functionalisation being confirmed by UV spectroscopy and Fourier Transformed Infra-red (FTIR) spectroscopy. The ability of these FAuNPs to bind, condense and protect siRNA were assessed using the band shift, SYBR Green II dye displacement and RNase A protection assays, respectively. *In vitro* cytotoxicity of the nanocomplexes was determined using the MTT, AlamarBlue® and acridine orange/ethidium bromide dual staining in the human embryonic kidney (HEK293), epithelial colorectal adenocarcinoma (Caco 2), breast adenocarcinoma (MCF-7) and colon adenocarcinoma (HT-29) cell lines. Cellular uptake studies were conducted using FITC-labelled siRNA in all 4 cell lines and the fluorescence quantitatively evaluated. The gene silencing efficiency of the FAuNP formulations were further assessed at the mRNA and protein levels by qRT-PCR and ELISA analysis following the introduction of *c-MYC* siRNA to the MCF-7 cell line, *in vitro*.

All FAuNP formulations were capable of successfully binding, condensing and protecting the siRNA against degradation. The FAuNPs were well tolerated by all the cell lines being tested

in vitro with observed cell death found to be apoptotic in nature. Enhanced cellular uptake of the siRNA nanocomplexes was observed which corresponded to successful silencing of the *c-MYC* gene at the mRNA level, exceeding that of commercially available Lipofectamine 3000[®]. PEG₄₀₀ Chito-AuNPs were the most successful with up to a 7 -fold decrease in *c-MYC* expression at the mRNA level, and up to 94.6% reduction in gene expression at the protein level. Overall, these FAuNP nanocomplexes have shown great potential as vehicles for enhancing cellular uptake and *c-MYC* siRNA gene silencing in the tested cancer cell culture model.

Key words: Gold nanoparticles, PEGylation, gene silencing, cytotoxicity

PREFACE

The experimental work described in this thesis was carried out in the School of Life Sciences, University of KwaZulu-Natal (Westville Campus), Durban, South Africa from February 2014 to January 2018, under the supervision of Professor M. Singh and the co-supervision of Dr. S. Singh.

These studies represent original work by the author and have not otherwise been submitted in any form for any degree or diploma to any tertiary institution. Where use has been made of the work of others it is duly acknowledged in the text.

DECLARATION 1 – PLAGIARISM

I, Aliscia Nicole Daniels declare that

1. The research reported in this thesis, except otherwise indicated, is my original research.
2. This thesis has not been submitted for any degree or examination at any other university.
3. This thesis does not contain any other persons' data, pictures graphs or other information, unless specifically acknowledged as being sourced from other persons.
4. This thesis does not contain other persons' writing unless specifically acknowledged as being sourced from other researchers. Where other written sources have been quoted, then:
 - a. Their words have been re-written but the general information attributed to them has been referenced.
 - b. Where their exact words have been used, then their writing has been placed in italics and inside quotation marks, and referenced.
5. This thesis does not contain text, graphics or tables copied and pasted from the internet, unless specifically acknowledged, and the source being detailed in the thesis and in the Reference Section.

Signed: _____

Declaration Plagiarism 22/05/08 FHDR Approved

DECLARATION 2 – PUBLICATIONS

DETAILS OF CONTRIBUTION TO PUBLICATIONS that form part and/or include research presented in this thesis (include publications in preparation, submitted, *in press* and published and give details of the contributions of each author to the experimental work and writing of each publication.

Publication: Peer Reviewed Published Abstract

Daniels A. and Singh M. (2016). *Pegylated Chitosan Functionalised Gold Nanoparticles for siRNA Delivery in vitro*. Human Gene Therapy **27**: A2- A185. (Appendix B)

Manuscript:

Daniels A.N., and Singh M. *Enhanced c-MYC oncogene silencing mediated by siRNA associated with sterically stabilised chitosan functionalised gold nanoparticles in a breast cancer cell model. In preparation.* (Appendix B).

Signed: _____

Declaration Publications FHDR 22/05/08 Approved

TABLE OF CONTENTS

	PAGE
ABSTRACT	ii
PREFACE	iv
DECLARATION 1 – PLAGIARISM	v
DECLARATION 2 – PUBLICATIONS	vi
TABLE OF CONTENTS	vii
LIST OF FIGURES	xii
LIST OF TABLES	xvii
ABBREVIATIONS AND SYMBOLS	xviii
ACKNOWLEDGEMENTS	xxiii
CHAPTER ONE	
INTRODUCTION	
1.1 BACKGROUND OF STUDY	1
1.2 SCOPE OF STUDY	2
1.2.1 Hypothesis	3
1.2.2 Aim	3
1.2.3 Objectives	3
1.3 NOVELTY OF STUDY	4
1.4 OVERVIEW OF THESIS	4
CHAPTER TWO	
LITERATURE REVIEW	
2.1 GENE THERAPY: AN OVERVIEW	6
2.2 GENE THERAPY FOR CANCER THERAPEUTICS	8
2.3 RNA INTERFERENCE	9
2.3.1 An overview of RNA Interference	9
2.3.2 siRNA mediated Gene Silencing	10
2.3.3 Potential of siRNA gene silencing therapeutics in cancer treatment	11
2.3.3 (a) Lung Cancer	12
2.3.3 (b) Liver Cancer	13

2.3.3 (c)	Prostrate Cancer	14
2.3.3 (d)	Breast Cancer	14
2.4	<i>c-MYC</i> ONCOGENE: A POSSIBLE TARGET FOR GENE THERAPY	15
2.4.1	MYC as a transcription factor	17
2.4.2	<i>c-MYC</i> and Metabolism	18
2.4.3	<i>c-MYC</i> and Apoptosis	19
2.5	Pharmacokinetic Challenges Associated with siRNA Delivery	20
2.6	GENE DELIVERY VECTORS	21
2.6.1	Viral Vectors	22
2.6.2	Non-Viral Vectors	22
2.6.2.1	Physical Methods	23
2.6.2.1 (a)	Hydrodynamic Injection	23
2.6.2.1 (b)	Electroporation and Nucleofection	23
2.6.2.1 (c)	Gene Gun Method	23
2.6.2.2	Chemical Methods	24
2.6.2.2.1	Advances in Nanotechnology	24
2.6.2.2.1 (a)	Lipid based Nanoparticles	25
2.6.2.2.1 (b)	Dendrimers	26
2.6.2.2.1 (c)	Carbon Nanotubes	27
2.6.2.2.1 (d)	Silica based Nanoparticles	28
2.6.2.2.1 (e)	Metal Nanoparticles	28
2.6.2.3	Gold Nanoparticles	29
2.6.2.4	Biomedical Applications of Gold Nanoparticles	30
2.6.2.4 (a)	Bio-Imaging	31
2.6.2.4 (b)	Gene and Drug Delivery	32
2.6.2.4 (c)	Thermal Therapy	34
2.6.2.5	Gold Nanoparticle Functionalisation	35
2.6.2.5 (a)	Polymer Functionalisation	36
2.6.2.5 (b)	PEGylation	38
2.7	CELLULAR UPTAKE	40

CHAPTER THREE

MATERIALS AND METHOD

3.1	GOLD NANOPARTICLE PREPARATION AND FUNCTIONALISATION	43
3.1.1	Materials	43
3.1.2	Method	43
3.1.2.1	Gold Nanoparticle preparation	43
3.1.2.2	Functionalisation of Gold Nanoparticles	43
3.1.2.3	PEGylation of Chitosan functionalised AuNPs	44
3.2	CHARACTERISATION OF PEGYLATED AND NON-PEGYLATED CHITO-AuNP AND siRNA INTERACTIONS WITH FUNCTIONALISED AuNPs	44
3.2.1	Materials	44
3.2.2	Preparation of siRNA Duplex	45
3.2.3	Preparation of PEGylated and non-PEGylated Chito-AuNP: siRNA complexes	45
3.2.4	siRNA: PEGylated and non-PEGylated Chito-AuNP Interactions	45
3.2.4.1	Band Shift Assay	45
3.2.4.2	RNase A Protection Assay	46
3.2.4.3	SYBR Green II Displacement Assay	47
3.2.5	Imaging and Sizing	48
3.2.5.1	UV Spectroscopy Analysis	48
3.2.5.2	Transmission Electron Microscopy (TEM) Analysis of AuNP, PEGylated and Non-PEGylated Chito-AuNPs	48
3.2.5.3	Inductively Coupled Plasma-Optical Emission Spectroscopy (ICP-OES) and Fourier Transform Infrared (FTIR) Analysis	48
3.2.5.4	Particle Size and Zeta Potential	49
3.3	<i>In Vitro</i> CELL CULTURE STUDIES	49
3.3.1	Materials	49
3.3.2	Preparation of siRNA Duplexes	50
3.3.3	Cell Line Maintenance	50
3.3.3.1	Reconstitution of Cell Lines	50
3.3.3.2	Propagation of Cell Lines	51

3.3.3.3 Cryopreservation of Cell Lines	51
3.3.4 TOXICITY STUDIES	51
3.3.4.1 MTT Assay	51
3.3.4.2 AlamarBlue® Assay	52
3.3.4.3 Apoptosis Analysis by Acridine Orange/Ethidium Bromide (AO/EB) Staining	53
3.3.5 <i>In vitro</i> TRANSFECTION ASSAYS	53
3.3.5.1 Cellular Uptake Studies	53
3.4 <i>c-MYC</i> GENE KNOCKDOWN STUDIES AT mRNA AND PROTEIN LEVELS	54
3.4.1 Materials	54
3.4.2 siRNA Duplexes	54
3.4.3 siRNA Transfection	55
3.4.4 RNA Isolation and qRT-PCR	55
3.4.4.1 RNA Isolation	55
3.4.4.2 Quantitative Real Time Polymerase Chain Reaction (qRT-PCR)	56
3.4.5 Protein Isolation and ELISA	57
3.4.5.1 Protein Isolation	57
3.4.5.2 Enzyme Linked Immunosorbent Assay (ELISA)	58
3.5 Statistical Analysis	58

CHAPTER FOUR

RESULTS AND DISCUSSION

4.1 GOLD NANOPARTICLE PREPARATION AND CHARACTERISATION	59
4.1.1 Synthesis and Functionalisation of AuNPs	59
4.1.2 Functionalised AuNP: siRNA Interactions	61
4.2 CHARACTERISATION OF FUNCTIONALISED AuNP and AuNP: siRNA INTERACTIONS	63
4.2.1 UV-Visible Spectrophotometry	63
4.2.2 ICP-OES and FTIR Analysis	65
4.2.3 PEGylated and non-PEGylated Chitosan AuNP: siRNA Interactions	66
4.2.3.1 siRNA Binding studies and Nuclease Protection Assays	66

4.2.3.1.1	Band Shift Assay	66
4.2.3.1.2	RNase A Protection Assay	69
4.2.3.1.3	SYBR Green II Displacement Assay	71
4.2.4	Imaging and Sizing	74
4.2.4.1	Transmission Electron Microscopy of PEGylated and non-PEGylated Chito-AuNPs and their complexes with siRNA	74
4.2.4.2	Nanoparticle Sizing and Zeta Potential	77
4.3	CELL CULTURE STUDIES	81
4.3.1	Cell Line Maintenance	81
4.3.2	Cytotoxicity Studies	83
4.3.2.1	MTT Reduction Assay	83
4.3.2.2	AlamarBlue® Toxicity Assay	87
4.3.3	Apoptosis Analysis using Acridine Orange/ Ethidium Bromide (AO/EB) Staining	90
4.3.4	Cellular Uptake Studies	96
4.3.5	<i>c-MYC</i> Gene Silencing in MCF-7 Cell Line	101
4.3.5.1	Quantitative Real Time PCR (qRT-PCR)	102
4.3.5.2	Enzyme Linked Immunosorbent Assay (ELISA)	107
CHAPTER FIVE		
CONCLUSION		
5.1	Concluding Remarks	111
REFERENCES		114
APPENDIX A1		151
APPENDIX A2		152
APPENDIX A3		155
APPENDIX B		157

LIST OF FIGURES

- Figure 2.1:** Graphical representation of diseases currently addressed by gene therapy trials (Misra *et al.*,2013).
- Figure 2.2:** Schematic representation of siRNA duplex
- Figure 2.3:** Illustration of the mechanism of RNA interference initiated by synthetic siRNA (Liao, *et al.*,2016).
- Figure 2.4:** Interaction between *c-MYC* and Max protein during transactivation of gene expression (Dang *et al.*, 1999).
- Figure 2.5:** Intracellular and Extracellular barriers encountered by siRNA (Xu and Wang, 2014).
- Figure 2.6:** Examples of nanodelivery systems (a) DOTMA, (b) DC-Chol, (c) Silica nanoparticles and (d) Carbon Nanotubes (Martin *et al.*,2005; Davis *et al.*, 2012; El Chaar *et al.*,2011) (Martin *et al.*,2005, Davis *et al.*,2012, El Chaar *et al.*,2011).
- Figure 2.7:** Biomedical applications of gold nanoparticles (AuNPs) (Gosh *et al.*,2008).
- Figure 2.8:** Sythesis of citrate capped AuNPs by reduction with sodium citrate (Makshin *et al.*,2012).
- Figure 2.9:** Commonly used polymers for AuNP functionalisation (Chattopadhyay and Inamdar, 2010; Antila *et al.*,2015; Hunter *et al.*,2012; Jokerst *et al.*,2011).
- Figure 2.10:** Schematic representation of the different densities of PEG polymers on the AuNP surface. High density PEG polymers result in a brush regime ($D < F$) (a) with low density PEG polymers exhibiting a mushroom conformation ($D > F$) (b).
- Figure 2.11:** Cellular Uptake mechanisms and intracellular trafficking of siRNA delivery systems (Adapted from Resnier *et al.*,2013).

- Figure 2.12:** Schematic representation of Proton Sponge Effect for the release of cationic AuNPs from the endosome following cellular uptake (Ding *et al.*, 2014).
- Figure 4.1:** Image depicting the colour change observed following the citrate reduction of the gold salt (yellow) to gold nanoparticles (deep red wine colour).
- Figure 4.2:** Schematic representation of the composition of the PEGylated and non-PEGylated Chito-AuNPs used in this study and its electrostatic interactions with siRNA.
- Figure 4.3:** Illustration of interactions between siRNA and functionalised AuNPs (Adapted from Hong and Nam, 2014).
- Figure 4.4:** UV-Vis Absorption Spectrum of AuNPs, PEGylated and non-PEGylated AuNPs.
- Figure 4.5:** Band Shift analysis the binding of various amounts of FAuNP preparations with a constant amount of siRNA (0.3µg) in a 10µl reaction mixture. (A) Chitosan, (B) Chito-AuNP, (C) 2% PEG₂₀₀₀ Chito-AuNP, (D) 5% PEG₂₀₀₀ Chito-AuNP, (E) 2% PEG₄₀₀ Chito-AuNP and (F) 5% PEG₄₀₀ Chito-AuNP. Lane 1: 0.3µg of uncomplexed siRNA in the absence of chitosan and FAuNPs; Lanes 2-8: the respective siRNA nanocomplexes prepared using various amounts of the FAuNPs and chitosan as indicated. Arrows or numbers in red indicate complete binding or point of electroneutrality.
- Figure 4.6:** RNase A protection assay of chitosan and FAuNP- siRNA nanocomplexes. Lane 1: 0.3 µg of untreated, naked siRNA, Lane 2: 0.3 µg of RNase A treated naked siRNA, (A) Lanes 3-5: Chitosan nanocomplexes, (A) Lanes 6-8: Chito-Au nanocomplexes, (B) Lanes 3-5: 2% PEG₂₀₀₀ Chito-Au nanocomplexes, (B) Lanes 6-8: 5% PEG₂₀₀₀ Chito-Au nanocomplexes, (C) Lanes 3-5 2% PEG₄₀₀ Chito-Au nanocomplexes (C) Lanes 6-8: 5% PEG₄₀₀ Chito-Au nanocomplexes. The siRNA was kept constant at 0.3 µg per well.
- Figure 4.7:** Graphical representation of the SYBR Green II dye intercalation between siRNA base pairs
- Figure 4.8:** SYBR Green II displacement assay of Chitosan, PEGylated and non-PEGylated Chito-AuNPs. The FAuNPs were added systemically to the siRNA/ SYBR Green II reaction mixture (0.28 µg siRNA) until the point of inflection was attained.

Figure 4.9: Transmission electron micrographs of (A) AuNP, (B) Chito-AuNP, (C) 2% PEG₂₀₀₀ Chito-AuNP, (D) 5% PEG₂₀₀₀ Chito-AuNP, (E) 2% PEG₄₀₀ Chito-AuNP and (F) 5% PEG₄₀₀ Chito-AuNP. Bar represents 50 nm (A-D) and 200 nm (E-F).

Figure 4.10: Transmission electron micrographs of siRNA:Au nanocomplexes prepared at the optimum binding or N/P ratios as determined from the band shift assay (A): Chito-AuNP, (B) 2% PEG₂₀₀₀ Chito-AuNP, (C) 5% PEG₂₀₀₀ Chito-AuNP (D) 2% PEG₄₀₀ Chito-AuNP and (E) 5% PEG₄₀₀ Chito-AuNP. Bar = 100 nm

Figure 4.11: Screenshot from recorded video showing the AuNPs light scatter and movement under Brownian motion.

Figure 4.12: Images of cell lines utilized during *in vitro* studies. Cells are viewed as a monolayer at confluence under 100 × magnification with an Olympus CKX41 inverted microscope (Tokyo, Japan). Bar = 100 nm

Figure 4.13: MTT conversion to the insoluble formazan product following a reduction reaction (Riss *et al.*,2013).

Figure 4.14: MTT reduction assay of siRNA nanocomplexes in (A) Caco 2, (B) HEK293, (C) MCF-7 and (D) HT-29 cell lines. Nanocomplexes were prepared with 50 nM control non-targeting siRNA at various siRNA: FAuNP ratios (^{w/w}). A control containing untreated cells was assumed to have 100% survival. The results are represented as means ± SD, *n* = 3 and shown as a percentage of the control sample. Statistical analysis was performed using one-way ANOVA which was followed by the Dunnett multiple comparison *post hoc* test (**P* < 0.05 and ***P* < 0.01 compared to the control).

Figure 4.15: Chemical structure of resazurin and its reduction to resafurin by viable cells (Adapted from Riss *et al.*,2013).

Figure 4.16: AlamarBlue® toxicity assay in (A) Caco 2, (B) HEK293, (C) MCF-7 and (D) HT-29 cell lines. Nanocomplexes were prepared with 50 nM control, non-targeting siRNA at various siRNA: FAuNP ratios (^{w/w}). The control containing cells only were assumed to have 100 % survival. Results represented as a means ± SD, *n* = 3.

Figure 4.17: Apoptotic Index in each cell line. Nanocomplexes were prepared with 50 nM control non-targeting siRNA at the ratios that exhibited the highest cytotoxic effects and were incubated with the Caco 2, HEK293, MCF-7 and HT-29 cell lines. A control of untreated cell was utilized for each cell line. The results are represented as a mean \pm SD, $n = 3$. Statistical analysis was performed using one-way ANOVA and Dunnett multiple comparison *post hoc* test (* $P < 0.05$, ** $P < 0.01$).

Figure 4.18 (A-D): AO/EB dual staining and fluorescence microscopy images illustrating the changes in morphology of the (A) Caco 2, (B) HEK293, (C) MCF-7 and (D) HT-29 cell lines treated with siRNA: Au nanocomplexes (containing 50 nM control, non-targeting siRNA). A control for each cell line is present. **L:** Live cells, **EA:** Early Apoptotic cells, **LA:** Late Apoptotic cells and **NV:** Non-viable cells. Bar = 100 μ m.

Figure 4.19: Evaluation of the cellular uptake of chitosan, PEGylated and non-PEGylated Chito-AuNPs at the sub-optimum, optimum and supra-optimum binding ratios in (A) Caco 2, (B) HEK293, (C) MCF-7 and (D) HT-29 cell lines with 50 nM (0.067 μ g) BLOCK-iT™ Fluorescent Oligo. Two controls were utilised which included non-treated cells and cells incubated with siRNA only. Results are represented as a mean \pm SD $n=3$. Statistical analysis was carried out using one-way ANOVA followed by Dunnett multiple comparison *post hoc* test (** $P < 0.01$) indicates a significant difference

Figure 4.20: Graphical representation of the SMARTpool™ siRNA design for the target mRNA (Adapted from Dharmacon™)

Figure 4.21: Analysis of *c-MYC* gene expression in the MCF-7 cell line. Reaction mixtures (10 μ l) were prepared at the optimum binding or N/P (+/-) ratios as determined from the band shift assay between chitosan, the FAuNP formulations and either *c-MYC* or non-targeting (NT) siRNA (0.065 μ g). Calibrator (cells only), NT siRNA only and *c-MYC* siRNA only were included as negative controls. Lipofectamine® 3000 was utilized as a positive control. The relative quantification of *c-MYC* normalized against β -Actin mRNA using the algorithm $2^{-\Delta\Delta C_t}$ (Livak and Schmittgen, 2001). Results are represented as a mean \pm SD $n = 3$. Statistical analysis was carried out using one-way ANOVA followed by Dunnett multiple comparison *post hoc* test (** $P < 0.01$) indicates a significant difference.

Figure 4.22: Diagrammatic representation of an Indirect ELISA assay (Thermo Fisher Scientific, 2010).

Figure 4.23: Analysis of MYC protein expression with ELISA. (A) Untreated cells, c-MYC siRNA only, NT-siRNA only and Lipofectamine® 3000 were utilized as controls. siRNA nanocomplexes were prepared at the optimum binding ratios with the FAuNP formulations and 50 nM of either (B) NT-siRNA or (C) *c-MYC* targeted siRNA. Data represented as a mean \pm SD, $n = 3$. Statistical analysis was conducted with one-way ANOVA followed by the Dunnett multiple comparison *post-hoc* test. ($*P < 0.05$) ($**P < 0.01$) is considered significant.

LIST OF TABLES

- Table 2.1:** Some of the disorders undergoing gene therapy clinical trials (Misra *et al.*, 2013; Hill *et al.*, 2016).
- Table 2.2:** Possible targets for siRNA in cancer therapy (Resnier *et al.*, 2013; Zhou *et al.*, 2012; Draz *et al.*, 2014).
- Table 3.1:** Composition of PEGylated and non-PEGylated Chito-AuNPs
- Table 3.2:** Varying amounts of Chitosan, PEGylated and non-PEGylated Chito-AuNPs used in band shift assay. siRNA was kept constant at 0.3 μg .
- Table 3.3:** Varying amounts of Chitosan, PEGylated and Non-PEGylated Chito-AuNPs. siRNA was kept constant at 0.3 μg .
- Table 3.4:** siRNA: Au nanocomplex ratios used for cytotoxicity and transfection studies
- Table 4.1:** siRNA:Au nanocomplexes at the optimum binding ratio and their corresponding charge ratios for the band shift and SYBR Green II displacement assays.
- Table 4.2:** Average particle size and zeta potential of AuNPs, FAuNPs and optimal siRNA: Au nanocomplex ratios

ABBREVIATIONS AND SYMBOLS

A	Apoptotic
Ago-2	Argonaute-2
ACTB	β Actin
AD5	Adenovirus type 5
ADA	Adenosine deaminase deficiency
AI	Apoptotic index
AIDS	Acquired immune deficiency syndrome
ATCC	American Type Tissue Culture Collection
ATP	Adenosine triphosphate
a.u	Fluorescence arbitrary units
Au	Gold
AuNP	Gold nanoparticles
AO	Acridine orange
BSA	Bovine Serum Albumin
C	Celsius
Caco 2	Human epithelial colorectal adenocarcinoma cell line
CDK-1	Cyclin dependant kinase 1
cDNA	Complimentary DNA
Chito-AuNP	Chitosan functionalised gold nanoparticles
Cl ⁻	Chloride ions
cm	Centimetre
cm ²	Square centimetre
CO ₂	Carbon Dioxide
C _t	Threshold cycle
CTD	Carboxy-terminal domain
Da	Daltons
DC-Chol	3 β [N,N',N'-dimethylaminoethane)-carbamoyl] cholesterol
DD	Degree of deacetylation
DLVO	Derjaguin-Landau-Verwey-Overbeek
DNA	Deoxyribonucleic acid

dNTP	Deoxyribonucleotide triphosphates
DMSO	Dimethylsulphoxide
DOTMA	N-[1-(2,3-dioleoyloxy)propyl]-N,N,N-trimethylammonium chloride
ds DNA	Double stranded DNA
EA	Early Apoptotic
EB	Ethidium bromide
EDTA	Ethylenediaminetetraacetic acid
EGFR	Epidermal growth factor receptor
ELISA	Enzyme Linked Immunosorbent Assay
EMEM	Eagles Minimum Essential Medium
EPR	Enhanced permeability and retention
ER α	Estrogen receptor alpha
etc	Etcetera
F	Flory radius
FAuNP	Functionalised gold nanoparticles
FBS	Foetal bovine serum
F ₀	Baseline Fluorescence
F _i	Fluorescence Intensity
F _{max}	Maximum Fluorescence
F _r	Relative Fluorescence
FTIR	Fourier Transform Infrared
g	Gram
gDNA	Genomic DNA
GPT	Glycerol propoxylate triacrylate
GSH	Glutathione
H	Hour
H ⁺	Hydrogen ions
HAuCl ₄	Gold (III) chloride trihydrate
HBS	HEPES buffered saline
HCC	Hepatocellular carcinoma
HCl	Hydrochloric acid
HDACs	Histone deacetylases

HEK293	Human embryonic kidney cell line
HER2	Human epidermal growth factor 2 receptor
HRP	Horse radish peroxidase
HT-29	Human colon adenocarcinoma cell line
hTERT	Human telomerase reverse transcriptase
ICP-OES	Inductively Coupled Plasma-Optical Emission Spectroscopy
IgG	Immunoglobulin G
IHC	Immunohistochemistry
kDa	Kilo daltons
KLK4	Kallikrein- related peptidase 4
LA	Late apoptotic
LDHA	Lactate Dehydrogenase A
LSPR	Localised surface plasmon resonance
M	Molar
MCF-7	Human breast adenocarcinoma cell line
Mg	Magnesium
mg	Milli gram
mL	Milli litre
mM	Milli molar
mRNA	Messenger RNA
miRNA	Micro RNA
Miz-1	MYC- interacting zinc finger protein-1
MPS	Mononuclear phagocytic system
MSN	Mesoporous silica nanoparticles
MTT	3-[4,5-dimethylthiazol-2-yl]-2,5-diphenyltetrazolium bromide
mV	Milli Volt
MW	Molecular weight
NIR	Near infrared region
nm	Nano meter
nM	Nano molar
N/P	Amine to Phosphate ratio
NT siRNA	Non-targeting siRNA

NTA	Nanoparticle Tracking Analysis
NV	Non-viable
OPN	Osteopotin
PANAM	Polyamidoamine
PBS	Phosphate buffered saline
PCR	Polymerase chain reaction
PEG	Poly(ethylene glycol)
PEI	Polyethyleneimine
PLL	Poly-L-lysine
pmol	Pico mole
PPI	Polypropylene imine
ppm	Parts per million
PTB	Polypyrimidine tract binding protein
qRT-PCR	Quantitative Real-Time Polymerase Chain Reaction
rcf	Relative centrifugal force
RISC	RNA-Induced Silencing Complex
RES	Reticuloendothelial system
RNA	Ribonucleic acid
RNAi	RNA Interference
RNase A	Ribonuclease A
RPN 2	Human- ribophorin II
rpm	Revolutions per minute
SAH	S-adenyl-L-homocysteine
SAHH	S-adenyl-L-homocysteine hydrolase
SD	Standard deviation
SDS	Sodium dodecyl sulphate
SE	Standard error
SERS	Surface- enhanced Raman scattering
siRNA	Small interfering RNA
SIS	Soft Imaging System
SPB	Surface plasmon band

SYBR Green	N',N'-dimethyl-N-[4-[(E)-3-methyl-1,3-benzothiazol-2-ylidene)methyl]-1-phenylquinolin-1-ium-2-yl]-N-propylpropane-1,3-diamine
TBS	Tris-buffered saline
TBS-T	Tris-buffered saline containing Tween 20
TF	Transcription Factor
TEM	Transmission electron microscopy
TMB	3,3',5,5'- tetramethylbenzidine
μg	Micro gram
μg/mL	Microgram per milli litre
μg/μL	Micro gram per Micro litre
μL	Micro Litre
μM	Micro molar
UV	Ultra violet
V	Viable
°	Degree
%	Percent
^w / _w	Weight to Weight ratio
^w / _v	Weight to Volume ratio
^v / _v	Volume to Volume ratio
λ	Wavelength (lambda)
ζ	Zeta Potential

ACKNOWLEDGEMENTS

I would like to express my deepest thanks and gratitude to the following people:

- My supervisor, Professor M. Singh and co-supervisor, Dr. S. Singh, for their patience, invaluable supervision, scientific knowledge and excitement towards this project.
- My parents, Mr. and Mrs. Daniels, for their constant prayers, support and guidance for the duration of this study.
- My brother, Graham Daniels, for his continuous support, encouragement and moments of light relief.
- The National Research Foundation (NRF) for financial support.
- Mr. S. Naidu, for his invaluable assistance with electron microscopy.
- Mr. T. Chiliza (Department of Microbiology) for assistance with qRT-PCR.
- My friends and colleagues from the Discipline of Biochemistry for their support and assistance.

CHAPTER ONE

INTRODUCTION

1.1 BACKGROUND OF STUDY

Since the discovery of RNA interference (RNAi) in 1998, a new paradigm for the treatment of various incurable genetic diseases has been created. RNAi is a post-transcriptional gene regulatory mechanism that is activated by small interfering RNA (siRNA), which are double stranded 21-25 nucleotide RNA molecules, that inhibit translation or lead to the degradation of target mRNA which suppresses the expression of that gene (Zhao *et al.*, 2012). The use of chemically synthesized siRNA molecules to target a specific mRNA sequence in mammalian cells can lead to sequence specific gene silencing. These siRNA molecules present a unique group of therapeutic agents comparable to protein-based drugs, namely, antibodies and vaccines. A siRNA-based drug can potentially target any gene of interest, irrespective of the location within the cell or the protein structure and, therefore, have emerged as a new generation of bio-drugs.

Malignant tumours are a result of a multistep process of alterations in several tumour suppressor genes, oncogenes or genes involved in the regulation of differentiation and growth of cells. Cancer is the leading cause of death worldwide with conventional cancer therapies including chemotherapy, radiation and surgery. However, due to the adaptive nature of cancer cells, most of these therapies fail. Furthermore, the exposure of the malignant tumours to chemical agents presents selective pressure which allows these cancerous cells to adapt, survive and grow which results in their resistance to treatment (Croce, 2008; Ashworth *et al.*, 2011). Hence the use of gene therapy as a viable alternative. Among the many proto-oncogenes causing the onset of cancer is the *c-MYC* oncogene. This oncogene is found to be upregulated in a variety of different human cancers and is believed to be involved in the initiation, maintenance and progression of the disease. Strategies aimed at eliminating the oncogenic activity of the *c-MYC* oncogene can be achieved using RNAi, mediated by specifically designed siRNA molecules which can inhibit the expression of the *c-MYC* gene, thereby eliminating its oncogenic activity.

Although RNAi, mediated by siRNA molecules, offers an attractive alternative to the conventional therapeutic strategies, there exists challenges in the systemic delivery of siRNA

to intracellular targets, which present limitations for the success of siRNA-based therapy. These hurdles include the high molecular weight, hydrophilic character and polyanionic nature of siRNA which minimizes its association with the cell membrane, thereby hampering the cellular entry of siRNA molecules (Whitehead *et al.*, 2009). Furthermore, these siRNA molecules are prone to nuclease degradation, activation of the immune response and short circulation times in the blood system which limits their gene knockdown potential. Hence, a major challenge for siRNA- based therapeutics is the development of a suitable carrier that is non-toxic and capable of introducing the siRNA to the target. Several experimental designs for gene therapy have utilised viral vectors that were based on recombinant viruses for the delivery of the therapeutic agent, however the hosts experienced inflammatory- type toxicities due to the adaptive immune response to the viral vectors. Furthermore, the large-scale production of viral vectors is also a major limitation. This led to an increased interest in non-viral vectors which became the delivery vehicles of choice as they provide possible solutions to the limitations associated with viral vectors. To date, there have been several nanoparticulate systems that have emerged to meet these challenges although the transfection and expression levels of the delivered gene needs to be enhanced. Hence, the cellular uptake and endosomal release of the gene of interest requires improvement. Due to the rapidly developing field of nanotechnology, inorganic nanoparticles have been utilised as gene delivery vehicles as they can effectively bind and release the siRNA from the endosome while preventing degradation. Among these, gold nanoparticles (AuNPs) have attracted much attention for their biological and biomedical applications due to their desirable physical and chemical properties, ease of synthesis, functionalisation with polymers, and low toxicity due to their inert core.

The study at hand aims to address the challenges associated with siRNA delivery by developing a AuNP delivery system that is non-toxic and efficient. The development of an ideal vector can overcome some of the associated obstacles and provide effective RNAi to target cells, thereby allowing for the possible cure and treatment of diseases, such as cancer, at a molecular level.

1.2 SCOPE OF STUDY

The delivery of siRNA molecules remains one of the major obstacles that needs to be overcome for the effectiveness of RNAi therapy to be achieved. Due to the safety concerns associated with viral vectors, non-viral vectors have become the delivery vehicles of choice. For the success of RNAi therapy to be achieved, a delivery vehicle needs to be formulated that is non-

toxic, safe, stable under storage conditions, capable of protecting the siRNA against degradation and have a high transfection potential. AuNPs have become increasingly popular as, once functionalised with suitable polymers, meet the requirements for an ideal delivery vehicle. However, their design and functionalisation need to be optimized for the efficient delivery of siRNA, for their potential use in clinical trials. In this study, five cationic AuNP formulations will be evaluated for their ability to enhance cellular uptake in four cell lines, as well as their ability to deliver *c-MYC* siRNA to a *c-MYC* over-expressing breast cancer cell line for effective gene silencing.

1.2.1 Hypothesis

AuNP delivery systems functionalised with the highly cationic, natural polymer chitosan and further modified with steric stabilising polyethylene glycol (PEG) can enhance the delivery of siRNA *in vitro*, as well as increase the *c-MYC* siRNA delivery to MCF-7 cells, thereby enhancing the oncogenic silencing potential of these siRNA molecules, while exhibiting minimal toxicity to the cell lines being tested.

1.2.2 Aim

The aim of this study was to develop cationic AuNPs functionalised with chitosan and further modified with PEG polymers (PEG₂₀₀₀ or PEG₄₀₀) at two different mass percentages, and to evaluate their physical and chemical characteristics, cytotoxicity and transfection abilities in four mammalian cell lines as well as the delivery of *c-MYC* siRNA for gene silencing in a breast cancer cell model.

1.2.3 Objectives

The following objectives form the premise to test the hypothesis and achieve the aim,

- Synthesis of five AuNP delivery systems, each functionalised with chitosan and to PEGylate four of the chitosan functionalised AuNP formulations with either 2 or 5 % (^{w/w}) of PEG₄₀₀ or PEG₂₀₀₀.
- Preparation of nanocomplexes between the siRNA and functionalised AuNP (FAuNP) and assessing the binding and protection efficiency using the band shift, SYBR Green II dye displacement and RNase A protection assays.

- Characterisation of the AuNP, FAuNPs and their nanocomplexes with siRNA by measuring the zeta potential and sizing using NTA and TEM analysis.
- To evaluate the toxicity of the FAuNP systems with the 3-(4,5-Dimethyl-2-thiazolyl)-2,5-diphenyl-2H-tetrazolium bromide (MTT), AlamarBlue® toxicity assays and apoptosis determination using Acridine orange/ Ethidium Bromide dual staining *in vitro* in four mammalian cell lines.
- To monitor the transfection activity of the FAuNP delivery systems using fluorescent cellular uptake studies.
- To assess gene silencing activity of the FAuNP delivered *c-MYC* siRNA by qRT-PCR and ELISA assays.

1.3 NOVELTY OF STUDY

AuNPs were synthesized using the modified Turkevich- Frens method. These AuNPs were then functionalised with 0.1% Chitosan (^{w/v}) and PEGylated with PEG₄₀₀ and PEG₂₀₀₀ at mass percentages varying between 0-5%. To date, the current focus is the interaction between AuNPs and DNA with target specific siRNA binding and delivery for gene silencing not been conducted. Furthermore, PEGylation of AuNPs with PEG₄₀₀ and PEG₂₀₀₀ has not been fully exploited. Accordingly, this study aims to evaluate the ability of these five AuNP formulations to efficiently deliver siRNA that targets the *c-MYC* oncogene *in vitro*.

1.4 OVERVIEW OF THESIS

Chapter One

This chapter outlines the background to the study and the challenges inherent in siRNA delivery. It also focuses on the scope, hypothesis, aim and objectives of the study.

Chapter Two

In this chapter, the relevant literature is reviewed. Firstly, an overview of RNAi is discussed and the potential of the *c-MYC* gene as a gene target for siRNA therapeutics. The obstacles faced in siRNA delivery and the use of non-viral delivery systems is outlined. Lastly, the cellular uptake mechanisms of the nanoparticles are discussed.

Chapter Three

Chapter three details the research design and laboratory methodologies undertaken in this study. The AuNP synthesis and functionalisation with chitosan and PEG is described, followed by the characterisation of their physical and chemical properties using UV spectroscopy, ICP-OES and FTIR. The siRNA binding and protection studies were conducted and siRNA nanocomplexes were further characterised with respect to size and zeta potential. Finally, the toxicity and transfection efficiency of the siRNA: FAuNP nanocomplexes were evaluated, *in vitro*, in the Caco 2, HEK293, MCF-7 and HT-29 cell lines., while the gene knockdown efficiency of the *c-MYC* siRNA: FAuNP nanocomplexes was assessed at the level of transcription and translation using qRT-PCR and ELISA assays in the MCF-7 cell line.

Chapter Four

This chapter highlights all the findings in this study with an interpretation of the results and comprehensive discussion which adds perspective to the investigation.

Chapter Five

This chapter provides the conclusion to the study and highlights the outcomes with respect to the aims and objectives. Contributions made by this investigation in siRNA therapeutics are discussed with possible limitations in this study being documented and assessed. Finally, further research recommendations are made to assist in optimising the current system for clinical studies.

CHAPTER TWO

LITERATURE REVIEW

2.1 Gene Therapy: An Overview

In the early 1850's, Gregor Mendel, an Austrian monk, began the study of genetics by conducting a number of experiments on peas. He observed that inheritance of characteristics occurred as separate units that we now know are genes (Misra, 2013). This work became the foundation for future scientific achievements in the field of genetics. A major breakthrough occurred in the 1950's by James Watson and Francis Crick when they discovered and developed their model of the double stranded helix of DNA. Genetic advances and DNA gene isolations that followed, resulted in the emergence of gene therapy in the 1980's.

Gene therapy has gained much interest in the field of science over the years and has become an important strategy to potentially treat or cure the development of genetically based diseases. The basis of this therapy is the introduction of a corrective or functional copy of a gene into a cell that possesses the defective gene. Hence, genetic defects can be corrected, and cancerous cells can be eliminated. Although it appears that gene therapy is a new field of research, it has been a point of interest for decades with the first proposal being expressed by Amos in the 1960's who discovered that nucleic acid uptake by cultured cells was enhanced following the complexation of RNA with protamine (Amos, 1961; Huang *et al.*, 1999). This was followed by the proposal of introducing exogenous DNA to the nuclei of cells for treatment of disease in 1972 (Kim *et al.*, 2013).

Many laboratories in medicine, biochemistry, and pharmacy are now focusing their attention on gene therapy and research into this concept has since expanded tremendously (El-Aneed, 2004). Following advances in research, gene therapy can now be defined as the introduction of nucleic acids, either DNA or RNA, which can be used to prevent or treat inherited or acquired diseases (El-Aneed, 2004; Robbins and Ghivizanni, 1998). However, one of the most important requirements is the identification of the disease-causing gene to be treated. This will, lead to the diagnosis of the disease and appropriate treatment for the defect. Approximately, 2000 gene therapy clinical trials have been conducted for the treatment of diseases over the past 25 years, some of which are outlined below (Table 2.1).

Table 2.1: Some of the disorders undergoing gene therapy clinical trials (Misra *et al.*, 2013; Hill *et al.*, 2016).

Disease
AIDS
ADA Deficiency
Asthma
Brain Tumours
Breast, Colon, Lung, Liver, Ovarian and Prostate cancers
Diabetes
Hemophilia
Melanoma
Muscular Dystrophy
Neurodegenerative Disease

Although gene therapy was discovered almost 5 decades ago, it has had moderate success with 95% of clinical trials not progressing beyond Phase II trials. Hence, there is still a need to overcome challenges which can produce an effective and clinically relevant treatment (Hill *et al.*, 2016). The majority of these trials have been conducted in Europe and the United States with a large portion used for the treatment of certain cancers (Figure 2.1) (Ferro *et al.*, 2016; Knoel and Yiu, 1998; Ginter, 2000). The potential use of gene therapy for cancer therapeutics will be discussed further.

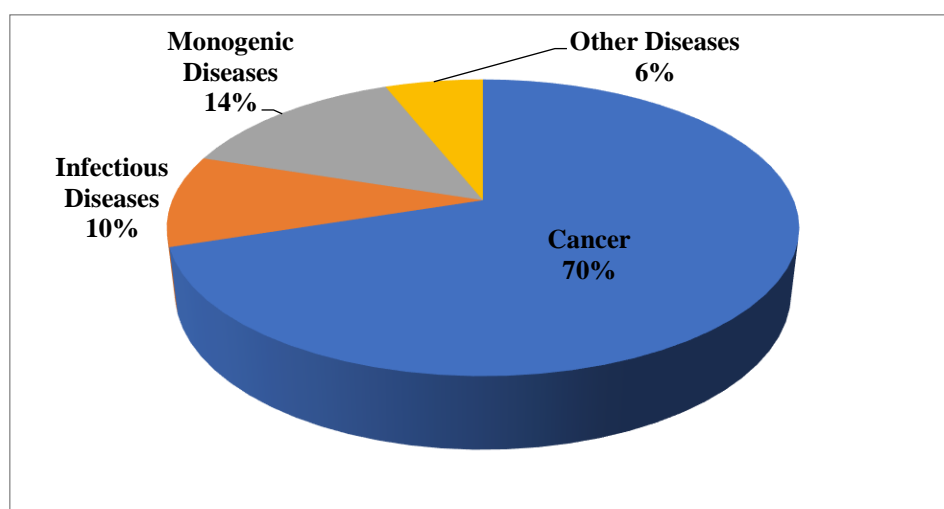


Figure 2.1: Graphical representation of diseases currently addressed by gene therapy trials (Adapted from Misra *et al.*, 2013).

2.2 Gene Therapy for Cancer Therapeutics

Cancer is said to be one of the leading causes of death worldwide and is a major health issue (Yamamoto and Curiel, 2005). Although knowledge into cancer biology has increased tremendously with time, fatalities that occur due to this disease seems to be on the rise with 8.2 million deaths and 14.1 million new cases in 2012 alone (Mendes *et al.*, 2017; Arvizer *et al.*, 2010; Amer, 2014).

Cancer is believed to be a result of a multi-step process of alterations or mutations to oncogenes, tumour suppressor genes or micro RNA genes which control cell growth (Figueiredo *et al.* 2010). When there is an increase in activity or overexpression of proto-oncogenes, proliferation signalling pathways become activated and these genes, therefore, become cancer causing genes and are referred to as oncogenes. Cell growth and division are controlled by tumour suppressor genes and when inactivated, results in uncontrolled cell division and tumour formation (Draz *et al.*, 2014).

There are many challenges present in the search for a treatment and possible cure for cancer due to the aggressive and invasive growth of tumours, their ability to avoid mechanisms that prevent apoptosis, as well as the complexity of the pathways involved in cancer development (Hanahan and Weinberg, 2000; Li *et al.*, 2013). The common and traditional methods of cancer treatment include chemotherapy, radiotherapy and surgery. These treatment strategies are not as effective due to the lack of specificity which results in negative side effects on normal cells and, in most cases, do not completely eradicate the invasive tumour. Furthermore, when a relapse occurs, multidrug resistance or cross-resistance with anticancer agents may take place, which could lead to an increased risk of developing other types of cancers (Fatemian *et al.*, 2014; Bassal *et al.*, 2006). Therefore, there is a need to develop new treatment options which can overcome these issues, and with gene therapy treatment can occur at the molecular level with the use of gene silencing, mutation correction, suicide gene therapies and antiangiogenic therapies (Cross and Burmester, 2006; Amer, 2014; Duarte *et al.*, 2012).

The identification of genes that play a role in tumour cell genetic alterations, that is, cancer causing genes, can lead to the possibility of designing silencing strategies that are selective and can treat cancer at the molecular level. Therefore, the use of siRNA gene therapy, that is, gene silencing, is an attractive method for the treatment of cancer at its source (Mendes *et al.*, 2017). Following several pre-clinical studies, it was reported that tumour cell growth, metastasis and chemotherapeutic drug resistance can be inhibited by gene silencing (Deng *et al.*, 2014). RNA

interference (RNAi) is a fairly new technology and it has become one of the most widely used and a powerful tool for sequence- specific gene silencing (Deng *et al.*,2014; Duarte *et al.*,2012).

2.3 RNA Interference

2.3.1 An Overview of RNA Interference

RNA interference (RNAi) is a natural, sequence specific, post transcriptional mechanism for gene regulation. It is known to control gene expression through the degradation of the corresponding mRNA, a process mediated by small double stranded RNA (ds RNA) molecules known as siRNA (Zhang *et al.*,2007). In recent years, RNAi has gained interest for the analysis of mammalian gene functions *in vitro* and *in vivo* as well as for the silencing of gene expression (Kim *et al.* 2010; Leung and Whittaker, 2005).

RNAi was first discovered in the late 1980's by plant biologists, Napoli and co-workers, who found gene silencing pathways in plants, however, the exact mechanism was unclear (Hammond, 2005; Zhang *et al.*,2007). Andrew Fire and Craig Mello made a ground-breaking discovery in the late 1990's, as their studies showed that ds RNA can elicit gene silencing in the nematode *Caenorhabditis elegans* (Fire *et al.*, 1988). Their research revealed that RNAi was an evolutionary conserved gene silencing mechanism, and that gene silencing was more effective when using ds RNA as opposed to either individual strand (Zhang *et al.*,2007). In 2001, El-Bashir and co-workers demonstrated that RNAi occurs in mammalian cell lines using synthetic siRNA. The siRNA duplex consists of short dsRNA molecules that are made up of 21- 23 nucleotides with a 19-base pair duplex region (Figure 2.3) (Kim *et al.*, 2010). A characteristic feature of siRNA is the presence of a two nucleotide 3' overhangs which is recognized by the enzymatic machinery of RNAi (Meister and Tuschl, 2001).

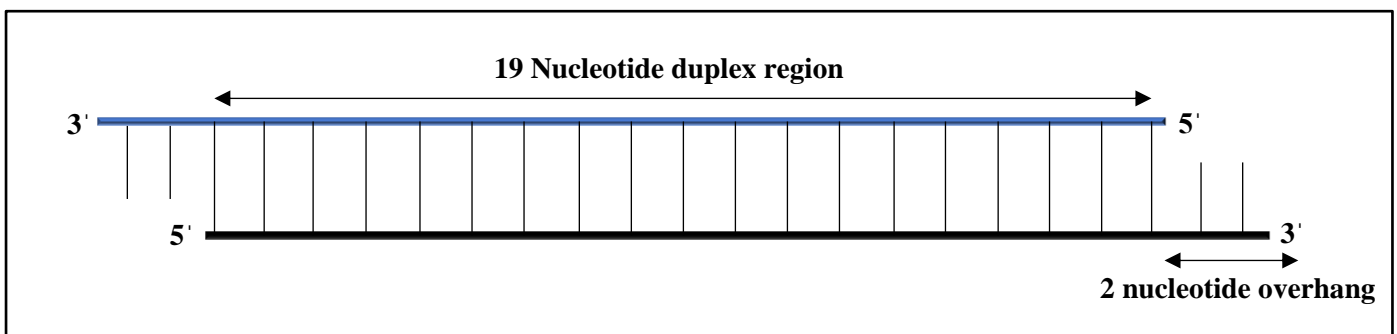


Figure 2.2: Schematic representation of siRNA duplex

The use of siRNA as a therapeutic agent has an advantage in affecting undruggable targets (Draz *et al.*,2014). Cancer has been shown to be heterogeneous in nature with each patient being unique and requiring individualized treatment. siRNA can be chemically synthesized to target any mRNA, and treat each individual based on the gene being overexpressed. These breakthroughs have showcased the great potential of this technology and have spurred intensive research on siRNA therapeutics and its applications (Davis, 2009; de Fougères, 2008). Potential targets for siRNA gene silencing are outlined in Table 2.2.

Table 2.2: Possible targets for siRNA in cancer therapy (Resnier *et al.*,2013; Zhou *et al.*, 2013; Draz *et al.*,2014).

siRNA Target	Disease
PLK 1	Breast Cancer
Cyclin B	Prostate Cancer
MAD 2	Colon Cancer
Mcl-1	Breast Cancer
c-MYC	Breast, Colon Cancer
PAR-1	Melanoma
E6/7	Renal Cancer
KRASG12D	Pancreatic Cancer

2.3.2 siRNA mediated Gene Silencing

The RNAi machinery is initiated following the introduction of siRNA. The siRNA macromolecule is produced from large ds RNA duplexes that are digested by the endonuclease, DICER-2 (Zhang *et al.*,2007; Kong *et al.*,2007; Tuschl *et al.*,1999). Alternately, siRNA can be synthesized chemically and introduced into the cytoplasm of mammalian cells to trigger the process. The process of RNAi is outlined in Figure 2.4.

The siRNA forms part of a nuclease complex called the RNA-Induced Silencing Complex (RISC) (Hammond, 2005; Aagaard and Rossi, 2007). The RISC complex contains Argonaute-2 (Ago-2) within its core, which is responsible for RISC activation by melting the ds RNA and cleaving the target mRNA (Wall and Shi, 2003). Ago-2 consists of three domains, namely, PAZ, MID and PIWI. The PAZ and MID domains anchor the RNA and PIWI is involved in the mRNA silencing (Kim *et al.*,2009). The duplex is unwound by ATP-dependant helicases and the sense strand is then cleaved by Ago-2 (Matranga *et al.*,2005; Rand *et al.*,2005). The cleavage of the ds RNA by Ago-2 results in the formation of the activated RISC complex which

contains a ss RNA molecule, being the anti-sense strand of siRNA, and remains bound to the RISC complex via Mg^{2+} (Ma *et al.*,2005). Complimentary mRNA sequences are then recognised by the activated RISC complex, a recognition is guided by the anti-sense RNA strand in the cytoplasm by Watson-Crick base pairing (Ryther *et al.*,2005). Cleavage of the mRNA strand by Ago-2 occurs between bases 10 and 11 relative to the 5' phosphorylated end of the antisense siRNA, inhibiting translation of the mRNA (Hammond, 2005; Elbashir *et al.*,2001). The guide strand is then recycled and allows for cleavage of other mRNA copies. A distinguishing feature of siRNA mediated gene silencing, as compared to other nucleic acid therapeutics, is RISC recycling which may result in a prolonged silencing effect, of up to 7 days in dividing cells and weeks in non-dividing cells. Furthermore, repeated siRNA administration can result in long term gene knockdown (Bartlett and Davis, 2006).

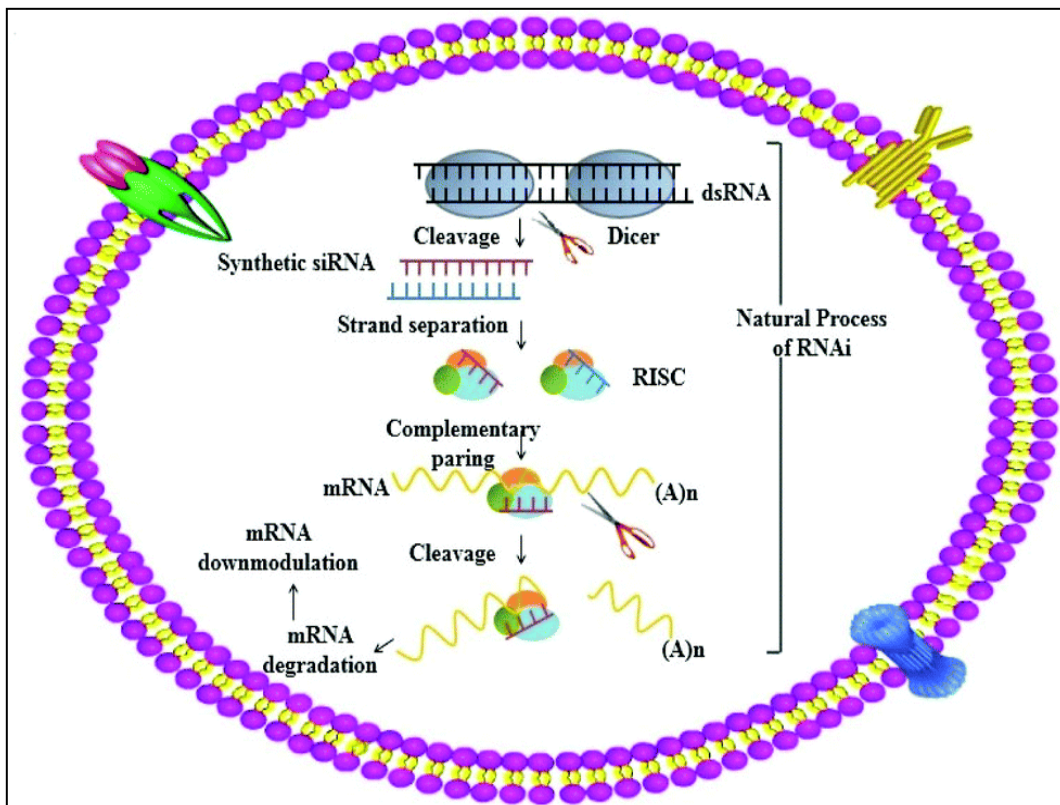


Figure 2.3: Illustration of the mechanism of RNA interference initiated by synthetic siRNA (Liao *et al.*,2016)

2.3.3 Potential of siRNA gene silencing therapeutics in cancer treatment

Cancer occurs due to a number of cellular gene mutations which usually involve a combination of oncogene activation or tumour suppressor gene inhibition which results in the suppression of the naturally occurring apoptotic processes and uncontrolled cell growth (McCleod, 2013;

Suva *et al.*,2013). The use of RNAi, induced by therapeutic siRNA, can be effective for cancer treatment as there are many key genetic mutations that lead to the onset of cancer. The specificity of the therapeutic siRNA molecule to target and inhibit various cancer related genes is a major advantage and allows for the treatment of ‘undruggable’ proteins, such as transcription factors, that are involved in the initiation of tumour formation, growth and metastasis. Therefore, the molecular targets need to be identified to allow for ‘personalised’ therapies for various cancers (Lee *et al.*,2016). The current targets for siRNA-based cancer therapies shall be discussed below.

2.3.3 (a) Lung Cancer

Lung cancer is the most common tumour type and among the three lung cancer types, non-small cell lung cancer is the most frequently occurring and makes up approximately 85% of lung cancers (Molina *et al.*,2008; Herbst *et al.*,2008). Treatment strategies for lung cancer, which include surgery and radiochemical therapies, often fail due to the metastatic nature associated with lung cancers, therefore, siRNA therapeutics can be considered.

Mutations of the epidermal growth factor receptor (EGFR) are found to be in various cancer types and is the most frequent in non-small cell lung cancer. Mutations usually occur on exons18-21 with the most common mutation involving the deletion of exon 19. This exon is involved in the activation of tyrosine kinase activity, and its deletion induces the downstream survival signalling and poor growth pathways. In 2003, Takahashi and colleagues found that the wet weight of tumours that were targeted by allele specific siRNA against the oncogenic EGFR mutant was much lower in the treated group as compared to the untreated control group. Moreover, the treated tumour tissue showed increased caspase-3 activity which indicates that apoptosis was induced. With this treatment, the oncogenic EGFR mutant was inhibited with the normal EGFR allele being unaffected (Takahashi *et al.*,2013).

KRAS mutations are often found in lung tumours and those found in EGFR mutant lung tumours are resistant to EGFR- directed treatment strategies. In 2014, Xue *et al.* used a combination treatment strategy targeting KRAS activation and p53 function loss in a genetically engineered mouse model. The authors utilized a polymer-based nanoparticle loaded with KRAS-targeted siRNA and miRNA that could partially restore p53 functions and injected these therapeutic molecules intravenously to mouse models. The authors found that 63% of tumour regression resulted in an increase in apoptotic cells. Furthermore, it was found that the

mice models treated with this combination therapeutic model survived much longer than those treated with either siRNA or miRNA treatment alone (Xue *et al.*, 2014). This combination treatment strategy allows for personalised treatment for multiple gene mutations identified in a particular cancer patient.

Resistance to chemotherapy drugs, such as docetaxel, is generally known to be facilitated by the protein Human- ribophorin II (RPN2), which is part of the N-oligosaccharyltransferase complex. Additionally, this protein is also known to be anti-apoptotic by stabilizing the p53 mutant which results in tumour survival (Kurashige *et al.*,2012). Fujita and co-workers delivered RPN2 targeted siRNA, via inhalation, to the lung and found that RPN2 expression was suppressed with inhibition of A549 lung xenograft growth (Fujita *et al.*,2013).

2.3.3 (b) Liver Cancer

Hepatocellular carcinoma (HCC) is a major type of liver cancer and is the most frequently occurring. HCC is a complicated form of liver cancer as it is not only caused due to environmental mutations but also occur as a result of viral infections including hepatitis virus infections. There is limited current treatment strategies for HCC, which include aggressive surgery and transplants.

Histone deacetylases (HDACs) are enzymes involved in gene expression regulation through the acetyl group deletion from histones (Lee *et al.*,2014). HDACs interact with transcription factors, such as Myc, β - catenin, p53, among others; which are known to regulate protein expression of those implicated in tumour development. Hence, HDAC mutations can result in tumour development. Lee and co-workers utilized HDAC targeted siRNA conjugated to lipid nanoparticles and found a reduction in the proliferation of liver cancer cells *in vitro* (Lee *et al.*,2014).

The protein Survivin, is an apoptosis inhibitor and is overexpressed in HCC. This results in the inhibition of caspase activation which prevents apoptosis and stimulates HCC proliferation (Ito *et al.*,2000). Mice models with tumours from HCC were treated with survivin targeted siRNA molecules by Wu *et al.* These siRNA molecules were conjugated to RGD-PEG-g-PEI-SPION nanoparticles and the authors found that tumour growth was delayed with an increase in the expression of cleaved caspase-3 (Wu *et al.*,2013).

The human telomerase reverse transcriptase (hTERT) is a human telomerase component required in the stable maintenance of telomere length in cancer cells. hTERT is overexpressed in lung and breast cancers which correlates with the activity of telomerase. Xia and co-workers studied the effects of hTERT siRNA, conjugated to PEI, in HepG2 cells *in vitro*, and found that cell proliferation and the activity of telomerase was reduced. Furthermore, following intratumoral injection into HepG2 tumour bearing mice, there was a reduction in tumour sizes as compared to the tumours treated with control siRNA (Xia *et al.*,2012).

2.3.3 (c) Prostate Cancer

Prostate cancer is the most common male malignant cancer with therapies including surgery, chemotherapy, hormone-therapy and radiotherapy. However, these treatment strategies reduce the quality of life or negatively impact healthy organs.

The transcription factor Myc is involved in biological processes which include replication, proliferation, transcription, cell division, among others (Dang, 2012). Myc is highly expressed in primary and metastatic prostate cancers. Civenni and colleagues reported the reduction in tumour initiation in prostate cancer stem cells *in vitro* and *in vivo* in cells treated with Myc targeted siRNA. Myc siRNA: PEI complexes were introduced into mouse models and the results showed a suppression of tumour masses with an increase in tumour progression in the control group (Civenni *et al.*,2013).

The Kallikrein- related peptidase 4 (KLK4) plays a role in the progression of prostate cancer and in the regulation of cell-cycle gene expression. This enzyme is normally expressed in prostate cells, however is found to be significantly overexpressed in the malignant form (Xi *et al.*,2004; Lai *et al.*,2010). Jin and colleagues found that the prostate cancer cells LNCaP and VCaP showed reduced KLK4 expression and AR-signalling down-regulation following treatment with KLK4 targeted siRNA/liposomes. Moreover, mice models treated with KLK4 siRNA showed a 90% reduction in tumour size (Jin *et al.*,2013).

2.3.3 (d) Breast Cancer

Breast cancer is the leading cause of cancer related deaths in females (Zhang *et al.*,2014). The different breast cancer subtypes can be divided using either molecular profiling or

immunohistochemical (IHC) staining for key receptors. Treatment strategies include surgery, chemotherapy, radiotherapy and targeted therapies with siRNA- based gene inhibition has been tested using models.

Breast cancers can be subdivided according to the expression of estrogen, progesterone and the human epidermal growth factor 2 receptor (HER2). The estrogen receptor alpha (ER- α) is found to be upregulated in approximately 70% of breast cancers and plays an important role in mammary epithelial cell cycle progression. Bouchlier and co-workers prepared nanocomplexes between PEG-*co*-poly(ϵ -caprolactone-*co*-dodecyl β -malate) and ER- α targeted siRNA which were introduced into MCF-7 xenografts and reported that tumour growth was reduced and ER- α was downregulated (Bouchlier *et al.*,2008).

Approximately 15% of breast cancers exhibit reduced expression following IHC in HER2 and progesterone receptors and are referred to as triple-negative breast cancer (Bosch *et al.*,2010; Reis-Filho and Tutt, 2008). Cyclin dependant kinase 1 (CDK1) inhibition results in the lethality of triple negative breast cancer that overexpresses *c-MYC*. In line with this, Liu and colleagues targeted CDK1 and utilized stealth lipid nanoparticles conjugated to CDK1-siRNA molecules to deliver the siRNA to mice via systemic injection. They found that there was a reduction in tumour growth with no toxicity or immune response (Liu *et al.*, 2014).

Osteopontin (OPN) protein is considered to be a marker in the progression of breast cancer as elevated levels have been detected in the plasma and blood of metastatic breast cancer patients. Minai-Tehrani and colleagues targeted OPN in mice models bearing xenografts of MDA-MB-231 by introducing OPN-siRNA molecules encapsulated nanoparticles composed of glycerol propoxylate triacrylate (GPT) and spermine and found that OPN knockdown occurred in the inhibition of tumour growth (Mirhai-Tehrani *et al.*,2012).

2.4 *c-MYC* Oncogene: A Possible Target for Cancer Gene Therapy

The human proto-oncogene, *c-MYC* was discovered approximately three decades ago as the cellular homolog of the retroviral *v-MYC* oncogene which was discovered during early studies of aggressive tumours in chickens (Dang, 1999; Hoffman and Lieberman, 2008). *c-MYC* is believed to play a role in cellular functions which include growth, metabolism, replication, differentiation and apoptosis (Dang *et.al.*, 2006). Furthermore, studies have marked this gene as a genuine human oncogene as it was found to consistently change due to chromosomal

translocations as in Burkitt's Lymphoma (Deusberg *et al.*,1979; Sheiness *et al.*,1979, Dalla-Favera *et al.*,1982; Shou *et al.*,2000). It is believed that overexpression of this oncogene is due to amplification in several human cancers, namely, lung, breast and in a few cases of colon carcinomas (Augenlicht *et al.*,1997; Little *et al.*,1983; Mariani- Constantini, 1988; Munzel *et al.*,1991).

The *c-MYC* gene is located on chromosome 8 and consists of three exons. The AUG start codon is located on exon 2 and translation of the major polypeptide (64 kDa) is initiated at this codon. Translation of a longer 67 kDa polypeptide is initiated on codon 1 at the CUG codon which is located 15 codons upstream of the AUG codon (Hann *et al.*, 1992). The *c-MYC* gene encodes a transcription factor with a base region/ helix-loop-helix/ leucine zipper domain, which is known to dimerize with its partner protein, Max, and trans-activate gene expression by binding to specific DNA sequences, namely, E-boxes with the consensus sequence 5'-CACGTG- 3' (Figure 2.2) (Blackwood *et al.*, 1991).

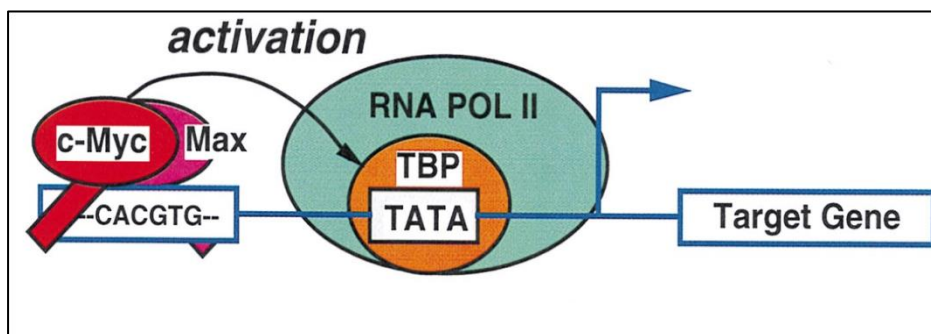


Figure 2.4: Interaction between *c-MYC* and Max protein during transactivation of gene expression (Dang, 1999).

The role of MYC in transcription activation has been established, however, the mechanism of MYC involvement in the repression of transcription is not fully understood (Pelengaris *et al.*,2002). It is believed that transcription may be inhibited by the interaction between the *c-MYC*- Max heterodimer and the MYC- interacting zinc finger protein-1 (Miz-1) (Eilers and Eisenman, 2008; Adhikary *et al.*,2005). Changes in cellular proliferation and metabolism occurs due to *c-MYC* regulation of several gene families, stimulating those genes that are involved in cancer metabolism, protein biosynthesis and transcription factors, while also inhibiting some tumour gene expression (Eilers and Eisenman, 2008).

The *c-MYC* oncogene is one of the most mutated oncogenes in human cancers (Wolfer and Ramaswamy, 2011). Studies have shown that changes on the chromosome 8q24 locus, not only increases tumour likelihood but also influences the expression of the MYC transcript. The overexpression of this gene is seen in pre-malignancy and invasive tumours. It has been estimated that 40% of all human cancers are due to an increase in MYC expression (Dang *et al.*, 2010). The most common feature observed in cancer cells is the abnormal activation of the *c-MYC* (MYC) oncogene. This may be due to overexpression during transcription, translocation, or alterations in upstream signalling pathways. (Koh *et al.*, 2016) In non-transformed cells or normal cells, sustained MYC expression results in arrested cell proliferation, apoptosis and differentiation. Overexpression of *c-MYC* is required by tumour cells, as high protein levels of MYC is essential for cancer cell maintenance and to drive tumour progression and initiation (Gabay *et al.*, 2014).

2.4.1 MYC as a Transcription Factor (TF)

MYC regulates the transcription of genes involved in protein synthesis, cell cycle, cell adhesion, metabolism, and micro-RNA expression (Hoffman and Lieberman, 2008). In non-transformed cells, *c-MYC* expression is well controlled by developmental signals. The *c-MYC* mRNA has a short life span and, in the absence of positive regulatory signals, transcription of *c-MYC* is reduced leading to low MYC protein levels, and minimal proliferation. MYC is capable of regulating non-coding and coding RNA during transcription which are produced by RNA polymerase I, II and III (Kress *et al.*, 2015; Gomez-Roman *et al.*, 2006). The emergence of genome-wide profiles has revealed that MYC binds to every active promoter and enhancer (Koh *et al.*, 2016).

Specific post-transcriptional capping of RNA Pol II consists of a 7-methyl guanosine addition at the 5' end of the first transcribed nucleotide which provides stability to the RNA and proper downstream processing of pre-mRNA. This cap addition is directly promoted by MYC with the assistance of TFIIF which results in the phosphorylation of the carboxy-terminal domain (CTD) of RNA Pol II, which is a requirement for capping (Cole and Cowling, 2009). MYC is also capable of upregulating transcription of S-adenyl-L-homocysteine hydrolase (SAHH) which is needed to metabolize SAH. SAH is an inhibitory by-product of the capping mechanism which can result in negative effects. MYC has been shown to control the transcription of splicing factors such as hnRNPA1, hnRNPA2 and the polypyrimidine tract

binding protein (PTB). These proteins, together with other events, control the splicing of pyruvate kinase which results in the formation of the tumour isoform PKM2, which is known to promote aerobic glycolysis, and PKM1, which is the adult isoform and brings about oxidative phosphorylation (Koh *et al.*,2016).

Splicing factor hnRNPH is regulated by *c-MYC* and is needed for the splicing of the *a-raf* pre-mRNA oncogene. Ras activation and transformation are suppressed in cells by low MYC and hnRNPH expression due to the production of the short A-raf isoform, which encodes a truncated A-Raf protein. However, in cancer cells, the overexpression of MYC and hnRNPH results in the production of a full-length A-raf protein, inhibiting the MST2 pro-apoptotic kinase activity (Rauch *et al.*,2011).

2.4.2 *c-MYC* and Metabolism

Due to transformations related to malignant cell growth abnormalities, metabolic changes in cancer cells occur in order to provide energy to drive the accelerated cell division. The *c-MYC* oncogene is known to have regulatory roles in transformation, however it is still not fully understood if the overexpression of MYC is primarily responsible for the metabolic changes during transformation, or whether the MYC overexpression may be a result of metabolic changes that occur due to malignant cell formation (Miller *et al.*,2012).

A crucial step in tumour progression is the adaptation of the tumour cell under anaerobic conditions. Cancer cells have the ability to use glucose as an energy source under hypoxic conditions and aerobically overproduce lactic acid, process termed the Warburg effect, which was discovered approximately eight decades ago as a characteristic in many tumour types (Koppenol *et al.*,2011; Fletcher *et al.*, 2008; Dang, 1999). Recently it has been shown that the Warburg effect is induced due to the activation of oncogenes with an observed increased consumption of glucose, oxidative phosphorylation and lactate production. Overexpression of the *c-MYC* oncogene results in changes that bring about malignancy. These changes allow for the production of cell growth and cell division intermediates and are known to be regulated by tumour suppressor genes and oncogenes (Miller *et al.*, 2012). It has been observed that lactate dehydrogenase A (LDHA), which is known to convert pyruvate to lactate during glycolysis, is a target gene for *c-MYC*, which suggests that this oncogene plays an important role in the glycolytic pathway (Lewis *et al.*,1997, Ramanathan *et al.*,2005). Various glucose metabolic

genes, namely, glucose transporter, hexokinase 2, phosphofructokinase and enolase 1 are also regulated by *c-MYC* (Dang *et al.*,2009). It is believed that *c-MYC* contributes to the Warburg effect due to the upregulation of these genes involved in glycolysis, further causing the transformed cells to convert glucose to pyruvate under hypoxic conditions. These effects were confirmed in studies with mice that overexpress *c-MYC* in the liver. The results showed that there was an overproduction of lactic acid and an increase in the activity of glycolytic enzymes in the liver (Valera *et al.*,1995).

Mammalian cells also obtain energy from glutamine catabolism. The normal expression of *c-MYC* results in the expression of genes required to metabolise glutamine in the cells, however, overexpression of *c-MYC* results in catabolism that exceeds the requirements for protein and nucleotide synthesis by cells. It has been reported that in some human tumours, there are reduced circulating levels of glutamine in the plasma due to high glutamine consumption (Klimberg *et al.*,1996; Chen *et al.*,1993). In cancer cells, glutamine metabolism is an important function in the mitochondria for the breakdown of glutamine to ATP and lactate (Deberardinis *et al.*,2008). Recent studies have shown that *c-MYC* expression influences cancer related changes in the metabolism of glucose and glutamine (Le *et al.*,2012).

2.4.3 *c-MYC* and Apoptosis

Approximately 25 years ago, it was shown that the *c-MYC* gene can play a role in the apoptotic response by cells. Apoptosis triggered by MYC provides a mechanism to limit uncontrolled cell growth in inappropriate conditions and, therefore, tumour growth and progression will be regulated. However, the apoptotic mechanism in cells that overexpress MYC is disabled in most cases due to mutations. *c-MYC* controlled apoptosis can either be dependant or independent of the p53 tumour suppressor gene. The p53 tumour suppressor gene is often referred to as the ‘guardian of the genome’ as it mediates mammalian cell apoptosis to stress stimuli (Hoffman and Lieberman, 2008).

In normal cells, the p53 protein is expressed at low levels, however, the expression of this protein increases in response to stress. The activation of p53 occurs with the downregulation of *c-MYC* expression and growth arrest (Guillouf *et al.*,1995). Studies have shown that p53 represses the expression of *c-MYC* during transcription, which results in the discontinuation of p53-mediated growth arrest. MYC mediated apoptosis may also occur independent of p53. The interaction between *c-MYC* and p53 has been found to be dependent on the cell type, e.g.

lymphoid and myeloid MYC apoptosis is p53 dependent (Hsu *et al.*, 1995; Hoffmann and Lieberman, 1998). Epithelial cells exhibit both p53 dependent and independent MYC activated apoptosis mechanisms (Sakamuro *et al.*, 1995).

Evidence also shows that *c-MYC* can change the balance of members of the *Bcl-2* family, which are anti and pro-apoptotic genes. Bcl-2 anti-apoptotic proteins inhibit MYC activated apoptosis in some cell systems, but the proliferative function of *c-MYC* is not affected (Nilsson and Cleveland, 2003). The *c-MYC* and Bcl-2 interaction provides an explanation on their role in cellular transformation, with the overexpression of *c-MYC* leading to a suppression of Bcl-2 RNA and protein levels (Eischen *et al.*, 2001).

Due to its ubiquitous role in human cancers, *c-MYC* is an ideal target in cancer therapy. Change in *c-MYC* expression is associated with the pathogenesis of most human cancers (Pelengaris *et al.*, 2002). Therefore, the specific downregulation of *c-MYC* could be a potential treatment strategy for human cancers.

2.5 Pharmacokinetic Challenges Associated with siRNA Delivery

The discovery of siRNA-mediated gene knockdown can be exploited for gene therapy. The ability to chemically synthesize siRNA to induce RNA interference in mammalian cells has stimulated interest in its therapeutic potential (Lu *et al.*, 2009). If siRNA can be targeted to a specific oncogene, it can be used in cancer therapy as a therapeutic agent (Gao and Huang, 2008). However, for RNAi to be effective, the siRNA has to reach its site of action, namely, the cytosol to induce its silencing effects. However, there are a number of hurdles that need to be overcome to allow for siRNA induced RNAi to take place. Although RNAi has a high specificity, off-target effects may be induced due to interactions between the siRNA and similar sequences, or targeted gene silencing may occur but not at the tissue of interest (Deng *et al.*, 2014; Song *et al.*, 2007; Li *et al.*, 2008). The physicochemical properties of siRNA, namely the anionic backbone, hydrophilicity and relatively large molecular weight (approximately 13 kDa), impedes cellular uptake by preventing the siRNA from crossing the cellular membrane (Thanki *et al.*, 2017). Biological barriers hinder extracellular as well as intracellular siRNA trafficking (Figure 2.5). The extracellular barriers encountered by siRNA include nuclease degradation, renal clearance and phagocytosis by the mononuclear phagocytic system (MPS) (Wang and Thanou, 2010). Furthermore, due to the size of the siRNA, which has an average diameter of less than 10 nm, they are rapidly removed from the blood circulation through renal

clearance (Zhou *et al.*,2013). It is believed that siRNA has a circulating half-life that is less than 10 minutes (Banan and Puri, 2004). If naked siRNA is taken up via endocytosis, endosomal escape is a challenge. The siRNA is susceptible to degradation when fusion occurs between the late endosome and the lysosome (Song *et al.*,2007).

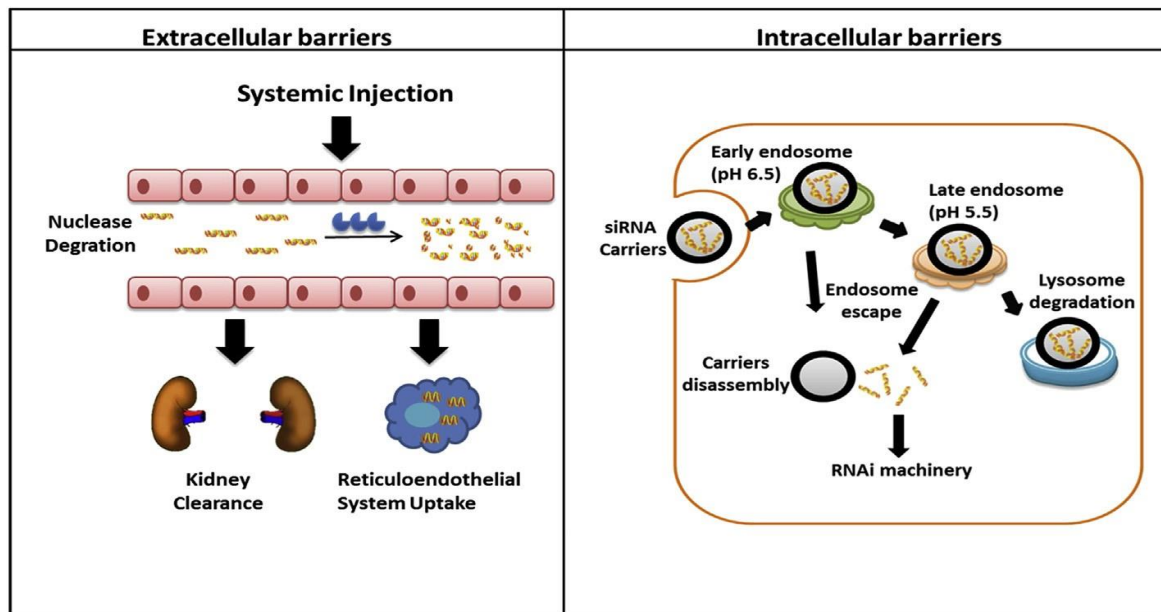


Figure 2.5: Intracellular and extracellular barriers encountered by siRNA (Xu and Wang, 2014)

Due to these barriers, effective and safe siRNA delivery vehicles are desired to deliver siRNA to the target site without any adverse effects (Lorenzer *et al.*,2015). Delivery systems must be developed that can be administered safely, efficiently and repeatedly (Kumar and Clarke, 2007). Furthermore, the gene delivery vector should be engineered to provide serum stability, be capable of binding and condensing siRNA, allow evasion of the immune system, mitigate interactions between serum proteins and non-cancer cells, resist renal clearance, permit cell entry and endosomal escape to enter the RNAi machinery, and have low toxicity (Alexis *et al.*,2008; Whitehead *et al.*,2009).

2.6 Gene Delivery Vectors

The success of gene therapy is dependent on the delivery vector as one of the main objectives is the transfer of genetic material to the cells being treated (Gao and Huang, 2008; El-Aneed, 2003). The question of delivery still remains a major hurdle which needs to be solved in order

to prevent any setbacks during therapeutic application (Shi *et al.*,2003). Delivery vehicles can be divided into two categories, namely, viral and non-viral vectors.

2.6.1 Viral Vectors

Viral vectors can be described as replication deficient viruses where a portion of their viral sequence is modified by deletion and replaced with the therapeutic gene (Li and Ma, 2001). Among the most common viral vectors are retroviruses, herpes simplex viruses, lentiviruses, adenoviruses and adeno-associated viruses. Each viral vector has its own characteristics and offer advantages such as high transfection rates and the very quick transcription of the genetic material that is incorporated into the viral genome (Oligino *et al.*, 2004). However, there are limitations that are associated with viral vectors. Firstly, the size of the genetic material that can be inserted into the viral genome is limited. Secondly, immune responses, toxicity and inflammatory responses are potential problems affecting patients and lastly, oncogenic effects and mutagenesis can occur following *in vivo* applications (Lee *et al.*,1998).

Due these limitations with respect to safety, non-viral vectors have become attractive alternatives for the therapeutic delivery of genes.

2.6.2 Non-Viral Vectors

Non-viral vectors have gained much attention as gene delivery vehicles due to the advantages associated with them which include their ease of synthesis, low immune response and the unrestricted size of the therapeutic agent to be delivered (Akhtar and Benter, 2007; Zhang *et al.*,2007). The main objective of a non-viral delivery system is to mimic the viral vectors in their ability to overcome the cellular barriers, while minimizing the toxicity associated with these viral methods (Balicki and Beutler, 2002). Non-viral delivery systems can be divided into two categories, namely, physical and chemical approaches. These delivery systems shall be discussed briefly.

2.6.2.1 Physical Methods

2.6.2.1 (a) Hydrodynamic Injection

The direct transfer of siRNA into cells can be achieved using the hydrodynamic injection approach, whereby siRNA in a large volume of physiological buffer, is rapidly introduced into the target tissue (Gao and Huang, 2008; Davis, 2002). Due to the invasive nature of the hydrodynamic injection as well as the high pressure that is generated following the injection of the genetic material, the application of this system is not currently viable for human clinical applications (Spagnou *et al.*,2004; Vandenbrouke *et al.*,2008; Gao and Huang, 2008).

2.6.2.1 (b) Electroporation and Nucleofection

Electroporation was designed to introduce molecules into a cell through the application of controlled, short bursts of electrical pulses. This electric shock creates pores in the cell membrane which allows for the nucleic acid to enter the cytoplasm (Ramon *et al.*,2008). Following this internalization, the negatively charged molecules become trapped within the cell (Nishikama and Huang, 2001; Nayerossadat *et al.*,2012). The application of this method on a large scale is difficult as the parameters for optimal gene expression varies in different tissues (Nishikama and Huang, 2001).

Nucleofection is an extension of electroporation and follows the same principle, however, it is cell type specific and uses less harmful electrical pulses (Gresch *et al.*,2004).

2.6.2.1 (c) Gene Gun Method

The gene gun method involves the shooting of nucleic acid coated gold, silver or tungsten particles with a gene gun and allows the nucleic acid to directly enter the target cell. This is achieved by bypassing the endosomal pathway (Ramon *et al.*,2008; Nishikama and Huang, 2001; Manjila *et al.*,2013). However, one of the drawbacks is that the target tissues have to be surgically exposed for gene delivery to be carried out (Huang *et al.*,2001; Ramon *et al.*,2005; Niidome and Huang, 2002), limiting its *in vivo* application.

2.6.2.2 Chemical Methods

Chemical approaches include the use of inorganic particles, lipid based, peptide based, or polymer-based particles and are categorised by their ability to form complexes with the therapeutic agent which can offer protection to the gene from degradation by nucleases and other components in the blood. Furthermore, these chemical or synthetic vectors can be designed to target a specific cell or tissue, enhance the delivery of the therapeutic gene to the cytosol or nucleus and allow for the controlled release of the therapeutic agent in the cytosol (Ramamoorth and Narvekar, 2015). Some of these chemical approaches shall be discussed below.

2.6.2.2.1 Advances in Nanotechnology

The emergence of nanotechnology in the last decade has proven to have an impact on diagnostic and therapeutic applications. With this type of technology, scientists are able to manipulate and understand materials at an atomic and molecular scale (Safari and Zarnegar, 2013). Through this control of matter at a nanometer range, the design, formulation, production and applications of new systems can be achieved (Jain *et al.* 2012). These nanostructures can have hydrodynamic diameters that range between 1-100 nm. They can also be designed with control over their chemical and physical properties of the resulting nanoparticle structure, with larger structures being formed through combination (Rocco, 2001). Furthermore, due to their size and greater surface area to volume ratio, vectorization of multiple biomolecules, which include antibodies, nucleic acids, drugs among others, can be incorporated onto a single nanoparticle.

Nanomedicine, which is the use of nanotechnology in medical applications, holds great promise for treatments and therapies in drug delivery, imaging, faster diagnosis and tissue regeneration (Sanvicens and Marco, 2008). The use of nanoparticle systems has many advantages that enables them to overcome a number of challenges, more especially with respect to the bioavailability and biodistribution of the therapeutic agent. Some of these properties is due to the nanoparticle surfaces that are immunochemically inert when in contact with the biological environment. Due to this interaction, the *in vivo* retention time of the nanoparticle is increased due to a decrease in enzymatic degradation and sequestration by phagocytes (Draz *et al.*, 2014). Nanoparticles can be divided into two categories, namely organic and inorganic. Organic nanoparticles include lipid-based nanoparticles such as liposomes, and polymers such

as dendrimers, while inorganic nanoparticles include carbon nanotubes, and metal nanoparticles such as gold and silver, and silica nanoparticles among others, most of which have been applied in cancer therapeutics (Mendes *et al.*, 2016).

2.6.2.2.1 (a) Lipid based Nanoparticles

Lipids are amphiphilic molecules, with one part of the molecule being hydrophilic, and the other hydrophobic (Çağdaş *et al.*, 2014). To date, there have been various lipid based systems that have been developed for siRNA delivery; these include liposomes, emulsions and solid lipid nanoparticles. Among these, cationic liposomes have been one of the most attractive systems due to the ease at which they form complexes with anionic siRNA, their relatively low toxicity and immunogenicity and high transfection efficiency (Oh and Park, 2009).

Liposomes may consist of natural or synthetic lipids, are biocompatible and biodegradable, making them suitable drug and gene delivery vehicles. Furthermore, they have the ability to naturally compartmentalize hydrophilic and hydrophobic material, and their surfaces can be easily modified to bear stealth like and targetable moieties (Grislain *et al.*, 1983). For cancer therapy, the surface modifications of the liposome allow for passive or active targeting to the specific cells, which enables efficient delivery of the therapeutic agent to the malignant cells with minimal impact on normal cells. The colloidal and physicochemical characteristics affect the capabilities of the liposome in drug and gene delivery. Although these cationic liposome formulations have demonstrated potential as gene delivery vehicles, some hurdles still remain, which include, low encapsulation, quick release of the therapeutic agent, lack of triggers for release of the drug or gene, and the release of the gene to extracellular fluids (Wangiaskara and Witharana, 2016). Studies have also described the appearance of unspecific interferon response in mice (Hornung *et al.*, 2005; Ma *et al.*, 2005). However, due to surface modifications, most of these hurdles can be overcome. Examples of cationic liposomes that have been used for the cellular delivery of nucleic acids include N-[1-(2,3-dioleoyloxy)propyl]-N,N,N-trimethylammonium chloride (DOTMA) (Figure 2.6 a) and 3β[N,N',N'-dimethylaminoethane)-carbamoyl] cholesterol (DC-Chol) (Figure 2.6 b).

2.6.2.2.1 (b) Dendrimers

Dendrimers are synthetic, spherical, highly branched molecules with three dimensional nanometric structures (Kesharwani *et al.*,2012; Safari and Zarnegar, 2012). In 1985, Tomalia first proposed the term dendrimer due to its structure that resembles a tree (Tomalia *et al.*, 1990). Dendrimers consist of three structural components, namely, a focal core, building blocks with multiple interior layers consisting of repeating units and several peripheral functional groups. The interior layers, which are the branched units, are referred to as generations and are repeating monomeric units of macromolecules (Bronstein and Shifrina, 2012). Dendrimers have a precise shape and size, are water soluble, biocompatible and elicit negligible immune responses (Biswas and Torchillin,2013; Wu *et al.*,2013, Menjoge *et al.*, 2010; Patil *et al.*,2008). Due to the high density of functional groups on the periphery of the dendrimer, multiple molecules can be introduced onto the surface, and the size of the dendrimer can be controlled, depending on the generation, satisfying various applications (Ciolkowski, *et al.*, 2012; Gurdag *et al.*,2006; Siewara and Watala, 2012). Furthermore, dendritic structures have high penetration ability which results in increased cellular uptake of the conjugated therapeutic agent (Yang *et al.*,2009). Dendrimers have non-polar cavities which allows for encapsulation of hydrophobic molecules (Gupta *et al.*,2006). Depending on the monomer units, a high density of either positive or negative charges will be present on the surface, which will allow for the conjugation of a therapeutic agent with an opposite charge to the surface (Cheng and Xu, 2005). Polyamidoamine (PANAM) and polypropylene imine (PPI) are examples of dendrimers that have been more commonly used in studies for delivery of hydrophobic and hydrophilic drugs (Pan *et al.*,2011).

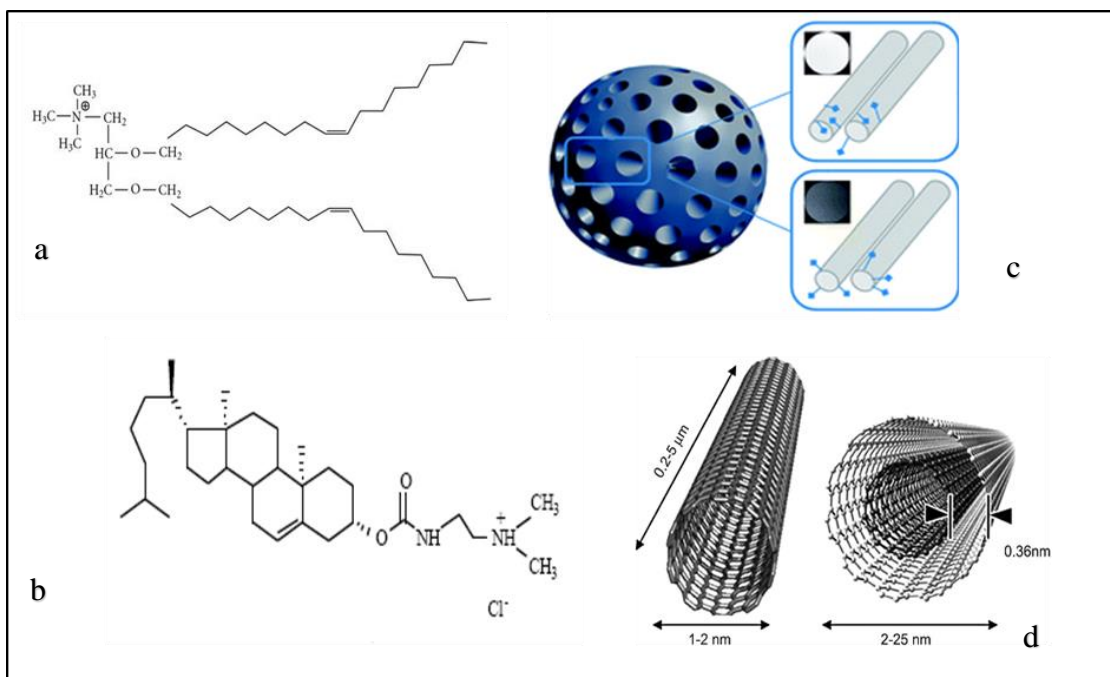


Figure 2.6: Examples of nanodelivery systems (a) DOTMA, (b) DC-Chol, (c) Silica nanoparticles and (d) Carbon Nanotubes (Martin *et al.*,2005; Davis *et al.*, 2012; El Chaar *et al.*,2011).

2.6.2.2.1 (c) Carbon Nanotubes

Carbon nanotubes were discovered in 1991 and have drawn much attention for applications as structural materials due to their surface, mechanical and electrical properties (Iijima, 1991; Guldi *et al.*,2006; Goldberger *et al.*,2006). Carbon nanotubes are one dimensional hollow carbon structures with diameters of 1-2 nm, and a range of lengths between 50 nm to 1 cm (Draz *et al.*,2014). They are cylindrical molecules made up of carbon atoms in a series of hexagonal lattice structures and can be divided into two categories, namely, single walled and multi-walled carbon nanotubes (Figure 2.6 d) (Kesharwani *et al.*,2012). Studies have shown that carbon nanotubes tend to aggregate, are insoluble in most types of solvents and are cytotoxic (Tasis *et al.*,2003; Colvin *et al.*,2003; Warheit *et al.*,2004). Hence, for biomedical applications, carbon nanotubes require functionalization which has been shown to improve their solubility and biocompatibility. Due to their diameter, which is approximately 5×10^4 times smaller than a human hair, it has been proposed that these molecules can cross the plasma membrane easily and enter the cytoplasm of the target cell through endocytosis- independent mechanisms (Pantarotto *et al.*,2004; Cai *et al.*, 2005). Due to their properties, carbon nanotubes show great potential for molecular diagnostics and targeted therapy of tumours. Furthermore,

the ability of functionalised carbon nanotubes to traverse the cell membrane make them attractive as a vector for gene delivery.

2.6.2.2.1 (d) Silica based nanoparticles

Mesoporous systems have gained much interest over the past decade due to their favourable pore size, stable structures and large surface area (Scott *et al.*,2001). Hence, mesoporous materials show potential for the encapsulation of drugs, proteins, nucleic acids, and other therapeutic macromolecules. Mesoporous silica is an example of a mesoporous material that can be used for biomedical and biotechnological applications. The pore size of these nanoparticles is one of their most important characteristics for biological and medical applications (Kesharwani, *et al.*,2012). The size of the mesoporous silica nanoparticles (MSNs) can be controlled from 50 to 300 nm. This permits their rapid endocytosis by cells. MSNs appear to be more stable to heat, mechanical stress, pH and degradation due to hydrolysis compared to other polymer-based nanoparticles. The uniformity of the pore size and tiny diameter of the MSNs (between 2-6 nm) allows one to adjust the amount of the therapeutic agent loaded onto the nanoparticles. Furthermore, the large surface area of the MSNs ($> 900 \text{ m}^2/\text{g}$), and pore volume ($> 0.9 \text{ cm}^3/\text{g}$) allows for high loadings of therapeutic agents (Slowing *et al.*,2008). Selective functionalization with different moieties can be conducted on MSNs due to the presence of an internal surface, that contain cylindrical pores, and the external particle surface (Figure 2.6 c). Due to their unique porous structure, MSNs have potential as drug and gene delivery vehicles (Slowing *et al.*,2008; Vallet -Regi *et al.*, 2001).

2.6.2.2.1 (e) Metal Nanoparticles

The use of metal nanoparticles in biomedical research has expanded in recent years due to their unique properties which include, small size, high reactivity to living cells, and large surface area to volume ratio. Hence, metal nanoparticles show immense potential for use in both diagnostics and therapeutics. Furthermore, their optical properties make them suitable for bioimaging applications due to their capability of producing quantum effects (Tiwari *et al.*,2011). To date, the most commonly studied metal nanoparticles include gold, silver, iron and titanium oxide nanoparticles, with gold nanoparticles (AuNPs) being the most extensively studied for drug and gene delivery, due to their inert nature and low cytotoxicity (El-Ansary

and Al-Daihon, 2009; Conner *et al.*,2005; Ghosh *et al.*,2008, Pissuwan *et al.*,2009). Gold nanoparticles which were used in this study shall be discussed in greater detail.

2.6.2.3 Gold Nanoparticles

Gold (Au) is a noble element and is naturally highly unreactive and therefore, does not deteriorate or undergo chemical oxidation. Nanostructured Au can be used for novel biomedical applications due to their chemical and physical properties. Gold is believed to be a highly functional metal. In its molecular form, they can serve as catalysts or anti-arthritis medications, while in its bulk form, gold is well known in its use for jewellery, electronics and coins (Greenwood and Earnshaw 1997; Chen and Goodman, 2004; Valden *et al.*,1998; Green *et al.*,2011). However, unlike these forms of gold, nanostructured gold exhibits different colours and are believed to be one of the best metals to form nanoparticles (Martínez *et al.*,2012).

Colloidal gold was used for therapeutic and decorative purposes in ancient China, Rome and Egypt with several ways being used to develop nanostructured gold (Boisselier and Astruc, 2009; Giljohann *et al.*, 2010). During the middle ages, soluble gold was used in the treatment of various diseases, such as epilepsy, dysentery, heart problems, tumours and the diagnosis of syphilis (Daniel and Astruc, 2004). The physicochemical properties of nanoscale gold differ from bulk gold in various ways with the most prominent being the colour change from yellow to ruby red. This colour change can be explained by the surface plasmonics theory which suggests that free electrons of gold atom clusters (six electrons in the case of Au) when in contact with an electromagnetic field of incoming light, begin to oscillate which creates a plasmon band with a peak absorbance in the visible region (Riviere *et al.*,2005; Eustis and El-Sayed, 2006). In 1857, Michael Faraday reported the first scientific finding of the deep red colour formation of colloidal gold following the reduction of chloroaurate aqueous solution with phosphorous, which was stabilised with carbon disulphide in a 2-phase system (Dreaden *et al.*,2011; Daniel and Astruc, 2004). Faraday also investigated the optical properties of the colloidal gold by preparing films from the dried solutions and noticed that upon mechanical compression, colour changes from bluish-purple to green occurred (Faraday,1857).

Gold nanoparticles (AuNPs) have attracted much attention for a variety of biomedical applications, and due to their unique properties have the potential as highly multifunctional and selective agents for anti- cancer therapeutics (Niemeyer and Ceyhan,2001). These properties

include their ease of synthesis into a variety of sizes (1-100 nm) and shapes (nanospheres, nanorods, nanoshells, nanodiamonds), relatively low toxicity, non-oxidative nature, and ease of functionalisation with a number of polymers which can provide biological stability, and target selectivity to the AuNPs (Spencer *et al.*,2011; Sandhu *et al.*,2002). Nanoscale gold can appear in a variety of colours that include red, blue, green or brown. The resulting colour is determined by the interaction between the conduction band electrons with the electric field of the incident light. The shape, size and surrounding medium of the gold nanoparticle are all parameters that play a role in the localised surface plasmon resonance (LSPR), as there are a limited number of incident light frequencies that exist that can induce the oscillations of the resonance electron band. The LSPR is found in the visible and near infrared portion of the gold nanoparticle spectrum (Alkilany and Murphy, 2010).

2.6.2.4 Biomedical Applications of Gold Nanoparticles

Nanomedicine is one of the most important research fields of nanotechnology which can allow for the diagnosis, treatment and prevention of diseases at a molecular scale (Boyes *et al.*, 2009). The application of AuNPs for the diagnosis and treatment of diseases in humans relies on the AuNPs being non-toxic, biocompatible, non-immunogenic, stable and environmentally friendly (Cornejo-Monroy *et al.*,2013). Furthermore, AuNPs require suitable properties for biomaterial conjugation, as well as cellular and sub-cellular targeting. AuNPs have been proposed as theranostic devices which refer to the combined diagnostic and therapeutic properties of an individual nanoparticle. The unique optical and electronic properties of AuNPs, due to their reduced size, can be used in bioimaging and therapeutic applications (Niemeyer and Ceyhan, 2001; Sandhu *et al.*,2002). Due to the optical properties of AuNPs, they can potentially serve in applications such as sensing, imaging as well as in cancer therapeutics (Figure 2.7) (Jelveh and Chithrani,2011; Dreaden *et al.*,2012; Daniel and Astruc, 2004; Cao-Milán and Liz-Marzán,2014). These applications are further discussed below.

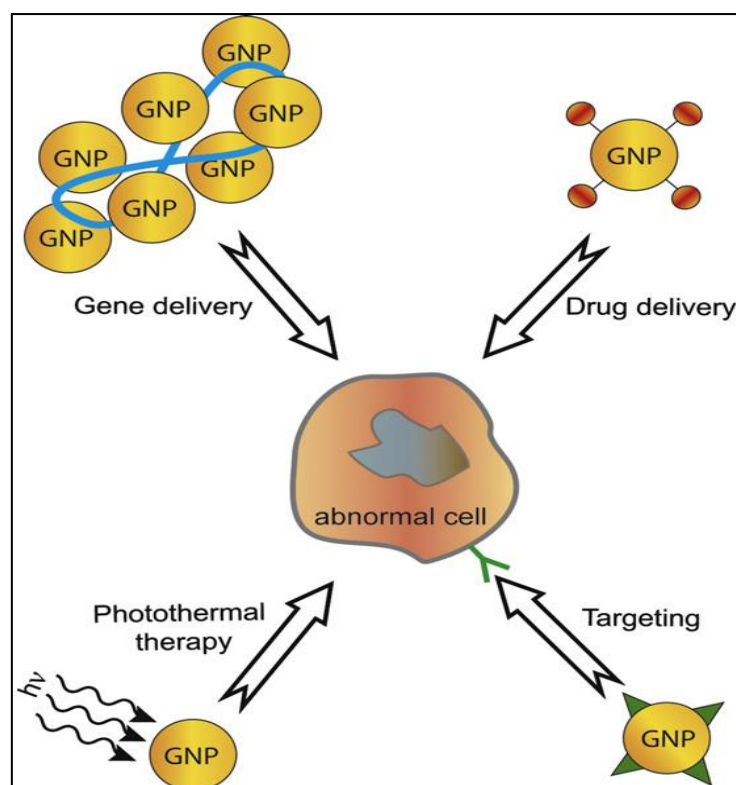


Figure 2.7: Biomedical Applications of gold nanoparticles (AuNP) (Gosh *et al.*,2008).

2.6.2.4 (a) Bio-imaging

AuNPs have optical properties that can be altered to a specific wavelength by changing the composition and shape of the nanoparticle (Conde *et al.*,2012). Hence, they have been used in imaging technology as enhancing agents for tracking and imaging cells, and *in situ* cancer diagnostics (Kim *et al.*,2011; Tseng *et al.*,2010). The high electron density of the AuNPs allows them to act as contrasting agents. Furthermore, by surface modification with antibodies or proteins and using the correct encapsulating agent, nanoparticles can be utilized for detection and treatment, simultaneously, of certain illnesses *in vivo* (Jiang *et al.*, 2008). The basic principle that is involved in the AuNP biosensor design is that the AuNPs should be capped or functionalised with thiolated biomolecules and, when identifying the biomolecule, the AuNP optical absorbance changes (West and Halas, 2003). Light absorption is reduced in the near infrared region (NIR) in many biological tissues. AuNPs can be developed which are activated in these compartments which can result in *in vivo* imaging and hyperthermia treatments (Conde *et al.*,2012). Furthermore, the limitations associated with NIR dyes can be overcome using AuNPs, which include hydrophilicity and photostability as well as low detection sensitivity and stability in biological systems. Pavlov and co-workers (2004) prepared AuNPs that were

functionalised with aptamers. These aptamer-AuNPs bound specifically to thrombin causing AuNP aggregation and a resulting red shift in the plasmon band compared to a control which involved exposing these aptamer-AuNPs to non-specific proteins, such as BSA, which showed no aggregation (Pavlov *et al.*, 2004).

AuNPs can also be utilized as contrast agents for magnetic resonance imaging, computed tomography and in surface-enhanced Raman scattering (SERS). SERS employing AuNPs with a specific receptor molecule attached that has a distinct Raman signature, can be utilized to identify cellular structures, and provide structural information in live cells (Conde *et al.*, 2012; Kniepp *et al.*, 2006). Furthermore, SERS can be used for the detection of trace amounts of biomolecules that may be in proximity to or adsorbed onto the AuNP surface (Kniepp *et al.*, 2002; Liu and Lee, 2005). The use of SERS will allow for the detection of biomolecules without any tags on the molecule, for example unmodified, label-free DNA conjugated to AuNPs can be detected within a cell or tissue upon introduction.

AuNPs can also serve as immune-sensors, which is based on the detection of specific binding between antigen and antibody. AuNPs have attracted much attention for this application as they are relatively simple and economical for mass production, they have excellent limits of detection with small volumes of the analyte and are robust. Dequaire and colleagues developed a novel electrochemical immunoassay that is sensitive for immunoglobulin G (IgG) detection by utilizing a colloidal Au label prepared using an acidic stripping voltammetry technology. Concentrations as low as 3×10^{-12} M could be detected which is competitive with detection limits obtained with ELISA and immunoassays based on fluorescent labels (Dequaire *et al.*, 2000; Parida and Nayak, 2012).

2.6.2.4 (b) Gene and Drug Delivery

As discussed previously, there are many obstacles that need to be overcome in order for gene and drug therapy to be successful. AuNPs are the most widely used of all metallic nanoparticles for gene and drug delivery studies, due to their ease of synthesis and functionalisation, their inert core, biocompatibility and low cytotoxicity (Duncan *et al.*, 2010). Furthermore, they have shown great potential as delivery vehicles for the intracellular delivery of genes due to protection of the therapeutic agent from nuclease degradation and targeting to specific tissues through functionalisation with targeting ligands. Due to the diversity in functionalisation of AuNPs, the therapeutic agent can be attached to the surface of the AuNP via non-covalent or

covalent approaches. The non-covalent method will incorporate the gene or drug to the AuNP surface, with no structural modification to the therapeutic agent required (Park *et al.*,2009).

The covalent attachment of drugs to the AuNP involves the use of cleavable linkages that are utilised for the delivery of the therapeutic agent, and its release into the cell through either internal or external stimuli (Han *et al.*,2006; Hong *et al.*,2006). Anticancer drugs that can be delivered by AuNPs include paclitaxel, 5-fluorouracil, and doxorubicin (Selveraj and Alagar, 2007). There have been various strategies that have been developed for the covalent attachment of drugs to the AuNP. These strategies include photo-regulated release and glutathione mediated release. The photo-regulated release mechanism uses an external stimulus to activate the release of the gene or drug, which also controls the rate of release and the site of action (Kim *et al.*,2006; Park *et al.*,2008; Park *et al.*,2008). This mechanism has been employed by several researchers. Radt and co-workers utilized AuNPs coated with polymers and were capable of releasing its contents by shining a laser onto the loaded nanoparticle (Radt *et al.*,2004). Nakanishi and colleagues used a near UV- irradiation to cleave the carbamate linkage of the 2-nitrobenzyl group of histamines and showed that following irradiation, the unreactive histamine became active (Nakanishi *et al.*,2009). Rotello and co-workers synthesized AuNPs with an o-nitrobenzyl ester moiety that was photocleavable and, upon the introduction of light irradiation, dissociation occurs, and the attached DNA is released intracellularly (Han *et al.*,2006). This controlled system can be potentially utilized for the delivery of various biomolecules. The second strategy involves the use of glutathione (GSH) and relies on the differences in the concentration of GSH within the cell (1-10 mM) and the extracellular concentration of thiols (cysteine 8 μ M, GSH 2 μ M) (Anderson, 1998; Sies, 1999; Jones *et al.*,1998; Jones *et al.*,2000). The bound therapeutic agent to the AuNP surface is released though disulphide exchanges with the intracellular GSH.

The non-covalent attachment of therapeutic agents on the AuNP surface assists in avoiding any potential hurdles that may arise with the covalent encapsulation methods. For this mechanism, appropriate ligands are required which creates a hydrophobic environment within which the therapeutic agent is incorporated. Rotello and colleagues synthesized AuNPs that were functionalised with a hydrophilic outer surface composed of tetra (ethylene glycol) and a hydrophobic alkanethiol interior. The ligand headgroup was zwitterionic which minimized any non-specific interaction with biomolecules and the cell surface. The therapeutic agent was incorporated into the monolayer of the AuNP and was found to be stable in buffer and serum. Furthermore, using fluorescence microscopy, the anti-cancer drug was shown to be delivered

to the cell by diffusion with no cellular entry of the nanoparticle (Kim *et al.*, 2009; Lin *et al.*, 2008; Rouhana *et al.*, 2007; D' Emanuele and Attwood, 2005). Regardless of the mechanism used for the incorporation of the therapeutic agent to the AuNP surface, the AuNP monolayer is of great importance in the eventual release of the gene or drug into the cells.

Although AuNPs are attractive gene delivery vehicles, the efficiency of delivery of the therapeutic agent still remains a major hurdle. This may be attributed to non-specific interactions between the functionalised AuNPs and serum proteins. Thus, PEGylation is a popular mechanism which can reduce AuNP aggregation and opsonization (Ramamoorth and Narvekar, 2015). PEGylation shall be discussed in greater detail in Section 2.6.2.7.

2.6.2.4 (c) Thermal Therapy

Hyperthermia is based on the principle that increasing the temperature above 42°C in living cells can result in cell death and, therefore, can be utilized as a therapeutic application for the immediate, irreversible destruction of malignant tissues. The effects that occur can range from the reduction of cell apoptosis and tumour metabolism, to the immediate destruction of the cancer cells. This is dependent on the temperature and time used. Due to the electron oscillation in the conduction band in noble metals, there is an induction of large electric fields on the surface and, therefore, upon interaction with electromagnetic radiation, the radiative properties of noble metals are enhanced (Nikoobakht and El-Sayed, 2003). This makes the absorption and light scattering properties of these nanoparticles much greater than absorbing molecules and organic dyes, respectively, and therefore, metal nanoparticles can serve as sensors and are excellent contrast agents during optical detection. Furthermore, the absorbed radiation is efficiently and rapidly converted to heat (picosecond time frame). This occurs as a result of electron-phonon and phonon-phonon processes making them potential agents in photothermal therapy (Varnavski *et al.*, 2003). Due to these favourable properties of metal nanoparticles functionalised with target-specific ligands, they can be employed to heat up the selected cancer tissue and destroy it. The heating of the nanoparticle can be achieved by exposing the target area or the patient to an intense light source, an altering magnetic field or radiofrequencies which results in the nanoparticle being heated to a temperature beyond the cancerous cell limits, causing ablation of the tumour (Jain *et al.*, 2011).

The first application was conducted in 2003 by Pitsillides *et al.* who showed that target cells were selectively damaged when using 20-30 nm spherical AuNPs which were irradiated with

laser pulses (20 nanosecond) at a wavelength of 532 nm. This treatment created local heating and, therefore, killed the target cells (Pitsillides *et al.*,2003). Huang and co-workers and Loo *et al.*, using antibodies conjugated to Au nanorods and Au nanospheres, respectively, also demonstrated the potential of gold in photothermal therapy as they reported that following treatment, cancer cells were selectively destroyed while healthy cells remained unaffected (Huang *et al.*,2005; Loo *et al.*,2005). For *in vivo* treatment, AuNPs have been utilized as photothermal agents as they have the ability to absorb in a broad-spectrum range between 650-900 nm and are capable of converting this radiation to heat in picoseconds (Conde *et al.*,2012). Due to the unique optical properties of AuNPs, they can be visualised over long periods of time in cells and hence can be irradiated with multiple laser pulses. This will allow for inactivation of the cell in a controlled and non-traumatic manner and can be applied for the treatment of cancers that are resistant to chemotherapy (Carpin *et al.*,2011).

2.6.2.5 Gold Nanoparticle Functionalisation

Gold nanoparticles have been synthesized by a variety of methods and follow a similar strategy where the gold salt is reduced in the presence of a stabilizing agent (Tiwari *et al.*,2011). The particle size of the colloidal gold can be controlled by varying the salt concentration, temperature and reducing agent (Dreaden *et al.*,2011). The two commonly employed methods for the synthesis of colloidal gold are the citrate reduction method and the Brust-Schuffron method. The latter being a two-phase synthesis and stabilisation process using thiols. The citrate reduction method was introduced by Turkevich and co-workers in 1951 which was later modified by Frens and colleagues in 1973 and involves the citrate reduction of HAuCl₄ in water (Figure 2.8). The citrate molecules offer stabilisation to the resultant anionic AuNPs (Remant-Bahadur *et al.*,2013, Oyelere *et al.*,2007). The citrate reduction method is the most popular method for AuNP synthesis, as it is simple and allows for large scale production of AuNPs.

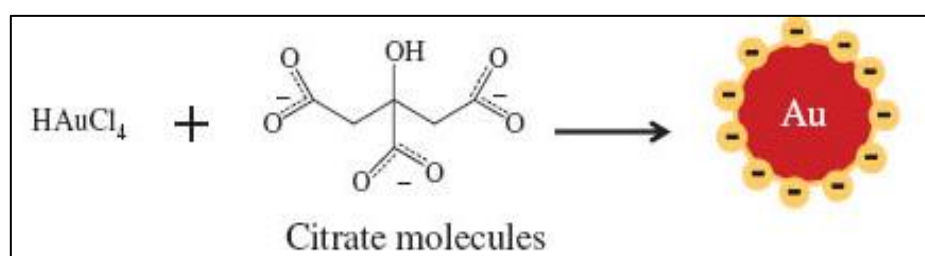


Figure 2.8: Synthesis of citrate capped AuNPs by reduction with sodium citrate (Makhsin *et al.*,2012)

One of the key issues for the integration of biological molecules into AuNPs is their surface chemistry which ultimately determines their stability, functionality and their biological applications. Uncoated AuNPs have a high sensitivity to environmental factors such as pH, temperature, electrolytes and solvent due to the free electrons on their surface which are highly reactive. This results in the tendency of AuNPs to easily aggregate in media (Boca *et al.*, 2010). Most biological applications of AuNPs requires the modification of their surface with ligands containing functional groups such as amines, thiols or phosphines, that have a high affinity for the AuNP surface, and additionally can be used to bind proteins, nucleic acids, antibodies and aptamers (Cornejo-Monroy *et al.*, 2013). AuNPs can be functionalised using synthetic and biological compounds. The choice of the functionalising agent depends on the application. Non-labile applications utilize thiol-based groups, while labile applications employ amine or carboxylate anchors. The non-covalent systems using amine functionalised anchors, are an attractive alternative to the covalent systems for nucleic acid delivery (Ding *et al.*, 2014). The coverage of the surface of the monolayer is of great importance as this modification influences the final charge of the AuNP and its hydrophobicity, in an attempt to maximise the transfection efficiency and with minimal cytotoxicity (Sandhu *et al.*, 2002).

2.6.2.6 Polymer Functionalisation

A non-covalent amine system can bind nucleic acids through electrostatic interactions and provide an effective means of gene delivery in mammalian cells. Polymers that have been commonly used for functionalisation include chitosan, poly-L-lysine (PLL), polyethyleneimine (PEI), polyethylene glycol (PEG) and various targeting ligands. Synthetic positively charged polymers include the commonly used PLL (Figure 2.8 a), and PEI (Figure 2.8 b), with PEI being the most popular to date. PEI has a wide range of molecular weights and a high number of protonable amino groups, which results in a high cationic charge at physiological pH. However, the use of synthetic polymers such as PLL and PEI can be toxic to living cells through apoptosis and necrosis. This toxicity can be attributed to the high molecular weight of these branching polymers (Hunter, 2006).

Natural polymers have been used due to their non-toxic nature, biocompatibility and biodegradability. Among the natural cationic polymers available, chitosan has been the most widely used for gene delivery and functionalisation of AuNPs. Chitosan is a natural biodegradable polysaccharide obtained by the deacetylation of chitin. Chitin is the structural

element found in the exoskeleton of crustaceans. Chitosan consists of repeating D-glucosamine and N-acetyl-D- glucosamine units which are linked via a (1-4) glycosidic bond (Figure 2.8 c) (Mao *et al.*,2010). Chitosan is non-toxic in humans and animals and can be characterised by its physicochemical properties that include the molecular weight, degree of deacetylation, crystallinity and viscosity (Kas, 1997). The solubility of chitosan in acidic media is attributed to each deacetylated subunit that contains a primary amine group with a pKa value of 6.5, therefore, chitosan is not soluble in alkaline or neutral media. The degree of deacetylation determines the positive charge density in acidic conditions. When there is a higher degree of deacetylation, there is an increased positive charge which can result in greater nucleic acid binding and cellular uptake. Deacetylation over 65% is required to form stable complexes with DNA whereas with siRNA, the degree of deacetylation should exceed 80% (Huang *et al.*,2005; Mao *et al.*,2010). Although synthetic polymers, in comparison to chitosan, have a higher charge density which is responsible for their transfection efficiency, they also induce a far greater cytotoxic effect. Due to its characteristics, chitosan is considered as one of the most important polymers for pharmaceutical and biological applications (Kumar, 2000). Furthermore, this natural polymer has shown great promise in the food industry as a preservative due to its anti-microbial properties and is currently been used in dietary supplements (Dutta *et al.*,2009; Li and Huang, 2000).

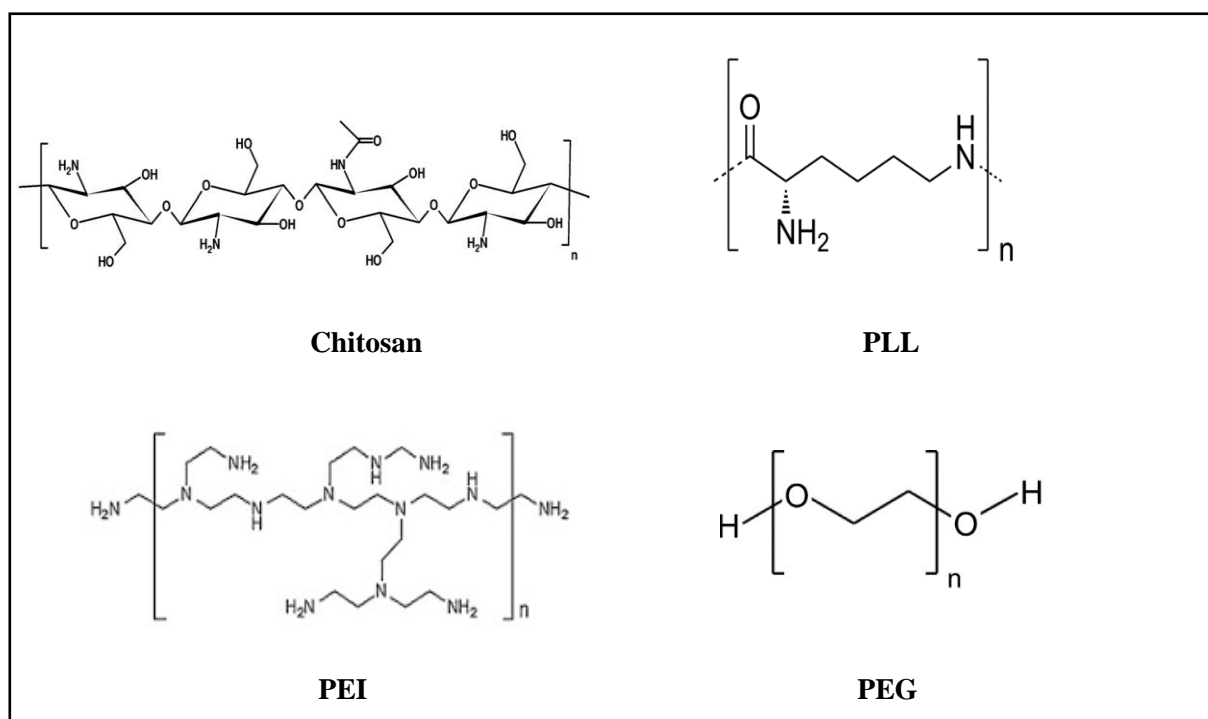


Figure 2.9: Commonly used polymers for AuNP functionalisation (Chattopadhyay and Inamdar, 2010; Antila *et al.*,2015; Hunter *et al.*,2012; Jokerst *et al.*,2011).

2.6.2.7 PEGylation

Biomedical applications require AuNPs that are highly stable in biological environments in the presence of high serum concentrations and ionic strengths. Despite the numerous advantages associated with AuNPs, there are some challenges that may affect their use in clinical applications. Some of these challenges include the reticuloendothelial system (RES) uptake which prevents the prolonged circulation of AuNPs, and the non-specific AuNP binding to non-diseased or non-target areas. Due to the RES accumulation, concerns have been raised about the toxicity of AuNPs (Jokerst *et al.*,2011).

Surface modification using polyethylene glycol (PEG) is one of the most commonly used methods of functionalization of AuNPs for biomedical applications, due to its ability to overcome some of these challenges. PEG is a coiled polymer comprising of repeating ethylene units (Figure 2.8 d). The addition of PEG to the surface of nanoparticles for delivery and imaging applications have been shown to reduce uptake by the RES, and increase the circulation time (van Vlerken *et al.*,2007). PEG has been described as amphiphilic and hence soluble in both hydrophilic and lipophilic solvents. Due to the hydrophilic nature of PEG, it allows for the dispersion of AuNPs conjugated with lipophilic molecules in aqueous environments (Dreadan *et al.*,2009). Furthermore, PEGylation is said to increase the circulatory half-life of the AuNPs by imparting stealth characteristics to them, which further prevents the adsorption of serum proteins and opsonins which facilitate the uptake and clearance of the nanoparticles by RES (Harris and Chess,2003; Zheng *et al.*,2003; Niidome *et al.*,2006; von Maltzahn *et al.*,2009). PEGylations are known to be non-immunogenic, biocompatible and are proposed to reduce cytotoxicity (Harris *et al.*,2001; Lai and Liao, 2003; Vonarbourg *et al.*,2006).

The basic structure of PEG molecules contains one end that attaches to the surface of the nanoparticle, and the distal terminal group that interacts with the solvent. These two ends are attached by varying numbers of ethylene glycol units that determines the size of the PEG molecule, with larger PEG polymers containing a greater number of monomer units. The thickness of the PEG layer grafted onto the surface of the nanoparticle correlates with the conformation of the polymer. This conformation can be described by the Flory radius (F) which takes into account the number of monomer units per PEG chain and the length of each monomer (Degennes, 1987; Degennes, 1980). PEG chains can acquire two main conformations depending on their grafting density. When the surface density is low, the polymer takes up a

‘mushroom’ conformation (Figure 2.9 b). Here the distance between the PEG points of attachment to the nanoparticle surface is greater than F , with the PEG chain making up approximately 50% of the sphere, with a radius comparable to F . When the grafting density is increased, PEG will acquire a ‘brush’ conformation (Figure 2.9 a). In this regime, PEG extends from the surface of the nanoparticle as long, thin bristles (Degennes, 1980). These different conformations of PEG illustrate the diversity of PEGylation. Nanoparticles with the brush PEG conformation are said to have longer circulation times due to the dense coating that offers greater protection to the nanoparticle from the RES (Moghimi and Szebeni, 2003).



Figure 2.10: Schematic representation of the different densities of PEG polymers on the AuNP surface. High density PEG polymers result in a brush regime ($D < F$) (a) with low density PEG polymers exhibiting a mushroom conformation ($D > F$) (b).

There are two spatial components present in all nanoparticles, namely the core and the outer surface, which can add complexity to the nanoparticle. However, all nanoparticles possess an area that interfaces with the solvent or surrounding environment. The modification of this interface with PEG chains can increase the circulation time of the nanoparticle. The circulation half time refers to the period where the circulating AuNP concentration is above 50% of the initial dose, analogous to the half time of the therapeutic agent. The efficacy of the nanoparticle requires a sufficient half time to reach the target area and remain in the affected area for an adequate amount of time to allow for delivery of the therapeutic agent and for imaging. However, this process is often prevented by the RES system, as it removes AuNPs from circulation which inhibits its delivery to the target site. The RES is part of the immune system that makes use of monocytes, macrophages, liver Kupffer cells, the spleen as well as other lymphatic vessels for the removal of foreign material from the body (Saba, 1970). Opsonin proteins adsorb to and coat the surface of foreign material, which are then engulfed by phagocytic cells which transport the foreign material to the liver or spleen for degradation and

excretion (Jokerst *et al.*,2011). The presence of PEG molecules on the AuNP surface reduces the opsonisation process, thereby increasing the blood circulation time of the AuNPs since the recognition by macrophages and monocytes is now prevented.

Poor circulation times of nanoparticles can also be attributed to aggregation, that is nanoparticle-nanoparticle interactions due to the stronger attraction between the particles as compared to their attraction to the solvent (van Vlerken *et al.*,2007; Zolnik and Sadreih, 2009). This phenomenon can be described by the Derjaguin-Landau-Verwey-Overbeek (DLVO) theory that states that nanoparticles have a greater tendency to aggregate due to their high surface energy. This interaction potential is attributed to the electrostatic repulsive potential and Van der Waals attraction potential (Guzman *et al.*,2006; Yang *et al.*,2010). The presence of the PEG polymer reduces the nanoparticle surface energy and hence decreases the Van der Waals attraction (Jun *et al.*,2003; Förster and Antonietti, 1998). Further reasons for this aggregation of AuNPs could include the high ionic strengths of the solvents (> 100mM) used, highly concentrated nanoparticle suspensions resulting in minimal space between nanoparticles, or preparation of AuNPs with a neutral zeta potential (between -10 and +10 mV) (Sze *et al.*,2003). The steric distance between nanoparticles is increased due to PEGylation, leading to a reduced attraction between the AuNPs. Furthermore, the hydrophilicity of the PEGylated AuNPs is increased due to the presence of ether groups which form hydrogen bonds with the solvent.

2.7 Cellular Uptake

An effective delivery system should favour cellular uptake and only target the tumour site or effected cells, while improving the therapeutic efficacy of the gene and limiting any side effects. Cellular uptake of AuNPs can occur voluntarily and is dependent on the characteristics of the nanoparticle which include size, shape, charge and surface modification (Zhang *et al.*,2009; Cho *et al.*,2011; Tkachenko *et al.*,2004). The concentration and exposure time of the AuNP to the cells can also play a role in their uptake. Vessels that are situated around the tumours have large fenestrations and poor lymphatic drainage which favours retention. This strongly favours the enhanced permeability and retention (EPR) effect, that was demonstrated by Maeda and colleagues which led to the development of passive targeting as a mechanism allowing for the natural accumulation of stealth nanoparticles at the tumour site. (Maeda *et al.*,2000). However, there are limitations associated with passive targeting. Although EPR will

allow for the entry of the delivery system into a tumour site, it will not lead to exclusive cancerous cell targeting. Furthermore, the host environment, type of tumour, angiogenesis and degree of vasculature all affect the EPR mechanism. Delivery can be further enhanced by active targeting, which allows for selective delivery of the therapeutic agent by grafting ligands such as peptides and antibodies, onto the surface of the nanoparticle that are recognised by cognate receptors overexpressed on the tumour cell surface (Figure 2.10) (Capco and Chen, 2014).

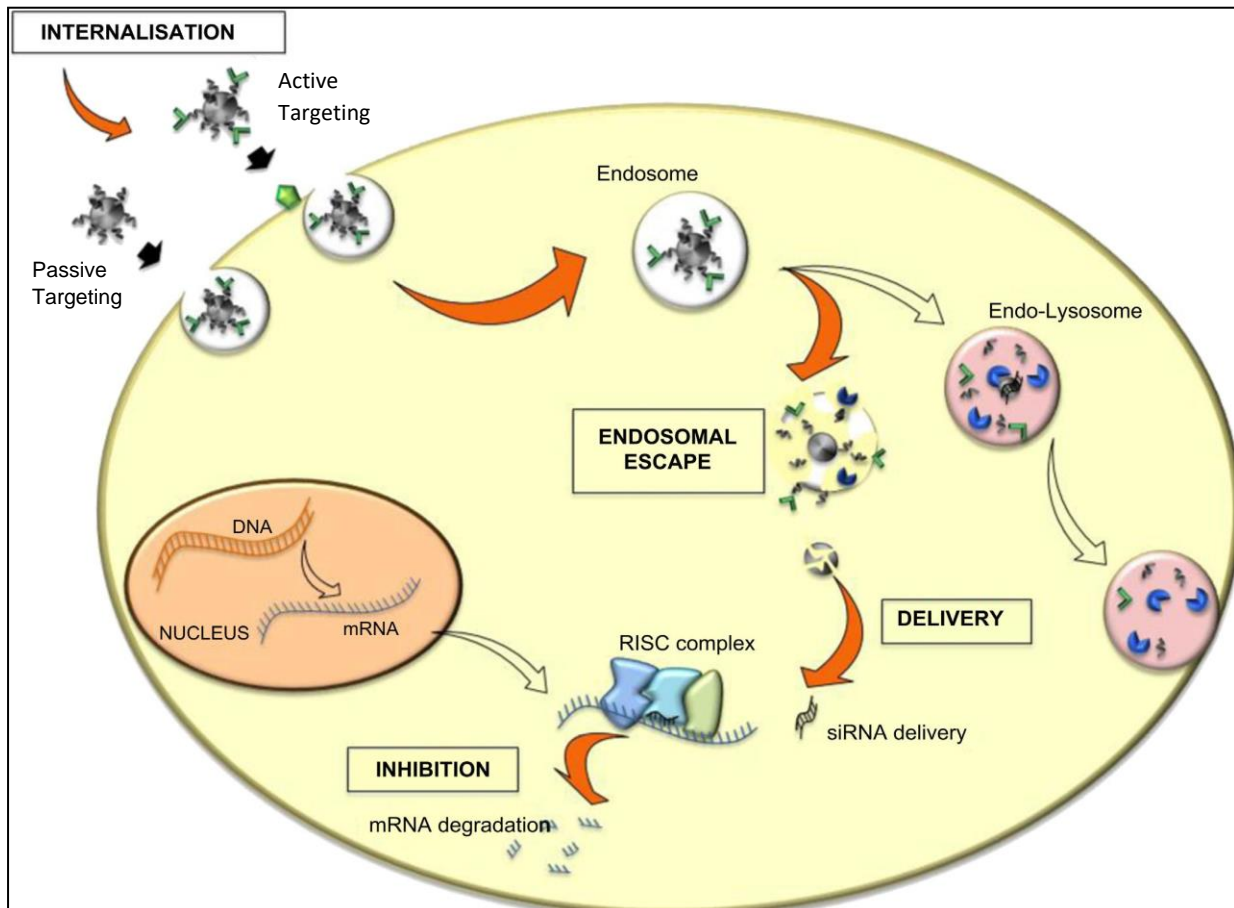


Figure 2.11: Cellular Uptake mechanisms and intracellular trafficking of siRNA delivery systems (Adapted from Resnier *et al.*, 2013).

The cellular mechanisms that are involved in the nanoparticle uptake include phagocytosis, and pinocytosis. Phagocytosis is facilitated through endosomes which are small membrane-bound vesicles, whereas pinocytosis utilizes an energy dependent and receptor mediated endocytosis. This process is believed to be the dominant cellular uptake mechanism in several cell lines (Cho *et al.*, 2011; Mironava *et al.*, 2010; Albanese *et al.*, 2012). Following internalization, the early endosomal vesicles mature into late endosomes. These late endosomes can be characterised by an acidic pH environment and active enzymes. These vesicles later fuse with the lysosomes. Within the endosomes, nanoparticles and nucleic acids can be degraded by

nucleases. Hence, for efficient siRNA delivery, the process of endosomal escape is a critical. Endosomal escape by nanoparticles has been described based on two principles. The first principle is attributed to the proton sponge effect or pH buffering. This is activated by protonation of the internalized molecules in the acidic pH of the vesicles, and results in the inflow of Cl^- and H^+ ions and water which produces osmotic swelling of the vesicles and rupture of the endosome. Nanoparticles that have amine groups are capable of sequestering protons once they enter the acidic environment of the lysosome (Figure 2.11) (Ding *et al.*,2014). The second mechanism involves membrane destabilization. This mechanism occurs in the presence of cationic lipids, peptides or polymers that are capable of fusing to the membrane of the endosome which perturbs the organization of the bilayer resulting in pore disruption (Brust *et al.*,1994).

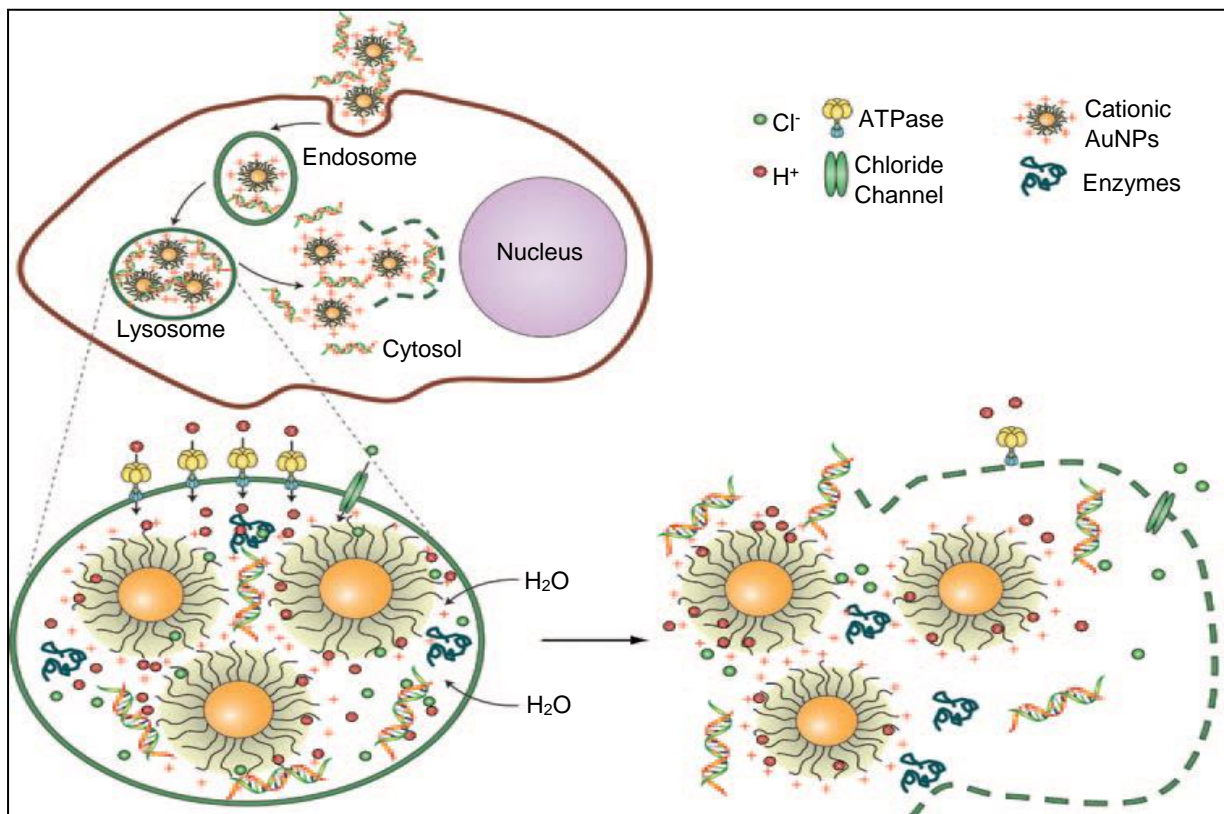


Figure 2.12: Schematic representation of the Proton Sponge Effect for the release of cationic AuNPs from the endosome following cellular uptake (Ding *et al.*,2014).

CHAPTER THREE

MATERIALS AND METHOD

3.1 Gold Nanoparticle Preparation and Functionalisation

3.1.1 Materials

Gold (III) chloride trihydrate 99% (HAuCl₄), sodium citrate (Na₃C₆H₅O₇), and polyethylene glycol 2000 (PEG₂₀₀₀) were purchased from Merck (Darmstadt, Germany). Chitosan (>75% DD, Mw: 25 kDa), polyethylene glycol 400 (PEG₄₀₀), and dialysis tubing (25 mm × 16 mm cellulose membrane) were obtained from Sigma Aldrich (St Louis, USA), Ultrapure water (Milli-Q50) was used in all preparations. All other reagents were of analytical grade.

3.1.2 Method

3.1.2.1 Gold Nanoparticle Preparation

Gold nanoparticles were prepared following a modified Turkevich-Frens method (Turkevich *et al.*, 1951; Frens, 1973). Approximately, 0.33 ml of a 3×10^{-3} M stock colloidal gold suspension was added to 25 ml ultrapure water which was boiled (approximately 85°C), with stirring, for 15 minutes in a 50 ml conical flask. Thereafter, 1 ml of 1% sodium citrate was rapidly added to the vortex of the solution, resulting in a colour change within the first 3 minutes, from pale yellow to dark blue. This colour gradually changed after a period of 15 minutes to a final deep red colour. The solution was boiled further for 5 minutes and thereafter, removed and cooled to room temperature. The resulting gold nanoparticle solution, at a final concentration of 0.45×10^{-3} M, was stored in a dark bottle at room temperature.

3.1.2.2 Functionalisation of Gold Nanoparticles

Gold nanoparticles were functionalised with a 1 mg/ml solution of chitosan (in 1% acetic acid) as outlined in Table 3.1. Approximately, 1 ml of the above colloidal AuNP suspension was added dropwise to 1 ml of the chitosan solution under constant stirring. The resulting 0.1 % chitosan AuNP (Chito-AuNP) suspension was then stirred for 24 hours at room temperature,

followed by dialysis in ultrapure water at a ratio of 100:1 (v/v buffer:sample) for 2 hours. The sample was then stored at room temperature for further use.

3.1.2.3 PEGylation of Chitosan Functionalised AuNPs

PEGylation of AuNPs was carried out by the method described by Manson *et al.* (2011). Gold nanoparticles were first functionalised as described in section 3.1.2.2. The Chito-AuNPs were then PEGylated with 2 and 5 mass percentages of polyethylene glycol 2000 (PEG₂₀₀₀) and polyethylene glycol 400 (PEG₄₀₀) as outlined in Table 3.1. PEG was gradually added to the Chito-AuNP suspension under constant stirring. Following the addition of PEG, the suspension was then stirred for a further 2 hours, and the resulting PEGylated Chito-AuNP suspension was then dialysed as described in section 3.1.2.2 and stored at room temperature.

Table 3.1: Composition of PEGylated and non-PEGylated Chito-AuNPs

Nanoparticle	AuNP (mg)	Chitosan (mg)	PEG ₂₀₀₀ (mg)	PEG ₄₀₀ (mg)
Chito- AuNP	0.08	1	-	-
2% PEG ₂₀₀₀ Chito-AuNP	0.08	1	0.02	-
5% PEG ₂₀₀₀ Chito-AuNP	0.08	1	0.05	-
2% PEG ₄₀₀ Chito-AuNP	0.08	1	-	0.02
5% PEG ₄₀₀ Chito-AuNP	0.08	1	-	0.05

3.2. Characterisation of PEGylated and non-PEGylated Chito-AuNPs and siRNA Interactions with Functionalised AuNPs

3.2.1 Materials

Control, siGENOME non-targeting siRNA (D-001210-01) and 5× siRNA buffer was purchased from Thermo Scientific Dharmacon Products (Lafayette, CO, USA). Ultrapure Agarose was purchased from Bio-Rad Laboratories (Richmond, VA, USA). Ethidium Bromide, glycerol, bromophenol blue, xylene cyanol, ethylenediaminetetraacetic acid (EDTA disodium salt), sodium dodecyl sulphate (SDS), tris [(hydroxymethyl)-aminoethane] and sodium dihydrogen phosphate were obtained from Merck (Darmstadt, Germany). SYBR Green

II RNA gel stain was purchased from Cambrex Bioscience (Rockland Inc., USA). RNase A was purchased from Novagen, Calbiochem (CA, USA). Ultrapure water (Milli-Q50) was utilized for all assays. All other reagents were of analytical grade.

3.2.2 Preparation of siRNA Duplex

To study the interactions between siRNA and the PEGylated and non-PEGylated Chito-AuNPs, a control non-targeting siRNA was used. The siRNA (20 μmole) was resuspended as per the manufacturer's protocol in $1\times$ siRNA buffer to a final concentration of $0.268 \mu\text{g}/\mu\text{L}$. The concentration of the siRNA suspension was verified using the NanoDrop 2000c spectrophotometer (Thermo Scientific, Wilmington, DE, USA) prior to their use and at regular intervals for the duration of the study.

3.2.3 Preparation of PEGylated and non-PEGylated Chito-AuNP: siRNA complexes

All functionalised AuNP preparations were vortexed for approximately 1 minute and sonicated for 15 minutes prior to use. Varying amounts of the AuNP suspensions were added to the siRNA to attain a range of mass ($^{\text{w/w}}$) or N/P ($^{\text{+/-}}$) ratios. These nanocomplexes were made up to a final volume of $10 \mu\text{l}$ in HBS and allowed to incubate at room temperature for 1 hour to allow for complex formation. All nanocomplexes were freshly prepared prior to each assay.

3.2.4 siRNA: PEGylated and non-PEGylated Chito-AuNP Interactions

3.2.4.1 Band Shift Assay

The ability of the PEGylated and non-PEGylated Chito-AuNPs (FAuNPs) to bind siRNA was determined using the band shift or gel retardation assay. Nanocomplexes were prepared as described in section 3.2.3, using increasing amounts of the AuNPs with $0.3 \mu\text{g}$ of control siRNA as outlined in Table 3.2. The reaction mixtures were made up to a final volume of $10 \mu\text{l}$ in HBS (pH 7.4), and incubated at room temperature for 1 hour. Following this incubation period, approximately $2 \mu\text{l}$ of gel loading buffer (50% glycerol, 0.05% bromophenol blue, 0.05% xylene cyanol) was added to each reaction mixture. The nanocomplexes were then subjected to agarose gel electrophoresis on a 2% ($^{\text{w/v}}$) agarose gel (0.4 g of agarose, 18 ml of ultrapure water, 2 ml $10\times$ electrophoresis buffer ($^{\text{w/v}}$)) containing $1 \mu\text{g}/\text{ml}$ of ethidium bromide.

Thereafter, the gel was transferred to a Mini-Sub® electrophoresis tank (BioRad Laboratories, Richmond, USA) containing 1× electrophoresis buffer (36 mM Tris-HCl, 30 mM sodium dihydrogen phosphate, 10 mM EDTA, pH 7.5). Electrophoresis was conducted at 50 V for 30 minutes at room temperature. Thereafter, the gels were viewed under UV₃₀₀ transillumination and the images were captured using a Vacutec Syngene G:Box BioImaging system (Syngene, Cambridge, UK).

Table 3.2: Varying amounts of Chitosan, PEGylated and non-PEGylated Chito-AuNPs used in band shift assay. siRNA was kept constant at 0.3 µg.

Nanoparticle	Functionalised AuNP Mass Range (µg)							
	0	0.12	0.15	0.18	0.21	0.24	0.27	0.3
Chitosan	0	0.12	0.15	0.18	0.21	0.24	0.27	0.3
Chito-AuNP	0	0.075	0.09	0.105	0.12	0.135	0.15	0.165
2% PEG ₂₀₀₀ Chito-AuNP	0	0.18	0.21	0.24	0.27	0.3	0.33	0.36
5% PEG ₂₀₀₀ Chito-AuNP	0	0.45	0.48	0.51	0.54	0.57	0.6	0.63
2% PEG ₄₀₀ Chito-AuNP	0	0.21	0.24	0.27	0.3	0.33	0.36	0.39
5% PEG ₄₀₀ Chito-AuNP	0	0.6	0.66	0.72	0.78	0.84	0.9	0.96

3.2.4.2 RNase A Protection Assay

The ability of the FAuNPs to protect the siRNA against enzymatic degradation was investigated by agarose gel electrophoresis following RNase A mediated digestion. Nanocomplexes were prepared using 0.3 µg siRNA at the sub-optimum, optimum and supra-optimum mass ratios (^w/_w), with their respective nanoparticles as determined from the band shift assay, and as outlined in Table 3.3. All reaction mixtures were made up to a final volume of 10 µl with HBS. Following a 1-hour incubation period, RNase A was added to each reaction mixture to a final concentration of 10% (^v/_v). Two controls were used for this assay, namely, a positive control which contains siRNA only in the absence of RNase A and nanoparticles and a negative control which is the uncomplexed siRNA in the presence of 10% RNase A. The reaction mixtures were then incubated at 37°C for 2 hours in a digital temperature controlled water bath (TriLab Scientific, Johannesburg, Gauteng, South Africa). Following incubation, ethylenediaminetetraacetic acid (EDTA) and sodium dodecyl sulphate (SDS) was introduced to the reaction mixtures to a final concentration of 10 mM and 0.5%, respectively. The samples

were then incubated for a further 20 minutes at 55 °C, followed by electrophoresis on a 2% agarose gel at 50 V for 30 minutes and images captured as previously described in section 3.4.2.1.

Table 3.3: Varying amounts of Chitosan, PEGylated and Non-PEGylated Chito-AuNPs. siRNA was kept constant at 0.3 µg.

Nanoparticle	Nanoparticle Amount (µg)		
	Sub-Optimum	Optimum	Supra-Optimum
Chitosan	0.18	0.21	0.24
Chito-AuNP	0.12	0.15	0.18
2% PEG ₂₀₀₀ Chito-AuNP	0.24	0.27	0.3
5% PEG ₂₀₀₀ Chito-AuNP	0.42	0.45	0.48
2% PEG ₄₀₀ Chito-AuNP	0.27	0.3	0.33
5% PEG ₄₀₀ Chito-AuNP	0.6	0.66	0.72

3.2.4.3 SYBR Green II Displacement Assay

The SYBR Green II dye is an alternative to ethidium bromide for siRNA visualization and measurements, due to its greater sensitivity. The assay was carried out using the method previously described by Dorasamy *et al.* (2009). The relative fluorescence was measured using the Glomax®-Multi Detection System (Promega Biosystems, Sunnyvale, USA) at excitation and emission wavelengths of 497 nm and 520 nm, respectively in a 96 well black flat-bottom FluorTrac plate. Approximately 1 µl of a 100× diluted SYBR Green II dye in 18 Mohm water was added to 100 µl HBS to produce a baseline fluorescence (0%). To this was added 0.28 µg siRNA and the fluorescence obtained was taken as 100%. The PEGylated and non-PEGylated Chito-AuNPs were then added in 1 µl aliquots to the respective wells containing the siRNA/SYBR Green II suspensions, and the fluorescence measured until a plateau in the readings were reached. The relative fluorescence was then calculated using the following equation:

$$F_r (\%) = (F_i - F_0) / (F_{\max} - F_0) \times 100$$

Where F_0 = baseline fluorescence, F_{\max} = fluorescence intensity of fully intercalated siRNA, F_i = fluorescence intensity for each nanoparticle concentration.

3.2.5 Imaging and Sizing

3.2.5.1 UV Spectroscopy Analysis

The optical properties of the AuNP, Chito-AuNP and PEGylated Chito-AuNP suspensions were analysed by examining the UV absorption spectra over a wavelength range of 400 nm to 800 nm. The spectra of the individual nanoparticle suspensions (1 ml) were measured using a Biomate 3 spectrophotometer (Thermo Scientific, Lafayette, CO, USA) in a quartz cuvette with a 1cm path length.

3.2.5.2 Transmission Electron Microscopy (TEM) of AuNPs, Chito-AuNPs and PEGylated Chito-AuNPs

The ultrastructural characteristics of the respective nanoparticles and their nanocomplexes with siRNA (prepared as described in section 3.2.3), were determined using TEM. Approximately, 1 μ l of the individual nanoparticle/nanocomplex suspensions were placed onto a 400-mesh carbon coated grid (Ted Pella Inc. Redding, USA), and allowed to air dry. Thereafter, they were viewed using a Jeol T-1010 transmission electron microscope (Tokyo, Japan), and images captured using a Soft Imaging Systems (SIS) MegaView III side mounted 3-megapixel digital camera.

3.2.5.3 Inductively Coupled Plasma-Optical Emission Spectroscopy (ICP-OES) and Fourier Transform Infrared (FTIR) Analysis

The synthesised AuNPs were analysed using ICP-OES for the quantification and elemental detection of the Au concentration. This analysis was performed using a Perkin Elmer Optima 5300DV Optical Emission Spectrophotometer. A standard 100 ppm Au solution (Fluka) was utilised to prepare a standard curve between 1 and 20 ppm.

FTIR analysis was performed using a Perkin Elmer Spectrum 100 FT-IR spectrometer with a universal ATR sampling accessory, to confirm surface functionalisation of the AuNPs with

chitosan and PEG (400 and 2000) at 25°C. Scanning was performed in the range of 380-4000 cm⁻¹.

3.2.5.4 Particle Size and Zeta Potential Analysis

The size and zeta potential of the AuNP, FAuNPs, as well as their nanocomplexes with siRNA were measured using Nanoparticle Tracking Analysis (NTA) facilitated by the Nanosight NS500 (Malvern Instruments, Malvern, Worcestershire, UK). The Nanosight NS500 has a sample chamber of approximately 0.25 ml, with a sCMOS camera and a laser wavelength of 430 nm. All AuNP preparations were vortexed and sonicated prior to analysis. Thereafter, a 1:600 dilution of each nanoparticle was prepared in 18 Mohm water. Nanocomplexes were prepared with siRNA at the optimum binding ratio, as described in section 3.2.3 and according to Table 3.3, and then diluted in 18 Mohm water. Images were captured and analysed using the NTA 3.2 analytical software.

3.3 *In Vitro* Cell Culture Studies

3.3.1 Materials

Control, non-targeting siRNA and Block-iT Fluorescent Oligo siRNA were purchased from Thermo Scientific Dharmacon Products (Lafayette, CO, USA). Eagles Minimum Essential Medium (EMEM) with L-glutamine (4.5 g/l), trypsin-versene mixture and penicillin-streptomycin mixtures (10 000 U/ml) were purchased from Lonza BioWhittaker (Walkersville, USA). Foetal bovine serum (FBS) was purchased from GIBCO, Life Technologies Ltd (Inchinnan, Scotland). All tissue culture plastic wear was purchased from Corning Incorporated (New York, USA). Phosphate buffered saline (PBS) tablets, 3-[4,5-dimethylthiazol-2-yl]-2,5-diphenyltetrazolium bromide (MTT), dimethylsulphoxide (DMSO), and acridine orange (AO) were obtained from Merck (Darmstadt, Germany). AlamarBlue® was purchased from Invitrogen (Carlsbad, CA, USA). Ultra-pure water was used throughout. All other reagents were of analytical grade.

3.3.2 Preparation of siRNA Duplexes

siGENOME Non-Targeting siRNA and BLOCK-iT™ Fluorescent Oligo were purchased from Thermo Scientific Dharmacon Products (Lafayette, CO). The non-targeting siRNA sequence has at least four mismatches with all known human genes and is used for *in vitro* studies to assess non-sequence specific effects of the siRNA nanocomplexes on the cell lines been studied. The target sequence of this duplex is 5'- UAG CGA CUA AAC ACA UCA A- 3'. BLOCK-iT™ Fluorescent Oligo is a double stranded RNA fluorescein labelled duplex with the same configuration, length and charge as the standard siRNA, and is not homologous to any known gene.

3.3.3 Cell Line Maintenance

Four cell lines were used for the duration of the study, namely, human embryonic kidney cells (HEK293) obtained from the Anti-Viral Gene Therapy Unit, Medical School, University of Witwatersrand, human epithelial colorectal adenocarcinoma cells (Caco 2), purchased from Highveld Biological (Pty) Ltd. (Kelvin, Gauteng, RSA), human breast adenocarcinoma cell line (MCF-7), supplied by the Department of Therapeutic and Medicines Management, Medical School, UKZN and the human colon adenocarcinoma cells (HT-29) purchased from the American Type Tissue Culture Collection (ATCC) , Manassas, VA, USA. All cell work was carried out in sterile class II biohazard hoods.

3.3.3.1 Reconstitution of Cell Lines

Each cryopreserved cell line was removed from a -80°C Nuair biofreezer and immediately placed in a 37°C water bath to thaw. The cell suspensions were then aseptically decanted into centrifuge tubes and were centrifuged at 1000 rpm for 5 minutes using an Eppendorf benchtop centrifuge. Following centrifugation, the supernatant was discarded, and the cells (pellet) was resuspended in 1 ml of sterile complete medium (EMEM +1% Antibiotic + 10 % FBS). The cell suspensions were then transferred to a 25 cm² tissue culture flask containing 4 ml of sterile complete medium. The cells were then placed in a 37°C incubator containing 5% CO₂ and monitored daily using an inverted microscope (Nikon TMS-F 6V, Tokyo, Japan). The medium was changed every two to three days until the cells were sub-cultured when confluent.

3.3.3.2 Propagation of Cell Lines

Once the cells had reached confluency, they were trypsinized. Briefly, the growth medium was discarded into a sterile waste bottle and the cells were washed with 5 ml of sterile PBS, pH 7.5. Thereafter, 1ml of pre-warmed trypsin-versene was introduced to the flask, and trypsinization of the cells was observed under the inverted microscope. The trypsinization time for each cell line varied from 1-3 minutes at room temperature or 37 °C. Once the cells had rounded off, 2 ml of complete medium was added to the cells. Thereafter, the flask was tapped gently against the palm of the hand to dislodge the cells. The cells were split into desired ratios into 25cm² tissue culture flasks or multiwell plates as required. Each tissue culture flask contained 4 ml of complete medium and were incubated at 37°C. The cells were then checked regularly, and the medium changed when necessary. Once the cells had reached confluence, they were trypsinized again and split into required ratios or the cells were frozen (section 3.3.3.3) and stored at -80°C for short term storage, or in liquid nitrogen for long term storage.

3.3.3.3 Cryopreservation of Cell Lines

Confluent cells were washed with PBS and trypsinized following the procedure outlined in section 3.3.3.2. Following trypsinization, the cells were transferred to a 15 ml centrifuge tube and were pelleted by centrifugation for 3 minutes at 1000 rpm. The medium was replaced with 0.9 ml complete medium and 0.1 ml DMSO. The cells were then resuspended by vortexing, and transferred to 2 ml cryogenic ampoules and frozen by placing the ampoule into a Nalgene™Cryo 1°C freezing container which contained isopropanol and facilitated freezing at a rate of -1°C per minute. This freezing container was placed directly into the -80°C biofreezer (Nuair, Lasec Laboratory and Scientific Equipment, Ndabeni, Cape Town, RSA).

3.3.4 Toxicity Studies

3.3.4.1 MTT Assay

Cells were trypsinized and seeded into clear 96 well plates at cell densities of 1.5- 1.8 × 10⁵ cells per well, and incubated at 37°C overnight to allow cells to attach. Nanocomplexes were prepared in triplicate using chitosan, Chito-AuNPs and PEGylated Chito-AuNPs with 50 nM siRNA (0.067 µg) as in Table 3.4. All the nanocomplexes were made up to a final volume of

10 μ l in sterile HBS and were incubated at room temperature for 30 minutes. A positive control containing untreated cells was included and was used to represent 100% survival. The cells were prepared by first replacing the growth medium with fresh complete medium. The nanocomplexes were then added to the cells and incubated at 37°C for 36 hours. Thereafter, the growth medium was aspirated and replaced with 0.1 ml of medium and 0.1 ml of MTT solution (5mg/ml in PBS), and cells incubated at 37°C for a further 4 hours. The MTT and medium was then removed and 0.1 ml dimethylsulphoxide (DMSO) was added to the wells and the absorbances were measured at 570 nm using a Mindray MR-96A microplate reader (Vacutec, Hamburg, Germany).

3.3.4.2 AlamarBlue® Assay

Once the cells had reached semi-confluency, they were seeded into 96 well plates at cell densities of $1.3-1.7 \times 10^5$ cells per well. The siRNA nanocomplexes were prepared as outlined in section 3.3.4.1 and Table 3.4. Following the incubation of the cells with the prepared reaction mixtures for 36 hours at 37°C, 10 μ l (10%, v/v) of 10 \times AlamarBlue® was added to the growth medium in the wells, and cells incubated at 37°C for 4 hours. Thereafter, the medium and AlamarBlue® solutions were transferred to a 96 well flat-bottomed black Fluor-Trac plate and fluorescence was measured at excitation and emission wavelengths of 570 nm and 585 nm respectively using a Glomax®-Multi Detection System (Promega BioSystems, Sunnyvale, CA, USA) operated by Instinct software.

Table 3.4: siRNA: Au nanocomplex ratios used for cytotoxicity and transfection studies

Nanoparticle	siRNA: Functionalised AuNP Ratios (w/w)		
	Sub-Optimum	Optimum	Supra-Optimum
Chitosan	1:0.6	1:0.7	1:0.8
Chito-AuNP	1:0.4	1:0.5	1:0.6
2% PEG ₂₀₀₀ Chito- AuNP	1:0.8	1:0.9	1:1
5% PEG ₂₀₀₀ Chito-AuNP	1:1.5	1:1.6	1:1.7
2% PEG ₄₀₀ Chito-AuNP	1:0.9	1:1	1:1.1
5% PEG ₄₀₀ Chito-AuNP	1:2	1:2.2	1:2.4

3.3.4.3 Apoptosis Analysis by Acridine Orange/Ethidium Bromide (AO/EB) Staining

Cells were seeded at densities of $1.2 - 1.5 \times 10^4$ cells per well in a clear 48 well plate and allowed to attach overnight at 37°C . Complexes were prepared with 50 nM siRNA (0.63 μg), the PEGylated Chito-AuNPs, Chito-AuNPs and chitosan as outlined in Table 3.4. The reaction mixtures were allowed to incubate at room temperature for 1 hour to allow for complex formation. Once the nanocomplexes were prepared, the growth medium was removed and replaced with 0.25 ml of complete medium. The nanocomplexes were then added and the cells incubated at 37°C for 24 hours. Following incubation, the growth medium was aspirated, and the cells washed twice with 0.2 ml PBS and stained with 10 μl of the dye (100 $\mu\text{g}/\text{ml}$ acridine orange, 100 $\mu\text{g}/\text{ml}$ ethidium bromide in PBS) for 5 minutes on a Stuart Scientific platform rocker at 30 rev/min. The cells were then washed with PBS and viewed under an inverted fluorescent microscope (Olympus CKX41, Tokyo, Japan) at excitation and emission wavelengths of 490 nm and 516 nm respectively. The apoptotic index was calculated as a quantification of apoptosis as below.

$$\text{Apoptotic index} = \text{number of apoptotic cells} / \text{number of total cells counted}$$

3.3.5 *In vitro* Transfection Studies

3.3.5.1 Cellular Uptake Studies

Confluent cells were seeded in 96 well plates at cell densities of $1.0 - 1.2 \times 10^5$ cells per well, and were incubated at 37°C overnight to allow for the attachment of the cells. Nanocomplexes were prepared in triplicate as outlined in Table 3.4 using 50 nM Block-It fluorescent oligo siRNA (0.067 μg), and incubated at room temperature for 1 hour. Thereafter, the growth medium from the plates were removed and replaced with complete medium, followed by the addition of the nanocomplexes and incubation at 37°C for 24 hours. Two controls were set up, viz., cells not treated with siRNA or nanocomplexes, and cells incubated with siRNA only. Following incubation, the growth medium was removed, cells washed twice with 0.2 ml PBS, and 80 μl of $1 \times$ cell culture lysis reagent (10mM Tris-HCl, 1mM EDTA, 0.5% SDS) was added to the cells. The plate gently rocked on a Stuart Scientific platform rocker for 15 min at 30 rev/min. The cells were dislodged from the multiwell plate using a cell scraper. Cell lysates were then transferred to a black 96 well flat-bottomed Fluor-Trac plate and fluorescence measured at excitation wavelengths of 419 nm and an emission wavelength of 512 nm using

the Glomax®-Multi Detection System. The results were represented as relative fluorescence units.

3.4 *c-MYC* Gene Knockdown Studies at mRNA and Protein Levels

3.4.1 Materials

ON-TARGET plus Human MYC siRNA- SMARTpool was purchased from Thermo Scientific Dharmacon Products (Lafayette, CO). TRIzol® reagent, Lipofectamine® 3000 and DNase/RNase free water were purchased from Life Technologies (Carlsbad, CA, USA). RIPA buffer was obtained from Sigma Aldrich (St. Louis, USA). Blotting grade buffer (non-fat dry milk), iScript™ gDNA Clear cDNA synthesis kit, SsoAdvanced™ Universal SYBR® Green Supermix, Prime PCR Assay Mix, 10× tris-buffered saline (TBS) and Tween 20 were acquired from Bio-Rad Laboratories (Richmond, CA, USA). Tris-(hydroxymethyl)-aminoethane, sodium chloride (NaCl), hydrochloric acid (HCl), absolute ethanol, chloroform, isopropanol, sodium carbonate (Na₂CO₃) and sodium bicarbonate (NaHCO₃) were purchased from Merck (Darmstadt, Germany). Anti-human c-myc (9E11); a mouse monoclonal antibody raised against a synthetic peptide corresponding to amino acid residues 408-439 from the c-terminus of c-myc (Mw = 64-67 kDa) was purchased from Invitrogen, Life Technologies (USA). β-Actin (8H10D10), a mouse monoclonal antibody raised against a synthetic peptide corresponding to amino-terminal residues of human β-Actin conjugated to KLH (Mw=42 kDa) was obtained from Novus Biologicals (Littleton, Colorado, USA). Goat anti-mouse IgG2a secondary antibody, an affinity purified antibody with characterised specificity for mouse immunoglobulins and conjugated to horse radish peroxidase and 3,3',5,5'-tetramethylbenzidine (TMB) was acquired from Thermo Scientific (Rockford, USA). Ultra-pure 18 Mohm water was used throughout. All other reagents were of analytical grade.

3.4.2 siRNA Duplexes

The siRNA utilised for gene knockdown studies consists of four different sequences of 19 nucleotides that all target the *c-MYC* gene (ON-TARGET plus SMARTpool). The sequences of these siRNA molecules are 5' ACG GAA CUC UUG UGC GUA A 3', 5' GAA CAC ACA ACG UCU UGG A 3', 5' AAC GUU AGC UUC ACC AAC A 3' and 5'CGA

UGU UGU UUC UGU GGA A 3'. The non-targeting siRNA was utilized as a control and contains at least four mismatches with any known gene (Section 3.4.2).

3.4.3 siRNA Transfection

For the *in vitro* gene silencing studies, MCF-7 cells were seeded into 6 well plates at a cell density of 3.3×10^5 cells per well, and incubated at 37 °C for 24 hours to allow for attachment of the cells. Nanocomplexes were then prepared with 50 nM *c-MYC* targeted siRNA (0.67 µg) and control non-targeting (NT) siRNA (0.67 µg) at the optimum binding ratios of chitosan, Chito-AuNPs and PEGylated Chito-AuNPs as per section 3.2.3 and Table 3.4. These nanocomplexes were allowed to mature at room temperature for 1 hour. Lipofectamine® 3000 was utilized as a positive control and complexes were prepared as per the manufacturer's instructions. Approximately, 5 µl of Lipofectamine® 3000 reagent was incubated with 2.5 µl of *c-MYC* siRNA in 0.25 ml of EMEM at room temperature for 5 minutes. Following nanocomplex formation, the growth medium from the wells were removed and replaced with 1.5 ml of complete medium (EMEM + 10% FBS + 1% Antibiotics). The nanocomplexes were added to the cells, and cells incubated at 37 °C for 48 and 72 hours, after which the cells were harvested to assess the knockdown of the *c-MYC* gene, using quantitative real-time polymerase chain reaction (qRT-PCR) and Enzyme Linked Immunosorbent Assay (ELISA).

3.4.4 RNA Isolation and qRT-PCR

3.4.4.1 RNA Isolation

The total cellular RNA was extracted for qRT-PCR analysis. The RNA was isolated using TRIzol® Reagent following the manufacturer's protocol. This procedure was carried out at room temperature under RNase free conditions in a Class II Biohazard laminar flow cabinet. The first step involved cellular homogenization. The growth medium was removed and replaced with 1 ml TRIzol® Reagent, and the cells were manually lysed with a pipette by homogenizing the cells several times (35-40 strokes). The homogenate was then incubated at room temperature for 5 minutes to allow for complete dissociation of the nucleoprotein. The samples were then transferred to sterile 2 ml microcentrifuge tubes, followed by the addition of 0.2 ml chloroform. The tubes were then vigorously shaken by hand for 15 seconds and left to stand at room temperature for 3 minutes. The samples were then centrifuged at 12 000 rcf

for 15 minutes at 4°C using an Eppendorf 5424R benchtop centrifuge. Following centrifugation, the mixture separated into an upper aqueous phase, an interphase and a lower red phenol-chloroform phase. The RNA remains in the colourless upper aqueous phase which was carefully removed by angling the tube and pipetting out this solution. This aqueous phase was then transferred to 2 ml microcentrifuge tubes, followed by the addition of 0.5 ml of 100% isopropanol for 15 minutes at - 20°C. The sample was then centrifuged at 12 000 rcf for 10 minutes at 4 °C. The supernatant was removed and the gel like pellet was washed twice in 75% ethanol by briefly vortexing and centrifuging at 7500 rcf for 5 minutes at 4 °C. The pellet was allowed to air dry and thereafter resuspended in 30 µl of RNase free water. This was conducted by pipetting the solution several times followed by incubation at 55 °C for 15 minutes. The concentration and quality of RNA was determined by measuring the absorbance at 260 nm and 280 nm, and the integrity was assessed by electrophoresis on a 2% agarose gel, as previously outlined in section 3.2.4.1.

3.4.4.2 Quantitative Real Time Polymerase Chain Reaction (qRT-PCR)

The total isolated RNA was converted to cDNA using the iScript™ gDNA clear cDNA synthesis kit following the manufacturer's detailed protocol. Approximately, 2 µg of the isolated RNA sample, diluted to 16 µl in nuclease free water, was treated with a DNase mastermix (iScript™ DNase, 0.5 µl; iScript DNase Buffer, 1.5 µl/ 16µl reaction) to remove any genomic DNA present. The reaction mixtures were incubated in 2 cycles with a Bio-Rad C1000 Touch™ Thermal Cycler at 25 °C (5 minutes) and 75 °C (5 minutes). Thereafter, 4 µl of the 5× iScript™ Reverse Transcription Supermix (RNase H⁺, Moloney murine leukaemia virus reverse transcriptase, dNTPs, oligo(dT), random primers, and RNase inhibitor) was added to the gDNA free RNA samples. The tubes were sealed and centrifuged briefly to remove any air bubbles and to spin down the solutions. Reactions with no reverse transcriptase were included for each sample as a negative control. The reverse transcription was conducted in a Bio-Rad C1000 Touch™ Thermal Cycler in 3 phases: step 1: 25 °C (5 minutes); step 2: 46 °C (20 minutes); 95°C (1 minute). Thereafter the resulting cDNA was diluted to 100 µl and stored at 4 °C.

The level of gene expression was determined and quantified by qRT-PCR using the Prime PCR Gene expression Assay with the SsoAdvanced™ Universal SYBR® Green Supermix. The primers used were the gene of interest, *MYC* (Assay ID: qHSACID002921) and the endogenous

control β Actin (ACTB) (Assay ID: qHSACED0036269). Each singleplex PCR reaction was carried out in triplicate for all the samples. The reaction mixtures (20 μ l) contained 10 μ l SsoAdvanced™ Universal SYBR® Green Supermix (Sso 7d-fusion polymerase, dNTPs, MgCl₂, SYBR® Green I dye, enhancers, stabilizers, and passive reference dyes (ROX and fluorescein)), 1 μ l of 10× Prime PCR Assay mix, 5 μ l (100 ng) cDNA, and 4 μ l nuclease free water. The reaction mixtures were mixed and transferred to Hard Shell® PCR 96 well plates (Biorad). The qRT-PCR amplification was performed using the following protocol: 98 °C (30 seconds) (initial), followed by 40 cycles of 98°C (15 seconds) (denature), 60 °C (30 seconds) (anneal/extension) on a CFX-96™ Real-Time System, C1000 Touch™ Thermal Cycler using the CFX Manager Software version 3.0 (Bio-Rad). The values of relative expression of the *c-MYC* mRNA normalised to the level of ACTB mRNA were determined by the $2^{-\Delta\Delta Ct}$ method (Livak and Schmittgen, 2001).

$$\text{Fold difference} = 2^{-\Delta\Delta Ct}$$

$$\Delta Ct_{\text{sample}} - \Delta Ct_{\text{calibrator}} = \Delta\Delta Ct$$

$$Ct_{\text{GOI}_s} - Ct_{\text{norm}_s} = \Delta Ct_{\text{sample}}$$

$$Ct_{\text{GOI}_c} - Ct_{\text{norm}_c} = \Delta Ct_{\text{calibrator}}$$

Where s represents the sample, c the calibrator (normal cells), GOI the gene of interest *c-MYC* and norm the normaliser gene ACTB.

3.4.5 Protein Isolation and ELISA

3.4.5.1 Protein Isolation

Proteins were isolated 72 hours after transfection. The growth medium was aspirated, and cells washed twice with 1.5 ml of PBS (pH 7.5). Thereafter, 1 ml of RIPA buffer was added to the cells, which were then incubated in the refrigerator (4 °C) for 5 minutes. The cells were then scraped with a pipette to remove and lyse the cells. The cell lysate was transferred to pre-cooled tubes on ice, followed by centrifugation at 8000 rcf at 4°C for 10 minutes to pellet the cell debris. The supernatant containing the protein was then transferred to cooled tubes and stored at - 80°C until further use.

3.4.5.2 Enzyme-Linked Immunosorbent Assay (ELISA)

To evaluate gene silencing efficiency of the *c-MYC* targeted siRNA nanocomplexes at the protein level, the concentration of MYC protein was determined using an adapted ELISA protocol outlined by Thermo Scientific technical bulletin (2010). Protein samples were diluted in a coating buffer (0.05 M carbonate-bicarbonate buffer, pH 9.6) to a final concentration of 50 µg/ml and were introduced into a 96 well, polystyrene, flat bottomed multi-well plate. The plate was sealed and incubated at 4°C overnight to allow for the attachment of the proteins to the wells. Following attachment, the coating buffer was removed, and the plates were washed twice with 200 µl Tris-buffered saline (20 mM Tris-HCl, pH 7.5, 150 mM NaCl) with 0.1% Tween 20 (TBS-T). Thereafter, unoccupied attachment sites within the well were saturated with 5% blocking agent (non-fat dry milk in TBS-T), at room temperature for 1 hour under constant agitation. The plate was then washed twice with TBS-T and the plate was incubated at room temperature for an hour with either MYC, (1:2000 in 1% blocking agent), or β-Actin, (1:10000 in 1% blocking agent) used as an internal control. The primary antibodies were removed, and the plates were washed for 5 minutes with constant agitation (total of 4 washes). Thereafter, the goat anti mouse IgG2a-HRP secondary antibody (1:2000 in 1% blocking agent) were added to all the wells and incubated at room temperature for one hour. The plate was then washed four times with TBS-T, followed by the addition of TMB (prepared as per the manufacturer's instructions) to the wells and incubation at room temperature for a period of 30 minutes for the desired colour to develop (colourless to blue). Thereafter, stop solution (2M H₂SO₄) was added, and the absorbance was then measured at 450 nm using a Mindray MR-96A microplate reader (Vacutec, Hamburg, Germany).

3.5 Statistical Analysis

Data are presented as a means ± SD ($n=3$). Statistical analysis among mean values was performed using one-way ANOVA followed by the Dunnett multiple comparison *post hoc* test for all formulations. All statistics were performed using a 95% confidence interval and were considered significant when the *P* value was less than 0.05 ($P < 0.05$).

CHAPTER FOUR

RESULTS AND DISCUSSION

4.1 Gold Nanoparticle Preparation and Characterization

4.1.1 Synthesis and Functionalisation of AuNPs

AuNPs have been synthesized by a variety of methods which follow a similar strategy whereby the gold salt is reduced in the presence of a stabilizing agent (Tiwari *et al.*,2011). The particle size of the colloidal gold can be controlled by varying the salt concentration, temperature and reducing agent (Dreaden *et al.*,2011). In this study, the citrate reduction method was employed.

Variations in the citrate concentration results in the formation of gold particles of different diameters within a range of 12- 160 nm (Frens, 1973). Following reduction of HAuCl_4 in water, the colloidal gold undergoes a colour change from yellow to a deep red wine colour (Figure 4.1). This colour change is associated with a decrease in particle size with larger particles ranging between 100- 200 nm and smaller particles between 5-15 nm, and predominantly spherical in shape (Peng *et al.*,2008).

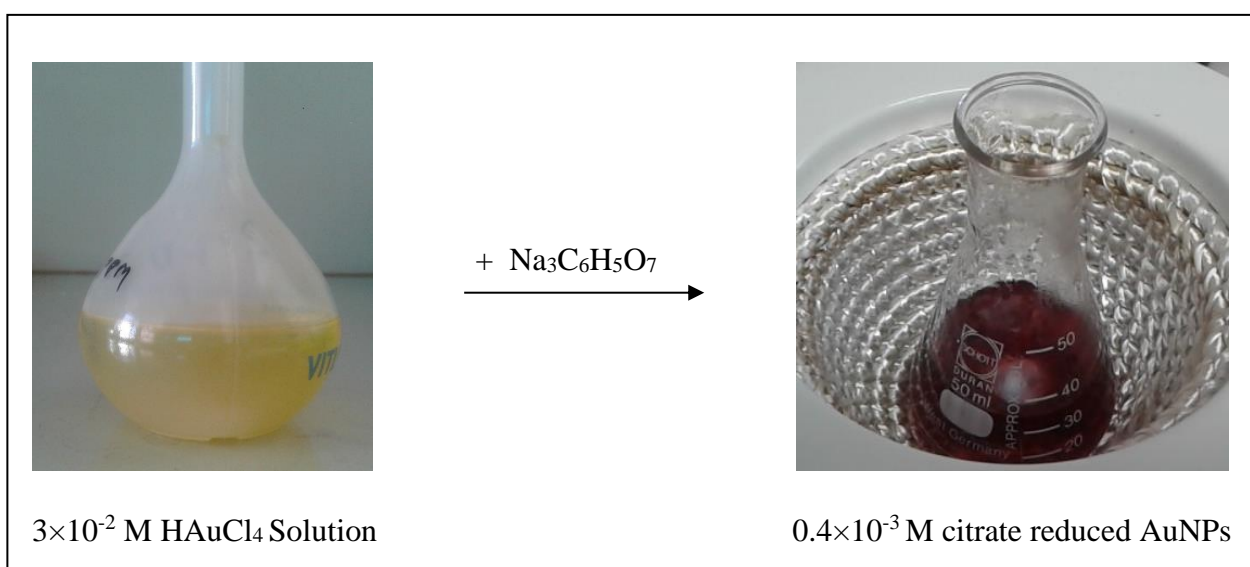


Figure 4.1: Image depicting the colour change observed following the citrate reduction of the gold salt (yellow) to gold nanoparticles (deep red wine colour).

Due to the citrate reduction, the resultant AuNPs are negatively charged which allows for the relative ease of functionalisation with positively charged polymers. For this study, five

functionalised AuNP preparations were utilized and the final concentration of the prepared AuNP suspension was determined by ICP-OES analysis.

Chitosan was the polymer of choice as it is a natural polysaccharide that is biodegradable, biocompatible and has characteristics that are desirable for siRNA delivery. Due to their cationic nature, they allow for complexation with anionic siRNA in a relatively quick and easy formulation process (Ragelle *et al.*,2013). For efficient gene silencing, the molecular weight and degree of deacetylation (DD) are important parameters for chitosan considering that there are different types of chitosan molecules. The molecular weight (MW) of chitosan further affects its morphological, physico-chemical and *in vitro* biological characteristics. For this study, low MW chitosan (25kDa) was utilized as it has been found that at this MW, the chitosan molecule was capable of completely binding to the siRNA when compared to very low MW chitosan (<10 kDa), which cannot completely bind siRNA due to their short chains. Interestingly, high MW chitosan molecules (80-300 kDa) that have been widely used for siRNA complexation, are incapable of forming suitable nanoparticles as their chain lengths were too long and therefore, the resulting particle size of the nanocomplex was too large for biological applications (Liu *et al.*,2007; Jackson and Linsley, 2007; Baldrick, 2010; Tapola *et al.*,2008; Garcia-Fuentes and Alonso, 2012; Cho *et al.*,2008; Howard *et al.*,2006). The charge density of the chitosan molecule is another important parameter and is determined by the degree of deacetylation (DD). This refers to the percentage of deacetylation of the primary amine groups of the chitosan molecule. Due to the short length and molecular topology of siRNA, a high number of positive charges is required to complex and keep the siRNA completely bound therefore, it has been reported that chitosan with a DD > 75% is required for nanoparticle formation and siRNA binding (Mao *et al.*,2010), as utilised in this study. The higher number of positive charges is also important for endosomal escape of the nanocomplex by the proton sponge effect following cellular uptake.

The chitosan functionalised AuNPs (Chito-AuNPs) were further modified by the addition of polyethylene glycol (PEG). PEG modifications are known to increase the blood circulation time of the nanoparticles by reducing opsonisation and preventing uptake by the reticuloendothelial system (RES) (Kah *et al.*, 2009; Niidome *et al.*,2006). The PEG molecules are known to be non-immunogenic, biocompatible and can reduce renal clearance of the nanoparticles (Lai and Liao,2003; Vonarbourg *et al.*,2006; Harris *et al.*,2001). It is also believed that the introduction of PEG molecules can stabilize nanoparticle structures. The

effect of high and low MW PEG molecules (2000 and 400 respectively) at different mass ratios were studied. Chitosan functionalization was based on the ability of the amine functional groups to spontaneously bind to the negatively charged citrate capped AuNP through electrostatic interactions. The addition of PEG to this delivery system was based on the findings by Manson and colleagues (2011) which stated that by introducing PEG to the citrate capped AuNPs, an exchange occurs between the citrate and PEG molecules which allows for the attachment of PEG to the AuNP surface (Manson *et al.*,2011). (Figure 4.2).

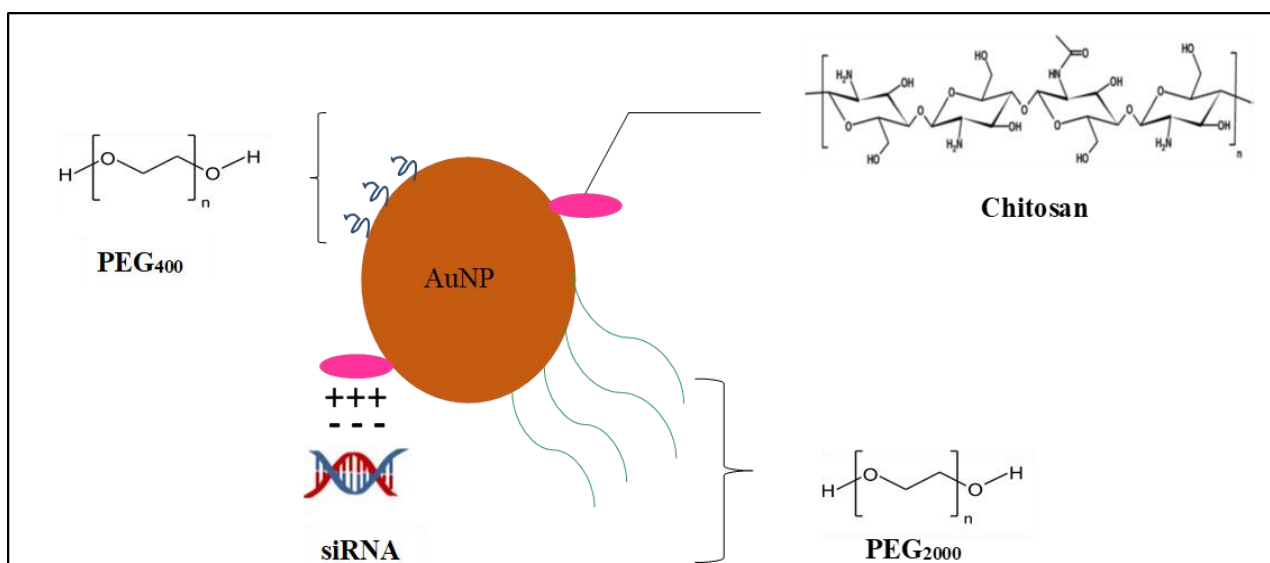


Figure 4.2: Schematic representation of the composition of the PEGylated and non-PEGylated Chito-AuNPs used in this study and its electrostatic interaction with siRNA.

4.1.2 Functionalised AuNP: siRNA Interactions

The unique surfaces of the AuNPs allow for functionalisation and the attachment of siRNA to their surfaces. The binding of the siRNA to the AuNP surface can occur through electrostatic interactions or chemical adsorption. These methods are relatively simple which involve the mixing and incubation of the siRNA with the positively charged functionalised AuNPs as represented in Figure 4.4.

The chemical adsorption of the siRNA to the AuNP surface relies on the use of chemically modified siRNA that usually bear thiol functional groups, usually at the 5' end of the sense strand. The siRNA then adsorbs onto the AuNP surface via a thiol- Au interaction (Figure 4.3 a). For this strategy, the AuNPs do not require surface functionalisation, however, the therapeutic agent as well as the ligands and PEG need to be chemically modified to allow for adsorption. The second strategy involves the electrostatic interaction between the siRNA and functionalised AuNP. Amine functionalised AuNPs possess a positive charge on their surface

and, therefore, due to ionic interactions with the anionic siRNA are able to spontaneously bind to the AuNP surface (Figure 4.3 b). The third approach involves a ‘layer by layer’ strategy which results in multiple layers on the AuNP surface. This is achieved by repeating oppositely charged electrolytes (Zaky *et al.*,2009). For example, negatively charged AuNPs were functionalised with PEI followed by the sequential addition of siRNA and PEI which results in the formation of an AuNP/PEI/siRNA/PEI complex (Figure 4.3 c). This method is an extension of the electrostatic interaction; however, it is believed that the addition of the second layer of the polymer offers a protective ‘shield’ around the siRNA, thereby offering greater protection against enzymatic degradation (Hong and Nam, 2014). For this study, the second strategy involving electrostatic interactions, was employed for preparation of nanocomplexes between the functionalised AuNPs and siRNA.

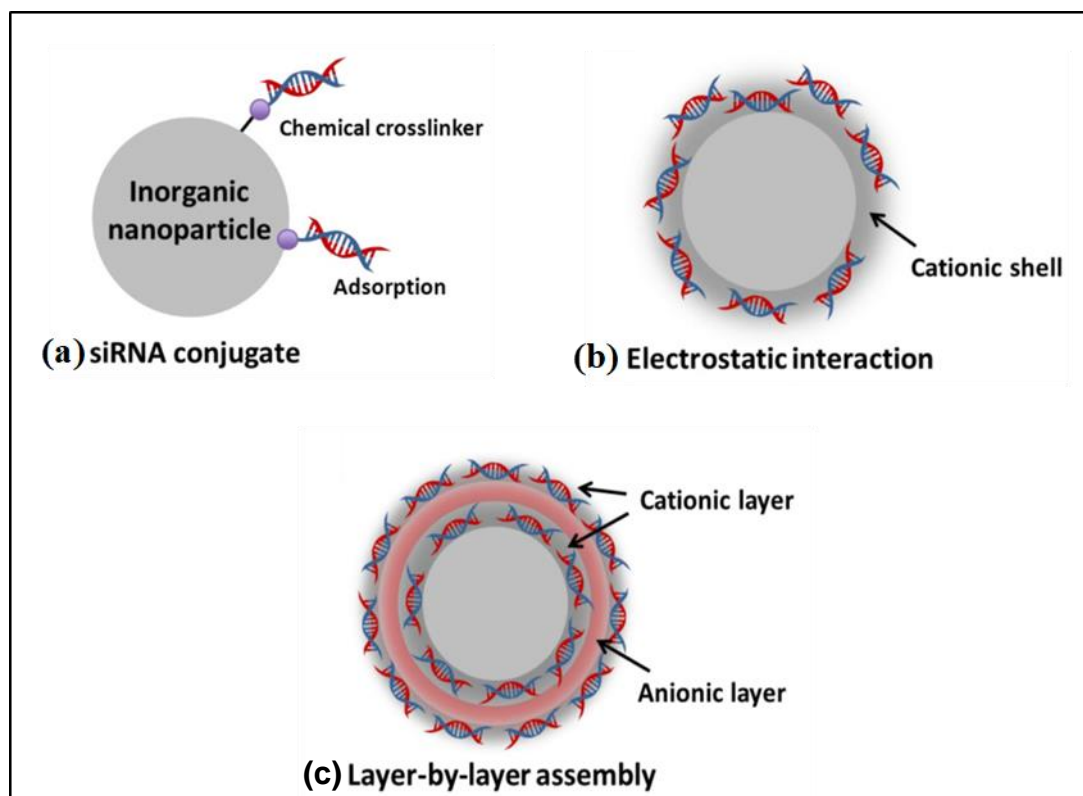


Figure 4.3: Illustration of interactions between siRNA and functionalised AuNPs (Adapted from Hong and Nam, 2014).

4.2 Characterisation of Functionalised AuNPs and AuNP: siRNA Interactions

4.2.1 UV-Visible spectrophotometry

UV-visible absorption spectroscopy can be utilised for the characterisation and confirmation of the synthesis of AuNPs. The spectroscopic properties associated with AuNPs can be used to provide an indication of the size of the resultant synthesized AuNP suspension by assessing their surface plasmon resonance and fitting the position to a wavelength function (Wolfgang *et al.*,2007; Nikhil *et al.*,2001; Kenneth *et al.*,2000; Martinez *et al.*,2012). The surface plasmon band (SPB) of spherical particles can be described using the Mie theory (1908). Maxwell's electromagnetic equations are the basis of the Mie theory which predicts the light scattering properties induced by spherical particles by measuring the difference in the refractive index between the particle and its medium (Malvern, 2010). Furthermore, this theory may also be used to describe the effect of the absorption characteristics of the particle with the amount of transmitted light and to determine how much of this light is either absorbed or refracted. According to this theory, the surface plasmon scattering and absorption is represented as magnetic and electric oscillations and attributes the SPB to the dipole oscillations of free electrons within the conduction band, which occupies energy states above the Fermi energy levels (Daniel and Astruc, 2004; Alvarez *et al.*, 1997). To date, the majority of reports correlate the AuNP spectroscopic behaviour to the Mie theory (Daniel and Astruc, 2004). The characteristics of the uncoated AuNP SPB are as follows: (i) should position near the 520 nm region, (ii) a decrease in the AuNP core size should result in a blue shift/ decrease in the SPB band, (iii) monodispersed AuNPs with a core size between 1.1 – 1.9 nm should exhibit step-like structures in the spectrum which indicates levels of the conduction band that are not occupied (Schaff *et al.*,1997; Zaitoun *et al.*,2001; Melinger *et al.*,2003). The UV absorption spectra of the AuNPs, PEGylated and non-PEGylated Chito-AuNPs are shown in Figure 4.4.

A well-defined adsorption band was observed for all AuNPs. The AuNPs showed a peak at 520 nm which is in agreement with the adsorption maxima of nanoscale AuNPs and the Mie theory, and is a characteristic feature of AuNPs. The addition of chitosan as well as PEG₂₀₀₀ and PEG₄₀₀ was confirmed by a red shift of the AuNP adsorption spectrum from λ_{max} of 520 nm for AuNP to λ_{max} of 524nm - 527 nm for the functionalised AuNPs. A red shift in the absorption spectrum is an indication of an increase in particle size which can be attributed to the addition of chitosan, PEG₂₀₀₀ and PEG₄₀₀, respectively. A similar result was observed by Manson and co-workers who showed that as the PEG density increased, the intensity of the surface plasmon band

increased. This effect was also previously reported by Oh and colleagues in 2008 (Oh *et al.*,2008). The spectral red shift can be attributed to the combining effects of polymer functionalisation and particle size increase.

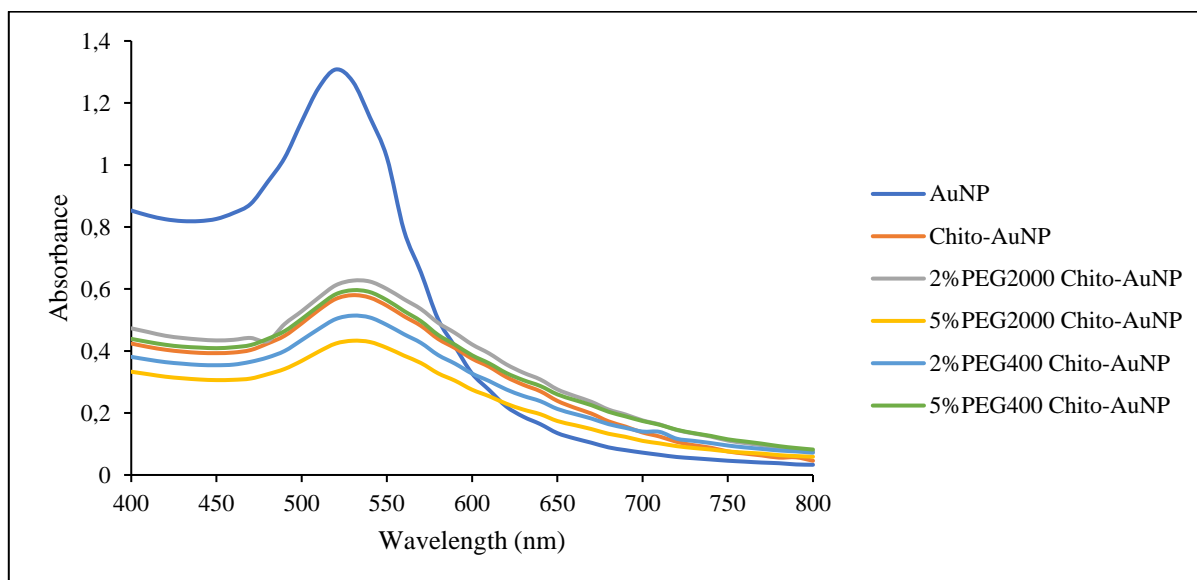


Figure 4.4: UV-vis Absorption Spectrum of AuNPs, Chito- AuNPs and PEGylated Chito-AuNPs

Standard citrate-capped AuNPs exhibit a single extinction band in the visible region at 520 nm and this is correlated to the size of the gold nanospheres being less than 50 nm (Boca *et al.*,2010). Since the AuNPs synthesized for this study exhibited a peak in the absorbance at this wavelength, it suggests that the size of the AuNPs are within this range. Interestingly, Chito-AuNPs PEGylated with PEG₄₀₀ showed an λ_{max} 524 nm which is similar to that exhibited by the Chito-AuNPs, whereas PEGylation with PEG₂₀₀₀ showed a red shift of the spectrum to a λ_{max} of 527 nm. The polymer coating of the AuNPs results in changes of the refractive index of the AuNPs, causing the red spectral shift, and hence, differs from that of the Mie theory which deals with uncoated AuNPs. The presence of the polymer shell results in an interaction with the electron cloud on the AuNP surface. The SPB of the functionalised AuNPs shifts to a higher wavelength upon the reduction between the spacing of the AuNPs (Daniel and Astruc,2004). This assists in understanding the highest λ_{max} exhibited by the 2 and 5% PEG₂₀₀₀ Chito-AuNPs. Since PEG₂₀₀₀ is a larger polymer than PEG₄₀₀, the space between individual AuNPs PEGylated with PEG₂₀₀₀ will be reduced when compared to the non-PEGylated and PEG₄₀₀ PEGylated Chito-AuNPs counterparts and hence, these PEG₂₀₀₀ PEGylated Chito-AuNPs exhibit the highest wavelength at 527 nm. Surface functionalisation was confirmed by

FTIR analysis. The sizes of all the AuNPs were further evaluated by TEM and NTA measurements.

4.2.2 ICP-OES and FTIR Analysis

ICP was conducted to determine the AuNP concentration within the prepared citrate reduced AuNP suspension. This technique is highly specific with excellent detection limits (18 parts per trillion for gold) (Alkilany and Murphy, 2010). It allows for a count of the number of Au atoms which results in a more precise quantification of the number of gold nanospheres. Furthermore, an elemental analysis can be carried out which provides an estimate of the number of nanoparticles within a sample (Lévy *et al.*, 2010). The results are represented in Appendix A1 and show that the average AuNP concentration is 8.862 mg/L.

Fourier Transmission Infrared analysis or FTIR is a method that can be used to determine the quality, components of a sample, and for identification of an unknown material. FTIR was used to analyse the surface functionalisation of the AuNPs with chitosan and PEG (400 and 2000) utilised in this study. Each material is unique, due to their atom combination; therefore, different materials will produce infrared spectrums that differ from each other. During FTIR analysis, the sample is exposed to IR radiation. The sample will absorb some of this radiation and also transmits a part of the IR radiation. Due to the vibration frequencies between the atomic bonds of a sample, various absorption peaks are generated that correspond to these frequencies and the spectrum that results serves as a 'molecular fingerprint' of the sample (Thermo Nicolet, 2001). From FTIR analysis, it was further confirmed that the AuNP surface was successfully functionalised with chitosan and PEG. The spectra are represented in Appendix A2 with characteristic peaks at approximately 1637 cm^{-1} and 2993 cm^{-1} due to the amino groups present in the chitosan molecule, and through the vibrations of repeated $\text{OCH}_2\text{-CH}_2$ units in PEG, distinct peaks are present in the 3200 cm^{-1} range. Slight differences exist within these ranges which confirm the variations in the quantity and molecular weight of the PEG molecules utilised during functionalisation.

4.2.3 PEGylated and non-PEGylated Chitosan AuNP: siRNA Interactions

4.2.3.1 siRNA Binding studies and Nuclease Protection Assays

Nanocomplexes were prepared between chitosan, FAuNPs and siRNA by simply mixing and incubating the two molecules at room temperature. Complex formation occurred through electrostatic interactions as described previously. Evaluation of these nanocomplexes to determine the optimum binding ratios and siRNA protection, was investigated using the band shift, SYBR Green II displacement, and RNase A protection assays.

4.2.3.1.1 Band Shift Assay

The band shift assay or gel retardation assay was introduced by Fried and Crothers to evaluate the interaction between DNA and proteins (Scott *et al.*, 1994; Hellman and Fried, 2007). It has been adapted for gene delivery studies to evaluate the interaction between DNA/RNA and cationic gene delivery vehicles. The principle of this study is that the migration of siRNA or DNA becomes retarded following complex formation between the nucleic acid and the cationic nanoparticles during electrophoresis. For this study, agarose gel electrophoresis was utilized to assess the binding efficiencies of the PEGylated and non-PEGylated Chito-AuNPs with siRNA. As the concentrations of the FAuNPs increases, the amount of siRNA associated with the FAuNPs increases until complete binding of the siRNA is achieved. At this point, the minimum amount of FAuNPs to completely bind and compact a constant amount of siRNA is achieved and the charge ratio which corresponds to that complex can be estimated (Percot *et al.*, 2004). At complete retardation, an electroneutral complex is formed, and it is at this ratio that the negative charges of the siRNA are completely titrated by the positive charges associated with the FAuNPs and the resultant complex will not migrate through the matrix of the gel, but will be retained in the well. Uncomplexed siRNA, that is the siRNA in the absence of any FAuNP, will migrate into the gel matrix upon electrophoresis, however, in the presence of increasing cationic FAuNPs, the siRNA becomes neutralised and does not migrate into the gel, but is seen fluorescing in the wells. The results of the PEGylated and non-PEGylated Chito-AuNPs binding with siRNA can be seen in Figure 4.5, and shows that all the FAuNP preparations were capable of successfully binding to the siRNA at various N/P or weight ratios (Table 4.1). The end points of each nanocomplex are indicated by the arrows.

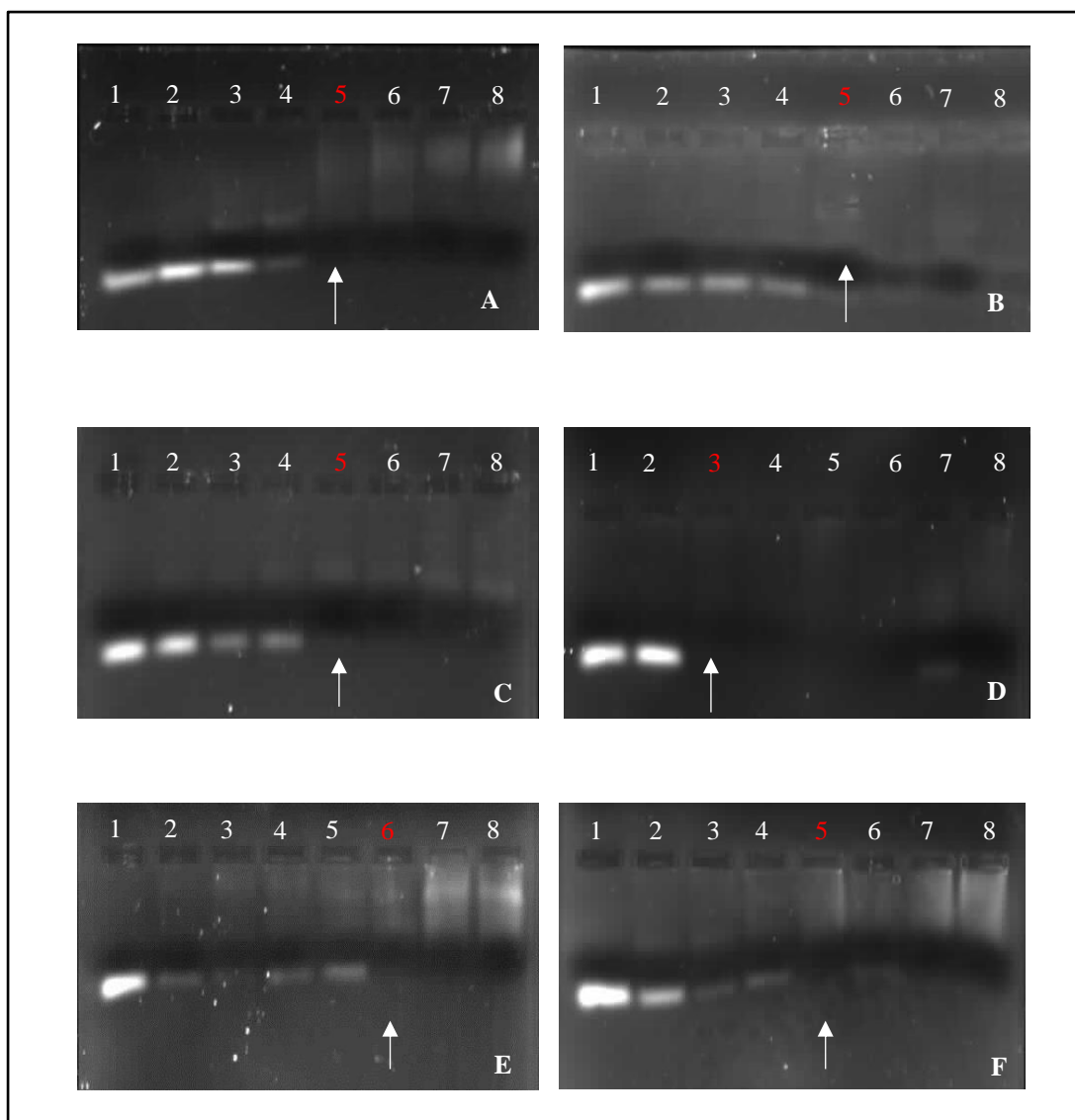


Figure 4.5: Band Shift analysis the binding of various amounts of FAuNP preparations with a constant amount of siRNA (0.3 μ g) in a 10 μ l reaction mixture. (A) Chitosan, (B) Chito-AuNP, (C) 2% PEG₂₀₀₀ Chito-AuNP, (D) 5% PEG₂₀₀₀ Chito-AuNP, (E) 2% PEG₄₀₀ Chito-AuNP and (F) 5% PEG₄₀₀ Chito-AuNP. Lane 1: 0.3 μ g of uncomplexed siRNA in the absence of chitosan and FAuNPs; Lanes 2-8: the respective siRNA nanocomplexes prepared using various amounts of the FAuNPs and chitosan as indicated. Arrows or numbers in red indicate complete binding or point of electroneutrality.

In lane 1, the naked siRNA serves as the control, against which retardation is measured. In this control lane, the siRNA exhibits a single band which is characteristic of the siRNA. In lanes 2-8, increasing amounts of chitosan and the FAuNPs are present. In these lanes, it can be seen that the amount of uncomplexed siRNA that migrates through the gel decreases until all the siRNA is completely bound to the FAuNPs and chitosan. The ratio at which this minimum amount of FAuNP is needed to completely bind the siRNA is referred to as the optimum binding ratio. The N/P and weight ratio for each FAuNP and chitosan at the optimum binding

ratio is outlined in Table 4.1. Interestingly, the amount of the PEGylated Chito-AuNPs to completely bind to the siRNA was higher than that required by the non-PEGylated Chito-AuNPs. Since 1 mg of chitosan was utilized in all the preparations, it suggests that the presence of PEG on the AuNP surface may be responsible for shielding some of the positive charges presented on the chitosan surface, resulting in more of the PEGylated Chito-AuNPs being required to bind the same amount of siRNA. Furthermore, PEG₄₀₀ Chito-AuNPs showed complete binding of the siRNA at a higher ratio compared to their PEG₂₀₀₀ Chito-AuNP counterparts. Since the PEG₄₀₀ chain is much smaller than that of the PEG₂₀₀₀, a greater number of PEG₄₀₀ molecules can attach to the nanoparticle surface, resulting in a higher number of positive charges being shielded, affecting the binding ability of the AuNP to the anionic siRNA. Hence, a greater amount of the Chito-AuNPs PEGylated with PEG₄₀₀ will be required to completely bind the same amount of siRNA.

Table 4.1: siRNA-Au nanocomplexes at the optimum binding ratio and their corresponding charge ratios for the band shift and SYBR Green II displacement assays.

FAuNPs	Band Shift Assay			SYBR Green II Displacement Assay	
	FAuNP Amount (µg)	siRNA: FAuNP Ratio ^(w/w)	N/P Ratio (+/-)	siRNA: FAuNP Ratio ^(w/w)	N/P Ratio (+/-)
Chitosan	0.21	1:0.7	0.01:1	1:17	0.35:1
Chito-AuNP	0.15	1:0.5	0.007:1	1:14	0.20:1
2% PEG ₂₀₀₀ Chito-AuNP	0.27	1:0.9	0.013:1	1:9	0.13:1
5% PEG ₂₀₀₀ Chito-AuNP	0.48	1:1.6	0.023:1	1:10	0.20:1
2% PEG ₄₀₀ Chito-AuNP	0.3	1:1	0.014:1	1:9	0.13:1
5% PEG ₄₀₀ Chito-AuNP	0.66	1:2.2	0.035:1	1:14	0.20:1

From the results, it was observed that the Chito-AuNP was capable of binding the siRNA at a lower ratio (^{w/w}) than chitosan on its own. This suggests that the presence of the AuNP introduced a positive influence on the delivery system by enhancing the interaction between the natural polysaccharide and the siRNA. Furthermore, the resulting nanocomplex formed may be smaller, thereby favouring cellular uptake and transfection efficiency of the AuNPs. The ratios that were obtained from this assay were then utilized for further characterisation and *in vitro* studies.

4.2.3.1.2 RNase A Protection Assay

One of the major hurdles in gene delivery is that the siRNA being introduced, is susceptible to nuclease degradation in circulation. These nucleases, which include RNase A, are present in the blood system during circulation and are also present in the interstitial spaces (Lu *et al.*,2009). An important and desirable feature of any nanoparticle is the protection that they afford to the siRNA against nuclease degradation. Hence, in this study, the ability of the prepared FAuNPs to protect the siRNA in the presence of RNase A was investigated *in vitro* using agarose gel electrophoresis.

Theoretically, the siRNA that is associated with the FAuNPs will be protected against degradation by nucleases as they are completely bound and, therefore, condensed and compacted into supramolecular structures, whereas uncomplexed siRNA is rapidly destroyed by nucleases as they are not afforded any protection by the FAuNPs. The results of the assay are represented in Figure 4.6. In this assay, two controls were included, namely, a positive control: untreated, naked siRNA which displays a single siRNA band, and a negative control which is the naked siRNA treated with 10% RNase A. These controls serve to evaluate the degree of RNase A digestion of uncomplexed siRNA compared to the siRNA associated with the PEGylated and non- PEGylated Chito-AuNPs. Following incubation with the enzyme, EDTA was then added to the reaction mixtures to terminate the action of the enzyme. This was followed by the addition of SDS which releases the compacted siRNA from the nanocomplexes. The resultant reaction mixtures containing the released siRNA were then evaluated by agarose gel electrophoresis as described in section 3.2.4.1.

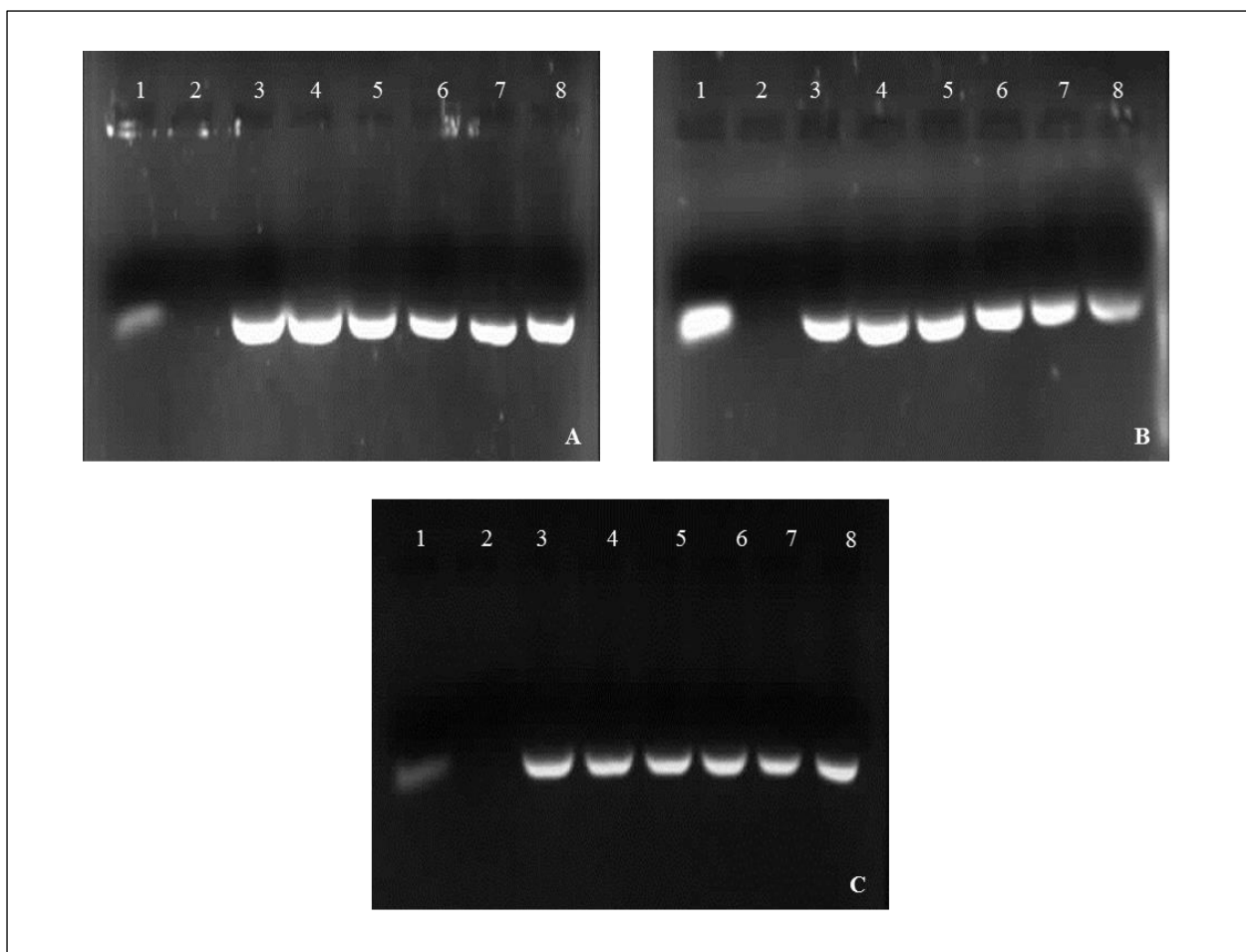


Figure 4.6: RNase A protection assay of chitosan and FAuNP- siRNA nanocomplexes. Lane 1: 0.3 μg of untreated, naked siRNA, Lane 2: 0.3 μg of RNase A treated naked siRNA, (A) Lanes 3-5: Chitosan nanocomplexes, (A) Lanes 6-8: Chito-Au nanocomplexes, (B) Lanes 3-5: 2% PEG₂₀₀₀ Chito-Au nanocomplexes, (B) Lanes 6-8: 5% PEG₂₀₀₀ Chito-Au nanocomplexes, (C) Lanes 3-5: 2% PEG₄₀₀ Chito-Au nanocomplexes (C) Lanes 6-8: 5% PEG₄₀₀ Chito-Au nanocomplexes. The siRNA was kept constant at 0.3 μg per well.

It can be seen from the results obtained, that all the FAuNPs were capable of fully protecting the siRNA against RNase A degradation across all the siRNA- FAuNP ratios (w/w), compared to the uncomplexed siRNA (lane 2) which was completely degraded. Chitosan also displayed protection of the siRNA. The chitosan utilized in this study has a MW of 25 kDa with a $>75\%$ DD. Studies conducted by Fernandes and co-workers (2012) showed that chitosan at this MW was capable of completely binding siRNA offered better protection against enzymatic degradation, when compared to higher or lower MW chitosan molecules (Alameh *et al.*, 2012). Furthermore, it was found that the DD should be greater than 75%, as this ensures complete binding and ensures that the siRNA remains complexed within the nanocomplex through electrostatic interactions. Therefore, from the results and as discussed above, it can be suggested that since the chitosan that was used for functionalisation met the above

requirements, the siRNA was completely complexed within the Au nanocomplex structure and was able to be fully protected against RNase A degradation. Overall, these results are an indication that the formulated PEGylated and non-PEGylated Chito-AuNPs are suitable as potential gene delivery vehicles, as treatment with of these siRNA-Au nanocomplexes with RNase A offered complete protection to the siRNA. This was a promising result for further transfection studies *in vitro* and future *in vivo* applications, with the anticipation of increased delivery of intact siRNA to the cells followed by efficient gene knockdown.

4.2.3.1.3 SYBR Green II Displacement Assay

The binding efficiency of the FAuNPs with siRNA attained from the band shift assay was further investigated using a fluorescence quenching assay based on that first reported by LePecq and Paoletti in 1967 which involved the use of ethidium bromide (Geall and Blagbrough, 2000; Duarte *et al.*, 2011). For this study, the assay was slightly modified by using the SYBR Green II dye in place of ethidium bromide. The fluorescence quantum yield of SYBR Green II with RNA complexes is believed to be seven times greater than that obtained with ethidium bromide/ RNA complexes (Dorasamy *et al.*, 2012). However, the principle of the assay remains the same. Free SYBR Green II dye, in aqueous solvents, exhibit low levels of fluorescence, however, when the dye becomes intercalated between the siRNA base pairs, it enters an environment that is hydrophobic which results in an increase in observed fluorescence (Figure 4.7). Upon the addition of FAuNPs, there is a competition between the dye and the nanoparticles. Since there is a greater affinity of the siRNA for the FAuNPs, this interaction is stronger and results in displacement of the SYBR Green II dye from the siRNA. This siRNA interaction with the FAuNPs results in the compaction of the siRNA. Hence, this displacement of the dye leads to a concomitant decrease in the measured fluorescence, which also correlates with the degree of interaction between the siRNA and FAuNPs.

In agreement with this principle, all the FAuNPs prepared were capable of successfully displacing the SYBR Green II dye that was intercalated between the siRNA base pairs. This was evident following the stepwise addition of the FAuNPs to the siRNA-SYBR Green II mixtures which resulted in a steady decrease of fluorescence and is illustrated in Figure 4.8.

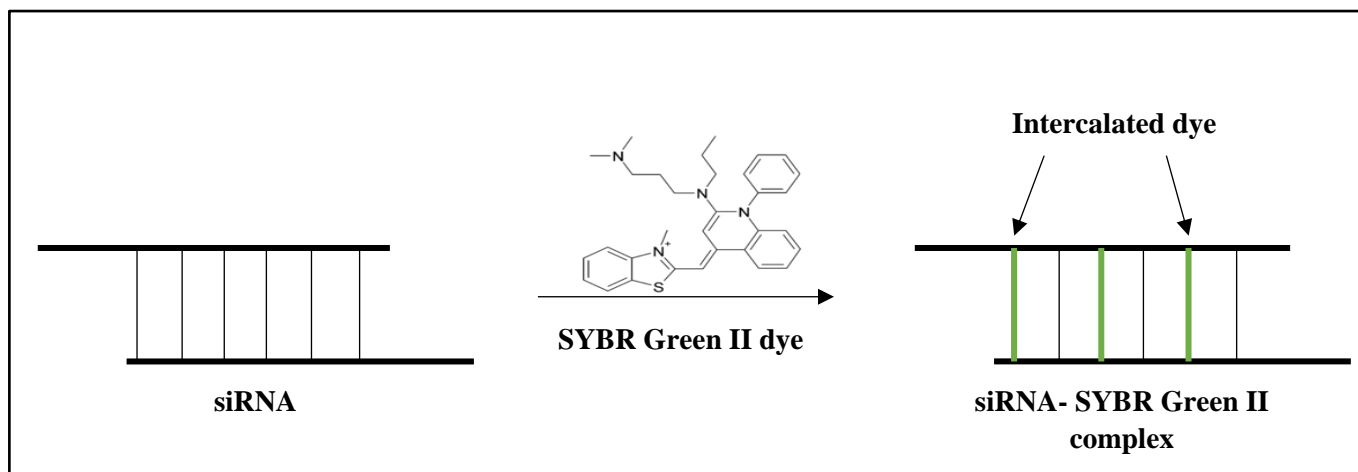


Figure 4.7: Graphical representation of the SYBR Green II dye intercalation between siRNA base pairs

The relative percentage fluorescence was calculated as per section 3.2.4.3 and was represented as a function of the amount (μg) of FAuNPs. The FAuNPs were added in varying amounts to the siRNA-SYBR Green II reaction mixture until the point of inflection or a plateau in readings was reached. It is at this point that the FAuNP ratio had maximally displaced the SYBR Green II dye and completely condensed the siRNA. The resulting mass and N/P ratios at the point of inflection are represented in Table 4.1.

The general trend observed for the chitosan, PEGylated and non-PEGylated nanocomplexes appear to correspond to that observed during the band shift assay with chitosan and Chito-AuNP showing similar levels of fluorescence decline (75.43% and 75.97%, respectively). Furthermore, the ratios correlate with the pattern attained in the band shift assay. The 2% PEGylated AuNPs showed higher levels of compaction at lower concentrations compared to their 5% PEGylated counterparts. This could be attributed to the amount of PEG present on the surface of the AuNP, with a lesser amount of PEG present for the 2% PEGylated AuNPs resulting in more positive charges being present on the nanoparticle surface allowing for greater interaction with the siRNA. These lower ratios are indicative of greater levels of nanocomplex compaction. However, PEG₂₀₀₀ Chito-AuNPs showed lower levels of fluorescence decrease (17.65%, 73.77%) with the siRNA compared to the PEG₄₀₀ Chito-AuNPs (81.16%, 78.74%). This could be due to the length of the PEG molecules which could hinder the compaction abilities of the PEG₂₀₀₀ Chito-AuNPs and hence, the resulting nanocomplexes with the siRNA were not as compact as the nanocomplexes achieved with the PEG₄₀₀ Chito-AuNPs.

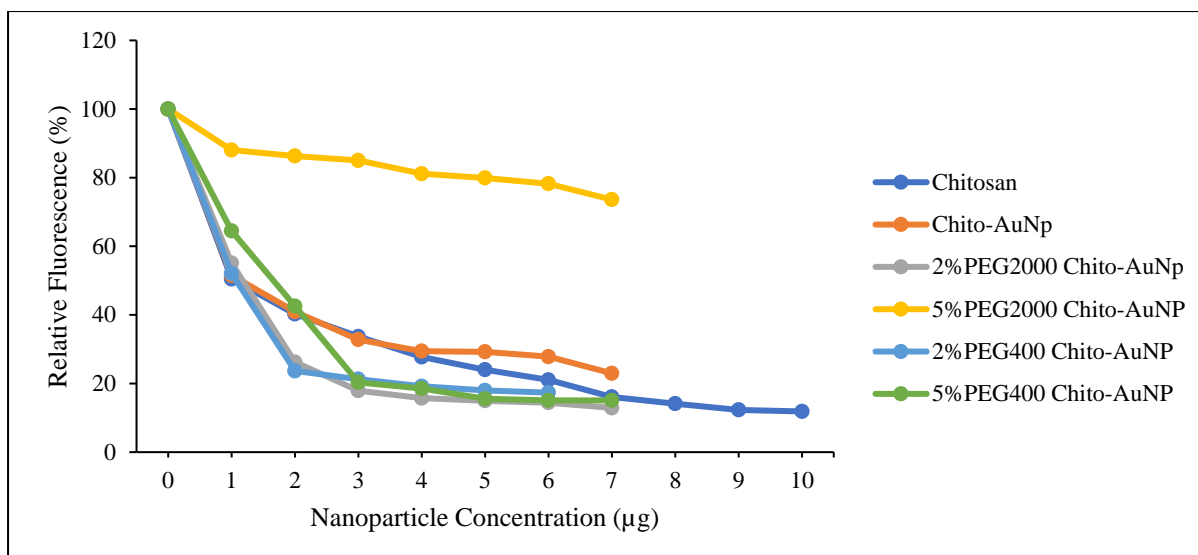


Figure 4.8: SYBR Green II displacement assay of Chitosan, PEGylated and non-PEGylated Chito-AuNPs. The FAuNPs were added systemically to the siRNA/ SYBR Green II reaction mixture (0.28 µg siRNA) until the point of inflection was attained.

All the prepared Chito-AuNP formulations, with the exception of 5% PEG₂₀₀₀ Chito-AuNP, exhibited good compaction of the siRNA and were capable of displacing large amounts of the intercalated SYBR Green II dye from the siRNA. The tight and compact binding of the siRNA to the FAuNPs had its advantages and disadvantages for future transfection studies. The strong interaction between the siRNA and FAuNPs also resulted in greater protection of the siRNA Au-nanocomplexes as seen in the RNase A protection assay. This further ensures the safe delivery of the siRNA to the cells being tested. However, this characteristic may also be unfavourable as the bound siRNA may not be easily released from the nanocomplex during the transfection process, and not able to undergo endosomal escape leading to lower levels of gene knockdown. Alternately, if a weak interaction exists between the siRNA and the FAuNPs, it may result in rapid dissociation of the siRNA: Au-nanocomplex, exposing the siRNA to degradation, which in turn limits the amount of siRNA that reaches the cell. Hence, an intermediary level of compaction is ideal for siRNA delivery.

There appears to be very little correlation between the mass (^{w/w}) and N/P ratios obtained with the band shift and dye displacement assays (Table 4.1). A possible reason for these discrepancies is that the ratios achieved during the band shift assay is based solely on charge neutralisation whereas the dye displacement assay is based on the condensation of the siRNA as well as charge neutralisation. However, the ratios that were obtained during the band shift

assay represent the minimum amount of the cationic FAuNPs to completely bind a constant amount of siRNA.

4.2.3 Imaging and Sizing

4.2.3.1 Transmission Electron Microscopy of PEGylated and non-PEGylated Chito-AuNPs and their complexes with siRNA

Transmission electron microscopy (TEM) was employed to analyse the ultrastructural characteristics of the AuNPs, Chito-AuNPs and the PEGylated Chito-AuNPs. Using this technique, one is able to study the ultrastructural morphology of the AuNPs. Due to the optical properties of the AuNPs, staining is not required to view the AuNPs in their native state. TEM can be characterised by the use of an electron beam which is concentrated onto the surface of the sample by a series of electromagnetic lenses. The electrons which are transmitted are then magnified and, due to the action of magnetic lenses, are focused resulting in an image which is projected onto a screen (Bibi *et al.*,2011; Kuntsche *et al.*,2011).

The TEM micrographs of the AuNPs, FAuNPs and siRNA containing nanocomplexes are represented in Figures 4.9 and 4.10, respectively. All the AuNP preparations appeared spherical in shape, which correlates with that reported in the literature when using the citrate reduction method for the synthesis of AuNPs. Moreover, the FAuNPs appear to exhibit a slight halo around their surface which may indicate the presence of functional groups. The uncoated AuNPs and Chito-AuNPs appear well dispersed whereas the PEGylated Chito-AuNPs appear to have very slight aggregation. These chain-like structures may be attributed to the exchange interaction between the PEG and the citrate molecules, following the PEGylation process during synthesis which may result in an organic double layer (Manson *et al.*,2011; Majzik *et al.*,2010). The siRNA nanocomplexes with the PEGylated and non-PEGylated Chito-AuNPs revealed aggregates that appear to be intact. These complexes further confirm the binding interaction between the FAuNPs and the siRNA as previously studied in the band shift, nuclease and dye displacement assays. An indication of the size of the AuNPs, FAuNPs and their complexes with siRNA was obtained with TEM (Table 4.2), however, for a more accurate measurement on the size distribution, nanoparticle tracking analysis (NTA) was utilized.

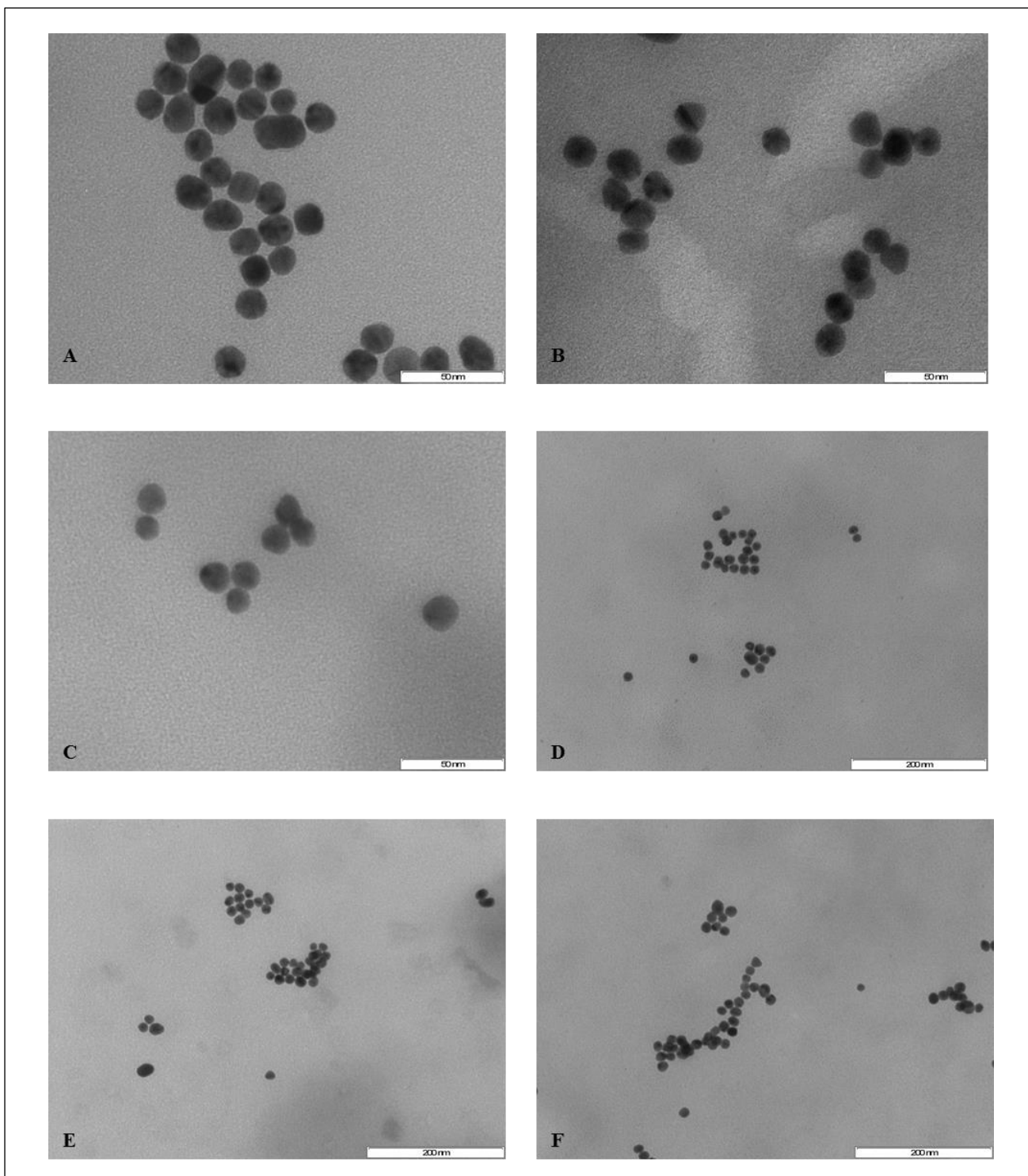


Figure 4.9: Transmission electron micrographs of (A) AuNP, (B) Chito-AuNP, (C) 2% PEG₂₀₀₀ Chito-AuNP, (D) 5% PEG₂₀₀₀ Chito-AuNP, (E) 2% PEG₄₀₀ Chito-AuNP and (F) 5% PEG₄₀₀ Chito-AuNP. Bar represents 50 nm (A-C) and 200 nm (D-F).

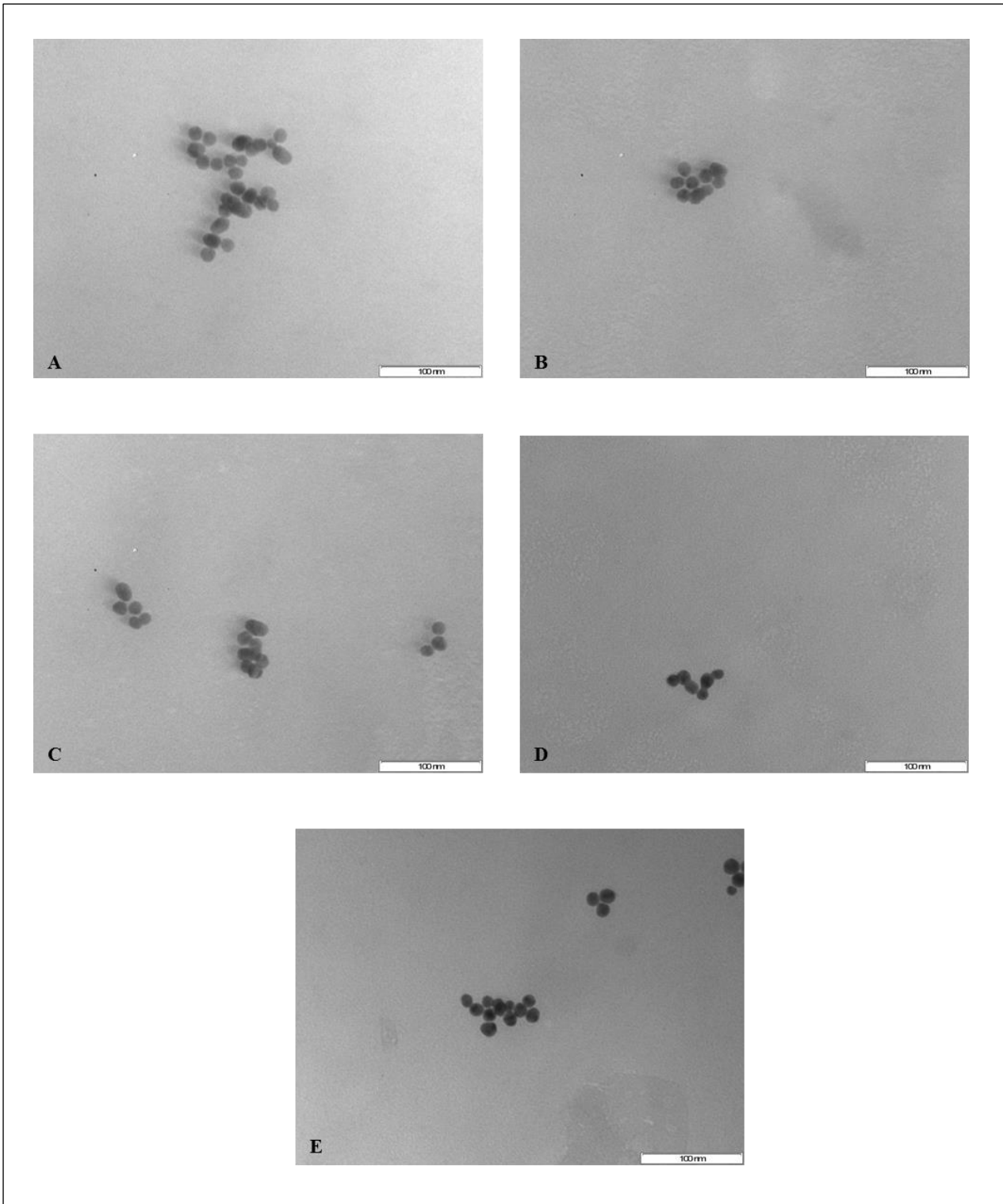


Figure 4.10: Transmission electron micrographs of siRNA: Au nanocomplexes prepared at the optimum binding or N/P ratios as determined from the band shift assay (A): Chito-AuNP, (B) 2% PEG₂₀₀₀ Chito-AuNP, (C) 5% PEG₂₀₀₀ Chito-AuNP (D) 2% PEG₄₀₀ Chito-AuNP and (E) 5% PEG₄₀₀ Chito-AuNP. Bar = 100 nm

4.2.3.2 Nanoparticle Sizing and Zeta Potential

An important parameter in the development of a nanoparticle delivery system is the particle size which is believed to have a great impact on its effectiveness during transfection. Furthermore, this morphological parameter can also influence the circulation time of the nanoparticle, its evasion from the RES as well as the nature of the nanoparticle cellular uptake, which can be either micropinocytosis or clathrin- or- caveolin mediated endocytosis (Ross and Hui, 1999; Ma *et al.*,2007; Marchini *et al.*,2009; Akbarzadeh *et al.*,2013). Another significant feature of the nanoparticles and the siRNA nanocomplexes, is their zeta potential which is a measure of the nanoparticle surface charge in a suspension. The zeta potential also acts as an indicator of the colloidal stability of the nanoparticle and nanocomplexes, which in turn affects the pharmacokinetic properties of these complexes in an *in vivo* system (Xu, 2008; Griffiths *et al.*,2011, Honary and Zahir, 2013).

As mentioned previously, sizing of the AuNP preparations was conducted during TEM analysis, however, the sizes and zeta potential of the AuNPs, PEGylated and non-PEGylated Chito-AuNPs as well as their complexes with siRNA at the optimum binding ratios were evaluated by NTA. The Brownian motion and light scattering properties of the nanoparticle is measured, and the diffusion constant of the nanoparticle is calculated. This is then applied to determine the hydrodynamic diameter of the nanoparticle (Gross *et al.*,2016; Nanosight, 2015). During NTA measurements, the sample is loaded onto a sample chamber and a laser beam at a wavelength of 430 nm is passed through this sample chamber, and the nanoparticles that are in the range of this beam are capable of scattering light allowing them to be visualised. A 20× magnification microscope objective which is attached to a sCMOS camera allows for the visualisation of these nanoparticles under Brownian motion (Figure 4.11) and videos are captured.

The videos were analysed using NTA 3.2 analytical software. The zeta potential of the nanoparticles is measured in a similar way; however, a variable electric current is passed through the sample chamber which is facilitated by the presence of two platinum electrodes within the sample chamber. The velocity of the particle motion under this electric current is recorded and measured on each nanoparticle which allows the zeta potential to be determined (Gross *et al.*,2011; Nanosight, 2013). A detailed NTA report is represented in Appendix A3.

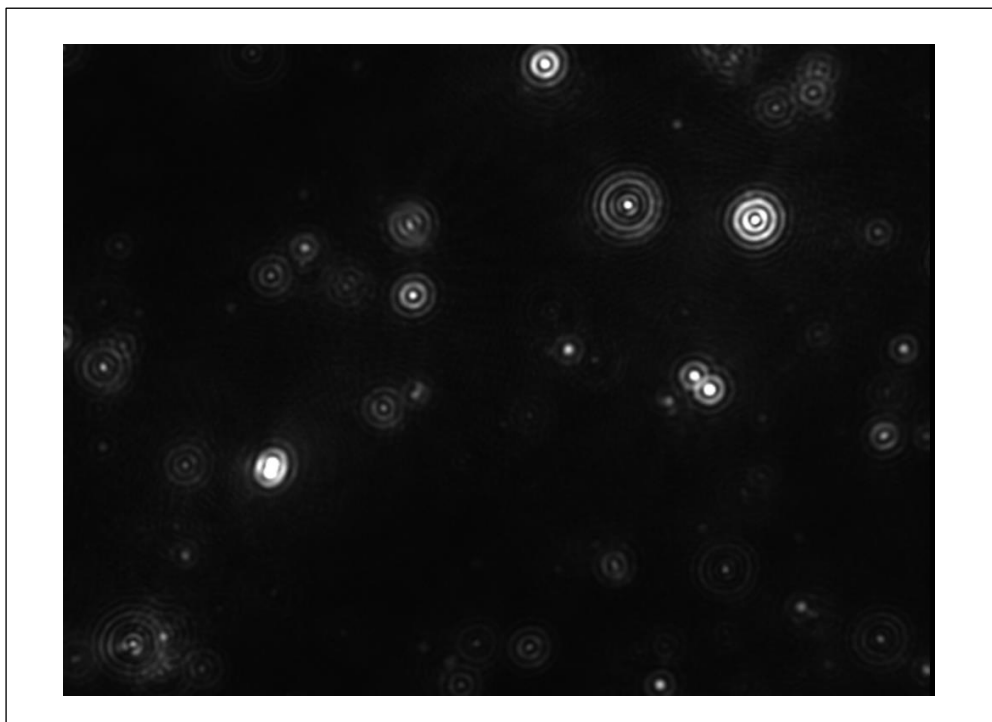


Figure 4.11: Screenshot from recorded video showing the AuNPs light scatter and movement under Brownian motion.

The sizes for the AuNPs and FAuNPs as well as their complexes with siRNA fell within low nanometre ranges. The size ranges determined during TEM analysis of the AuNPs were between 14.29 nm - 17.8 nm and their siRNA nanocomplexes were between 42.5 nm- 58.9 nm whereas the NTA showed sizes between 65.9 nm – 160.8 nm for AuNPs and FAuNPs and 144.3 nm – 164.5 nm for their corresponding siRNA nanocomplexes. These discrepancies in the size measurements could be attributed to the sample preparation prior to analysis. During TEM analysis, the AuNP samples are dried on the copper grid and visualised whereas during NTA, the samples are prepared in a suspension and analysed which results in a hydrodynamic diameter measurement. Hence, the results achieved during NTA may be more reliable for the potential clinical use of these AuNPs, as they will be exposed to a hydrodynamic environment. However, although there are differences in the actual measurements, the trend observed for the AuNPs and their siRNA nanocomplexes using both analyses appear to be the same. The AuNPs have a smaller size range which increases following functionalisation with chitosan and PEG. This result correlates with the data obtained during UV spectroscopy which showed a red shift in the spectrum of the FAuNPs when compared to the uncoated AuNPs.

A similar trend was observed with the corresponding siRNA: Au nanocomplexes. The sizes of the resulting nanocomplexes increased in size depending on the PEGylation. Chito-AuNPs PEGylated with PEG₂₀₀₀ had formed larger complexes with siRNA compared to those PEGylated with PEG₄₀₀. As discussed previously, the resultant siRNA: Au nanocomplex sizes could be due to the size of the PEG polymer, and since PEG₂₀₀₀ is larger than PEG₄₀₀ in size, the nanocomplex that is formed is larger. Furthermore, the presence of PEG on the AuNP surface resulted in a greater nanocomplex size, as all the PEGylated AuNPs formed larger nanocomplexes with the siRNA compared to the non-PEGylated Chito-AuNP. This result is reinforced by those achieved in the band shift and dye displacement assays, as a greater amount of the PEGylated AuNPs were required to bind the same amount of siRNA and furthermore, the Chito-AuNPs that were PEGylated with PEG₄₀₀ showed higher degrees of compaction with the siRNA compared to those Chito-AuNPs PEGylated with PEG₂₀₀₀. The average sizes and zeta potential of the AuNPs, FAuNPs and their complexes with siRNA are represented in Table 4.2.

Previous studies have suggested that the size of the resulting nanocomplex may affect its transfection efficiency as size plays a role in the cellular internalisation pathway (Zuhorn *et al.*, 2002; Ross and Hui, 1999, Ma *et al.*, 2007; Marchini *et al.*, 2009). Furthermore, the size range of the nanoparticle for efficient gene delivery is also conflicting. Some studies suggest that larger nanocomplexes result in higher degrees of transfection while others believe that smaller nanoparticles are superior (Ma *et al.*, 2007; Marchini *et al.*, 2009; Masotti *et al.*, 2009; Wang *et al.*, 2012). For this study, the FAuNPs are proposed to be taken up by cells via a passive cellular uptake mechanism, that is, a combination of clathrin mediated endocytosis and micropinocytosis. This is a non-specific cellular uptake process where particles within a broad size range (up to 5 μm) can be internalised. Therefore, this may not be a limiting parameter of the AuNPs in determining efficient uptake *in vitro*, however, this feature may be of vital importance for *in vivo* applications.

Table 4.2: Average particle size and zeta potential of AuNPs, FAuNPs and optimal siRNA: Au nanocomplex ratios

FAuNPs	TEM (n= 3)		NTA (n=3)			
	Nanoparticle Size (nm) \pm SE	Nanocomplex Size (nm) \pm SE	Nanoparticle		Nanocomplex	
			Size (nm) \pm SE	ζ Potential (mV) \pm SE	Size (nm) \pm SE	ζ Potential (mV) \pm SE
AuNP	14.29 \pm 1.69	-	65.9 \pm 9.8	-15.5 \pm 1.6	-	-
Chito-AuNP	15.27 \pm 1.75	42.7 \pm 9.8	69.6 \pm 15.2	55.5 \pm 1.2	144.3 \pm 7.3	- 35.8 \pm 1.3
2% PEG ₂₀₀₀ Chito-AuNP	16.12 \pm 2.3	57.7 \pm 9.06	90.9 \pm 3.4	29.5 \pm 1.6	164.6 \pm 15.2	-25.8 \pm 0.7
5% PEG ₂₀₀₀ Chito-AuNP	16.5 \pm 0.97	58.9 \pm 4.7	160.8 \pm 3.9	34.6 \pm 1.4	171.6 \pm 5.9	-25.5 \pm 0.3
2% PEG ₄₀₀ Chito-AuNP	16.7 \pm 1.6	48.5 \pm 13	140.3 \pm 0.2	36 \pm 0.5	147.1 \pm 5.7	-44.5 \pm 0.1
5% PEG ₄₀₀ Chito-AuNP	16.6 \pm 3.18	44.4 \pm 12.7	160.3 \pm 7.1	26.9 \pm 0.1	153.3 \pm 12.4	-33.2 \pm 2.6

Abbreviation: SE=Standard Error

The zeta potential refers to the electrostatic value of the nanoparticle and correlates to the nanoparticle surface charge (Honary and Zahir, 2013). Hence, a desirable zeta potential for nanoparticles should be greater than 25 mV or less than – 30 mV. Nanoparticles that have zeta potentials within this range are believed to be more stable due to the greater levels of mobility in solution and higher levels of electrostatic repulsion which will, therefore, minimise aggregation of the nanoparticles (Griffiths *et al.*,2013). The results obtained show that uncoated AuNPs had a negative zeta potential that measured – 15.5 mV. This suggests that these AuNPs have a low level of colloidal stability and require stabilization by a polymer which will interact with the electron cloud present on the AuNP surface (Daniel and Astruc,2004). The results obtained confirm this theory as the AuNPs that were functionalised with chitosan and PEG exhibited greater colloidal stability with their zeta potential ranging between 29.5 mV and 55.5 mV. Furthermore, due to the overall positive charge, the interaction of these FAuNPs with siRNA will be enhanced. The surface charges can also assist in explaining the optimal ratios attained during the binding studies, which shows that Chito-AuNP has the highest charge 55.5 mV and 5% PEG₄₀₀ Chito-AuNP has a charge of 29.5 mV, hence, 5% PEG₄₀₀ Chito-AuNP required a higher mass (^w/_w) and N/P ratio to bind siRNA compared to Chito-AuNP which required much less.

The results obtained during the zeta potential analysis show that the siRNA nanocomplexes have a negative charge. Previous studies suggest that this is not a limiting factor as they have shown that nanoparticles with a negative zeta potential have been successfully internalised by cells. This is due to the formation of nanoparticle clusters as well as non-specific cell membrane adsorption by the nanoparticle (Honary and Zahir, 2013 (a)). It was also shown by Honary and Zahir that negatively charged nanoparticles show lower cytotoxicity and enhanced circulation times in rats (Honary and Zahir, 2013 (b)). The cellular toxicity of highly positively charged nanoparticles are increased as they can combine with plasma proteins. Therefore, the siRNA nanocomplexes prepared and utilised in this study possess a negative zeta potential and have shown minimal toxicity to the cell lines being studied as determined from the AlamarBlue® an MTT toxicity assays and shall be further discussed below.

4.3 Cell Culture Studies

4.3.1 Cell Line Maintenance

The human epithelial colorectal adenocarcinoma cell line (Caco 2), human embryonic kidney cell line (HEK293), human breast adenocarcinoma cell line (MCF-7) and human colon adenocarcinoma cell line (HT-29) were utilized for *in vitro* cell culture studies. The HEK293 cell line is semi-adherent and was derived from human primary embryonic kidney cells of an aborted embryo that was exposed to fragments of the adenovirus type 5 (AD5) DNA that was mechanically sheared (Thomas and Smart, 2005; Stepanenko and Dmitrenko, 2015). The Caco2 cell line grows as a monolayer and are adherent cells. They are differentiated cells that exhibit various morphological and functional characteristics of small bowel enterocytes (Lea, 2012). The HT-29 cell line was isolated by Fogh and Tremp in 1964 from a primary tumour of a Caucasian female (Martínez-Maqueda *et al.*, 2015). They are undifferentiated cells that grow as a multilayer and can express characteristics of intestinal cells and have therefore, attracted much attention. The MCF-7 cell line was isolated from the pleural effusion of a Caucasian female with metastatic breast cancer (Levenson and Jordan, 1997). This cell line exhibits an epithelial-like morphology and grows as monolayers with dome structures. These 4 cell lines are shown in Figure 4.12.

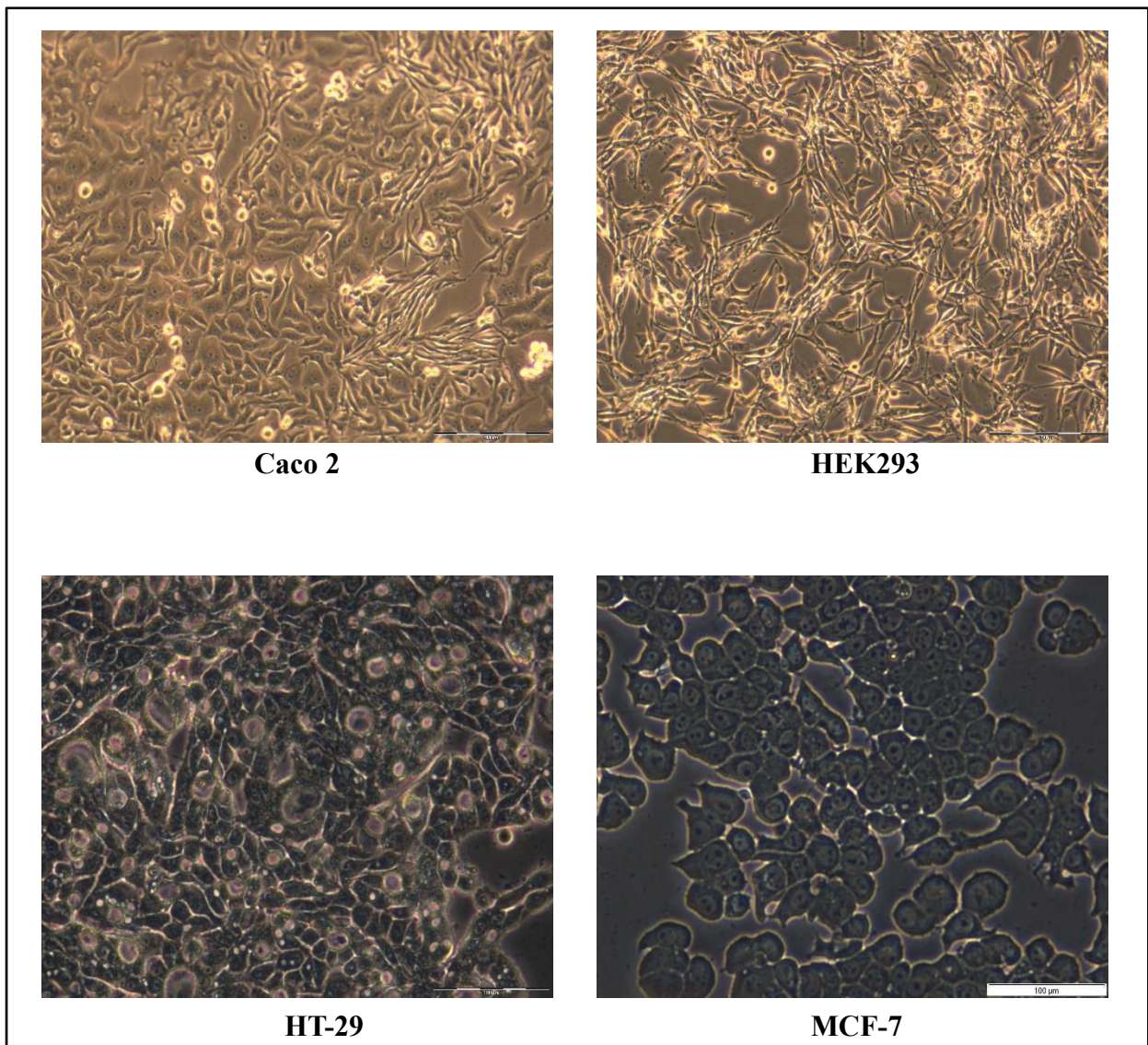


Figure 4.12: Images of cell lines utilized during *in vitro* studies. Cells are viewed as a monolayer at confluence under 100 × magnification with an Olympus CKX41 inverted microscope (Tokyo, Japan). Bar = 100nm.

To maintain healthy cells under *in vitro* conditions, the original environment of the cells need to be mimicked which include the temperature, pH, availability of nutrients and vitamins, etc. The minimal essential nutrients are provided by the medium which is supplemented with foetal bovine serum (FBS). The medium also serves as a means of monitoring the pH. The temperature and humidity are controlled using the CO₂ incubator which maintains the temperature at 37°C with 5% humidity. Most cell lines in culture grow as a monolayer and upon reaching confluency, their cell growth may be suppressed leading to cell death. To avoid

this from occurring, the cell lines need to be sub-cultured regularly to ensure the propagation of healthy cells.

In this study, all cell lines were maintained in Eagle's Minimal Essential Medium (EMEM) supplemented with 10% FBS and 1% antibiotics. Initial cell propagation was slow with confluence being reached within 5-7 days, thereafter, cell growth was exponential as the cell lines reached confluence within 3-4 days and were regularly sub-divided into 1:2 or 1:3 ratios by trypsinization or utilized for cell culture studies.

4.3.2 Cytotoxicity Studies

A safe and efficient vector is an important requirement for siRNA delivery. The use of cell lines for pre-clinical screenings of compounds is an accepted system as cell lines are well established for *in vitro* analyses (van Tonder, *et al.*, 2015). In this study, *in vitro* cytotoxicity of the PEGylated and non-PEGylated AuNPs were investigated using two cell viability assays, namely, the MTT reduction and AlamarBlue® assays on the HEK293, Caco 2, HT-29 and MCF-7 cell lines.

4.3.2.1 MTT Reduction Assay

The MTT Assay was developed by Mosmann in the 1980's and was the first cytotoxicity assay developed that could be utilized for high throughput screenings (Mosmann, 1983). MTT is a tetrazolium compound that is utilized for the detection of viable cells. The principle of this assay is based on the active metabolism of viable cells that are capable of converting MTT into a purple formazan product (Figure 4.13). This product absorbs light maximally at 570 nm. The mechanism of this conversion is not well understood; however, it is believed that a reaction with NADH is involved which transfers electrons to MTT (Marshall *et al.*, 1995).

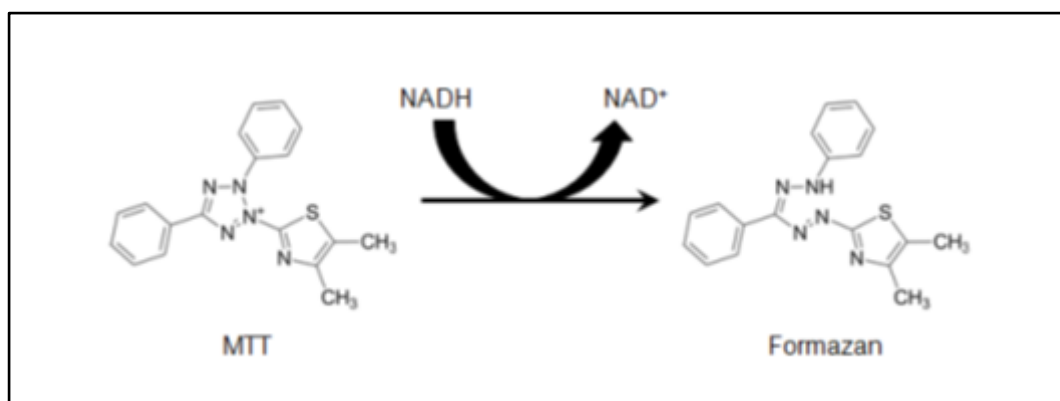
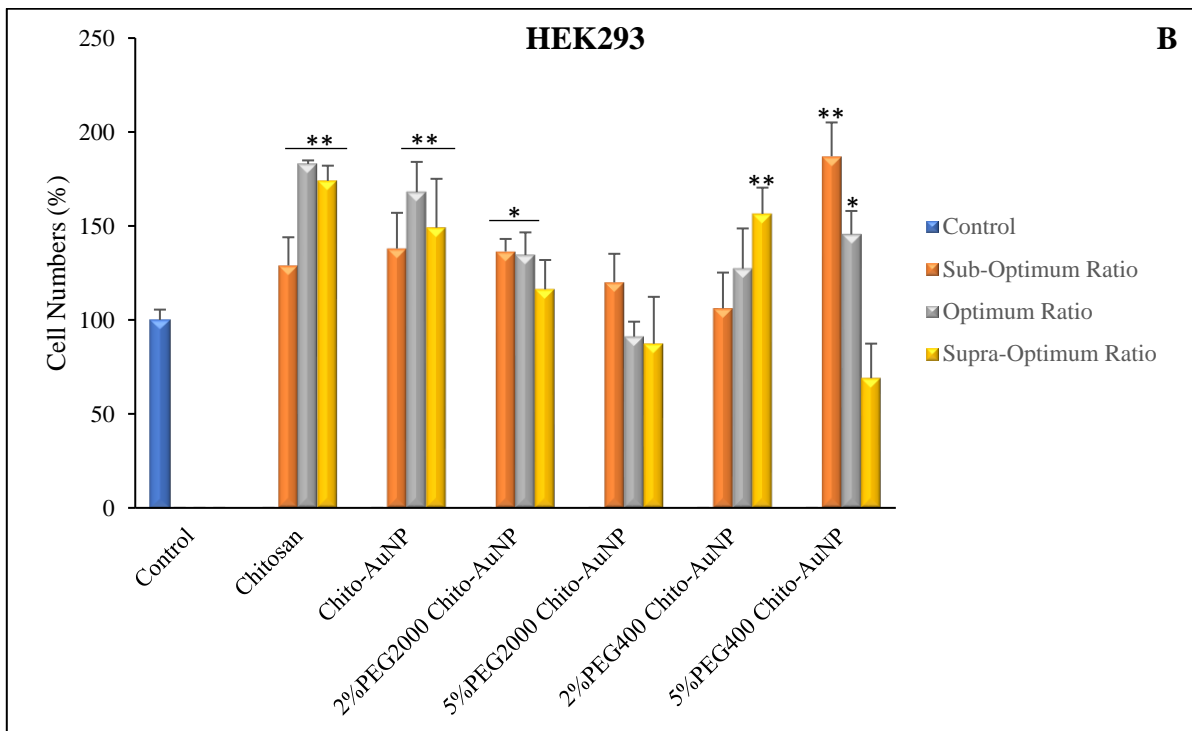
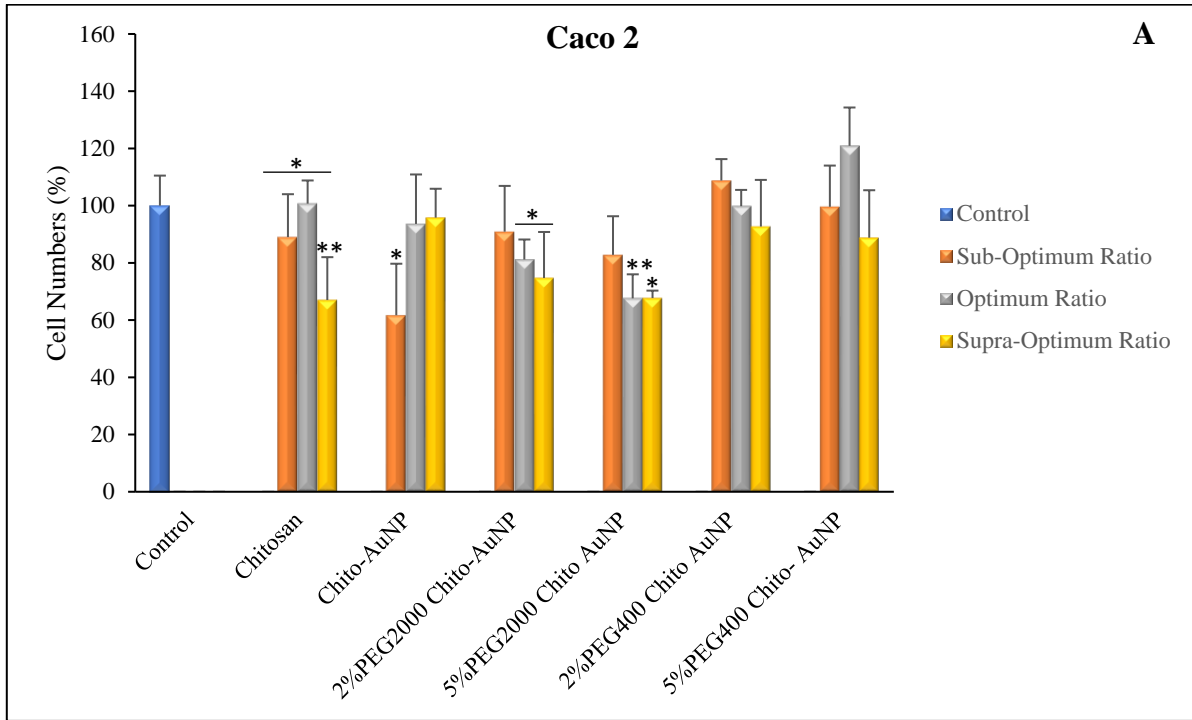


Figure 4.13: MTT conversion to the insoluble formazan product following a reduction reaction (Riss *et al.*,2013).

The resulting formazan product accumulates within the cell as well as near the surface of the cell and cell culture medium as an insoluble product which requires solubilisation prior to measurement of the absorbance. The solubilisation method utilized in this investigation involved the use of DMSO which allowed for absorbance readings to be recorded (Tada *et al.*,1986; Hansen *et al.*,1989; Denizot and Lang, 1986). The results achieved for this assay are represented in Figure 4.14.

From the results obtained (Figure 4.14 A-D), it is evident that all nanocomplexes were well tolerated by the different cell lines with cell survival over 65%, and minimal toxicity in the MCF-7 and HT-29 cell lines. In these cell lines, cell survival was very high, with some cases, the percentage cell viability was higher than the control. Cell viabilities of the Caco 2, HEK293, MCF-7 and HT-29 cell lines respectively were: Chitosan (89-67, 129-174, 286.9- 190.4, 132.2-145.2) %; Chito-AuNP (66.7- 95.8, 138-149.1,237-241, 124-118.4) %; 2% PEG₂₀₀₀ Chito-AuNP (90.9-74.7, 136.4-116.3, 259-248, 100.8-99.35) %, 5% PEG₂₀₀₀ Chito-AuNP (82.8-67.7, 120-87.3, 149-173.6, 84.2-83.5) %; 2% PEG₄₀₀ Chito-AuNP (108.8-92.7, 106.2-156.4, 318-80, 133.2-132.9) % and 5% PEG₄₀₀ Chito-AuNP (99.6-88.8, 187.1-69, 93-79.5, 130.4-124.9) %. Of the cell lines being tested, the Caco 2 appears to have been most adversely affected, however cell viability was still over 65%. Overall there appears to be no severe cytotoxic effect of the nanocomplexes in the different cell lines. However, in most cases, cell survival of the treated cells appeared to be greater than the control. This could be attributed to the presence of chitosan in the preparations which allow the AuNPs to interact with the cell membranes and resulted in stimulation of growth factors (Rajam *et al.*,2011).



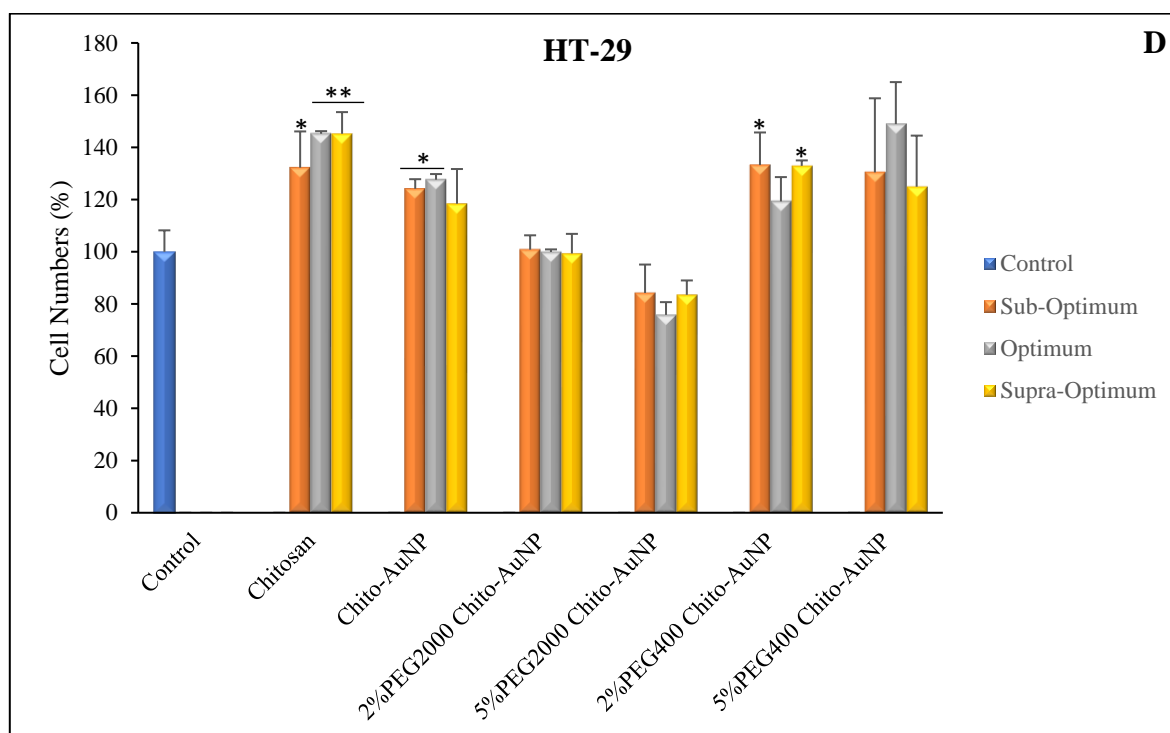
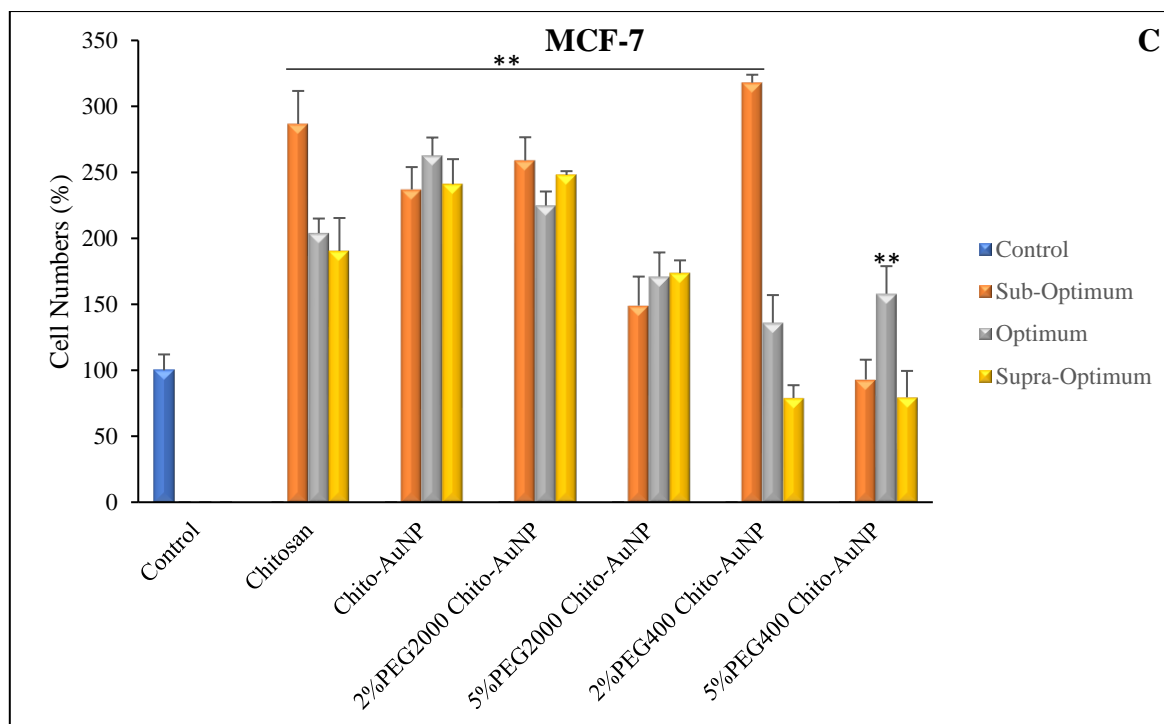


Figure 4.14: MTT reduction assay of siRNA nanocomplexes in (A) Caco 2, (B) HEK293, (C) MCF-7 and (D) HT-29 cell lines. Nanocomplexes were prepared with 50 nM control, non-targeting siRNA at various siRNA:FAuNP ratios (^w/_w). A control containing untreated cells was assumed to have 100% survival. The results are represented as means \pm SD, $n = 3$ and shown as a percentage of the control sample. Statistical analysis was performed using one-way ANOVA which was followed by the Dunnett multiple comparison *post hoc* test ($*P < 0.05$ and $**P < 0.01$ compared to the control).

4.3.2.2 AlamarBlue® Toxicity Assay

The AlamarBlue® assay utilizes the dye resazurin which is cell permeable and a redox indicator. Resazurin has been widely used as a viable cell indicator and the principle of this assay lies in the ability of cells with an active metabolism to reduce the blue resazurin to a resorufin product which is pink in colour and fluoresces (Figure 4.15). It is said that mitochondrial enzymes such as NADPH dehydrogenases are involved in the reduction reaction and are responsible for transferring electrons from $\text{NADPH} + \text{H}^+$ to resazurin (O'Brien *et al.*,2000). The amount of resorufin that is produced during this reduction is directly proportional to the number of viable cells present.

Figure 4.16 represents the results obtained following the incubation of all four cell lines with the various siRNA nanocomplexes. Similar to the results obtained from the MTT assay, all prepared siRNA: Au nanocomplexes were well tolerated by all cell lines with cell viability greater than 75%. In most cases, the percentage of resazurin reduction was much higher in the treated cells compared to the control (represented as ---- on the graphs). Following the AlamarBlue® assay, it appears that the Caco 2 cells showed resistance to cytotoxic effects (Figure 4.16 A) which contrasts with the results obtained from the MTT assay (Figure 4.14 A).

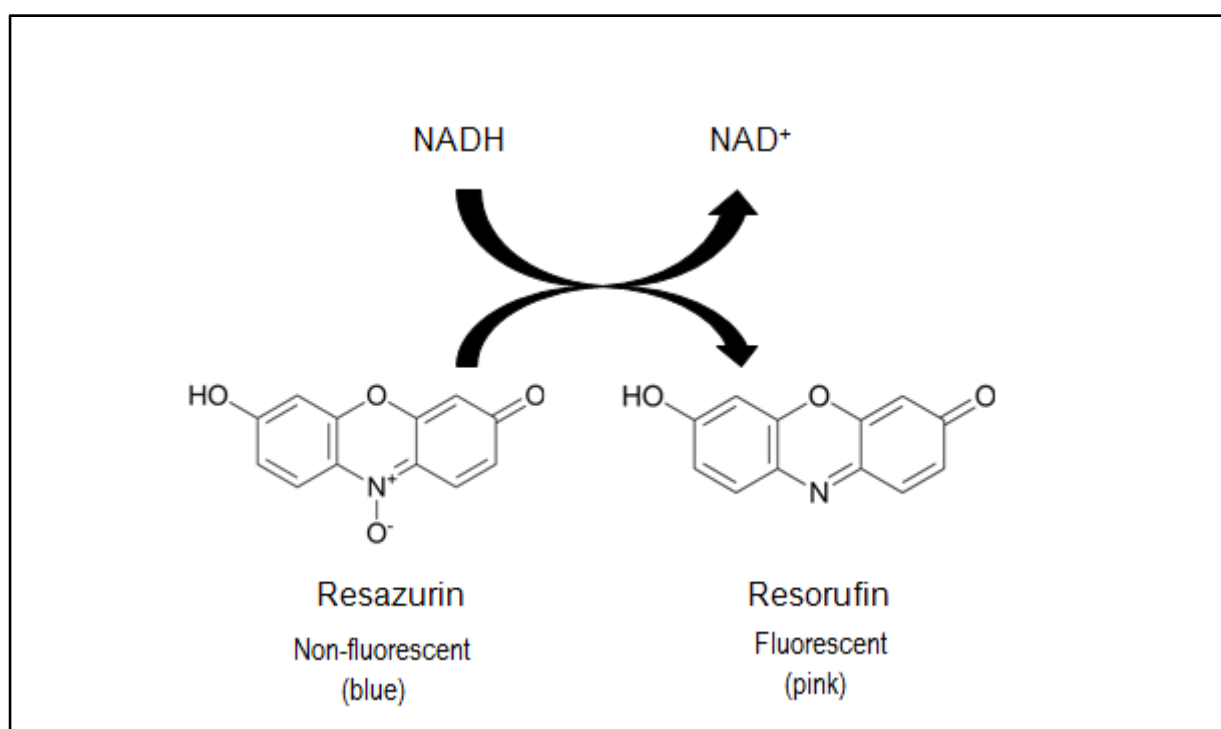
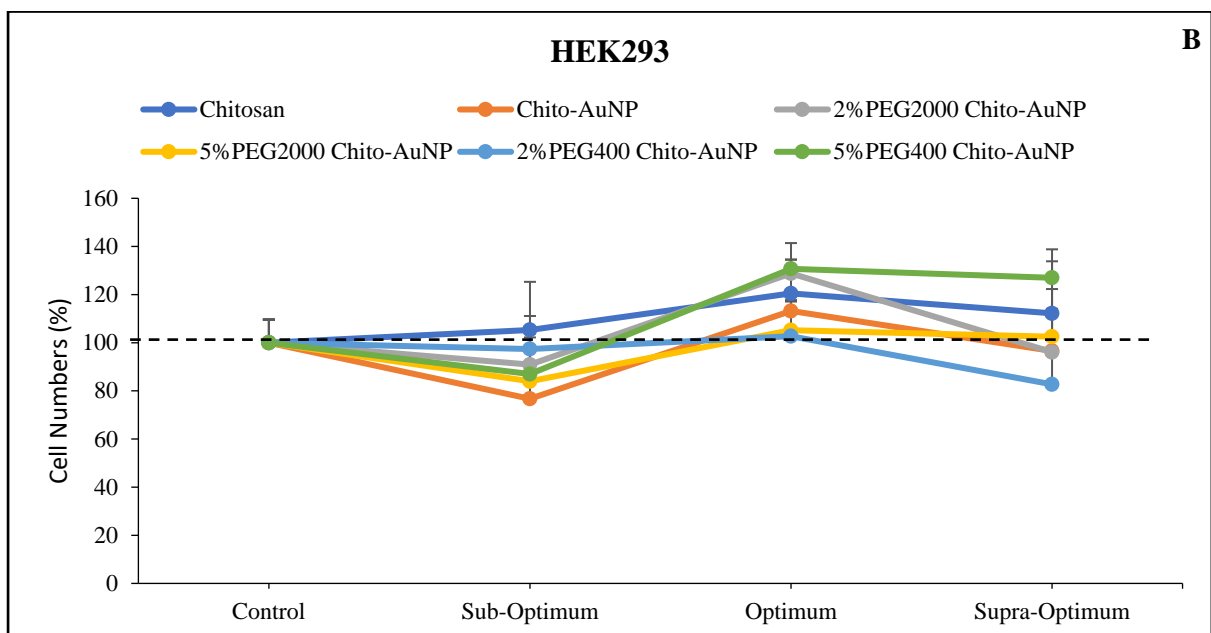
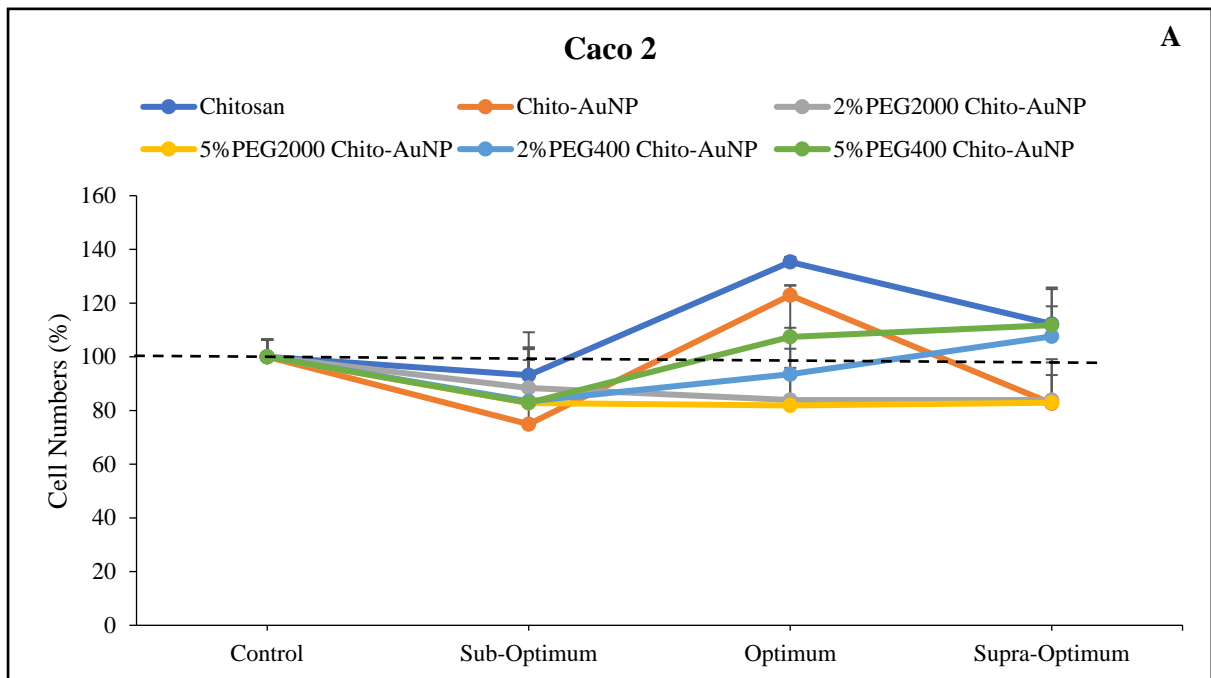


Figure 4.15: Chemical structure of resazurin and its reduction to resorufin by viable cells (Adapted from Riss *et al.*,2013).



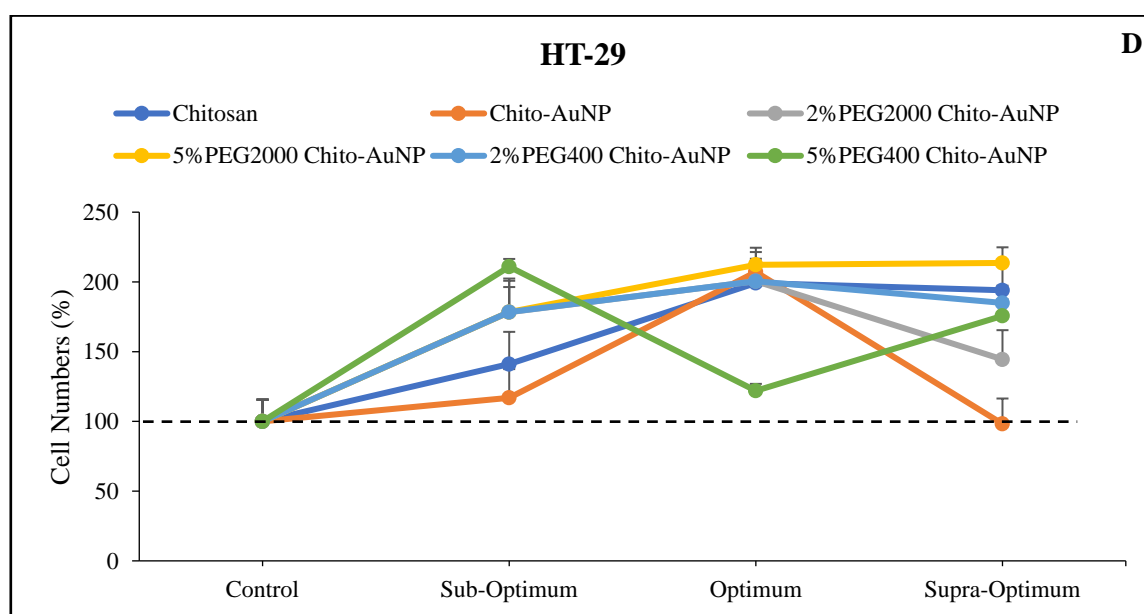
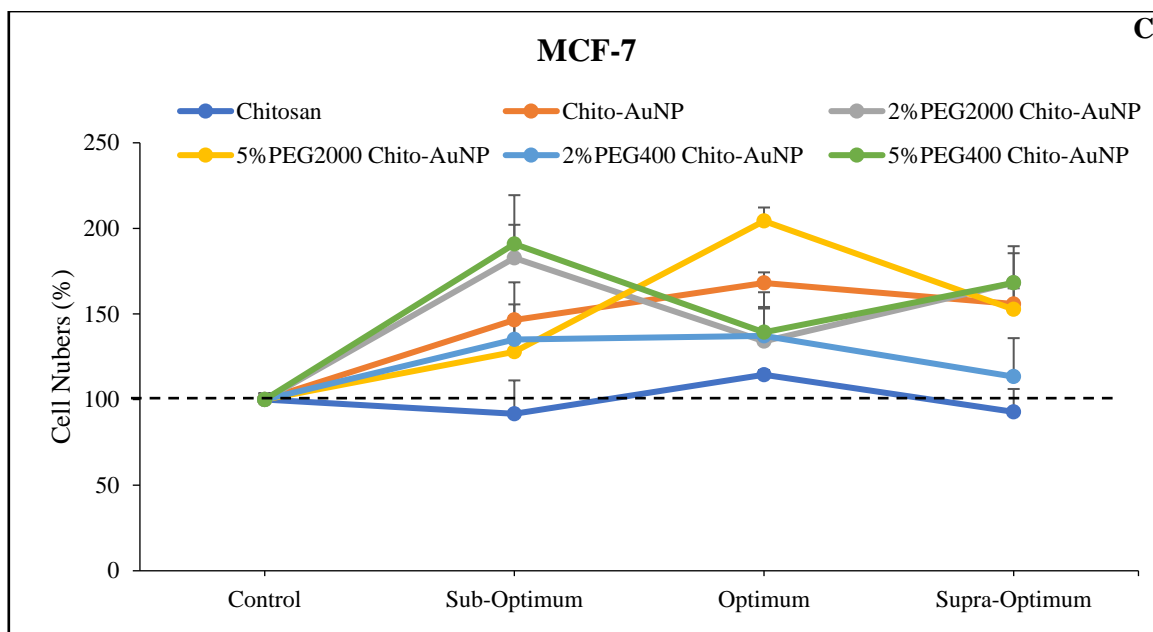


Figure 4.16: AlamarBlue® toxicity assay in (A) Caco 2, (B) HEK 293, (C) MCF-7 and (D) HT-29 cell lines. Nanocomplexes were prepared with 50 nM control, non-targeting siRNA at various siRNA: FAuNP ratios (^{w/w}). The control containing cells only were assumed to have 100 % survival. Results represented as a means \pm SD, $n = 3$.

Overall, this assay showed that all the AuNP formulations were capable of greater reduction of AlamarBlue® which correlates to a higher level of cell viability compared to the MTT assay. This can be attributed to the higher sensitivity of the AlamarBlue® assay, and therefore

suggests that it may have a higher degree of accuracy than the MTT assay. Further advantages include its higher stability, lower toxicity for cells and resazurin has a high solubility in medium (Al-Nasiry *et al.*,2007). Furthermore, the AlamarBlue® assay can be multiplexed with various other methods, for example, caspase activity may be measured, which will allow one to gain more information on cytotoxicity whereas, with the MTT assay, follow up investigations cannot be conducted on the same cells as the cell integrity may be damaged (Riss *et al.*,2013; Al-Nasiry *et al.*,2007; Rampersad, 2012).

The results obtained from both cytotoxicity assays show that all the siRNA nanocomplexes were well tolerated by all four cell lines, however, *in vivo* outcomes cannot be predicted and, hence, analysis of the data is vitally important.

4.3.3 Apoptosis Analysis using Acridine Orange/ Ethidium Bromide (AO/EB) Staining

The average cell number of multicellular eukaryotes is regulated by a combination of cell division and death during the normal function and growth of the cells. Apoptosis is a term used to describe this initiation of cell death (Kerr *et al.*,1972; Liegler *et al.*,1995). This programmed cell death is controlled genetically and is intrinsic to each cell. Apoptosis differs from necrosis, that is accidental cell death, which arises due to detrimental changes in the environment such as toxins or trauma. Apoptosis is an important study in biology as a deficiency of this cellular function is believed to be the major cause of certain diseases such as Alzheimer's, cancers, autoimmune diseases, degeneration of the central nervous system and AIDS (Ribble *et al.*,2005; Liegler *et al.*, 1995). The morphological changes of cells following apoptosis include condensation of the nucleus and chromatin, reduction of membrane integrity, cell shrinkage and membrane blebbing. Despite the many morphological changes, nuclear fragmentation and chromatin condensation are the characteristic features of apoptotic cells. There are many methods that can be utilized to study apoptotic cells, however, for this investigation, fluorescence microscopy coupled with the differential uptake of acridine orange (AO) and ethidium bromide (EB) DNA binding dyes, was employed due to its rapidity, accuracy and simplicity.

In this study, the cell viability assays, that is the MTT and AlamarBlue® assays, that were utilized showed that the AuNP preparations induced minimal cytotoxic effects to the cell lines being studied, and the AO/EB technique was conducted to evaluate if the cell death that did occur was due to apoptosis or necrosis. The siRNA: FAuNP nanocomplexes were prepared at

the ratios that exhibited the highest level of cytotoxicity and were incubated with the cell lines for 24 hours, followed by staining with AO/EB, the fluorescent images of which are depicted in Figure 4.18 (A-D). Acridine orange is a nucleic acid dye and is taken up by viable and non-viable cells and the nucleus appears green. Ethidium bromide permeates cells that have lost their membrane integrity, thereby allowing the dye to enter the cell and bind to the DNA, and hence, viable cells appear green with a normal nucleus, early apoptotic cells have a fragmented and condensed chromatin that appears as yellow-green dots with the cells appearing green. The nuclei of late apoptotic cells appear orange due to the incorporation of ethidium bromide and is fragmented and condensed. Necrotic cells differ from late apoptotic cells as they have a structurally normal nucleus and appear orange (Ribble *et al.*, 2005; Renvoize *et al.*, 1998). The apoptotic index (AI) was determined following the evaluation of the morphological changes of the cell lines from their fluorescent images. The AI is the percentage of apoptotic cells within the population and is represented as a function of the respective cell lines. These results are illustrated in Figure 4.17.

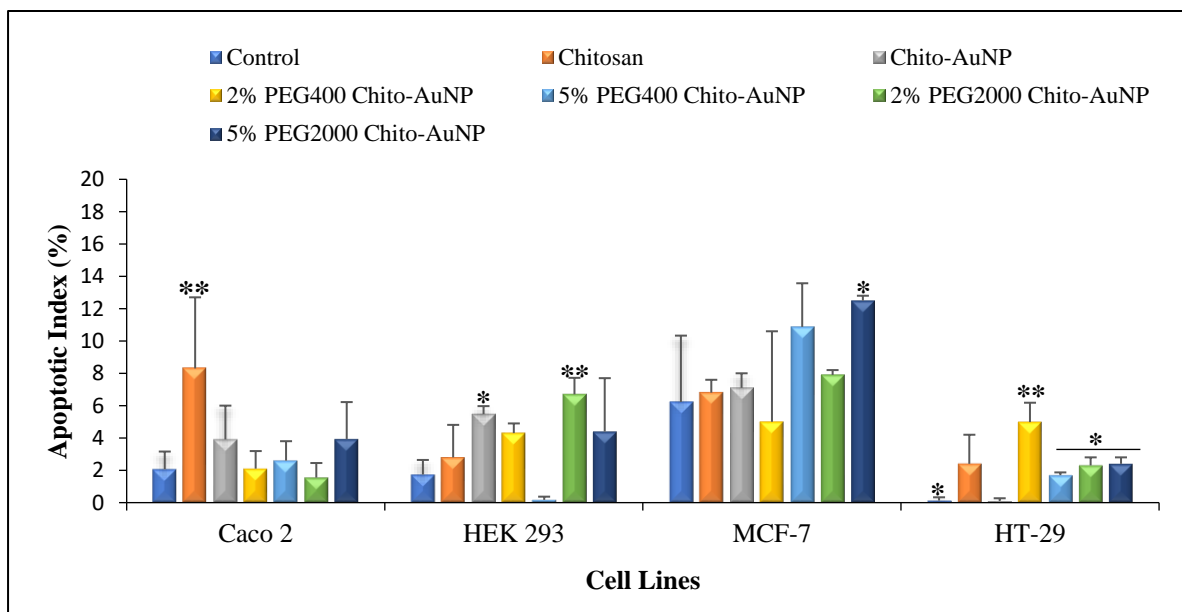


Figure 4.17: Apoptotic Index in each cell line. Nanocomplexes were prepared with 50 nM control non-targeting siRNA at the ratios that exhibited the highest cytotoxic effects and were incubated with the Caco 2, HEK293, MCF-7 and HT-29 cell lines. A control of untreated cell was utilized for each cell line. The results are represented as a mean \pm SD, $n = 3$. Statistical analysis was performed using one-way ANOVA and Dunnett multiple comparison *post hoc* test (* $P < 0.05$, ** $P < 0.01$).

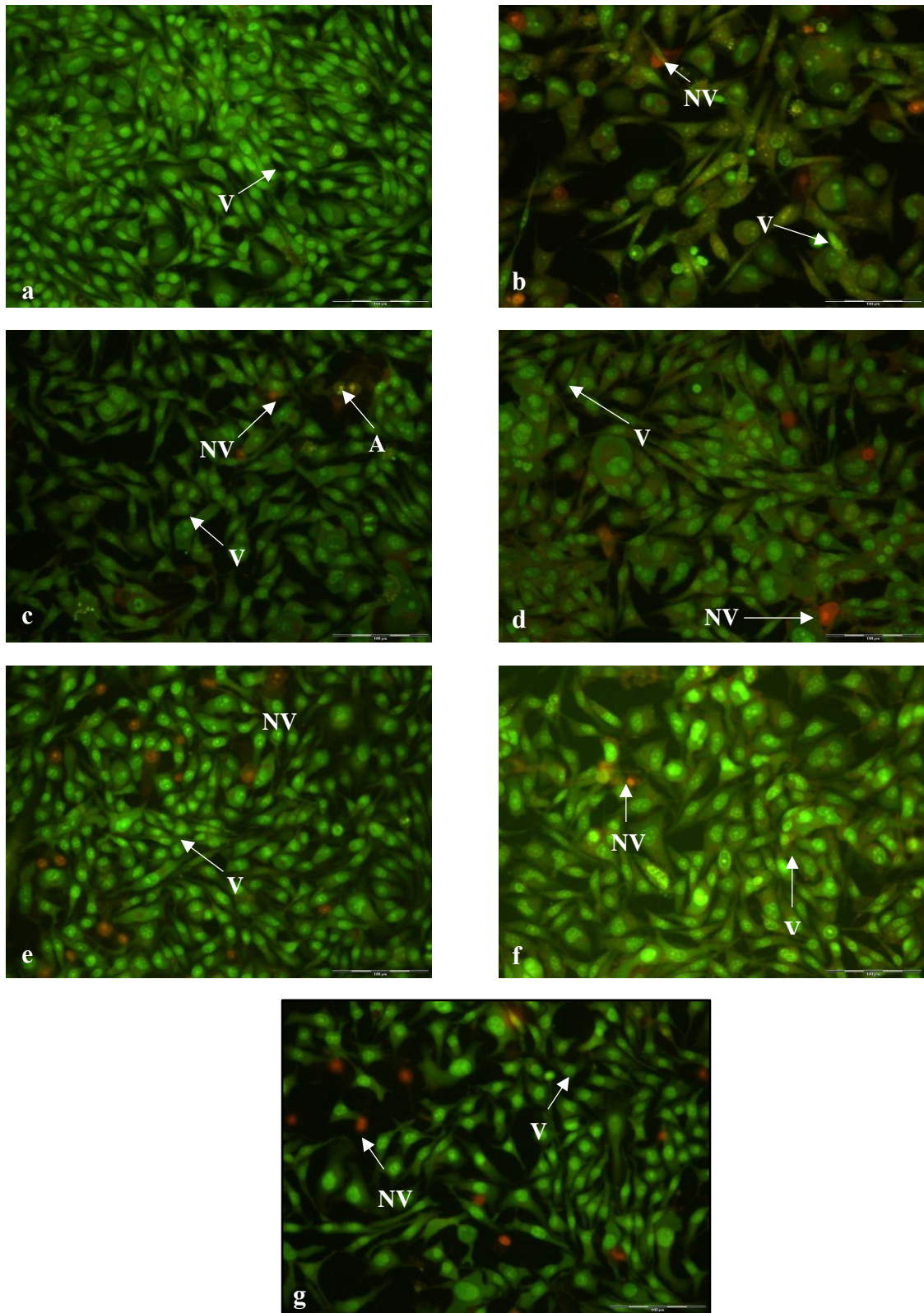


Figure 4.18 A: AO/EB dual staining and fluorescence microscopy images illustrating the changes in morphology of the Caco 2 cell line treated with (b) Chitosan, (c) Chito-AuNP, (d) 2% PEG₂₀₀₀ Chito-AuNP, (e) 5% PEG₂₀₀₀ Chito-AuNP, (f) 2% PEG₄₀₀ Chito-AuNP and (g) 5% PEG₄₀₀ Chito-AuNP nanocomplexes (containing 50 nM control, non-targeting siRNA). A control being the untreated Caco 2 cells (a) was included. **L:** Live cells and **NV:** Non-viable cells. Bar = 100 µm.

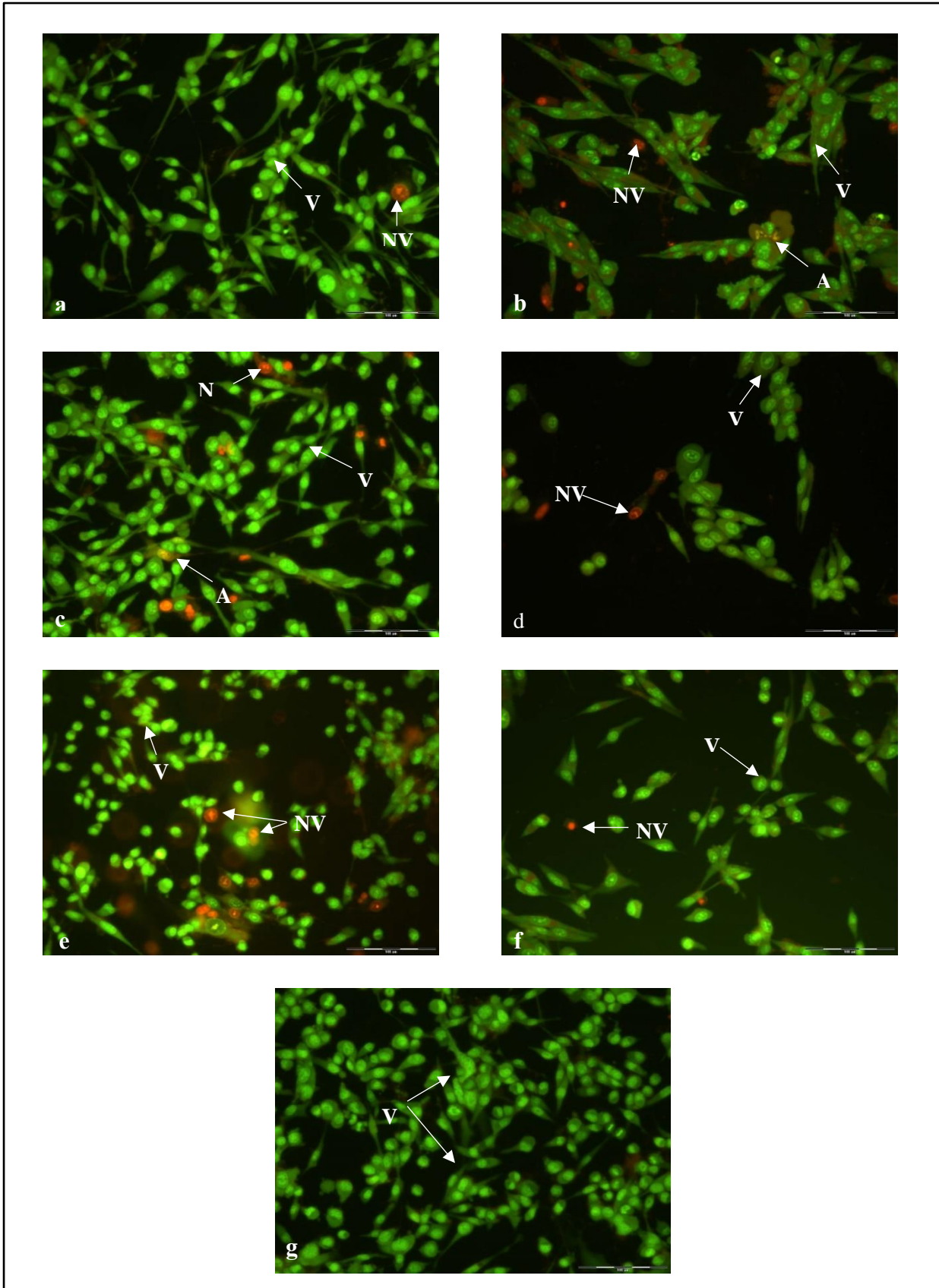


Figure 4.18 B: AO/EB dual staining and fluorescence microscopy images illustrating the changes in morphology of the HEK293 cell line treated with (b) Chitosan, (c) Chito-AuNP, (d) 2% PEG₂₀₀₀ Chito-AuNP, (e) 5% PEG₂₀₀₀ Chito-AuNP, (f) 2% PEG₄₀₀ Chito-AuNP and (g) 5% PEG₄₀₀ Chito-AuNP nanocomplexes (containing 50 nM control, non-targeting siRNA). A control being the untreated HEK293 cells (a) was included. L: Live cells, A: Apoptotic cells and NV: Non-viable cells. Bar = 100 μ m.

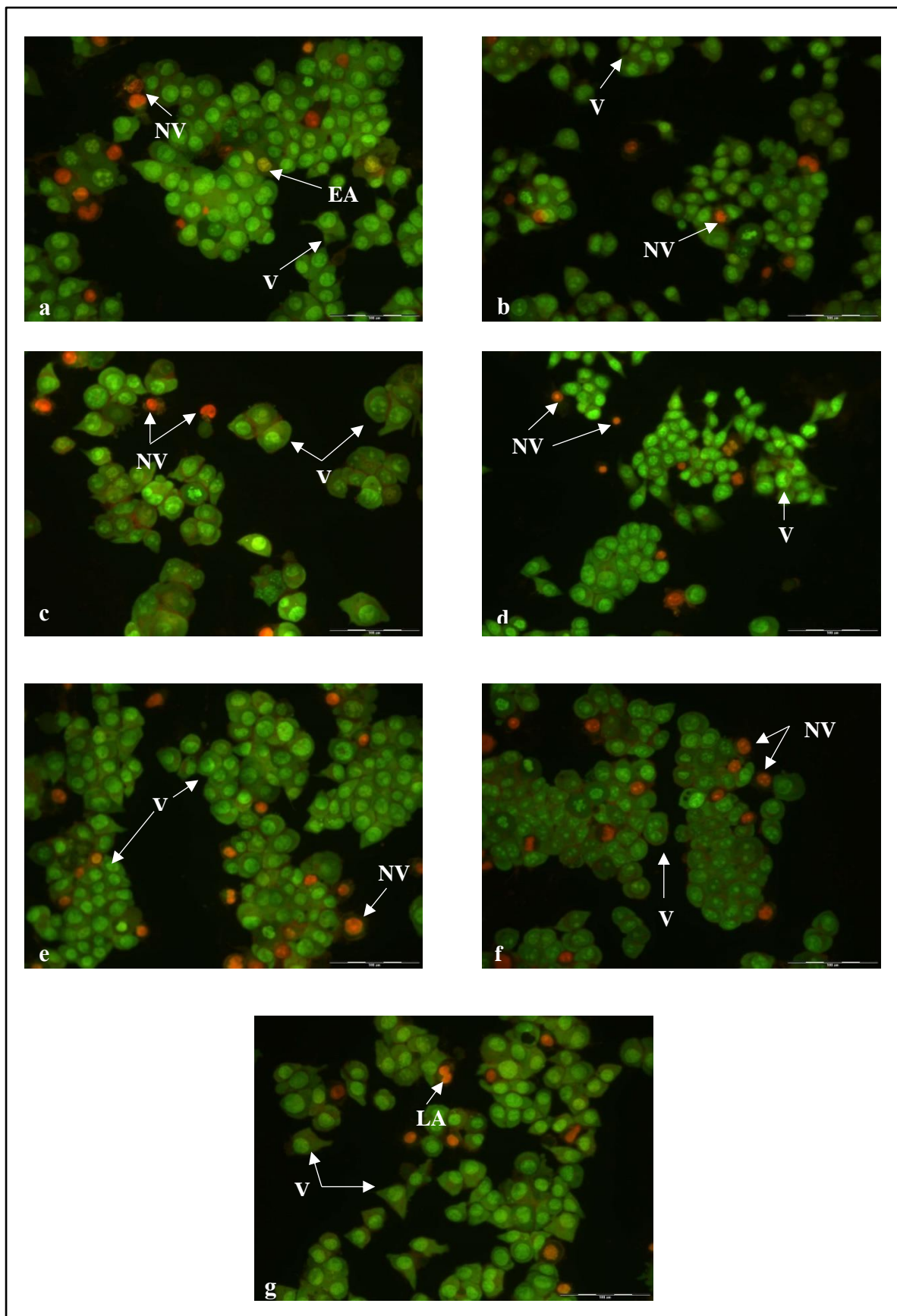


Figure 4.18 C: AO/EB dual staining and fluorescence microscopy images illustrating the changes in morphology of the MCF-7 cell line treated with (b) Chitosan, (c) Chito-AuNP, (d) 2% PEG₂₀₀₀ Chito-AuNP, (e) 5% PEG₂₀₀₀ Chito-AuNP, (f) 2% PEG₄₀₀ Chito-AuNP and (g) 5% PEG₄₀₀ Chito-AuNP nanocomplexes (containing 50 nM control, non-targeting siRNA). A control being the untreated MCF-7 cells (a) was included. L: Live cells, EA: Early Apoptotic cells, LA: Late Apoptotic cells and NV: Non-viable cells. Bar = 100 μ m

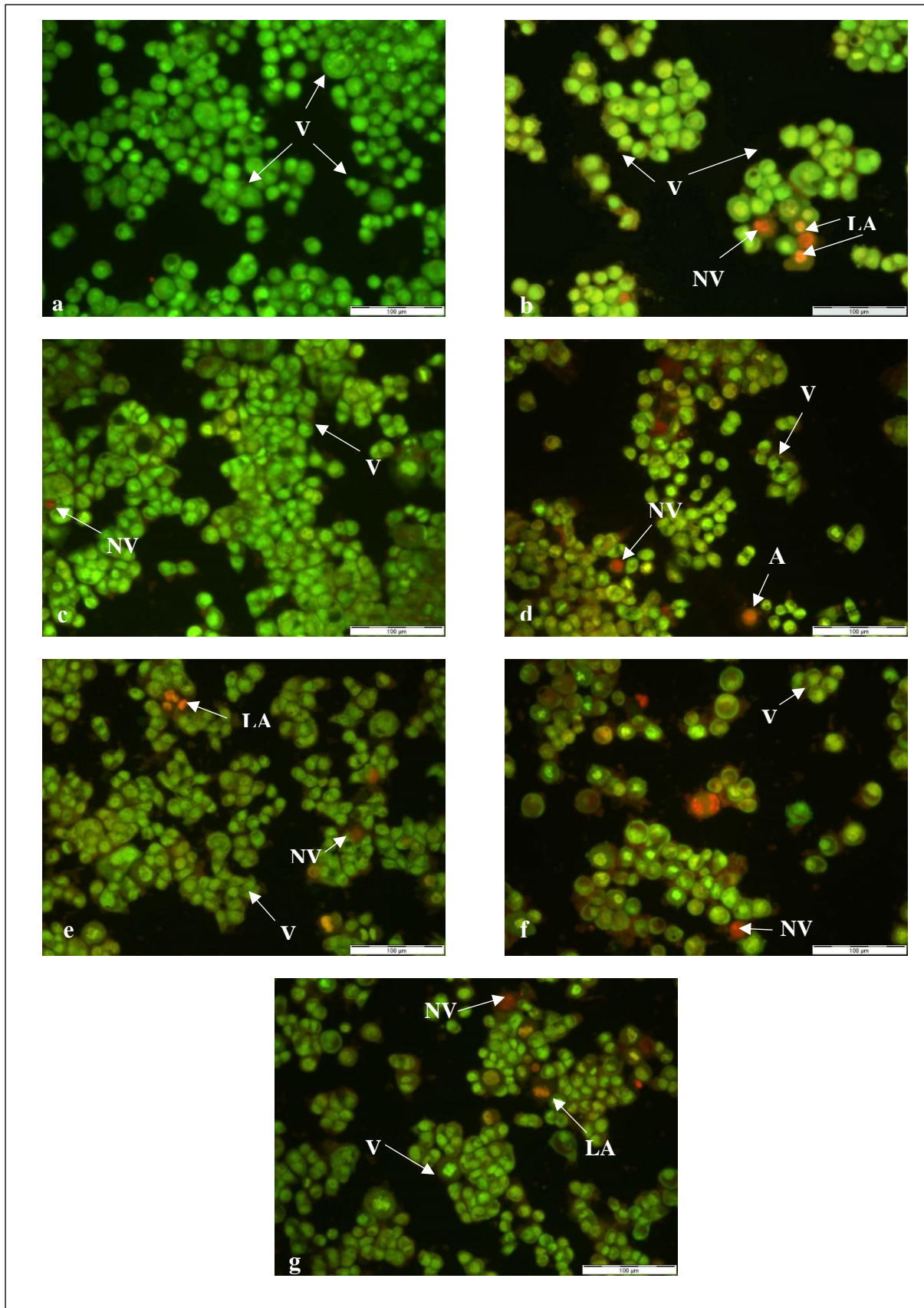


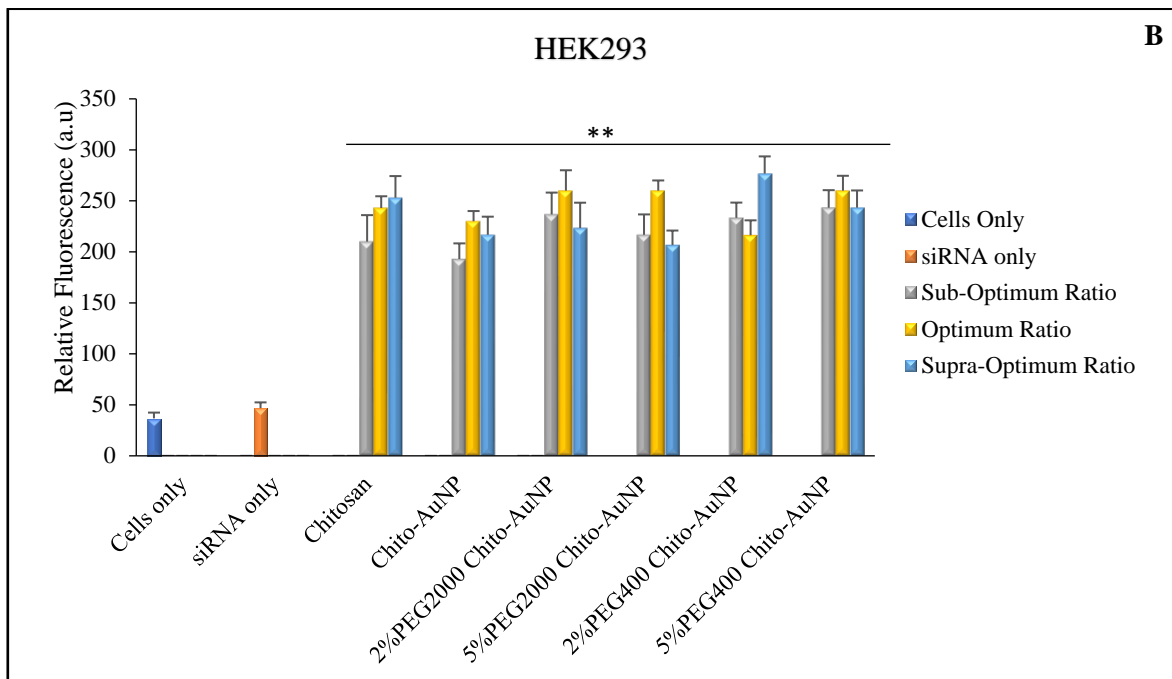
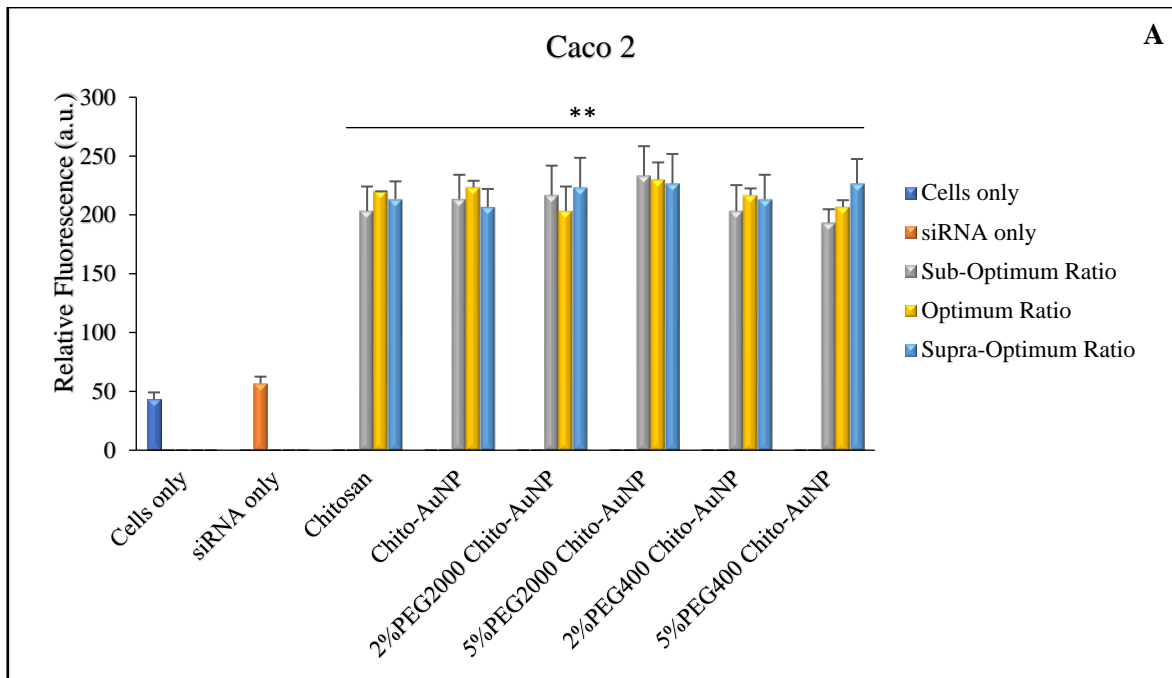
Figure 4.18 D: AO/EB dual staining and fluorescence microscopy images illustrating the changes in morphology of the HT-29 cell line treated with (b) Chitosan, (c) Chito-AuNP, (d) 2% PEG₂₀₀₀ Chito-AuNP, (e) 5% PEG₂₀₀₀ Chito-AuNP, (f) 2% PEG₄₀₀ Chito-AuNP and (g) 5% PEG₄₀₀ Chito-AuNP nanocomplexes (containing 50 nM control, non-targeting siRNA). A control being the untreated HT-29 cells (a) was included. **L:** Live cells, **A:** Apoptotic cells, **LA:** Late Apoptotic cells and **NV:** Non-viable cells. Bar = 100 µm

From the results, it can be observed that all the cell lines appear to have similar levels of apoptosis with the MCF-7 cell line exhibiting the highest level. Furthermore, cells that were treated with the different siRNA: FAuNP formulations appear to have higher levels of apoptotic cells, which can be expected. In most cases, however, these levels are extremely low and are comparable to those obtained from the control (non-treated) cells. These results do correspond with the previous cell viability assays that were conducted which showed that these AuNP preparations possess minimal cytotoxic effects, and that any cell death that did occur may be due to apoptosis and not necrosis.

4.3.4 Cellular Uptake Studies

The transfection efficiency of the PEGylated and non-PEGylated Chito-AuNPs was assessed using the BLOCK-iT™ fluorescent oligo (Dharmacon) in the Caco 2, HEK293, MCF-7 and HT-29 cell lines. The BLOCK-iT™ fluorescent oligo is a siRNA molecule that has the same length and configuration as the non-targeted control siRNA, however, this siRNA molecule is labelled with the FITC fluorescent tag. Hence, upon successful transfection, a fluorescent signal will be emitted and can be measured.

Initial attempts at this evaluation utilizing fluorescence microscopy were unsuccessful due to the optical properties of the AuNPs which quenched the fluorescent signal emitted by the FITC-tag on the siRNA and, therefore, no fluorescence was detected. Thus, the quantitative measurement of fluorescence became the method utilised as it is more sensitive, and a better interpretation of the results could be presented. The fluorescence was measured in cell homogenates following lysis of each cell line and are represented below in Figure 4.19 A-D.



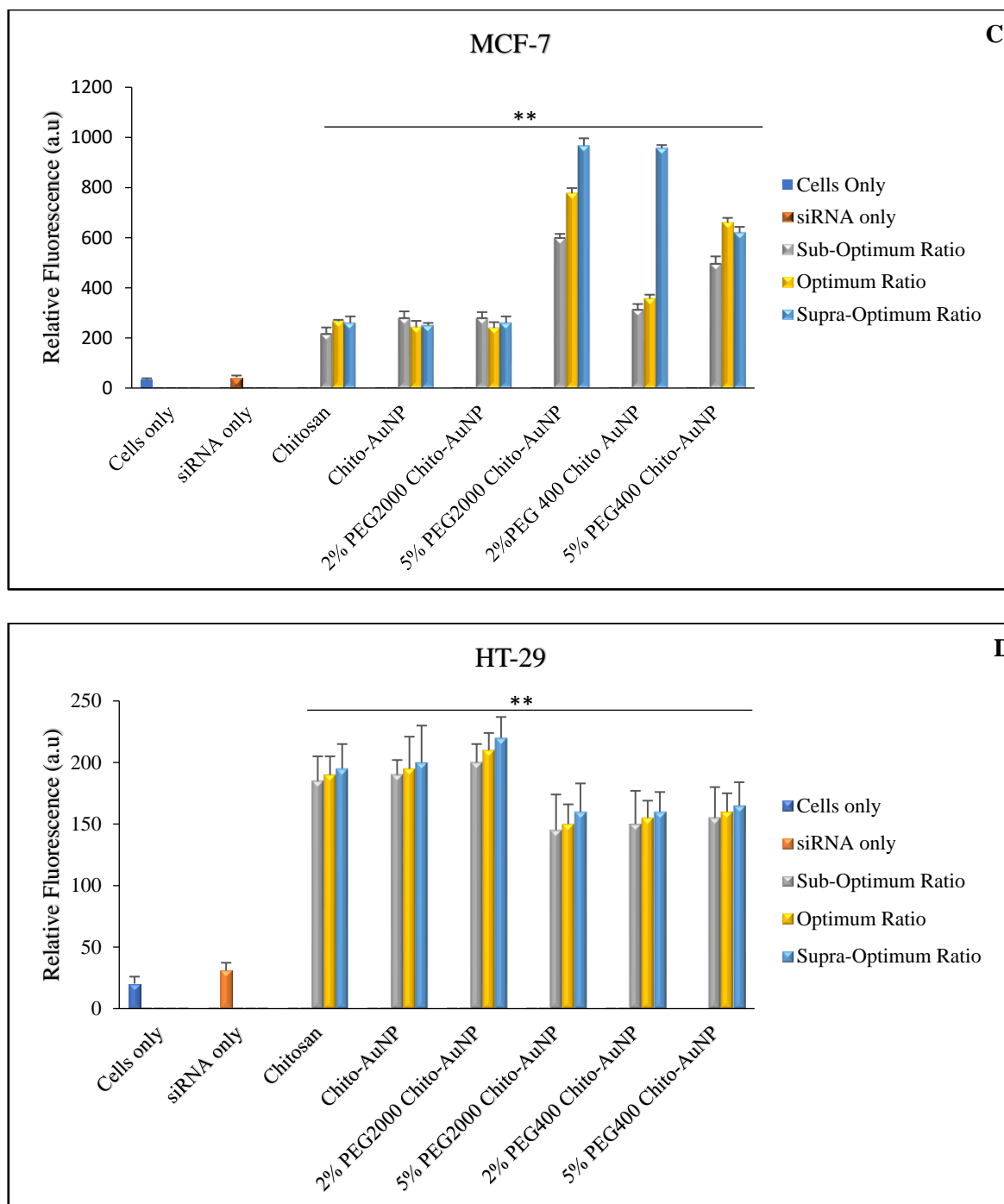


Figure 4.19: Evaluation of the cellular uptake of chitosan, PEGylated and non-PEGylated Chito-AuNPs at the sub-optimum, optimum and supra-optimum binding ratios in (A) Caco 2, (B) HEK 293, (C) MCF-7 and (D) HT-29 cell lines with 50 nM (0.067 μ g) BLOCK-iT™ Fluorescent Oligo. Two controls were utilised which included non-treated cells and cells incubated with siRNA only. Results are represented as a mean \pm SD $n=3$. Statistical analysis was carried out using one-way ANOVA followed by Dunnett multiple comparison *post hoc* test (** $P < 0.01$) indicates a significant difference.

For this study, both controls (untreated cells only and uncomplexed siRNA) exhibited very low levels of fluorescence in all four cell lines which is expected as the first control should have no

discernible fluorescence, while the cells treated with the uncomplexed BLOCK-iT™ fluorescent oligo siRNA would be degraded by serum nucleases present in the complete medium. There appears to be slight variances in the cellular uptake of the FAuNPs with respect to the different cell lines. This may be due to the differences in the cellular uptake mechanisms and plasma membrane properties of the different cell lines. The plasma membrane separates the cell interior from its environment and allows for the diffusion of non-polar and small molecules into the cell due to the semi-permeability of the membrane. AuNPs are voluntarily taken up by the cells, however, the AuNP size, shape, charge and surface modification influence their uptake (Heufner *et al.*,2014). In this investigation, the PEGylated and non-PEGylated AuNPs will be taken up by a non-specific cellular uptake mechanism. Studies that have been previously conducted have shown that the cell size and topography also have an effect on the cellular uptake mechanism. This is due to the regulation of the tension of the cell membrane and cell spreading (Huang *et al.*,2013; Huang *et al.*,2016). For this study, all the PEGylated and non-PEGylated Chito-AuNPs were successful in the delivery of the siRNA to the cell lines studied. The results show that the MCF-7 cell line exhibited the greatest level of nucleic acid uptake (Figure 4.19 C) with HT-29 exhibiting very low fluorescence levels (Figure 4.19 D). The larger the cell size, the greater the surface area for the adhesion of the AuNPs to the cell membrane which can enhance the efficiency of cellular uptake (Wang *et al.*,2016; Lesniak *et al.*,2013). This could assist in the understanding of the low transfection efficiency exhibited by the HT-29 cell line as their cell size is much smaller as compared to the other cell lines being studied which resulted in the lowest level of transfection.

Interestingly, there appears to be very small difference in the cellular uptake ability of Chitosan and the PEGylated and non-PEGylated Chito-AuNPs in the Caco 2, HEK 293 and HT-29 cell lines. However, this similarity in the results may be attributed to the fluorescence quenching of the AuNPs. The distance of the FITC tag on the siRNA molecule from the AuNP core during nanoparticle formation determines the amount fluorescence that may be emitted by the FITC tag due to the transfer of energy which prevents the emission of photons (Lévy *et al.*, 2010). The closer the FITC tag is to the AuNP core, the greater the amount of fluorescence that is inhibited. The results obtained from the dye displacement assay showed that all the AuNP preparations were capable of high levels of compaction (> 70%), which suggests that the bound siRNA will have a highly condensed nanocomplex and, hence, the FITC tag will be in close proximity to the AuNP core which will result in fluorescence quenching.

A limiting factor in the transfection efficiency of nanocomplexes is their interaction with serum proteins. The growth media utilized during *in vitro* studies contains serum proteins, amino acids, electrolytes, vitamins and antibiotics that can interact with nanoparticles. Upon interaction, the nanoparticle characteristics may change which can result in aggregation. This aggregation can affect cellular uptake due to their larger size. Plasma proteins may also adsorb to the nanoparticle surface which results in a protein shell also referred to as a protein corona (Alkilany and Murphy, 2010). It is believed that the adsorption of the negatively charged protein to the cationic AuNP formulations may result in a reversal of their charge. However, the resulting nanocomplexes utilised in this study all exhibited negative surface charges during zeta potential analysis. This may have prevented the formation of the protein corona due to repulsive electrostatic forces. Furthermore, PEGylation stabilises the nanocomplexes by inhibiting protein adsorption onto the nanocomplex and thus, aggregation is prevented and the size of the resulting nanocomplex may remain unaltered allowing for successful cellular uptake and transfection. This is the case in the MCF-7 cell line where the PEGylated Chito-AuNPs have a better cellular uptake capacity compared to the non-PEGylated Chito-AuNPs as the fluorescence levels of the cells transfected with these FAuNPs were significantly higher than the controls and their non-PEGylated counterparts. There also appears to be a dose dependant increase in the uptake levels in this cell line as at the supra-optimum ratio of 5% PEG₂₀₀₀ Chito-AuNP exhibited the highest level of fluorescence (956.6 a.u). This was also evident for the nanocomplexes prepared with 2% PEG₄₀₀ Chito-AuNP (925 a.u). This dose dependant trend was also observed in the HT-29 cell line, with 2% PEG₂₀₀₀ showing the highest level of transfection (220 a.u), however, this cell line also exhibited the greatest resistance to nanocomplex uptake.

Since all the AuNP formulations contained chitosan, this enabled the release of the siRNA nanocomplexes from the endosome due to chitosan's high amine content, which introduces positive charges into the acidic environment and allows for the release of the nanocomplex due to the proton sponge effect (Crayton and Tsourkas, 2011). This is evident due to the fluorescence measured in all four cell lines following cellular uptake of the FAuNPs which was significantly higher than that measured in the controls.

The results obtained have shown that both the PEGylated and non-PEGylated Chito-AuNPs were capable of enhancing the cellular uptake of the siRNA compared to the controls ($P < 0.01$). However, the use of a fluorescently-tagged siRNA molecule may not be a completely reliable method for the measurement of the transfection efficiency of AuNPs due to the fluorescence

quenching properties of the AuNP core. Overall, we can deduce that the use of the PEGylated and non-PEGylated Chito-AuNPs had a beneficial effect on the cellular uptake of the siRNA *in vitro*.

4.3.5 *c-MYC* Gene Silencing in MCF-7 cell line

The success of RNAi for the treatment of genetic diseases lies in the delivery of sequence specific siRNA molecules that can target the mRNA strand of interest. To evaluate the efficiency of the prepared PEGylated and non-PEGylated Chito-AuNP formulations in the delivery of *c-MYC* oncogene targeted siRNA in the MCF-7 cell line was conducted. The *c-MYC* oncogene is believed to be involved in many cellular function activities and upregulated in a variety of human cancers especially in human breast cancers. Studies conducted by Kozbar and Croce (1984) have shown elevated *c-MYC* oncogene levels in the MCF-7 cell line. Furthermore, the MCF-7 cell line has been used previously in various studies for *c-MYC* gene silencing evaluations as it is known to express high levels of this oncogene. Orr and colleagues showed that a reduction of *c-MYC* expression in the MCF-7 cell line parallels the inhibition of cell growth (Orr *et al.*, 1995). A similar result was achieved by Magnet *et al.* in 2001 and Wang *et al.* in 2005 who showed that suppression of *c-MYC* mRNA expression results in inhibition of MCF-7 tumour cells (Magnet *et al.*, 2001; Wang *et al.*, 2005). Hypoxia is found in most tumours and is involved in the malignancy associated with cancers, including breast cancers. Wu and co-workers demonstrated that exposing the MCF-7 cell line to hypoxic conditions resulted in an upregulation of *c-MYC* expression (Wu *et al.*, 2014). Due to these previous studies, it is evident that the *c-MYC* oncogene is expressed at elevated levels in the MCF-7 cell line and plays a vital role in cell growth and tumour formation, therefore, this cell line was utilized for *c-MYC* gene silencing evaluation in this study. Furthermore, the MCF-7 cell line exhibited the highest level of transfection following cellular uptake studies with the FITC-tagged siRNA (Section 4.3.4).

The siRNA utilized in the gene silencing studies was the SMARTpool™ siRNA (Dharmacon™) which consist of siRNA molecules that are designed to target four regions of the target mRNA strand (Figure 4.20). Gene silencing efficiency was measured at the mRNA and protein levels using qRT-PCR and ELISA analyses.

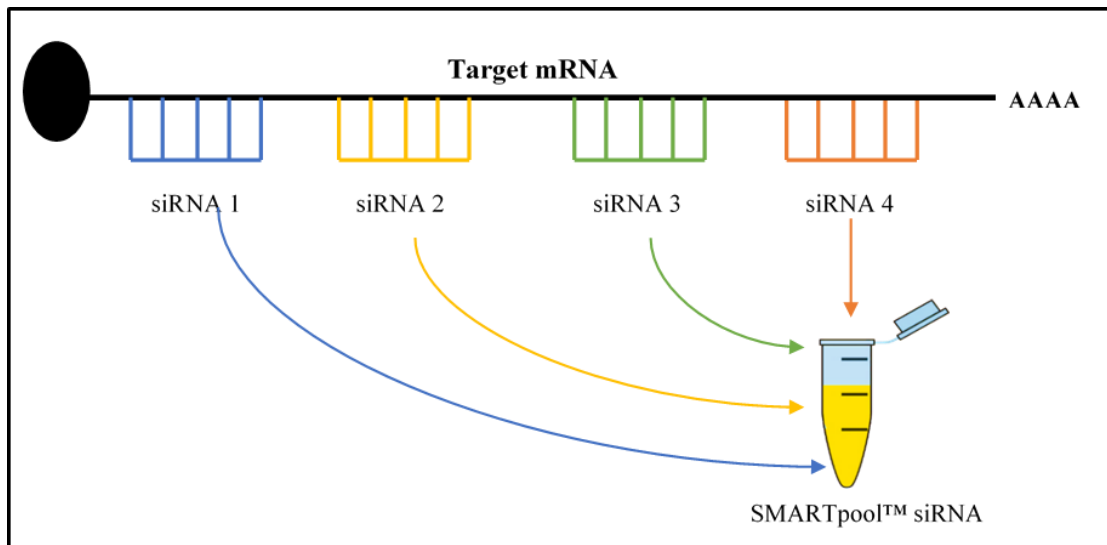


Figure 4.20: Graphical representation of the SMARTpool™ siRNA design for the target mRNA (Adapted from Dharmacon™).

4.3.5.1 Quantitative Real-Time PCR

Quantitative Real-Time PCR (qRT-PCR) has become the method of choice for the detection of low concentrations of RNA targets and is a powerful tool in molecular biology (Stephens *et al.*, 2011). There are several advantages associated with RT-PCR over PCR which include the use of a fluorescent detection system that monitors the amplification products during each PCR cycle, post-PCR processing is not required as the steps for DNA amplification and detection are in one assay, the results attained are reproducible and reliable due to minimal variations between assays, and RT-PCR is a quantitative rather than qualitative assay (Bustin and Mueller, 2005). The difference between qRT-PCR and PCR lies in the addition of an initial step which involves the conversion of RNA to cDNA by reverse transcriptase that is a RNA-dependant DNA polymerase. Following cDNA synthesis, PCR is carried that consists of three cycles, namely; exponential, linear and plateau. During the exponential phase of PCR, there is an exponential amplification of the target DNA sequence, provided that the conditions are ideal and there is 100% reaction efficiency. It is this phase that is exploited during RT-PCR for data quantification due to the doubling of the amplicon following every PCR cycle. This exponential amplification of the amplicon occurs due to the abundance of reagents and the kinetics of the reaction and results in data that is accurate and reproducible. Two values are calculated during this exponential phase, namely, the threshold fluorescence and the threshold cycle (C_t). The threshold fluorescence refers to the level of the signal that shows an increase in fluorescent intensity over the background fluorescence signal that is statistically significant. The cycle

number during the PCR reaction at which the reporter dye's fluorescent signal reaches the threshold is referred to as the C_t and is known as the qualitative end-point of the reaction and is used in relative and absolute quantification (Pfaffl,2001; Schmittgen and Livak, 2008). The reaction then begins to slow down during the linear phase due to a limitation in the reagents that are used during the reaction, and a linear production of the amplicon occurs. Once all the reagents are utilized in the PCR reaction, a plateau is reached, and the product quantity remains constant (Heid, *et al.*,1996; Yuan, *et al.*,2006).

For this study, Prime PCR™ was utilised which is a non-probe based system. This detection method makes use of the SYBR Green I dye as a fluorescent detection system which binds to dsDNA. Unbound SYBR Green I, in solution, emits little fluorescence, however, during PCR, there is an increase in the amount of dye that binds to the nascent dsDNA which results in an increase in fluorescence during polymerisation. The increase in fluorescence intensity is a direct indication of an increase in dsDNA which can monitored in real time (Morrison *et al.*,1988). An important parameter in RT-PCR is the normalization of the data which can account for any differences that may have occurred during the multi-step process (Hugget *et al.*,2005). There have been various methods for data normalization that have been used which include cell numbers, RNA and genomic DNA input, however, the most commonly employed strategy is the normalisation to housekeeper genes which are internal controls. Housekeeping genes are stably expressed in all samples and, thus, can adjust for variations between samples. This method of data normalisation was employed in this study with β -Actin (ACTB) used as the normaliser gene.

The transfection efficiency of the PEGylated and non-PEGylated Chito-AuNP formulations were assessed following the delivery of complexed c-MYC siRNA to the MCF-7 cell line. The controls used for the transfection study were the non-treated cells (calibrator); a scrambled, non-targeting siRNA (NT siRNA) sequence complexed with the FAuNPs; uncomplexed c-MYC siRNA and non-targeting siRNA and Lipofectamine® 3000 which served as a positive control. Lipofectamine® 3000 is the most extensively used, commercially available reagent for siRNA transfection and the transfection efficiency achieved with this reagent will be compared to that achieved by the FAuNPs. The control, NT siRNA was also included as a negative control as the sequence of this siRNA molecule is scrambled and is not homologous to any mRNA sequence and, thus, would be incapable of gene knockdown and will be used to confirm that sequence specific gene knockdown occurred following transfection. The prepared complexes were introduced to the MCF-7 cell line and following a 48-hour incubation the total cellular

RNA was isolated, and the concentration, quality and purity was assessed. The $^{260}/_{280}$ ratios for all the RNA samples were between 1.95-2.1 and were considered pure and of a high quality. The concentration of the isolated RNA ranged between 0.4 - 0.9 $\mu\text{g}/\mu\text{L}$.

The process of qRT-PCR was then carried out to determine gene expression and silencing with *c-MYC* specific primers. Normalization of the expression of *c-MYC* was carried out relative to ACTB. The $2^{-\Delta\Delta C_t}$ method was used to analyse the results obtained during qRT-PCR and are represented as a percentage of the fold-change in gene expression of the treated cells relative to the calibrator, that is, the non-treated MCF-7 cells and are shown in Figure 4.21. Hence, $\Delta\Delta C_t$ for the calibrator equals 0 and, therefore, 2^0 is 1 which, by definition, means that the fold change in gene expression for the MCF-7 cells is 1, and is therefore represented as 100% *c-MYC* expression. From the results, both uncomplexed siRNA molecules, i.e., the *c-MYC* and control non-targeting siRNA were incapable of eliciting any gene knockdown. This unsuccessful transfection was expected and can be attributed to the degradation of unprotected siRNA molecules by serum nucleases as seen in the RNase protection assay, hence, they were not taken up by the MCF-7 cell line and were incapable of gene knockdown. siRNA nanocomplexes were prepared between chitosan, the FAuNP formulations and the siRNA molecules at the optimum binding ratios as determined from the band shift assay. The results obtained show that the nanocomplexes prepared with the NT siRNA showed no gene knockdown with fold differences between 1.1- 1.23 (87-91%) This confirmed that the reduction of *c-MYC* expression observed in the MCF-7 cell line treated with *c-MYC* siRNA nanocomplexes was a result of sequence specific gene knockdown.

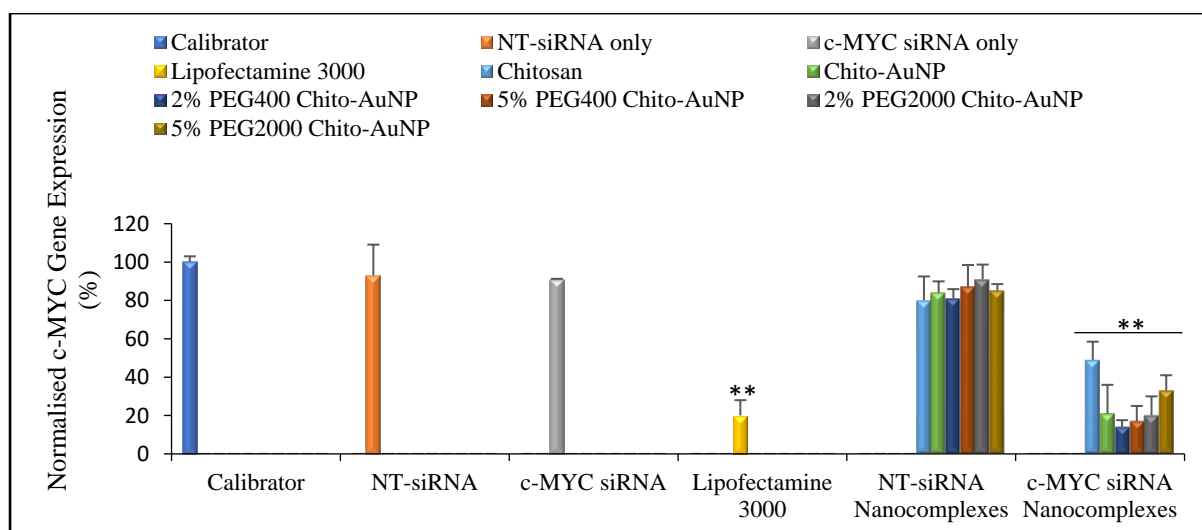


Figure 4.21: Analysis of *c-MYC* gene expression in the MCF-7 cell line. Reaction mixtures (10 μ l) were prepared at the optimum binding or N/P (+/-) ratios as determined from the band shift assay between chitosan, the FAuNP formulations and either *c-MYC* or non-targeting (NT) siRNA (0.065 μ g). Calibrator (cells only), NT siRNA only and *c-MYC* siRNA only were included as negative controls. Lipofectamine® 3000 was utilized as a positive control. The relative quantification of *c-MYC* normalized against β -Actin mRNA using the algorithm $2^{-\Delta\Delta C_t}$ (Livak and Schmittgen, 2001). Results are represented as a mean \pm SD $n = 3$. Statistical analysis was carried out using one-way ANOVA followed by Dunnett multiple comparison *post hoc* test (** $P < 0.01$) indicates a significant difference.

The five nanocomplexes prepared between the *c-MYC* siRNA and the FAuNP formulations exhibited high levels of *c-MYC* gene silencing of following qRT-PCR. This suggests that all five of the FAuNP formulations were successfully taken up by the MCF-7 cells by a passive, non-specific cellular uptake mechanism, that is, clathrin mediated endocytosis and that the reduction of *c-MYC* expression was due to sequence specific gene silencing as there was a significant difference in the gene expression levels of the siRNA nanocomplexes compared to the controls ($P < 0.01$). Chitosan was also capable of successful transfection and since all the FAuNP formulations were prepared with a constant amount of chitosan (1 mg), it can be noted that cellular uptake was enhanced and endosomal escape of the siRNA nanocomplexes occurred via the proton sponge effect due to the high amine content present in the chitosan molecule which provides a positive charge in the acidic environment within the endosome. This amine content also enhances cellular uptake by cancerous cells (Crayton and Tsourkas, 2011). The FAuNPs exhibited higher levels of gene silencing compared to chitosan alone which suggests that the presence of the AuNPs increased the efficiency of cellular uptake which resulted in better gene silencing through the stabilization of the siRNA nanocomplexes. This prevented interactions with the serum proteins and allowed the siRNA to reach the target

mRNA producing significant gene knockdown, with recorded normalized gene expressions ranging between 0.14 – 0.33 (3.01- 7.06-fold differences) (Figure 4.21). The PEG₄₀₀ PEGylated Chito-AuNPs showed gene knockdown levels that exceeded those obtained by Lipofectamine® 3000 (4.7-fold difference, 80% gene knockdown) which served as a positive control and is a commercially available transfection reagent. These PEGylated FAuNPs further enhanced the transfection efficiency of the nanocomplexes with 2% and 5% PEG₄₀₀ Chito-AuNPs exhibiting the highest level of gene knockdown (7.06-fold difference, 86% gene knockdown and 6.02-fold difference, 84% gene knockdown respectively). It does appear that the presence of PEG in these formulations further stabilized the nanocomplexes against the formation of the ‘protein corona’ and therefore, cellular uptake of these nanocomplexes was enhanced. Furthermore, the nanocomplexes that formed between the siRNA and these AuNP formulations with PEG₄₀₀ showed high levels of compaction, as determined from the dye displacement assay, which resulted in the formation of compact and condensed nanocomplexes with high levels of colloidal stability. Chito-AuNP and 2% PEG₂₀₀₀ Chito-AuNP produced a similar reduction of *c-MYC* expression (4.6 -fold difference, 79% gene knockdown and 4.7 - fold difference, 80% gene knockdown, respectively) and are comparable to Lipofectamine® 3000 (80% gene knockdown). Similarly, Gilojohann and co-workers (2009) showed that the stability of the siRNA was increased following complexation with AuNPs which resulted in gene silencing when compared to Lipofectamine® 2000 (Gilojohann *et al.*, 2009).

The trend observed following qRT-PCR mirrored that achieved following cellular uptake studies of the MCF-7 cell line where Chito-AuNP and 2% PEG₂₀₀₀ Chito-AuNP showed similar levels of cellular uptake with higher levels achieved using 2% and 5% PEG₄₀₀ Chito-AuNPs. Interestingly, in contrast to those results, 5% PEG₂₀₀₀ Chito-AuNP exhibited the lowest gene silencing of the five FAuNP formulations (3.01-fold difference, 67% gene knockdown). However, it should be noted that the cellular uptake studies utilized a FITC-tagged siRNA and the fluorescence intensity of the siRNA nanocomplex depends on the proximity of the tag to the AuNP core. Hence, due to the low levels of compaction obtained by 5% PEG₂₀₀₀ Chito-AuNP, the FITC-tag may have been further away from the AuNP core which resulted in higher fluorescence being measured. Although this AuNP preparation exhibited the lowest transfection ability of the five AuNP formulations, reduction of *c-MYC* expression was quite significant ($P < 0.01$) and comparable to their non-PEGylated and PEGylated counterparts. Overall, the qRT-PCR studies have revealed that all the PEGylated and non-PEGylated Chito-

AuNP formulations displayed significant levels of reduction of *c-MYC* gene expression in the MCF-7 cell line.

4.3.5.2 Enzyme-Linked Immunosorbent Assay (ELISA)

The level of *c-MYC* oncoprotein expression was analysed by ELISA, a powerful technique for the detection of a specific protein within a complex protein mixture. This technique was first described by Engvall and Perlmann in 1971 and allows for the analysis of immobilized protein samples in microplate wells with specific antibodies (Engvall and Perlmann, 1971). The ELISA assay comprises of four basic steps that include (i) Coating which involves the immobilisation of the protein (Antigen) to the surface of the microplate wells, (ii) Well blocking, where unsaturated sites for surface binding are covered by an irrelevant protein, (iii) Probing, where antigen-specific antibodies are incubated and bind to the antigen and (iv) Detection, which involves the measurement of the signal emitted by the tag on the specific antibody. For this study, an indirect ELISA assay was conducted which utilized a secondary antibody that was tagged with horse radish peroxidase (HRP) and its sole purpose was to deliver a signal that can be measured following specific attachment to the primary antibody that was bound to the protein of interest (Figure 4.22).

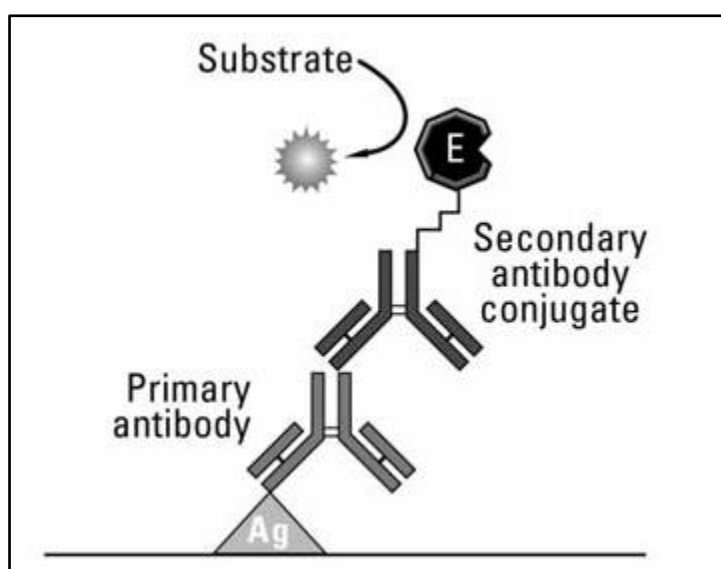


Figure 4.22: Diagrammatic representation of an Indirect ELISA assay (Thermo Fisher Scientific, 2010).

The assay set up for ELISA paralleled that of qRT-PCR, however, protein isolation was conducted 72 hours following transfection. The reference protein utilized in this assay was β -actin, which, when expressed, is a cytoskeleton protein. β -actin is known to be expressed in all cells and tissues with minimal variations among samples. The controls included in this study were the untreated MCF-7 cells, uncomplexed *c-MYC* and non-targeting (NT) siRNA and the positive control, Lipofectamine® 3000. Nanocomplexes were prepared between the FAuNPs and NT- siRNA which served as negative controls as the NT-siRNA molecule has a scrambled sequence and is not homologous to any gene. The test samples comprised of nanocomplexes prepared between chitosan, FAuNPs and *c-MYC* siRNA. The results shown in Figure 4.25 are represented as a percentage of protein expression relative to the untreated MCF-7 cells (control). The MCF-7 cells alone showed the highest level of MYC protein expression which was expected as this control group was untreated and was represented as 100% protein expression (Figure 4.23 A). The cells treated with either uncomplexed *c-MYC* or NT-siRNA also exhibited high levels of MYC oncoprotein expression, comparable to that of the untreated cells, as these siRNA molecules may have been degraded by serum nucleases during the delivery process (Figure 4.23 A). β -actin was present in all samples being tested and was expressed in high amounts, with some reaction mixtures exceeding that of the control (Figure 4.23). This protein expression was expected as β -actin is a housekeeping gene and is expressed in all cells with minimal variance. MCF-7 cells treated with NT siRNA: Au nanocomplexes did not elicit any gene knockdown which was expected, and confirmed that the reduction of MYC protein levels following transfection was due to *c-MYC* specific siRNA gene silencing (Figure 4.23 B).

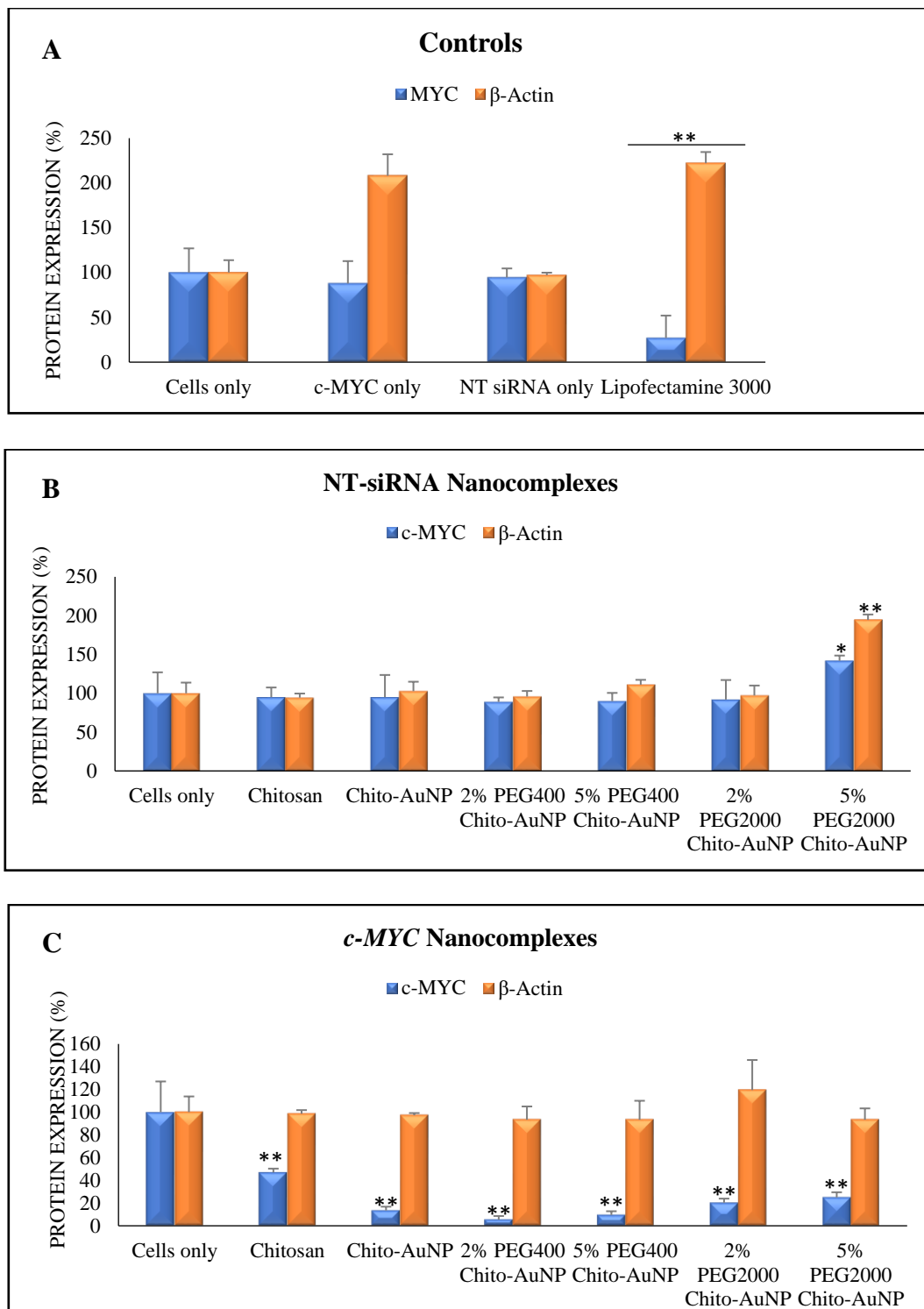


Figure 4.23: Analysis of MYC protein expression with ELISA. (A) Untreated cells, c-MYC siRNA only, NT-siRNA only, NT-siRNA only and Lipofectamine® 3000 were utilized as controls. siRNA nanocomplexes were prepared at the optimum binding ratios with the FAuNP formulations and 50 nM of either (B) NT-siRNA or (C) *c-MYC* targeted siRNA. Data represented as a mean \pm SD, $n = 3$. Statistical analysis was conducted with one-way ANOVA followed by the Dunnett multiple comparison *post-hoc* test. ($*P < 0.05$) ($**P < 0.01$) is considered significant.

All five FAuNP preparations exhibited considerable levels of transgene knockdown with MYC oncoprotein expression reduced between 75-95% (Figure 4.23 C). All five FAuNP formulations showed higher levels of knockdown when compared to chitosan alone (53% knockdown), which further suggests that the presence of AuNPs enhanced the transfection ability of chitosan, which could be also attributed to the inert core of the AuNP. Four of the five FAuNP preparations showed higher levels of transfection efficiency compared to the positive control, Lipofectamine® 3000 (75% knockdown), with 5% PEG₂₀₀₀ Chito-AuNP exhibiting similar knockdown activity.

In line with these findings, the results corroborated those attained during qRT-PCR studies with comparable levels of knockdown achieved by the PEGylated and non-PEGylated Chito-AuNPs. Following ELISA analysis, it was found that the 2 and 5% PEG₄₀₀ Chito-AuNP exhibited the highest level of *c-MYC* knockdown with protein levels reduced by 95% and 90.5%, respectively. Chito-AuNPs showed considerable knockdown levels of 86.5% with 2 and 5% PEG₂₀₀₀ Chito-AuNP exhibiting knockdown levels of 79.7% and 75%, respectively. This trend was also present after gene expression analysis following qRT-PCR. Vinhas and colleagues (2017) showed similar findings with AuNPs functionalised with thiolated PEG (356.48 Da) and incorporating a thiolated oligonucleotide for silencing of the *BCR-ABL 1* gene in the K562 cell line. They obtained a reduced gene expression using these PEGylated AuNPs suggesting that the incorporation of the PEG moiety enhanced the transfection of the oligonucleotide *in vitro* (Vinhas *et al.*, 2017).

The results obtained show that the overall negative charge of the resulting siRNA nanocomplexes, as determined by NTA analysis, was not a limiting factor as all the AuNP formulations showed significantly lower levels of MYC protein expression when compared to the control ($P < 0.01$). However, the size of the resulting nanocomplex did impact cellular uptake, as the nanocomplexes prepared with 2 and 5% PEG₂₀₀₀ Chito-AuNP were larger with lower levels of siRNA compaction and resulted in slightly higher levels of MYC oncoprotein expression. The Chito-AuNPs and 2 and 5% PEG₄₀₀ Chito-AuNPs from earlier studies have shown greater protection to the siRNA, thus resulting in safer delivery of the siRNA followed by higher levels of gene knockdown. Overall, the gene expression analysis at the mRNA and protein levels following qRT-PCR and ELISA have shown that the formulated non-PEGylated and PEGylated Chito-AuNPs can function as siRNA delivery vehicles, as evidenced by their enhanced gene silencing abilities in the MCF-7 cell line following transfection with these novel AuNP formulations

CHAPTER FIVE

CONCLUSION

5.1 Concluding Remarks

The emergence of siRNA in recent years has shown great promise and potential for the treatment of diseases through the silencing of aberrant levels of expression of various oncogenes or genes involved in cancer progression and the regulation of cell cycles. Provided that the sequence of the gene of interest is known, siRNA molecules can be designed to target and potentially knockdown the overexpression of the disease-causing gene. Despite the development of numerous non-viral gene vectors over the past two decades, the use of siRNA-based gene therapy remains at a juncture due to poor cellular uptake, cytotoxicity and the degradation of the siRNA molecules in the presence of nucleases limits their application both *in vitro* and *in vivo*. Therefore, the challenge facing the use of siRNA-based therapeutics is the development of a delivery vehicle that is safe and efficient while enhancing cellular uptake and endosomal escape of the siRNA molecule.

This study assessed the ability of five cationic AuNP-based formulations to enhance the cellular uptake efficiency of siRNA in four cell culture models and to evaluate the effect of the *c-MYC* targeted siRNA in *c-MYC* oncogene silencing in the *MYC*-overexpressing MCF-7 cell line. The sterically stabilised, cationic FAuNPs containing PEG₄₀₀ or PEG₂₀₀₀ were capable of successfully binding and protecting the siRNA molecules against degradation from RNase A. The particle sizes and zeta potentials of the FAuNPs and their corresponding nanocomplexes with siRNA were favourable and were found to be spherical in shape. These FAuNP preparations were stable at room temperature with minimal aggregation observed for the duration of the study (36 months). The FAuNP formulations were well tolerated by the HEK293, Caco 2, MCF-7 and HT-29 cell culture models and exhibited minimal cytotoxicity with cell survival exceeding 75%. Further evaluation of the cytotoxicity indicated that apoptosis was the predominant mechanism of cell death.

Cellular uptake studies of all nanocomplexes were significantly enhanced when compared to the two controls utilized ($P < 0.01$), which showed indiscernible fluorescence. However, the FITC-labelled siRNA complexed to the FAuNPs exhibited considerably higher levels of fluorescence in all four cell line models *in vitro*. This suggests a relative ease in the mechanism

of cellular uptake, that is endocytosis, and endosomal escape of the siRNA: FAuNP nanocomplexes which resulted in the delivery of intact siRNA. This is a promising feature as the main site of action of the siRNA molecules is in the cytoplasm.

With regards to *c-MYC* siRNA delivery, gene expression studies revealed that the nanocomplexes produced superior levels of transfection compared to chitosan alone. This may be attributed to the presence of the AuNP core which is electrokinetically stable. Furthermore, four of the five FAuNP formulations exhibited higher levels of gene silencing than that of the Lipofectamine 3000[®] (80% gene knockdown), and the FAuNPs that were PEGylated with PEG₄₀₀ induced the highest *c-MYC* oncogene silencing effect (86% and 83%) and showed comparable levels of gene knockdown to the non-PEGylated and PEG₂₀₀₀ PEGylated Chito-AuNPs (> 77% gene knockdown). This trend was further confirmed by ELISA studies which showed decreased c-MYC protein levels in cells treated with the FAuNP formulations (> 75%) with the highest level of gene knockdown exhibited by 2 and 5% PEG₄₀₀ Chito-AuNPs (94.6% and 90.5%, respectively). All the FAuNP formulations displayed high levels of compaction and binding of siRNA, and low cytotoxicity as determined from the dye displacement, MTT and AlamarBlue[®] assays, respectively. These results have suggested that the FAuNPs can enhance the *in vitro* transfection of the siRNA in the model MCF-7 cell line.

The results obtained further confirm the potential of all FAuNP formulations to enhance cellular uptake in the cell culture models studied and silencing of the *c-MYC* oncogene in the MCF-7 cell line, supporting the hypothesis that the PEGylated and non-PEGylated Chito-AuNPs hold great potential for future siRNA gene-based delivery. These findings will allow for the treatment of human diseases at the post-transcriptional level and with optimizations can be further developed and enhanced for clinical applications.

Possible limitations to this investigation included the use of a fluorescent oligo to assess the cellular uptake efficiency of the FAuNPs. Although all FAuNP preparations exhibited enhanced cellular uptake capabilities compared to the uncomplexed siRNA, the fluorescence quenching by the AuNP core may have hindered the evaluation of the true potential of these FAuNP preparations. A possible solution to determine the efficiency of siRNA delivery by the FAuNPs across various cell lines may be the use of siTOX siRNA molecules that induce cell death upon successful transfection. Since all the FAuNPs showed minimal cytotoxicity, one can conclude that a decrease in cell viability using siTOX is due to successful delivery and cellular uptake of the intact siRNA molecule.

Future studies and recommendations, can include the addition of targeting ligands incorporated into the FAuNP formulation, which will allow for specificity of the AuNP vector to the target tissue. For example, the addition of an asialoglycoprotein moiety to the AuNP preparation can be used to target hepatocytes, or the inclusion of a transferrin ligand can be beneficial in crossing the blood-brain barrier. Further investigations are required to understand the cellular uptake mechanisms and intracellular trafficking of the nanocomplexes which will allow for improvement of the efficiency of the delivery vehicle. Furthermore, due to the optical properties associated with the AuNP core, these nanoparticles can be used for bioimaging and can, therefore, be used in medicine as diagnostic tools.

In summary, the FAuNP formulations used in this study were capable of successfully binding and protecting the siRNA against degradation, with minimal toxicity and enhanced gene silencing ability, making these nanoparticles attractive options for the therapeutic delivery of siRNA *in vivo*.

REFERENCES

- Aargaard L., and Rossi J.J. (2007). *RNAi therapeutics: Principles, prospects and challenges*. *Advanced Drug Delivery Reviews*. **59**: 75-86.
- Aigner A. (2006). *Gene Silencing through RNA interference (RNAi) in vivo: strategies based on the direct application of siRNAs*. *Journal of Biotechnology*. **124**: 12-25.
- Adhikary S., and Eilers M. (2005). *Transcriptional regulation and transformation by MYC protein*. *Nature Reviews Molecular Cell Biology*. **6**: 635-645.
- Akbarzadeh A., Razaeei-Sodabody R., Davaran S., Jao S.W., Zarghami N., Hanifehpour Y., Samiei M., Kouhi M., and Nejati-Koshk K. (2013). *Liposome: classification, preparation and applications*. *Nanoscale Research Letters*. **8**: 102-111. doi: 10.1186/1556-276X-8-102.
- Akhtar S., and Benter I. (2007). *Toxicogenomics of non-viral drug delivery systems for RNA interference: Potential impact on small interfering RNA mediated gene silencing activity and specificity*. *Advanced Drug Delivery Reviews*. **59**:164-182.
- Akinc A., Thomas M., Klivanov A.M., and Langer R. (2005). *Exploring polyethyleneimine-mediated DNA transfection and the proton sponge hypothesis*. *The Journal of Gene Medicine*. **7**: 657-663.
- Al-Nasiry S., Geusens N., Hansens M., Luyten C., and Pijenenborg R. (2007). *The use of Alamar Blue assay for quantitative analysis of viability, migration and invasion of choriocarcinoma cells*. *Human Reproduction*. **22**: 1304-1309.
- Alameh M., Dejesus D., Jean M., Darras V., Thibault M., Lavertu M., Buschmann M.D., and Merzouki A. (2012). *Low molecular weight chitosan nanoparticulate system at low N:P ratios for non-toxic polynucleotide delivery*. *International Journal of Nanomedicine*. **7**: 1399-1414.
- Albanese A., and Cha W.C.W. (2003). *Effect of Gold Nanoparticle Aggregation on Cell Uptake and Toxicity*. *ACS Nano*. **5(7)**: 5478-5489.
- Albanese A., Tang P.S., and Chan W.C.W. (2012). *The Effect of Nanoparticle Size, Shape and Surface Chemistry on Biological Systems*. *Annual Review of Biomedical Engineering*. **14(1)**: 1-16.
- Alexis F., Pridgen E., Molnar L.K., and Farokhzad O.C. (2008). *Factors affecting the clearance and biodistribution of polymeric nanoparticles*. *Molecular Pharmaceutics*. **5(4)**: 505-515.

- Alivisatos P. (2003). *The use of nanocrystals in biological detection*. Nature Biotechnology. **22**: 47-51.
- Alkilany A.M., and Murphy C.J. (2010). *Toxicity and cellular uptake of gold nanoparticles: what we have learned so far?* Journal of Nanoparticle Research. **12**: 2313-2333.
- Alvarez M.M., Khoury J.T., Schaff T.G., Shafiqullin M.N., Vezmar I., and Whetten R.L. (1997). *Optical Absorption Spectra of Nanocrystal Gold Molecules*. The Journal of Physical Chemistry B. **101**: 3706-3712.
- Amer M.H. (2014). *Gene Therapy for cancer: present status and future perspective*. Molecular and Cellular Therapies. **2**:27-46. doi: 10.1186/2052-8426-2-27.
- Anderson M.E. (1998). *Glutathione: An overview of biosynthesis and modulation*. Chemico-Biological Interactions. **111(112)**: 1-14.
- Antila H.S., Härkönen M., and Sammalkorpi M. (2015). *Chemistry specificity of DNA-polycation complex salt response: a simulation study of DNA, polylysine and polyethyleneimine*. Physical Chemistry Chemical Physics. **17**: 5279-5289.
- Avizo R., Bhattacharya R., and Mukherjee P. (2010). *Gold nanoparticles: Opportunities and challenges in nanomedicine*. Expert Opinion Drug Delivery. **7**: 753-763.
- Ashworth A, Lord C.J., and Reis-Filho J.S. (2011). *Genetic interactions in cancer progression and treatment*. Cell. **145(1)**: 30-38.
- Augenlicht L.H., Wadler S., Corner G., Richards C., Ryan L., Multani A.S., Pathak S., Benson A., Haller D., and Heerdt B.G. (1997). *Low level c-MYC amplification in human colonic carcinoma cell lines and tumours: a frequent p53- independent mutation associated with improved outcome in a randomized multi-institutional trial*. Cancer Research. **48**: 199-205.
- Baldrick P. (2010). *The safety of chitosan as a pharmaceutical excipient*. Regulatory toxicology and Pharmacology. **56**: 290-299.
- Baliki D., and Beutler E. (2002). *Gene therapy of human disease*. Medicine. **81(1)**: 69-86.
- Banan M., and Puri N. (2004). *The ins and outs of RNAi in mammalian cells*. Current Pharmaceutical Biotechnology Journals. **5(5)**: 441-450.

- Bartlett D.W., and Davis M.E. (2006). *Insights into the kinetics of siRNA-mediated gene silencing from live-cell and live animal bioluminescent imaging*. *Nucleic Acids Research*. **34**: 322-333.
- Basal M., Mertens A.C., Taylor L., Neglia J.P., Greffe B.S., Hammond S., Ronckers C.M., Friedman D.L., Stovall M., Yasui Y.Y., Robinson L.L., Meadows A.T., and Kadan-Lottick N.S. (2006). *Risk of selected subsequent carcinomas in survivors of childhood cancer: a report from the child cancer survivor study*. *Journal of Clinical Oncology*. **24(3)**:476-483.
- Bertram J.S. (2001). *The molecular biology of cancer*. *Molecular Aspects of Medicine*. **21**: 167-223.
- Bhattarai S.R., Bahadur R., Bahadur R.K.C., Aryal S., Bhattarai N., Kim S.Y., Yi H.K., Hang P.H., and Kim H.Y. (2008). *N- hexanoyl chitosan stabilized magnetic nanoparticles: Implication for cellular labelling and magnetic resonance imaging*. *Journal of Nanobiotechnology*. **6**:1-9. doi: 10.1186/1477-3155-6-1.
- Bibi S., Kaur R., Henriksen-Lacey M., McNeil S.E., Wilkhu J., Lattman E., Christensen E., Mohammed R.A., and Perrie Y. (2011). *Microscopy imaging of liposomes: From coverslips to environmental SEM*. *International Journal of Pharmaceutics*. **417**: 138-150.
- Biswas S., and Torchillin V. (2013). *Dendrimers for siRNA delivery*. *Pharmaceutics*. **6**: 161-183.
- Blackwood E.M., and Eisenmann R.N. (1991). *Max: a helix-loop-helix zipper protein that forms a sequence- specific DNA- binding complex with MYC*. *Science*. **251**: 1211-1217.
- Boca S.C., Potara M., Toderas F., Stephan O., Baldeck P.L., and Astilean S. (2010). *Uptake and biological effects of chitosan -capped gold nanoparticles on Chinese Hamster ovary cells*. *Materials Science and Engineering C*. **31**: 184-189.
- Boisselier E., and Astruc D. (2009). *Gold nanoparticles in nanomedicine: preparations, imaging, diagnostics, therapies and toxicity*. *Chemical Society Reviews*. **38(6)**: 1759-1782.
- Bosch A., Eroles P., Zaragoza R., Vina J.R., and Lluch A. (2010). *Triple-negative breast cancer molecular features, pathogenesis treatment and current lines of research*. *Cancer Treatment Reviews*. **36**: 206-215.
- Bouclier C., Maine L., Hillaireau H., Marsoud V., Connault E., Opolon P., Couvreur P., Fattal E., and Renoir J.M. (2008). *Physicochemical characteristics and preliminary in vivo biological*

evaluation of nanocapsules loaded with siRNA targeting estrogen receptor alpha. Biomacromolecules. **9**:2881-2890.

Boyes S.G., Rowe M.D., and Hotchkiss J. (2009). *Gold nanoparticle conjugate and uses thereof.* US20090060839A1.

Brigger J., Dubernett C., and Couvreur P. (2012). *Nanoparticles in cancer therapy and diagnosis.* Advanced Drug Delivery Reviews. **59**: 24-36.

Bronstein L.M., and Shifrina Z.B. (2012). *Dendrimers as Encapsulating, Stabilizing, or Directing Agents for Inorganic Nanoparticles.* Chemical Reviews. **111(9)**: 5301-5344.

Brust M., Fink J., Bethell D., Schiffron D.J., and Kiely C.J. (1994). *Synthesis and Reactions of Functionalised Gold Nanoparticles.* Journal of the Chemical Society, Chemical Communications. **16**: 1655-1656.

Brust M., Walker M., Bethell D., Schiffrin D.J., and Whyman R.J. (1994). *Synthesis of Thiol-Derivatized Gold Nanoparticles in a two-phase Liquid-Liquid System.* Journal of the Chemical Society, Chemical Communications. **7**:801-802.

Bustin S.A., and Mueller R. (2005). *Real-time reverse transcription PCR (qRT-PCR) and its potential use in clinical diagnosis.* Clinical Science. **109(4)**: 365-379.

Cabral R.M., and Baptista P.V. (2013). *The Chemistry and Biology of Gold Nanoparticle Mediated Photothermal Therapy: Promises and Challenges.* NanoLIFE. doi: 10.1142/5179398441330001X.

Cai D., Montarazza J.M., Qin Z.H., Huang Z., Huang J., Chiles T.C., Carnahan D., Kempa K., and Ren Z. (2005). *Highly efficient molecular delivery into mammalian cells using carbon nanotube spearing.* Nature Methods. **2**: 449-454.

Cai W., Gao T., Hong H., and Sun J. (2008). *Applications of gold nanoparticles in cancer technology.* Nanotechnology, Science and Applications. **1**:17-32.

Çağdaş M., Sezer A.D., and Bucak S. (2014). *Liposomes as Potential Drug Carrier Systems for Drug delivery.* Nanotechnology and Nanomaterials. doi: 10.5772/58459.

Cao-Milán R., and Liz-Marzán L.M. (2014). *Gold nanoparticle conjugates: recent advances toward clinical application.* Expert Opinion in Drug Delivery. **11(5)**: 741-752.

- Capco D.G., and Chen Y. (2014). *Nanomaterial Impacts on Cell Biology and Medicine*. Volume 811 of Advances in experimental medicine and biology. Springerlink: Bücher. Springer Science and Business Media. ISBN: 9401787395, 9789401787390.
- Carpin L.B., Bicford L.R., Agollah G., Yu T.K., Schiff R., Li Y., and Drezek R.A. (2011). *Immunoconjugated gold nanoshell-mediated photothermal ablation of trastuzumab-resistant breast cancer cells*. Breast Cancer Research and Treatment. **125**:27-34.
- Chattopadhyay D.P., and Inamdar M.S. (2010). *Aqueous Behaviour of Chitosan*. International Journal of Polymer Science. **2010**:1-7. doi: 10.1155/2010/939536.
- Chen M.K., Espat N.J., Bland K.I., Copeland E.M. 3rd., and Souba W.W. (1993). *Influence of progressive tumour growth on glutamine metabolism in skeletal muscle and kidney*. Annals of Surgery. **217**: 655-666, discussion 66-67.
- Chen M.S., and Goodman D.N. (2004). *The structure of catalytically active gold in titania*. Science. **306(5694)**: 252-255.
- Cheng Y.Y., and Xu T.W. (2005). *Dendrimers as potential drug carriers. Part I. Solubilization of non-steroidal anti-inflammatory drugs in the presence of polyamidoamine dendrimers*. European Journal of Medicinal Chemistry. **40**: 1188-1192.
- Cho B.C., Kim E.H., Choi H.J., Kim J.H., Roh J.K., Chung H.C., Ahn J.B., Lee J.D., Lee J.T., Yoo N.C., and Sohn J.H. (2005). *A pilot study of trans-arterial injection of 166 holium-chitosan complex for treatment of small hepatocellular carcinoma treatment*. Yonsei Medical Journal. **46**: 799-805.
- Cho E.C., Zhang Q., and Xia Y. (2011). *The effect of sedimentation and diffusion on cellular uptake of gold nanoparticles*. Nature Nanotechnology. **6**: 385-391.
- Ciolkowski M., Palecz B., Appelhans D., Voit B., Klajnert B., and Bryszewska M. (2012). *The influence of maltose modified poly(propylene imine) dendrimers on hen egg white lysozyme structure and thermal stability*. Colloids and Surfaces B: Biointerfaces. **95**: 103-108.
- Cole M.D., and Cowling V.H. (2009). *Specific regulation of mRNA cap methylation by c-Myc and E2F1 transcription factors*. Oncogene. **28**: 1169-1175.
- Colvin V.L. (2003). *The potential environmental impact of engineered nanomaterials*. Nature Biotechnology. **10**:1166-1170.

- Conde J., Doria G., and Baptista P. (2012). *Noble metal nanoparticles applications in cancer*. Journal of Drug Delivery. doi: 10.1155/2012/751075.
- Conner E.E., Mwamuka J., Gole A., Murphy C.J., and Wyatt M.D. (2005). *Gold nanoparticles are taken up by human cells but do not cause acute toxicity*. Small. **1**: 325-327.
- Cornejo-Monroy D., Acosta-Torres L.S., Morena-Vega A.I., Saldana C., Morales-Tlalpan V., and Castaño V.M. (2013). *Gold nanostructures in medicine: past, present and future*. Journal of Nanoscience Letters. **3(25)**: 1-9.
- Crayton S.H., and Tsourkas A. (2011). *A pH-titratable superparamagnetic iron oxide for improved nanoparticle accumulation in acidic tumour microenvironments*. ACS Nano. **5(12)**: 9592-9601.
- Croce C.M. (2008). *Oncogenes and cancer*. New England Journal of Medicine. **358(5)**: 502-511.
- Cross D., and Burmester J.K. (2006). *Gene Therapy for Cancer Treatment: Past, Present and Future*. Clinical Medicine and Research. **4(3)**: 218-227.
- Dalla-Favera R., Bregni M., Erikson J., Patterson D., Gallo R.C., and Croce C.M. (1982). *Human c-myc onc gene is located on the region of chromosome 8 that is translocated in Burkitt lymphoma cells*. Proceedings of the National Academy of Sciences of the United States of America. **79**:7824-7827.
- Dalla-Favera R., Gelmann E.P., Martinotti S., Franchini G., Papas T.S., Gallo R.C., and Wang-Stall F. (1982). *Cloning and characterisation of different human sequences related to the oncogene (v-myc) of avian myelo-cytomatosis virus (MC29)*. Proceedings of the National Academy of Sciences of the United States of America. **79**:6497-6501.
- Dang C.V. (1999). *c-MYC Target Genes Involved in Cell Growth, Apoptosis and Metabolism*. Molecular and Cellular Biology. **19(1)**: 1-11.
- Dang C.V. (2010). *Rethinking the Warburg effect with Myc micromanaging glutamine metabolism*. Cancer Research. **70**: 859-862.
- Dang C.V., Le A., and Gao P. (2009). *MYC-induced Cancer Cell Energy Metabolism and Therapeutic Opportunities*. Clinical Cancer Research. **15(21)**: 6479-6483.

- Dang C.V., O'Donnell K.A., Zeller K.I., Nguyen T., Ostus R.C., and Li F. (2006). *The c-Myc target gene network*. *Seminars in Cancer Biology*. **16**:253-264.
- Daniel M.C., and Astruc D. (2004). *Gold Nanoparticles: Assembly Supramolecular Chemistry, Quantum-size related properties and Applications toward Biology, Catalysis and Nanotechnology*. *Chemical Reviews*. **104**: 293-346.
- David S., Pitard B., Benoît B., and Passira J.P. (2010). *Non-viral nanosystems for systemic siRNA delivery*. *Pharmacological Reviews*. **61**: 850-862.
- Davis J.J., Huang W-Y., and Davies G-L. (2012). *Location- tuned relaxivity in Gd-doped mesoporous silica nanoparticles*. *Journal of Materials Chemistry*. **22**:22848-22850.
- Davis M.E. (2002). *Non-viral gene delivery systems*. *Current Opinion in Biotechnology*. **13**: 128-131.
- Davis M.E. (2009). *The first targeted delivery of siRNA in humans via a self-assembling, cyclodextrin polymer based nanoparticle: from concept to clinic*. *Molecular Pharmaceutics*. **6**: 659-668.
- Deberardinis R.J., Sayed N., Ditsworth D., and Thompson C.B. (2008). *Brick by brick: metabolism and tumour cell growth*. *Current Opinion in Genetics and Development*. **18**: 54-61.
- D'Emanuele, A., and Attwood D. (2005). *Dendrimer-drug interactions*. *Advanced Drug Delivery Reviews*. **57(15)**: 2147-2162.
- Deusberg P.H., and Vogt P.K. (1979). *Avian acute leukaemia viruses MC29 and MHZ share specific RNA sequences: evidence for a second class of transforming genes*. *Proc Natl. Acad. Sci. USA*. **76**:1633-1637.
- de Fourgerolles A.R. (2008). *The first targeted delivery of siRNA in humans via a self-assembly, cyclodextrin polymer- based nanoparticle from concept to clinic*. *Molecular Pharmaceutics*. **6**: 659-668.
- Degennes P.G. (1980). *Conformations of polymers attached to an interface*. *Macromolecules*. **16(5)**: 1069-1075.
- Degennes P.G. (1987). *Polymers at an interface- a simplified view*. *Advances in Colloid and Interface Science*. **27(3-4)**: 189-209.

- Dequaire M., Degrand C., and Limoges B. (2000). *An electrochemical metaloimmunoassay based on a colloidal gold label*. *Analytical Chemistry*. **72(22)**: 5521-5528.
- Dharmacon™. (2016/2017). *Gene Editing, RNAi and Gene Expression*. Dharmacon™ Product Guide 2016/17. GE Life Sciences, General Electric Company.
- Deng Y., Wang C.C., Choy K.W., Du Q., Chen J., Wang Q., Lii L., Chung T.K.H., and Tang T. (2014). *Therapeutic potentials of gene silencing by RNA interference: Principles, challenges, and new strategies*. *Gene*. **538**: 217-227.
- Denizot F., and Lang R. (1986). *Rapid colorimetric assay for cell growth and survival. Modifications to the tetrazolium dye procedure giving improved sensitivity and reliability*. *Journal of Immunological Methods*. **89**: 271-277.
- Ding Y., Jiang Z., Saha K., Kim C.S., Kim S.T., Landis R.F., and Rotello V.M. (2014). *Gold Nanoparticles for Nucleic Acid Delivery*. *Molecular Therapy*. **22(6)**: 1075-1083.
- Dorasamy S., Singh M., and Ariatti M. (2009). *Rapid and Sensitive fluorometric analysis of novel galactosylated cationic liposome interaction with siRNA*. *African Journal of Pharmacy and Pharmacology*. **3(12)**: 632-635.
- Draz M.S., Fang B.A., Zhang P., Hu Z., Gu S., Weng K.C. Gray J.W., and Chen F.F. (2014). *Nanoparticle mediated systemic delivery of siRNA for treatment of cancers and viral infections*. *Theranostics*. **4(9)**: 872-892.
- Dreaden E.C., Alkilany A.M., Huang X., Murphy C.J., and El-Sayed M.A. (2012). *The Golden Age: Gold Nanoparticles for Biomedicine*. *Chemical Society Reviews*. **41**: 2740-2779.
- Dreaden E.C., Mackey M.A., Huang X., Kong B., and El-Sayed M.A. (2011). *Beating cancer in multiple ways using nanogold*. *Chemical Society Reviews*. **40(7)**: 3391-3404.
- Dreaden E.C., Mwakwari S.C., Soji Q.H., Oyelere A.K., and El-Sayed MA. (2009). *Tamoxifen-poly(ethylene glycol)- thiol gold nanoparticle conjugates: enhanced potency and selective delivery for breast cancer treatment*. *Bioconjugate Chemistry*. **20(12)**: 2247-2253.
- Duarte S., Carte G., Faneca H, de Lima M.C.P., and Pierrefite-Carle V. (2012). *Suicide gene therapy in cancer: where do we stand now?* *Cancer Letters*. **324**: 160-170.

- Duarte S., Faneca H., and Pedroso de Lima M.C. (2011). *Non-covalent association of folate to lipoplexes: A promising strategy to improve gene delivery on the presence of serum*. Journal of Controlled Release. **149**: 264-272.
- Duncan B., Kim C., and Rotello V.M. (2010). *Gold nanoparticle platforms as drug and biomolecule delivery systems*. Journal of Controlled Release. **148**: 122-127.
- Dutta D.K., Tripath S., Mehrotra G.K., and Dutta J. (2009). *Perspectives for chitosan based antimicrobial films in food applications*. Food Chemistry. **114**: 1173-1182.
- Dykman L., and Khlebtsov N. (2012). *Gold nanoparticles in biomedical applications: recent advances and perspectives*. Chemical Society Reviews. **41**:2256-2282.
- Dykhhoorn D.M., and Lieberman J. (2006). *Knocking down disease with siRNAs*. Cell. **126**: 231-235.
- Dykhhoorn D.M., Palliser D., and Lieberman J. (2006). *The silent treatment: siRNAs as small molecule drugs*. Gene Therapy. **13**: 541-552.
- Eilers M., and Eisenman R.N. (2008). *MYC's broad reach*. Genes and Development. **22**: 2755-2766.
- Eischen C.M., Packham G., Nip J., Fee B.E., Hiebert S.W., Zambetti G.P., and Cleveland J.L. (2001). *Bcl-2 is an apoptotic target suppressed by both c-Myc and E2F-1*. Oncogene. **20(48)**: 6983-6993.
- El-Aneed A. (2004). *An overview of current delivery systems in cancer gene therapy*. Journal of Controlled Release. **94**:1-14.
- El-Ansary A., and Al-Daihan S. (2009). *On the toxicity of therapeutically used nanoparticles: An overview*. Journal of Toxicology. **2009(754180)**: 1-9.
- Elbashir S.M., Lendeckel W., and Tuschl T. (2001). *RNA interference is mediated by 21-22 nucleotide RNAs*. Genes and Development. **15**:188-200.
- El Chaar L., Lamant L.A., and El Zein N. (2011). *Review of photovoltaic technologies*. Renewable and Sustainable Energy Reviews. **15(5)**: 2165-2175.
- El-Sayed M.A. (2001). *Some interesting properties of metals confined in time and nanometer space of different shapes*. Accounts of Chemical Research. **41(12)**: 1578-1586.

Engvall E., and Perlmann P. (1971). *Enzyme linked immunosorbent assay (ELISA) quantitative assay of immunoglobulin G*. *Immunochemistry*. **8**: 871-875.

Eustis S., and El-Sayed M. (2005). *Aspect ratio dependence of enhanced fluorescence intensity of gold nanorods: Experimental and simulation study*. *Journal of Physical Chemistry B*. **109(34)**:16350- 16353.

Eustis S., and El-Sayed M. (2006). *Why gold nanoparticles are more precious than pretty gold: Noble metal surface plasmon resonance and its enhancement of the radiative and non-radiative properties of nanocrystals of different shapes*. *Chemical Society Reviews*. **35(3)**: 209-217.

Faraday M. (1857). *Experimental Relations of Gold (and other Metals) to Light*. *Philosophical Transactions of the Royal Society*. **147**:145-181.

Fatemian T.L., Othman L., and Chowdury E.H. (2014). *Strategies and validation for siRNA-based therapeutics for the reversal of multi-drug resistance in cancer*. *Drug Discovery Today*. **19**: 71-78.

Fatin F.M., Kifah A-K., AL-Imarah A.F., AL-Hasnawi I.A., Angelmashotjafar L., and Abdul-Majeed B.A. (2013). *A simple method for synthesis, purification and concentration stabilised gold nanoparticles*. *International Journal of Engineering Research and Applications*. **3(6)**: 21-30.

Ferro S., Fabre I., and Chenivresse X. (2016). *Optimising a Method for the Quantification by Quantitative Real-Time Polymerase Chain Reaction of Host Cell DNA in Plasmid Vector Batches Used in Human Gene Therapy*. *Human Gene Therapy Methods*. **27(4)**: 159-170.

Figueiredo J.C., Grau M.V., Wallace K., Levine A.J., Shen L., Hamdan R., Chen X., Bresliar R.S., McKeown-Eyssen G., Haile R.W., Baron J.A., and Issa J.P.J. (2009). *Global DNA hypomethylation (LINE-1) in their normal colon and lifestyle characteristics and dietary and genetic factors*. *Cancer Epidemiology, Biomarkers and Prevention*. **18(4)**: 1041-1049.

Figueiredo S., Cabral R., Luis D., Fernandes A.R., and Baptista P.V. (2014). *Conjugation of Gold nanoparticles and liposomes for combined vehicles of drug delivery in cancer*. *Nanomedicine In: Seifalian A (ed). Nanomedicine, University College London (UK) 2014. Chapter 3: available from <http://www.onecentralpres.com/nanomedicine/>*

- Fire A., Xu S., Montgomery M.K., Kostas S.A., Driver S.E., and Mello C.C. (1998). *Potent and specific genetic interference by double stranded RNA in Caenorhabditis elegans*. *Nature*. **391**: 806-911.
- Fletcher J.W., Djulbegovic B., Soares H.P., Siegel B.A., Lowe V.J., Lyman G.H., Colean R.E., Wahl R., Paschold J.C., Avril N., Einhorn L.H., Suh W.W., Samson D., Delbeke D., Gorman M., and Shields F. (2008). *Recommendations on the use of 18F-FDG PET in oncology*. *Journal of Nuclear Medicine*. **49**: 480-508.
- Förster S., and Antonietti M. (1998). *Amphiphilic Block Copolymers in Structure-Controlled Nanomaterial Hybrids*. *Advanced Materials*. **10(3)**: 195-219.
- Frens G. (1973). *Controlled Nucleation for the Regulation of the Particle Size in Monodisperse Gold Suspensions*. *Nature Physical Science*. **241**: 20-22.
- Friedmann T. (1992). *A Brief history of gene therapy*. *Nature Genetics*. **2**: 93-98.
- Gabay M. Li Y., and Felsher D.W. (2014). *MYC activation is a hallmark of cancer initiation and maintenance*. *Col Spring Harbor Perspectives in Medicine*. **4**:ao14241.
- Gao K., and Huang L. (2008). *Non-viral methods for siRNA delivery*. *Molecular Pharmaceutics*. **6(3)**: 651-658.
- Garcia-Fuentes M., and Alonso M.J. (2012). *Chitosan based nanocarriers: where do we stand?* *Journal of Controlled Release*. **161**: 496-504.
- Gartell A.L. (1989). *A new mode of transcriptional repression by c-myc methylation*. *Oncogene*. **25**: 1989-1990.
- Geall A.J., and Blagbrough I.S. (2000). *Rapid and sensitive ethidium bromide fluorescence quenching assay of polyamine conjugate-DNA interactions for the analysis of lipoplex formation in gene therapy*. *Journal of Pharmaceutical and Biomedical Analysis*. **22**: 849-859.
- Ghosh P., Han G., De M., Kim C.K., and Rotelo V/M. (2008). *Gold nanoparticles in delivery applications*. *Advanced Drug Delivery Reviews*. **60**: 1307-1315.
- Gilojohann D.A., Seferos D.S., Daniel W.L., Massich M.D., Patel P.C., and Mirkin C.A. (2010). *Gold Nanoparticles for Biology and Medicine*. *Angewandte Chemie International Edition in English*. **49(19)**: 3280-3294.

Gilojohann D.A., Seferos D.S., Prigodich A.E., Patel P.C., and Mirkin C.A. (2009). *Gene regulation with polyvalent siRNA nanoparticle conjugates*. Journal of the American Chemical Society. **131**: 2072-2073.

Ginter E.K. (2000). *Gene Therapy of hereditary disease*. Voprosy Meditsinskoi Khimii. **46**: 265-278.

Goldberger J., Fan R., and Yang P. (2006). *Inorganic Nanotubes: A Novel Platform for Nanofluidics*. Accounts of Chemical Research. **39(4)**: 239-248.

Gomez-Raman N., Felton-Edkins Z.A., Kenneth N.S., Goodfellow S.J., Athineos D., Zhang J., Ramsbottom B.A., Innes F., Kantidakis T., Kerr E.R., Brodie J., Grandori C., and White R.J. (2006). *Activation by c-MYC of transcription by RNA polymerase I, II and III*. Biochemical Society Symposium. **73**: 141-154.

Green I.X., Tang W., Neurock M., and Yates J.T. (2011). *Spectroscopic Observation of Dual Catalytic Sites During Oxidation of CO on a Au/TiO₂ Catalyst*. Science. **333(6043)**: 736-739.

Greenwood N.N., and Earnshaw A. (1997). *Chemistry of the Elements 2nd Edition*. Butterworth-Heinemann, Burlington, MA.

Gresch O., Engel F.B., Nestic D., Tran T.T., England H.M., Hickman E.S., Körner I., Gon L., Chen S., Castrol-O bregan S., Hammermann R., Wolf J., Müller-Harfmann H., Nix M., Siebenkotten G., Kraus G., and Luna K. (2004). *New non-viral method for gene transfer into primary cells*. Methods. **33**: 151-163.

Griffiths D., Bernt W., Hole P., Smith J., Mallay A., and Carr B. (2011). *Zeta potential measurement of nanoparticles by Nanoparticle Tracking Analysis (NTA)*. NSTI-Nanotech. www.nsti.org.

Grislain L., Couvreur P., Lenaerts V., Roland M., Deprez-Decampeneere D., and Speiser P. (1983). *Pharmokinetics and distribution of a biodegradable drug-carrier*. International Journal of Pharmaceutics. **15**: 335-345.

Gross J., Sayle S., Karaw A.R., Bakowsky U., and Garidel P. (2016). *Nanoparticle tracking analysis of particle size and concentration detection in suspensions of polymer and protein samples: Influence of experimental and data evaluation parameters*. European Journal of Pharmaceutics and Biopharmaceutics. **104**: 30-41.

- Guillouf C., Brona X., Selvakumaran M., Giordana A., Hoffmann B., and Liebermann D.A. (1995). *Dissection of the genetic programs of 53-mediated G1 growth arrest and apoptosis: Blocking p53-induced apoptosis unmasks G1 arrest*. *Blood*. **85**: 2691-2698.
- Guldi D.M., Rahman G.M.A., Sgobba V., and Ehli C. (2006). *Multifunctional molecular carbon materials-from fullerenes to carbon nanotubes*. *Chemical Society Reviews*. **35**: 471-487.
- Guo J., O'Driscall C.M., Holmes J.D., and Rahme K. (2016). *Bioconjugated Gold Nanoparticles Enhance Cellular Uptake: A Proof of Concept Study for siRNA Delivery in Prostate Cancer Cells*. *International Journal of Pharmaceutics*. doi: <http://dx.doi.org/doi:10.1016/j.ijpharm.2016.05.027>.
- Guo P., Coban O., Snead N.M., Trebley J., Hoeprich S., Guo S., and Shu Y. (2010). *Engineering RNA for targeted siRNA delivery and medical application*. *Advanced Drug Delivery Reviews*. **62(6)**: 650-666.
- Gupta U., Agashe H.B., Asthana A., and Jain N.K. (2006). *Dendrimers: novel polymeric nanoarchitectures for solubility enhancement*. *Biomacromolecules*. **7(3)**: 649-658.
- Gurdag S., Khandare J., Stapels S., Matherly L.H., and Kannan R.M. (2006). *Activity of dendrimer-methotrexate conjugates on methotrexate-sensitive and resistant cell lines*. *Bioconjugate Chemistry*. **17(2)**: 275-283.
- Guzman K., Finnegan M., and Banfield J. (2006). *Influence of Surface Potential on Aggregation and Transport of Titania Nanoparticles*. *Environmental Science and Technology*. **40(24)**: 7688-7693.
- Hammond S.M. (2005). *Dicing and slicing, the core machinery of RNA interference pathway*. *FEBS Letters*. **579**:5822-5829.
- Han G., You C-C., Kim B-J., Turingan R.S., Forbes N.S., Martin C.T., and Rotello V.M. (2006). *Light regulated release of DNA and its delivery to nuclei by means of photolabile gold nanoparticles*. *Angewandte Chemie International Edition*. **45(19)**: 3165-3169.
- Hann S.R., Sloan-Brown K., and Spotts G.D. (1992). *Translational activation of the non-AUG-initiated c-myc 1 protein at high cell densities due to the methionine deprivation*. *Genes and Development*. **6**:1229-2240.
- Hanahan D., and Weinberg R.A. (2000). *The hallmarks of cancer*. *Cell*. **100**: 57-70.

- Hansen M.B., Nielsen S.E., and Berg K. (1989). *Re-examination and further development of a precise and rapid dye method for measuring cell growth/ cell kill*. Journal of Immunological Methods. **119**: 203-210.
- Harris J.M., and Chess R.B. (2003). *Effect of pegylation on pharmaceuticals*. Nature Reviews Drug Discovery. **2**: 214-221.
- Harris J.M., Martin V.E., and Modi M. (2001). *Pegylation: a novel process for modifying pharmacokinetics*. Clinical Pharmacokinetics. **40**: 539-551.
- Heid C.A., Stevens J., Livak K.J., and Williams P.K. (1996). *Real time quantitative PCR*. Genome Research. **6**: 986-994.
- Hellman L.M., and Fried M.G. (2007). *Electrophoretic mobility shift assay (EMSA) for detecting protein-nucleic acid interactions*. Nature Protocols. **2**: 1849-1861.
- Herket B., and Eilers M. (2010). *Transcriptional repression: the dark side of myc*. Genes and Cancer. **1**: 580-586.
- Hill A.B., Chen M., Chen C.K., Pfeifer B.A., and Jones C.H. (2016). *Overcoming gene-delivery hurdles: Physiological considerations for non-viral vectors*. Trends in Biotechnology. **34**: 91-105.
- Hoffman B., and Liebermann D.A. (1998). *The proto-oncogene c-Myc and apoptosis*. Oncogene. **17**: 3351-3357.
- Hoffman B., and Liebermann D.A. (2008). *Apoptotic signalling by c-MYC oncogene*. **27**: 6402-6472.
- Hole P., Sillence K., Hannell C., Maguire C.M., Rosslein M., Suarez G., Capracotta S., Magdolenova Z., Horev-Azaria L., Dybowska A., Cooke L., Hase A., Contal S., Mano S., Vennemann A., Sauvain J-J., Stauntan K.C., Anguissola S., Luch A., Dusinska M., Korenstein R., Gutleb A.C., Wiemann M., Prina- Mello A., Riediker M., and Wicj P. (2013). *Interlaboratory comparison of size measurements on nanoparticles using nanoparticle tracking analysis (NTA)*. Journal of Nanoparticle Research. **15**: 2101-2113.
- Honary S., and Zahir F. (2013a). *Effect of zeta potential on the properties of nano-drug delivery systems- A review (Part I)*. Tropical Journal of Pharmaceutical Research. **12**: 255-264.

- Honary S., and Zahir F. (2013b). *Effect of zeta potential on the properties of nano-drug delivery systems- A review (Part 2)*. Tropical Journal of Pharmaceutical Research. **12**: 265-273.
- Hong R., Han G., Fernandez J.M., Kim B-J., Forbes N.S., and Rotello V.M. (2006). *Glutathione mediated delivery and release using monolayer protected nanoparticles carriers*. Journal of the American Chemical Society. **128(4)**: 1078-1079.
- Hong C.A., and Nam Y.S. (2014). *Functional Nanostructures for Effective Delivery of Small Interfering RNA Therapeutics*. Theranostics. **4(12)**: 1211-1232.
- Hornung V., Guenther-Biller M., Bourquin C., Ablasser A., Schlee M., Uematsu S., Noronha A., Manoharan M., Akira S., de Fougerolles A., Endres S., and Hartmann G. (2005). *Sequence-specific potent induction of IFN-alpha by short interfering RNA in plasmacytoid dendritic cells through TLR-7*. Nature Medicine. **11**: 263-270.
- Howard K.A., Rahbek U.L., Liu X., Damgaard C.K., Glud S.Z., Anderson M.O., Hovgaard M.B., Schmitz A., Nyengaard J.R., Basenbacher F., and Kjems J. (2006). *RNA Interference in vitro and in vivo using novel chitosan/ siRNA nanoparticle system*. Molecular Therapy. **14**: 799-805.
- Hsu B., Marin M.C., el-Naggar A.K., Stephens L.C., Brisbay S., and McDaniel T.J. (1995). *Evidence that c-Myc mediated apoptosis does not require wild-type during lymphomagenesis*. Oncogene. **11**: 175-179.
- Huang C, Butler P.J., Tang S., Muddana H.S., Bao G., and Zhang S. (2013). *Substrate Stiffness Regulates Cellular Uptake of Nanoparticles*. Nano Letters. **13(4)**: 1611-1615.
- Huang C., Ozdemir T., Xu L-C., Butler P.J., Siedlecki C.A., Brown J.L., and Zhang S. (2016). *The role of substrate topography on the cellular uptake of nanoparticles*. Journal of Biomedical Materials Research. **104(3)**: 488-495.
- Huang L., Hung M., and Wagner E. (1999). *Non-viral vectors for Gene Therapy*. San Diego, California, Academic Press. ISBN: 9780080479774.
- Huang M., Fang C.W., Khorc E., and Lim L.Y. (2005). *Transfection efficiency of chitosan vectors: effect of polymer molecular weight and degree of deacetylation*. Journal of Controlled Release. **106**: 391-406.
- Huang X., El-Sayed I.H., Qian W., and El-Sayed M.A. (2005). *Cancer Cells Assemble and Align Gold Nanorods Conjugated to Antibodies to Produce Highly Enhanced, Sharp and*

Polarized Surface Raman Spectra: A Potential Cancer Diagnostic Marker. Nano Letters. **7(6)**: 1591-1597.

Huefner A., Septiadi D., Wilts B.D., Patel I.I., Kuan W-L., Fragniese A., Barker R.A., and Mahajan S. (2014). *Gold nanoparticles explore cells: Cellular uptake and their use as intracellular probes.* Methods. **68**: 354-363.

Huggett J., Dheda K., Bustin S., and Zumla A. (2005). *Real-Time RT-PCR normalisation, strategies and considerations.* Genes and Immunity. **6**: 279-284.

Hunter A.C. (2006). *Molecular Hurdles in polyfection, design and mechanistic background to poycation induced cytotoxicity.* Advanced Drug Delivery Reviews. **58**: 1523-1531.

Hunter A.C., Elsom J., Wibroe P.P., and Moghimi S.M. (2012). *Polymeric particulate technologies for oral drug delivery and targeting: A pathophysiological perspective.* Maturitas. **73(1)**: 5-18.

Iijima S. (1991). *Helical microtubules of graphite carbon.* Nature. **354**: 56-58.

Jackson A.L. and Linsley P.S. (2010). *Recognizing and avoiding siRNA off target effects for target identification and therapeutic application.* Nature Reviews Drug Discovery. **9**: 57-67.

Jain S., Hirst D.G., and O'Sullivan J.M. (2012). *Gold nanoparticles as novel agents for cancer therapy.* The British Journal of Radiology. **85**: 101-113.

Jiang W., Kim B.Y.S., Rutka J.T., and Chan W.C.W. (2008). *Nanoparticle- mediated cellular response in size-dependant.* Nature Nanotechnology. **3(3)**: 145-150.

Jin Q., Xu J-P., Ji J., and Shen J-C. (2008). *Zwitterionic phosphorylcholine as a better ligand for stabilising large biocompatible gold nanoparticles.* Chemical Communications. **26**: 3058-3060.

Jelveh S., and Chithrani D.B. (2011). *Gold nanostructures as a Platform for Combination Therapy in Future Cancer Therapeutics.* Cancers. **3**: 1081-1110.

Jokerst J.V., Labovkina T., Zare R.N., and Gambhir S. (2010). *Nanoparticle PEGylation for Imaging and Therapy.* Nanomedicine. **6(4)**: 715-728.

Jones D.P., Carlon J.L., Samiec P.S., Sternberg P., Mody V.C., Reed R.L., and Brown L.A.S. (1998). *Glutathione measured in human plasma: evaluation of sample collection, storage and*

derivatization conditions for analysis of dansyl derivatives by HPLC. Clinica Chemica Acta. **275(2)**: 175-184.

Jones D.P., Carlson J.L., Mody V.C., Cai J., Lyn M.J., and Sternberg P. (2000). *Redox state of glutathione in human plasma.* Free Radical Biology and Medicine. **28(4)**: 625-635.

Jun Y-W., Casula M.F., Sim J-H., Kim S.Y., Cheon J., and Alivisatos A.P. (2003). *Surfactant-Assisted Elimination of a High Energy Facet as a Means of Controlling the Shapes of TiO₂ Nanocrystals.* Journal of the American Chemical Society. **125(51)**: 15981-15985.

Kah J.C., Wong K.Y., Neoh K.G., Song J.H., Fu J.W., Mhaucalkar S., Olivo M., and Sheppard C.J. (2009). *Critical parameters in the pegylation of gold nanoshells for biomedical applications: an in vitro macrophage study.* Journal of Drug Targeting. **17**: 181-193.

Kas H.S. (1997). *Chitosan: properties, preparations and application to microparticulate systems.* Journal of Microencapsulation. **14**: 689-711.

Kenneth R.B., Daniel G.W., and Michael J.N. (2000). *Seeding of Colloidal Gold Nanoparticle Solutions 2. Improved Control of Particle Size and Shape.* Chemistry of Materials. **12(2)**: 306-313.

Kerr J.F.R., Wyllie H., and Currie A.R. (1972). *Apoptosis: a basic biological phenomenon with wide-ranging implications in tissue kinetics.* British Journal of Cancer. **26**: 239-257.

Kesharwani P., Gajbhiye V., and Jain N.K. (2012). *A review of the nanocarriers for the delivery of small interfering RNA.* Biomaterials. **33**: 7138-7150.

Kim C.K., Ghosh P., Pagliuca, Zhu Z-J, Menichetti S., and Rotello V.M. (2009). *Entrapment of hydrophobic drugs in nanoparticle monolayers with efficient release into cancer cells.* Journal of the American Chemical Society. **131(4)**: 1360-1361.

Kim D., Yu M.K., Lee T.S., Park J.J. Jeong Y.Y., and Jon S. (2011). *Amphiphilic polymer-coated hybrid nanoparticles as CT/MRI dual contrast agents.* Nanotechnology. **22(15)**: 155101.

Kim H.J., Matsuda H., Zhou H., and Honma I. (2006). *Ultrasound-triggered smart drug release from a poly(dimethyl siloxane) mesoporous silica composite.* Advanced Materials. **18(23)**: 3083-3088.

- Kim H.-K., Davaa E., Myung C.-S., and Park J.-S. (2010). *Enhanced siRNA delivery of cationic liposomes by using new polyarginine-conjugated PEG-lipid*. International Journal of Pharmaceutics. **392(1-2)**:141-147.
- Kim H.S., Song I.H., Kim J.C., Kim E.J., Jang D.O., and Park Y.S. (2006). *In vitro and in vivo gene transferring characteristics of novel cationic lipids, DMKD (O,O'-dimyristyl-N-lysyl aspartate) and DMKE (O,O'-dimyristyl-N-lysyl glutamate)*. Journal of Controlled Release. **115**: 234-241.
- Kim T.H., Choi H., Yu G.S., Lee J., and Choi J.S. (2013). *Novel hyperbranched polyethyleneimine conjugate as an efficient, non-viral gene delivery vector*. Macromolecular Research. **21(10)**: 1097-1104.
- Klimberg V.S., and McClellan J.L. (1996). *Claude H. Organ Honorary Lectureship. Glutamine, cancer and its therapy*. The American Journal of Surgery. **172**: 418-424.
- Kniepp J., Kniepp H., McLaughlin M., Brown D., and Kniepp K. (2006). *In vivo molecular probing of cellular compartments with gold nanoparticles and nanoaggregates*. Nano Letters. **6(10)**: 2225-2231.
- Kniepp K., Kniepp H., Itzkan I., Dasari R.R., and Feld M.S. (2002). *Surface-enhanced Raman Scattering and biophysics*. Journal of Physics and Condensed Matter. **14(18)**: R597-R624.
- Knoell D.M., and Yiu I.M. (1998). *Human Gene Therapy for hereditary diseases: a review of trials*. American Journal of Health-System Pharmacy. **55**:899-904.
- Knoell D.M., and Yiu I.M. (2005). *Human Gene Therapy: Twenty-first century medicine*. Annual Review of Biochemistry. **74**: 711-738.
- Koh C.M., Sabó A., and Guccione E. (2016). *Targeting MYC in cancer therapy: RNA processing offers new opportunities*. Prospects and Overviews, BioEssays. **38(3)**: 266-275.
- Kong Y., Ruan L., Ma L., Cui Y., Wong J.M., and Le Y. (2007). *RNA interference as a novel agent and powerful tool in immunopharmacological research*. International Immunopharmacology. **7**: 417-426.
- Koppenol W.H., Bounds P.L., and Dang C.V. (2011). *Otto Warburg's contributions to current concepts of cancer metabolism*. Nature Reviews Cancer. **11**: 325-337.

- Kreiberg U., and Vollmer M. (1995). *Optical Properties of Metal Clusters*. New York: Springer. ISBN 978-3-662-09109-8.
- Kress T.R., Sao A., and Amati B. (2015). *MYC: connecting selective transcriptional control to global RNA productions*. *Nature Reviews Cancer*. **15**: 593-607.
- Kumar L.D., and Clarke A.R. (2007). *Gene Manipulation through the use of small interfering RNA (siRNA): from in vitro to in vivo applications*. *Advanced Drug Delivery Reviews*. **59**: 87-100.
- Kumar R. (2000). *A review of chitin and chitosan applications*. *Reactive and Functional Polymers*. **46**:1-27.
- Kuntsche J., Horst J.C., and Bunjes H. (2011). *Cryogenic transmission electron microscopy (cryo-TEM) for studying the morphology of colloidal drug delivery systems*. *International Journal of Pharmaceutics*. **417**: 120-137.
- Lai W.C., and Liao W.B. (2003). *Thermo-oxidative degradation of poly (ethylene glycol)/ poly (L-lactic acid) blends*. *Polymer (Guildf)*. **44**: 8103-8109.
- Lagunov S.L., Ahmodi T.S., El-Sayed M.A., Khoury J.T., and Whetten R.L. (1997). *Electron Dynamics of Passivated Gold Nanocrystals Probed by Subpicosecond Transient Absorption Spectroscopy*. *The Journal of Physical Chemistry B*. **101**: 3713-3719.
- Le A., Lane A.N., Hamaker M., Bose S., Gouw A., Barbi J., Tsukamoto T., Rojas C.J., Slusher B.S., Zhang H., Zimmerman L.J., Liebler D.C., Slebos R.J., Lorkiewicz P.K., Higashi R.M., Fan T.W., and Dang C.V. (2012). *Glucose-independent glutamine metabolism via TCA cycling for proliferation and survival in B cells*. *Cell Metabolism*. **15(1)**: 110-121.
- Lea T. (2015). *Caco 2 Cell Line*. In: Verhoeckx K *et al.* (eds) *The Impact of Food Bioactives on Health*. Springer, Cham.
- Lee K.Y., Kwan J.C., Kim Y.H., Jo W.H., and Jeong S.Y. (1998). *Preparation of chitosan self-aggregates as a gene delivery system*. *Journal of Controlled Release*. **51**: 213-220.
- Lesniak A., Salvati A., Santes-Martinez M.J., Radomski M.W., Dawson K.A., and Aberg C. (2013). *Nanoparticle adhesion to the cell membrane and its effect on nanoparticle uptake efficiency*. *Journal of the American Chemical Society*. **135(4)**: 1438-1444.

- Leung R.K.M., and Whittaker P.A. (2005). *RNA Interference: From gene silencing to gene specific therapeutics*. *Pharmacology and Therapeutics*. **107**: 222-239.
- Levenson A.S., and Jordan V.C. (1997). *MCF-7: The First Hormone Responsive Breast Cancer Cell Line*. *Cancer Research*. **57**:3071-3078.
- Lévy R., Shaheen U., Cesbron Y., and Sée V. (2010). *Gold nanoparticle delivery in mammalian live cells: a critical review*. *Nano Reviews*. **1**: 4889-4907.
- Lewis B.C., Shim H., Li Q., Wu C.S., Lee L.A., Maity A., and Dang C.V. (1997). *Identification of putative c-myc- responsive genes: characterisation of rcl, a novel growth-related gene*. *Molecular and Cellular Biology*. **17**: 4967-4978.
- Li J., Wang Y., Zhu Y., and Oupický D. (2013). *Recent Advances in delivery of drug -nucleic acid combinations for cancer treatment*. *Journal of Controlled Release*. **172**: 589-600.
- Li S., and Huang L. (2000). *Non-viral gene therapy: promises and challenges*. *Gene Therapy*. **7**:31-34.
- Li S-D., and Huang L. (2006). *Gene Therapy Progress and Prospects: no-viral gene therapy by systemic delivery*. *Gene Therapy*. **13**: 1313-1319.
- Li S., and Ma Z. (2001). *Nonviral gene therapy*. *Current Gene Therapy*. **1**:1-35.
- Li S-D., Chano S., and Huang L. (2008). *Efficient oncogene silencing and metastasis inhibition via systemic delivery of siRNA*. *Molecular Therapy*. **16**: 942-946.
- Liao W., Li W., Zhang T., Kirberger M., Liu J., Wang P., Chen W., and Wang Y. (2016). *Powering up the molecular therapy of RNA Interference by novel nanoparticles*. *Biomaterial Science*. **4**: 1051-1061.
- Liegler T.J., Hyum W., Yen B., and Stites D.P. (1995). *Detection and Quantification of Live, Apoptotic and Necrotic Human Peripheral Lymphocytes by Single- Laser Flow Cytometry*. *Clinical and Diagnostic Laboratory Immunology*. **2(3)**: 369-376.
- Lin M.M., Kim D.K., Haj A.J.E., and Dobson J. (2008). *Development of Superparamagnetic Iron Oxide Nanoparticles (SPIONS) for Translation to Clinical Applications*. *IEEE Transactions on NanoBioscience*. **7(4)**: 298-305.

Link S., and El-Sayed M.A. (2000). *Spectral properties and relaxation dynamics of surface plasmon electronic oscillations in gold and silver nanorods*. The Journal of Physical Chemistry B. **103(40)**: 8410-8426.

Little C.D., Nau M.M., Carney D.N., Gazdar D.N., and Minna J.D. (1983). *Amplification and expression of the c-myc oncogene in human lung cancer cell lines*. Nature. **306**: 194-196.

Liu G.K., and Lee L.P. (2005). *Nanowell surface enhanced Raman scattering arrays fabricated by soft-lithography for label-free biomolecular detections in integrated microfluidics*. Applied Physics Letters. **87(7)**: 074101-1-3. doi: org/10.1063/1.2031935.

Liu X., Howard K.A., Dang M., Anderson M.O., Rahbek U.L., Johnsen M.G., Hansen O.C., Besenbacher F., and Kjem S.J. (2007). *The Influence of polymeric properties on chitosan/siRNA nanoparticle formulations and gene silencing*. Biomaterials. **28**: 1280-1288.

Liu Y., Zhu Y.H., Mao C.Q., Dou S., Shen S., Ton Z.B., and Wang J. (2014). *Triple-negative breast cancer therapy and CDK1 siRNA delivered by cationic lipid assisted PEG-PLA nanoparticles*. Journal of Controlled Release. **192**: 114-121.

Loo C., Lowery A., Halas N., West J., and Drezek R. (2005). *Immunotargeted Nanoshells for Integrated Cancer Imaging and Therapy*. Nano Letters. **5(4)**:709-711.

Lorenzer C., Dirin M., Winkler A.M., Baumann V., and Winkler J. (2015). *Going beyond the liver: Progress and challenges of targeted delivery of siRNA therapeutics*. Journal of Controlled Release. **203**: 1-15.

Lu J.J., Langer R., and Chen J. (2009). *A novel mechanism is involved in cationic lipid mediated functional siRNA delivery*. Molecular Pharmaceutics. **6(3)**: 763-771.

Lynch I., Cedervall T., Lundqvist M., Cabeleiro-Lago C., and Dawson K.A. (2007). *The nanoparticle-protein complex as a biological entity; a complex fluids and surface science challenge for the 21st century*. Advances in Colloid and Interface Science. **134-135**: 167-174.

Ma B., Zhang S., Jiang H., Zhao B., and Lv H. (2007). *Lipoplex morphologies and their influences on transfection efficiency in gene delivery*. Journal of Controlled Release. **123**: 184-194.

Ma J.B., Yuan Y.R., Meister G., Pei Y., Tusel T., and Patel D.J. (2005). *Structural basis for 5' end specific recognition of guide RNA by the A. fulgidus PIWI protein*. Nature. **434**: 666-670.

- Ma Z., Li J., He F., Wilson A., Pitt B., and Li S. (2005). *Cationic lipids enhance siRNA mediated interferon response in mice*. *Biochemical and Biophysical Research Communications*. **350**: 755-759.
- Maeda H., Wu J., Sawa T., Matsumura Y., and Hori K. (2000). *Tumour vascular permeability and the EPR effect in macromolecular therapeutics: a review*. *Journal of Controlled Release*. **65(1-2)**: 271-284.
- Maghimi S., and Szebeni J. (2003). *Stealth liposomes and long circulating nanoparticles: critical issues in pharmacokinetics, opsonization and protein-binding properties*. *Progress in Lipid Research*. **42(6)**: 463-478.
- Majzik A., Fülöpb L., Csapó E., Bogár B., Martinecs T., Penke B., Bírád G., and Dékány I. (2010). *Functionalization of gold nanoparticles with amino acid-amyloid peptides and fragments*. *Colloids and Surfaces B: Bioinformatics*. **81**: 235-241.
- Makhsin S.R., Razak K.A., Noordin R., Dyana Zakaria N., and Chun T.S. (2012). *The effects of size and synthesis methods of gold nanoparticle-conjugated MoHlgG₄ for use in an immunochromatographic strip test to detect brugian filariasis*. *Nanotechnology*. **23**: 49-57.
- Malvern. (2010). *Mie Theory- The first 100 years*. Malvern Instruments Limited.
- Manjila S.B., Baby J.N., Bijin E.N., Constantine I., Pramod K., and Valsalakumar J. (2013). *Novel gene delivery systems*. *International Journal of Pharmaceutical Investigation*. **3**: 1-7.
- Manson J., Kumar D., and Meenan B.J. (2011). *Polyethylene glycol functionalized gold nanoparticles: the influence of capping density on stability in various media*. *Gold Bulletin*. **44**: 99-105.
- Mao S., Sun W., and Kissel T. (2010). *Chitosan- based formulations for delivery of DNA and siRNA*. *Advanced Drug Delivery Reviews*. **62**: 12-27.
- Marchini C., Montani M., Amici A., Amenitsch H., Marianecci C., Pozzi P., and Caracciolo G. (2009). *Structural stability and increase in size rationalize the efficiency of lipoplexes in serum*. *Langmuir*. **25**: 3013-3021.
- Mariani-Constantini R., Escot C., Theillet C., Gentile A., Merlo G., Lidereau R., and Callahan R. (1988). *In situ c-myc expression and genomic status of the c-myc locus in infiltrating ductal carcinomas at the breast*. *Cancer Research*. **48**: 199-205.

- Marshall N.J., Goodwin C.J., and Holt S.J. (1995). *A critical assessment of the use of microculture tetrazolium assays to measure cell growth and function*. *Growth Regulation*. **5(2)**: 69-84.
- Martin B., Sainlos M., Aissaoui A., Oudrhiri N., Hauchecorne M., Vigneron J.P., Lehn J.M., and Lehn P. (2005). *The design of cationic lipids for gene delivery*. *Current Pharmaceutical Design*. **11**: 375-394.
- Martínez J.C., Chequer N.A., González J.L., and Cardova T. (2012). *Alternative Methodology for Gold Nanoparticle Diameter Characterisation using PCA Technique and UV-vis Spectrophotometry*. *Nanoscience and Nanotechnology*. **2(6)**: 184-189.
- Martinez-Maqueda D., Miralles B., and Recio I. (2015). *HT-29 Cell Line*. In: Verhoeckx K *et al.* (eds). *The Impact of Food Bioactives on Health*. Springer, Cham.
- Masotti A., Massa G., Cametti C., Ortoggi G., Binaco A., Del Grosso N., Malizia D., and Espasito C. (2009). *Comparison of different commercially available cationic liposome-DNA lipoplexes: Parameters influencing toxicity and transfection efficiency*. *Colloids and Surfaces B: Biointerfaces*. **68**: 136-144.
- Matranga C., Tomari Y., Shin C., Bartell D.P., and Zamore P.D. (2005). *Passenger- strand cleavage facilitates assembly of siRNA into AGO-2 containing RNAi enzyme complexes*. *Cell*. **123**: 607-620.
- McLeod H.L. (2013). *Cancer pharmacogenomics: early promise, but concerted effort needed*. *Science*. **339**:1563-1566.
- Meister G., and Tuschl T. (2004). *Mechanisms of gene silencing by double stranded RNA*. *Nature*. **431**: 343-349.
- Melinger J.S., Kleiman V.D., McMarrow D., Gröhn F., Bauer B.J., and Amis E. (2003). *Ultrafast Dynamics of Gold based Nanocomposite Materials*. *The Journal of Physical Chemistry A*. **107**: 3424-3431.
- Mendes R., Carrira B., Baptista P.V., and Fernandes A.R. (2016). *Non-small cell lung cancer biomarkers and targeted therapy- Two faces of the same coin fostered by nanotechnology*. *Expert Review of Precision Medicine and Drug Development*. **1(2)**:155-168.

- Mendes R., Fernandes A.R., and Baptista P.V. (2017). *Gold Nanoparticle Approach to the Selective Delivery of Gene Silencing in Cancer-The case for Combined Delivery*. *Genes*. **8**: 94-110. doi: 10.3390/genes8030094.
- Menjoge A.R., Kannan R.M., and Tomalia D.A. (2010). *Dendrimer-based drug and imaging conjugates: design considerations for nanomedical applications*. *Drug Discovery Today*. **15**: 171-185.
- Mie G. (1908). *Beiträge zur Optik Trüber Medien, Speziell Kolloidaler Metallösungen*. *Annals of Physics*. **25**: 377-445.
- Mironava T., Hadjiargyrou M., Simon M., Jurukovski V., and Rafailovich M.H. (2010). *Gold nanoparticles cellular toxicity and recovery: effect of size, concentration and exposure time*. *Nanotoxicology*. **4(1)**: 120-137.
- Miller D.M., Thomas S.D., Islam A., Muench D., and Sedoris K. (2012). *C-MYC and cancer Metabolism*. *Clinical Cancer Research*. **18(20)**: 5546-5553.
- Mina-Tehrani A., Jiang H.L., Kim Y.K., Chung Y.S., Yu K.N., Kim J.E., Shin J.Y., Hong S.H., Lee J.H., Kim H.J., Chang S.H., Park S., Kong B.N., Cho C.S., and Cho M.H. (2012). *Suppression of tumour growth in xenograft model mice by small interfering RNA targeting osteopontin delivery using biocompatible poly (amino ester)*. *International Journal of Pharmaceutics*. **431**: 197-203.
- Misra S. (2013). *Human Gene Therapy: A brief overview of the genetic revolution*. *Journal of the Association of Physicians of India*. **61(2)**: 127-133.
- Moghimi S., and Szebeni J. (2003). *Stealth liposomes and long circulating nanoparticles: critical issues in pharmacokinetics, opsonization and protein-binding properties*. *Progress in Lipid Research*. **42(6)**: 463-478.
- Morrison T.M., Weiss J.J., and Wittwer C.T. (1998). *Quantification of low copy transcripts by continuous SYBR Green I monitoring during amplification*. *Biotechniques*. **24**: 954-962.
- Mossman T. (1983). *Rapid colorimetric assay for cellular growth and survival: Application to proliferation and cytotoxicity assays*. *Journal of Immunological Methods*. **65**: 55-63.
- Munzel P., Marx D., Kochel H., Schauer A., and Back K.W. (1991). *Genomic alterations of the c-myc protooncogene in relation to the overexpression of c-erbB2 and Ki-67 in human*

breast and cervix carcinomas. Journal of Cancer Research and Clinical Oncology. **117**: 603-607.

Nakanishi J., Nakayama H., Shimizu T., Ishida H., Kikuchi Y., Yamaguchi K., and Horiike Y. (2009). *Light regulated activation of cellular signalling by gold nanoparticles that capture and release amines*. Journal of the American Chemical Society. **131(11)**: 3822-3823.

Nanosight (2015). *NTA: Principles and Methodology*. Malvern Instruments Limited. www.malvern.com.

Nath S., Kaittanis C., Tinkham A., and Perez J.M. (2008). *Dextran-coated gold nanoparticles for the assessment of antimicrobial susceptibility*. Analytical Chemistry. **80(4)**: 1033-1038.

Nayerossadat N., Maedeh T., and Abas Ali P. (2012). *Viral and non-viral delivery systems for gene delivery*. Advanced Biomedical Research. **1**:27.

Nguyen J., and Szoka F.C. (2012). *Nucleic acid delivery: the missing pieces of the puzzle?* Accounts of Chemical Research. **45**: 1153-1162.

Niemeyer C.M., and Ceyhan B. (2001). *DNA-directed functionalization of colloidal gold with proteins*. Angewandte Chemie International Edition. **40(19)**: 3685-3688.

Niidome T., and Huang L. (2002). *Gene therapy progress and prospects of non-viral vectors*. Gene Therapy. **9**:1647-1652.

Niidome T., Yamagata M., Okamoto Y., Akiyama Y., Takahashi H., Kawana T., Katayama Y., and Niidome Y. (2006). *PEG-modified gold nanorods with a stealth character for in vivo applications*. Journal of Controlled Release. **114**: 343-347.

Nikhil R.J., Latha G., and Catherine J.M. (2001). *Seeding Growth for size control of 5-40 nm Diameter Gold Nanoparticles*. Langmuir. **17**: 6782-6786.

Nikoobakht B., and El-Sayed M.A. (2003). *Preparation and Growth Mechanism of Gold Nanorods (NRs) using seed-mediated Growth Methods*. Chemistry of Materials. **15(10)**: 1957-1962.

Nilsson J.A., and Cleveland J.L. (2003). *Myc pathways provoking cell suicide and cancer*. Oncogene. **22**: 9007-9021.

Nishikawa M., and Huang L. (2001). *Nonviral vectors in the new millennium: Delivery barriers in gene transfer*. Human Gene Therapy. **12**: 861-870.

- Obata Y., Suzuki D., and Takeoka S. (2008). *Evaluation of cationic assemblies constructed with amino acid based lipids for plasmid DNA delivery*. *Bioconjugate Chemistry*. **19**: 1055-1063.
- O'Brien J., Wilson I., Orten T., and Pagnan F. (2000). *Investigation of the Alamar Blue (resazurin) fluorescent dye for the assessment of mammalian cell cytotoxicity*. *European Journal of Biochemistry*. **267(17)**: 5421-5426.
- Oh K.S., Kim R.S., Lee J., Kim D., Cho S.H., and Yuk S.H. (2008). *Gold/chitosan/pluronic composite nanoparticles for drug delivery*. *Journal of Applied Polymer Science*. **108(5)**: 3239-3244.
- Oh Y-K., and Park T.G. (2009). *siRNA delivery systems for cancer treatment*. *Advanced Drug Delivery Reviews*. **61**: 850-862.
- Oligino T.j., Yao Q., Ghivizzani S.C., and Robbins P. (2008). *Vector systems for gene transfer to joints*. *Clinical Orthopaedics*. **379**:517-530.
- Oyelere, A.K., Chen P.C., Huang X., El-Sayed I.H., and El-Sayed M.A. (2007). *Peptide conjugated gold nanorods for nuclear targeting*. *Bioconjugate Chemistry*. **18**: 1490-1497.
- Parida U.K., and Nayak P.L. (2012). *Biomedical Applications of Gold Nanoparticles: Opportunity and Challenges*. *World Journal of Nano Science and Technology*. **1(2)**: 10-25.
- Pan S., Wang C., Zeng X., Wen Y., Hongmei W., and Feng M. (2011). *Short multi-armed polylysine-graft-polyamidoamine copolymer as efficient gene vectors*. *International Journal of Pharmaceutics*. **420**: 206-215.
- Panariti A., Miseroch G., and Rivolta I. (2012). *The effect of nanoparticle uptake on cellular behaviour: disrupting or enabling functions?* *Nanotechnology, Science and Applications*. **5**: 87-100.
- Pantarotto D., Singh R., McCarthy D., Erhardt M., Briand J.P., Prato M., Kostarelas K., and Bianco A. (2004). *Functionalised carbon nanotubes for plasmid DNA gene delivery*. *Angewandte Chemie International Edition*. **43**: 5242-5246.
- Park C., Lim J., Yun M., and Kim C. (2008). *Photoinduced release of guest molecules by supramolecular transformation of self-assembled aggregates derived from dendrons*. *Angewandte Chemie International Edition*. **47(16)**: 2959-2963.

- Park C., Yun H., Kim T.H. Noh T., Kook Y.H., Oh E.T., Park H.J., and Kim C. (2009). *Cyclodextrin-covered gold nanoparticles for targeted delivery of an anti-cancer drug*. Journal of Materials Chemistry. **19(16)**: 2310-2315.
- Park H., Yang J., Seo S., Kim K., Suh J., Kim D., Haom S., and Yao K-H. (2008). *Multifunctional nanoparticles for photothermally controlled drug delivery and magnetic resonance imaging enhancement*. Small. **4(2)**: 192-196.
- Patil M.L., Zhang M., Betigeri S., Taratula O., He H., and Minko T. (2008). *Surface modified and internally cationic Polyamidoamine Dendrimers for efficient siRNA delivery*. Bioconjugate Chemistry. **19**: 1396-1403.
- Pavlov V., Xiao Y., Shlyahovsky B., and Willner I. (2004). *Aptamer functionalized Au nanoparticles for amplified optical detection of thrombin*. Journal of the American Chemical Society. **126(38)**: 11768-11769.
- Pelengaris S., Khan M., and Evan G. (2002). *c-Myc: more than just a matter of life and death*. Nature Reviews Cancer. **2**: 764-776.
- Peng S., Lee Y., Wang C., Yin H., Dai S., and Sun S. (2008). *A facile synthesis of monodisperse Au nanoparticles and their catalysis of CO oxidation*. Nano Research. **1(3)**: 229-234.
- Percot A., Briane D., Coudert R., Reynier P., Bauchemal N., Lieure N., Hantz E., Salzmann J.L., and Cao A. (2004). *A hydroxyethylated cholesterol-based cationic lipid for DNA delivery: effect of conditioning*. International Journal of Pharmaceutics. **278**: 143-163.
- Pfaffl M.W. (2001). *A new mathematical model for relative quantification in real time RT-PCR*. Nucleic Acid Research. **29**: 2002-2007.
- Pissuwan D., Niidome T., and Cortie M.B. (2009). *The forthcoming applications of gold nanoparticles in drug and gene delivery*. Journal of Controlled Release. **149**: 65-71.
- Pitsillides C.M., Joe E.K., Wei X., Anderson R.R., and Linc P. (2003). *Selective cell targeting with light-absorbing microparticles and nanoparticles*. Biophysical Journal. **84**: 4023-4032.
- Radt B., Smith T.A., and Caruso F. (2004). *Optically addressable nanostructured capsules*. Advanced Materials. **16**: 2184-2189
- Ragelle H., Riva R., Vandermeulen G., Naeye B., Pourcelle V., Le Duff C.S., D'Haese C., Nysten B., Braeckmans K., DeSmedt S.C. Jérôme C., and Préat V. (2014). *Chitosan*

nanoparticles for siRNA delivery: Optimizing formulation to increase the stability and efficiency. Journal of Controlled Release. **176**: 54-63.

Ragelle H., Vandermeulen G., and Pr at V. (2013). *Chitosan based siRNA delivery systems.* Journal of Controlled Release. **172**: 207-218.

Rajam M., Pulovendran S., Rose C., and Mandal A.B. (2011). *Chitosan nanoparticles as a dual growth factor delivery system for tissue engineering applications.* International Journal of Pharmaceutics. **410**: 145-152.

Ramamoorth M. and Narvekar A. (2015). *Non-Viral Vectors in Gene Therapy- An Overview.* Journal of Clinical and Diagnostic Research. **9(1)**: GE01-GE06.

Ramanathan A., Wang C., and Schreiber S.L. (2005). *Perturbational profiling of a cell-line model of tumorigenesis by using metabolic measurements.* Proceedings of the National Academy of Sciences of the United States of America. **102**: 5992-5997.

Rampersad S.N. (2012). *Multiple applications of alamar blue as an indicator of metabolic function and cellular health in cell viability bioassays.* Sensors. **12**: 12347-12360.

Ramon A-L., Bertrand J-R., and Malvy C. (2008). *Delivery of small interfering RNA: A review and an example of application to a junction oncogene.* Tumori. **94**: 254-263.

Rand T.A., Peterson S., Du F., and Wang X. (2005). *Argonaute-2 cleaves the anti-guide strand of siRNA during RISC activation.* Cell. **123**: 621-629.

Rauch J., Moran-Jones K., Albrecht V., Scwarzl T., Hunter K., Gires O., and Kolch W. (2011). *c-Myc regulates RNA splicing of the A-Raf kinase and its activation of the ERK pathway.* Cancer research. **71(13)**: 4664-4674.

Reis-Filho J.S., and Tutt A.N. (2008). *Triple-negative tumours: a critical review.* Histopathology. **52**:108-118.

Remant Bahadur K.C., Thapa B., and Bhattaria N. (2013). *Gold nanoparticle-based gene delivery: promises and challenges.* Nanotechnology Reviews. **3**: 269-280.

Renvoize C., Biola A., Pallardy M., and Breard J. (1998). *Apoptosis: Identification of dying cells.* Cell Biology and Toxicology. **14(2)**: 111-120.

Resnier P., Montier T., Mathieu V., Benoit J-P., and Passirani C. (2013). *A review of the current status of siRNA nanomedicines in the treatment of cancer.* Biomaterials. **34**: 6429-6443.

- Ribble D., Goldstein N., Norris D., and Shellman Y. (2005). *A simple technique for quantifying apoptosis in 96-well plates*. BMC Biotechnology. **5(12)**: 1-7.
- Riss T.L., Moravec R.A., Niles A.L., Duellman S., Benink H.A., Worzella T.J., and Minor L. (2013). *Cell Viability Assays*. In Assays Guide Manual. Sittampalam G.S., Caussens N.P. ed Creature Commons Attribution-NonCommercial-ShareAlike.
- Riviere C., Boudghene F.P., Gazeau F., Roger J., Pons J.N., Laissy P., Allaire E., Michel J-P., Letourneur D., and Deux J-F. (2005). *Iron oxide nanoparticle-labelled rat smooth muscle cells: Cardiac MR imaging for cell graft monitoring and quantitation*. Radiology. **235(3)**: 959-967.
- Robbins P.D., and Ghivizzani S.C. (1998). *Viral vectors for gene therapy*. Pharmacological Therapy. **(80)1**: 35-47.
- Rocco M.C., and Bainbridge W.S. (2001). *Societal Implications of Nanoscience and Nanotechnology*. Science Foundation 285. Scientific American 3. (online: www.wtech.org/loyola/nano/societalimpact/nanocsci.pdf).
- Ross P.C., and Hui S.W. (1999). *Lipoplex size is a major determinant of in vitro lipofection efficiency*. Gene Therapy. **6**: 651-659.
- Rouhana L.L., Jaber J.A., and Schlenoff J.B. (2007). *Aggregation-resistant water-soluble gold nanoparticles*. Langmuir. **23(26)**: 12799-12801.
- Ryther R.C.C., Flynt A.S., Phillips III J.A., and Patton J.G. (2005). *Small interfering RNA therapeutics: Big potential for small RNA's*. Gene Therapy. **12**:5-11.
- Saba T.M. (1970). *Physiology and physiopathology of the reticuloendothelial system*. Archives of Internal Medicine. **126(6)**: 1031-1052.
- Safari J., and Zarnegar Z. *Advanced drug delivery systems: Nanotechnology of health design: A review*. Journal of Saudi Chemical Society. **18**: 85-99.
- Sakamuro D., Eviner V., Elliot K.J., Showe L., White E., and Prendergast G.C. (1995). *c-Myc induces apoptosis in epithelial cells by both p53- dependent and p53- independent mechanisms*. Oncogene. **11**: 2411-2418.
- Sandhu K.K., McIntosh C.M., Simard J.M., Smith S.W., and Rotello V.M. (2002). *Gold nanoparticle- mediated transfection of mammalian cells*. Bioconjugate Chemistry. **13**:3-6.

- Sanvicens W., and Marco M.P. (2008). *Multifunctional nanoparticles-properties and prospects for their use in human medicine*. Trends in Biotechnology. **26(8)**: 425-433.
- Scaglioni L., Mondelli R., Artoli R., Sirtori F.R., and Mazzini S. (2016). *Nemorubicin and doxorubicin bind the G-quadruplex sequences of the human telomeres and of the c-MYC promoter element PU22*. Biochimica et Biophysica Acta. **1860**: 1129-1138.
- Schaff T.G., Shafigullen M.N., Khoury J.T., Vezmar I., Whettan R.L., Cullen W.G., First P.N., Guttierrez-Wing C., Ascencio J., and Jose-Yacamun M.J. (1997). *Isolation of smaller nanocrystal gold molecules: Robust Quantum Effects in Optical Spectra*. The Journal of Physical Chemistry B. **101**: 7885-7891.
- Schmittgen T.D., and Livak K.J. (2008). *Analysing real time PCR data by the comparative Ct method*. Nature Protocols. **3**: 1101-1108.
- Scott V., Clark A.R., and Docherty K. (1994). *Gel Retardation Assay*. Methods in Molecular Biology. Harwood AS ed. New York, Humana Press. 31:399.
- Scott B.J., Wirnsberger G., and Stucky G. (2001). *Mesoporous and mesostructured materials for optical applications*. Chemistry of Materials. **13**: 3140-3150.
- Selvaraj V., and Alagar M. (2007). *Analytical detection and biological assay of antileukemic drug 5-fluorouracil using gold nanoparticles as a probe*. International Journal of Pharmaceutics. **337(1-2)**: 275-281.
- Sheiness D., and Bishop J.M. (1979). *DNA and RNA from uninfected vertebrate cells contain nucleotide sequences related to the putative transforming gene of avian myelocytomatosis virus*. Journal of Virology. **31**:514-521.
- Shi Y. (2003). *Mammalian RNA interference for the masses*. TRENDS in Genetics. **19(1)**: 9-12.
- Shou Y., Martelli M.L., Gabrea A., Qi Y., Brents L.A., Rosch L.E., Dewald G., Kirsch I.R., Bergsagel P.L., and Kuchl W.M. (2000). *Diverse karyotypic abnormalities of the c-myc locus associated with c-myc dysregulation and tumour progression in multiple myeloma*. Proceedings of the National Academy of Sciences of the United States of America. **97**: 228-233.

- Shukla R., Bonsal V., Choudhary M., Basu A., Bhonde R.R., and Sastry M. (2005). *Biocompatibility of gold nanoparticles and their endocytotic fate inside the cellular compartment: a microscopic overview*. *Langmuir*. **21**: 10644-10654.
- Sies H. (1999). *Glutathione and its role in cellular functions*. *Free Radical Biology and Medicine*. **27(9-10)**: 916-921.
- Siewiera K., and Labieniec-Watala M. (2012). *Ambiguous effect of dendrimer PAMAM G3 on rat heart respiration in a model of an experimental diabetes- Objective causes of laboratory misfortune or unpredictable G3 activity?* *International Journal of Pharmaceutics*. **430**: 258-265.
- Sioud M. (2005). *On the delivery of small interfering RNAs into mammalian cells*. *Expert Opinion on Drug Delivery*. **62**:12-27.
- Slowing J.J., Vivero-Escoto J.L., Wen Wu C., and Lin V. (2008). *Mesoporous silica nanoparticles as controlled release drug delivery and gene transfection carriers*. *Advanced Drug Delivery Reviews*. **60**: 1278-1288.
- Sokolov K., Follen M., Aaron J., Pavlova I., Malpica A., Loctari R., and Richartz-Kortum R. (2003). *Real-time vital optical imaging of precancer using anti-epidermal growth factor receptor antibodies conjugated to gold nanoparticles*. *Cancer Research*. **63(9)**:1999-2004.
- Sokolova V., and Epple M. (2008). *Inorganic nanoparticles as carriers of nucleic acids into cells*. *Angewandte Chemie International Edition Eng*. **47**: 1382-1395.
- Song C-Z. (2007). *Gene Silencing Therapy Against Cancer*. In *Cancer Drug Discovery and Development: Gene Therapy for Cancer*. Eds: Human Press: Totewa, NJ, USA. 185-196.
- Spagnou S., Miller A.D., and Keller M. (2004). *Lipidic carriers of siRNA: Differences in formulation, cellular uptake and delivery with plasmid DNA*. *Biochemistry*. **43(42)**: 13348-13356.
- Spencer D., Chirra H.D., and Hilt J.Z. (2011). *Functionalization of Gold Nanoparticles (GNPs) using the Isolate, Functionalize and Release (ISOFURE) Methodology*. *UKnowledge Kaleidoscope*. **10(32)**: 1-17.
- Sperling R.A., and Parack W.J. (2010). *Surface modification, functionalisation and bioconjugation of colloidal inorganic nanoparticles*. *Philosophical Transactions of The Royal Society A*. **368**: 1333-1383.

- Stephaneko A.A., and Dmitrenko V.V. (2015). *HEK293 in cell biology and cancer research: Phenotype, karyotype, tumorigenicity, and stress-induced genome-phenotype evolution*. *Gene*. **569**: 182-190.
- Stephens A.S., Stephens S.R., and Morrison W.A. (2011). *Internal control genes for quantitative RT-PCR expression analysis in mouse osteoblasts, osteoclasts and macrophages*. *BMC Research Notes*. **4**: 410-419.
- Suva M.L., Riggi N., and Bernstein B.E. (2013). *Epigenetic reprogramming in cancer*. *Science*. **339**:1567-1570.
- Sze A., Erickson D., Ren L., and Li D. (2003). *Zeta potential measurement using the Smoluchowski equation and the slope of the current- time relationship in electroosmotic flow*. *Journal of Colloid and Interface Science*. **261(2)**: 402-410.
- Tada H., Shiho O., Kuroshima K., Koyama M., and Tsukamoto K. (1986). *An improved colorimetric assay for interleukin 2*. *Journal of Immunological Methods*. **93(2)**: 157-165.
- Tasis D., Tagmatarchis N., Georgakilas V., and Prato M. (2003). *Soluble Carbon Nanotubes*. *Chemistry A European Journal*. **9(17)**: 4000-4008.
- Tapola N.S., Lyyra M.L., Kolehmainen R.M., Sarkkinen E.S., and Schauss A.G. (2006). *Safety aspects and cholesterol- lowering efficacy of chitosan tablets*. *The Journal of the American College of Nutrition*. **27**: 22-30.
- Thanki K., Zeng X., Justesen S., Tejlmann S., Falkenberg E., Van Driessche E., Nielsen H.M., Franzyk H., and Fayed C. (2017). *Engineering of Small Interfering RNA-loaded Lipidoid-Poly (DL-LLactic-Co-Glycidic Acid) Hybrid Nanoparticles for Highly Efficient and Safe Gene Silencing. A Quality by Design -Based Approach*. *European Journal of Pharmaceutics and Biopharmaceutics*. **120**: 22-33.
- The Theory of the Photographic Process. (1977). 4th ed. James T.H. Ed. MacMillian Press: New York.
- Thermo Nicolet. (2001). *Introduction Fourier Transform Infrared Spectrometry*. Thermo Nicolet Corporation. www.thermonicolet.com.
- Thermo Scientific. (2010). *ELISA technical guide and protocols. Tech tip #65*. Thermo Fisher Scientific Inc. USA.

- Thomas P., and Smart T.G. (2005). *HEK293 cell line: A vehicle for the expression of recombinant proteins*. Journal of Pharmacological and Toxicological Methods. **51**: 187-200.
- Tiwari P.M., Vig K., Dennis V.A., and Singh S.R. (2011). *Functionalised Gold Nanoparticles and Their Biomedical Applications*. Nanomaterials. **1**: 31-63. doi: 10.3390/nano1010031.
- Tkachenko A.G., Xie H., Liu Y., Coleman D., Ryan J., Glomm W.R., Shipton M.K., Franzen S., and Feldman D.L. (2004). *Cellular trajectories of peptide-modified gold particle complexes: comparison of nuclear localization signals and peptide transduction domains*. Bioconjugate Chemistry. **15(3)**: 482-490.
- Tomalia D.A., Nayler A.M., and Goddard W.A. (1990). *Starburst dendrimers: Molecular-level control of size, shape, surface chemistry, topology and flexibility from atoms to microscopic matter*. Angewandte Chemie International Edition in English. **29**: 138-175.
- Torchillin V.P. (2012). *Multifunctional nanocarriers*. Advanced Drug Delivery Reviews. **64**: 302-315.
- Tseng H-Y., Lee C-K., Wu S-Y., Chi T-T., Yang K-M., Wang J-Y., Kiang Y-W., Yang C.C. Tsai M-T., Wu Y-C., Chou Y-C., and Chiang C-P. (2010). *Au nanorings for enhancing absorption and backscattering monitored with optical coherence tomography*. Nanomedicine. **21(29)**: 295102
- Tseng Y-C., Chano S., and Huang L. (2009). *Lipid-based systemic delivery of siRNA*. Advanced Drug Delivery Reviews. **61**: 721-731.
- Turkevitch J., Stevenson P.C., and Hillier J. (1951). *A Study of the Nucleation and Growth Processes I the Synthesis of Colloidal Gold*. Discussions of the Faraday Society. **11**: 55-75.
- Tuschl T., Zamore P.D., Lehmann R., Bartel D.P., and Sharp P.A. (1999). *Targeted mRNA degradation by double-stranded RNA in vitro*. Genes and Development. **13**: 3191-3197.
- Valden M., Lai X., and Goodman D.N. (1998). *Onset of catalytic activity of gold clusters on titania with the appearance of non-metallic properties*. Science. **281(5383)**: 1647-1650.
- Vale R.D. (2003). *The molecular motor toolbox for intracellular transport*. Cell. **112(4)**: 467-480.
- Valera A., Pujol A., Gregor X., Riu E., Visa J., and Bosch F. (1995). *Evidence from transgenic mice that myc regulates hepatic glycolysis*. The Faseb Journal. **9**: 1067-1078.

Vallet-Regi M., Ramilia A., del Real D.P., and Pereze-Parietne J. (2001). *A New Property of MCN-41: Drug Delivery System*. Chemistry of Materials. **13(2)**: 308-311.

van de Water F.M., Boerman O.C., Wouterse A.C., Peters J.G. Russel F.G., and Masereeuw R. (2006). *Intravenously administered short interfering RNA accumulates in the kidney and selectively suppresses gene function in renal proximal tubules*. Drug Metabolism and Disposition. **34**: 1393-1397.

van Tonder A., Joubert A.M., and Cromarty A.D. (2015). *Limitations of the 3-(4,5-dimethylthiazole-2-yl)-2,5-diphenyl-2H-tetrazolium bromide (MTT) assay when compared to three commonly used cell enumeration assays*. BMC Research Notes. **8**:47-57. doi: 101186/513104-015-1000-8.

van Vlerken L.E., Vyas T.K., and Amiji M.M. (2007). *Poly (ethylene glycol)- modified nanocarriers for tumor-targeted and intracellular delivery*. Pharmaceutical Research. **24(8)**: 1405-1414.

Vandenbroucke R.E., Lentacker I., Demeester J., De Smedt S.C., and Sanders N.N. (2008). *Ultrasound assisted siRNA delivery using PEG-siPlex loaded microbubbles*. Journal of Controlled Release. **126**: 265-273.

Varnavski O.P., Mohamed M.B., El-Sayed M.A., and Goodson T. (2003). *Relative Enhancement of Ultrafast Emission in Gold nanorods*. The Journal of Physical Chemistry B. **107(14)**: 3101-3104.

von Maltzahn G., Park J.H., Agrawal A., Bandaru N.K., Das S.K., Sailor M.J., and Bhatia S.N. (2009). *Computationally guided photothermal tumor therapy using long- circulating gold nanorod antennas*. Cancer Research. **69**: 3892-3900.

Villiers C.L., Freitas H., Cauderc R., Villiers M.B., and Marche P.N. (2009). *Analysis of the toxicity of gold nanoparticles on the immune system: effect on dendritic cell functions*. Journal of Nanoparticle Research. **12**: 55-60.

Vinhas R., Fernandes A.R., and Baptista P.V. (2017). *Gold nanoparticle for BCR-ABL 1 Gene Silencing: Improving Tyrosine Kinase Inhibitor Efficacy in Chronic Myeloid Leukaemia*. Molecular Therapy: Nucleic Acids. **7**: 408-416.

Vonarbourg A., Passirani C., Saulnier P., and Benoit J.P. (2006). *Parameters influencing the stealthiness of colloidal drug delivery systems*. Biomaterials. **27**: 4356-4373.

- Wall N.R., and Shi Y. (2003). *Small RNA: can RNA interference be exploited for therapy?* Lancet. **362(9393)**: 1401-1403.
- Wang B., Zhou J., Cui S., Yang B., Zhao Y., Duan Y., and Zhang S. (2012). *Cationic liposomes as carriers for gene delivery: Physico-chemical characterization and mechanism of cell transfection.* African Journal of Biotechnology. **11**: 2763-2773.
- Wang M., and Thanou M. (2010). *Targeting nanoparticles to cancer.* Pharmacological Research. **62**: 90-99.
- Wang X., Hu X., Li J., Rusie A.C.M., Kawazoe N., Yang Y., and Chen G. (2016). *Influence of cell size on cellular uptake of gold nanoparticles.* Biomaterials Science. **4**: 970-978.
- Wanigasekara J., and Witharana C. (2016). *Applications of Nanotechnology in Drug Delivery and Design- An Insight.* Current Trends in Biotechnology and Pharmacy. **10(1)**: 78-91.
- Warheit D.B., Laurence B.R., Reed K.L., Roach D.H., Reynolds G.A., and Webb T.R. (2004). *Comparative pulmonary toxicity assessment of single-wall carbon nanotubes in rats.* Toxicological Sciences. **77**: 117-125.
- West J.L., and Halas N.J. (2003). *Engineered nanomaterials for biophotonics applications: Improving sensing, imaging and therapeutics.* Annual Review of Biomedical Engineering. **5**: 285-292.
- Whitehead K.A., Langer R., and Anderson D.G. (2009). *Knocking down barriers: advances in siRNA delivery.* Nature Reviews Drug Discovery. **8**:129-138.
- WHO: World Health Organisation: <http://www.who.int/en/> (Accessed on 23 August 2016).
- Wolfgang H., Nguyen T.R., Thanh J., and David G.F. (2007). *Determination of size and concentration of Gold nanoparticles from UV-vis spectra.* Analytical Chemistry. **79**: 4215-4221.
- Wolfer A., and Ramaswamy S. (2011). *MYC and Metastasis.* Cancer Research. **71(6)**: 2034-2037.
- Wu J., Huang W., and He Z. (2013). *Dendrimers for siRNA delivery and gene silencing: a review.* The Scientific World Journal. **1**:1-16.
- Xu C.F., and Wang J. (2014). *Delivery systems for siRNA drug development in cancer therapy.* Asian Journal of Pharmaceutical Science. **10**: 1-12.

- Xu R. (2008). *Progress I nanoparticle characterization: Sizing and zeta potential measurements*. *Particuology*. **6**: 112-115.
- Yamamoto M., and Curiel D.T. (2005). *Cancer Gene Therapy*. *Technology in Cancer Research and Treatment*. **4(4)**: 315-330.
- Yang W., Cheng Y., Wang X., and Wen L.P. (2009). *Targeting cancer cells with biotin-dendrimer conjugates*. *European Journal of Medicinal Chemistry*. **44**: 862-868.
- Yang P., Ando M., and Murase N. (2010). *Various Au Nanoparticle Organizations Fabricated through SiO₂ Monomer Induced Self-Assembly*. *Langmuir*. **27(3)**: 895-901.
- Yuan J.S., Reed A., Chen F., and Stewart Jr. C.N. (2006). *Statistical analysis of real time PCR data*. *BMC Bioinformatics*. **7**:85. Doi: 10/1186/1471-2150-7-85.
- Zaitoun M.A., Mason W.R., and Lin C.T. (2001). *Magnetic Circular Dichroism Spectra for colloidal Gold Nanoparticles in xerogels at 5.5K*. *The Journal of Physical Chemistry B*. **105**: 6780-6784.
- Zaky A., Liebl R., Rachel R., Goepferich A., and Breunig M. (2009). *Layer-by-layer assembled gold nanoparticles for siRNA delivery*. *Nano Letters*. **9**: 2059-2064.
- Zhang F., Skoda M.W., Jacobs R.M., Zorn S., Martin R.A., Martin C.M., Clark G.F., Goerigk G., and Schreiber F. (2007). *Gold Nanoparticles Decorated with Oligo (ethylene glycol) Thiols: Protein Resistance and Colloidal Stability*. *The Journal of Physical Chemistry A*. **111(49)**: 12229-12237.
- Zhang J., Li X., and Huang L. (2004). *Non-viral nanocarriers for siRNA delivery in breast cancer*. *Journal of Controlled Release*. **190**:440-450.
- Zhang S., Li J., Lykotrafitis G., Bao G., and Suresh S. (2009). *Size-Dependant Endocytosis of Nanoparticles*. *Advanced Materials*. **21(4)**: 419-424.
- Zhang S., Zhao B., Jiang H., Wang B., and Ma B. (2007). *Cationic lipids and polymer mediated vectors for delivery of siRNA*. *Journal of Controlled Release*. **123**: 1-10.
- Zhang Y., Li H., Sun J., Gao J., Liu W., Li B., Guo Y., and Chen J. (2010). *DC-Chol/DOPE cationic liposomes: A comparative study of the influence factors on plasmid pDNA and siRNA gene delivery*. *International Journal of Pharmaceutics*. **390(2)**: 198-207.

Zhao W., Brook M.A., and Li Y. (2008). *Design of gold nanoparticle- based colorimetric biosensing assays*. ChemBioChem. **9(15)**: 2363-2371.

Zhao Z.X., Gao S.Y., Wang J.C., Chen C-J., Zhao E.Y., Hou W.J., Feng Q., Gao L.Y., Liu X.Y., Zhong L.R., and Zhang Q. (2012). *Self- assembly nanomicelles based on cationic mPEG-PLA-b-Polyarginine (RI5) triblock co-polymer for siRNA delivery*. Biomaterials. **33**:6793-6807.

Zheng M., Davidson F., and Huang X. (2003). *Ethylene glycol monolayer protected nanoparticles for eliminating nonspecific binding with biological molecules*. Journal of the American Chemical Society. **125(26)**: 7790-7791.

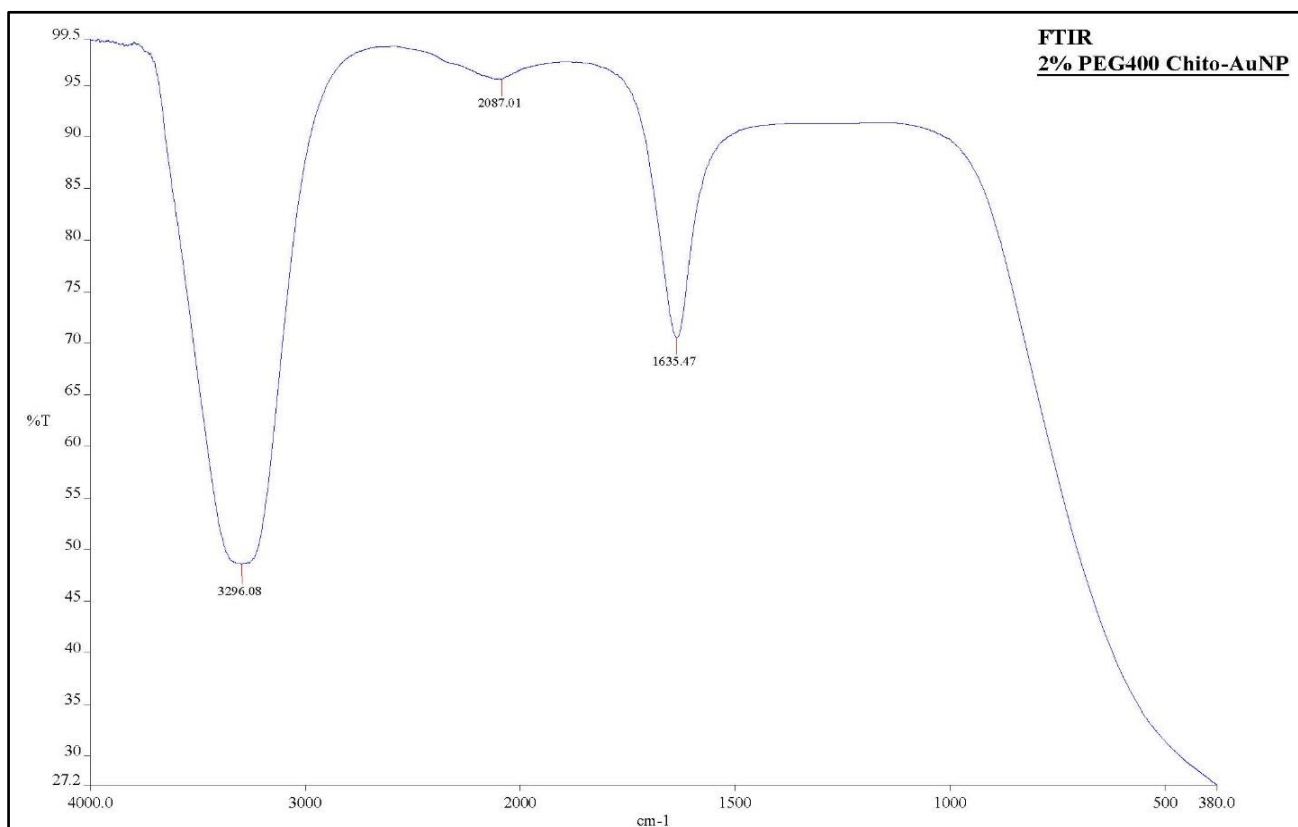
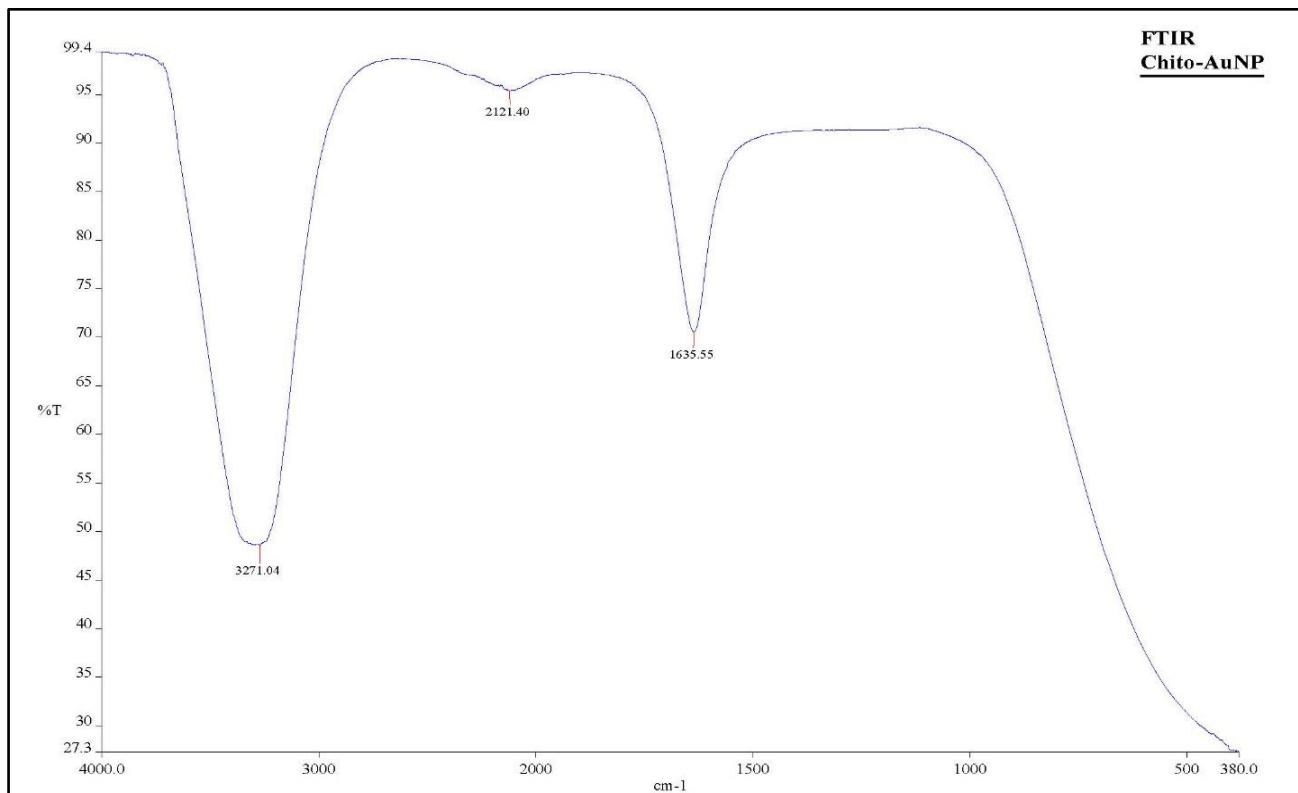
Zheng D., Gilijohann D.A., Chen D.L., Massich M.D., Wang X.Q. Iordanov H., Mirkin C.A., and Paller A.S. (2012). *Topical delivery of siRNA-based spherical nucleic acid nanoparticle conjugates for gene regulation*. Proceedings of the National Academy of Sciences of the United States of America. **109**: 11975-11980.

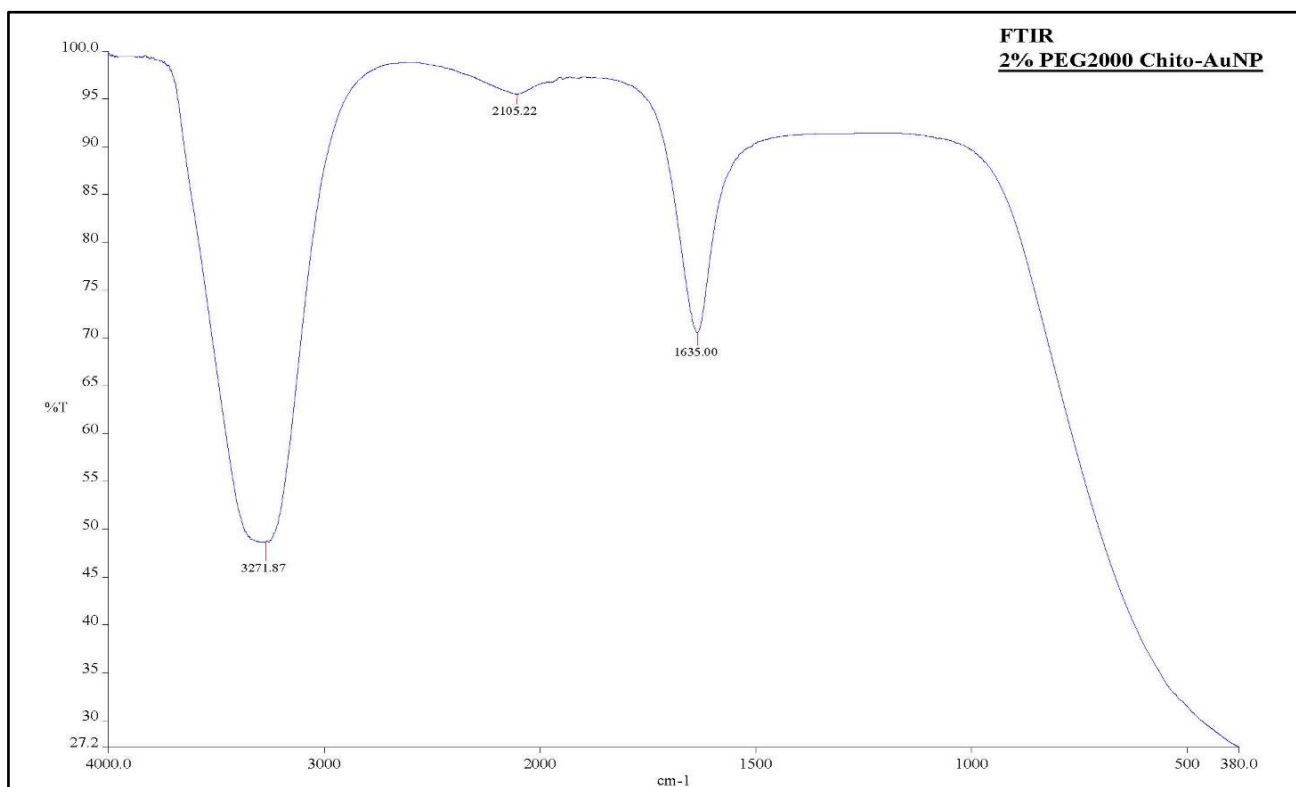
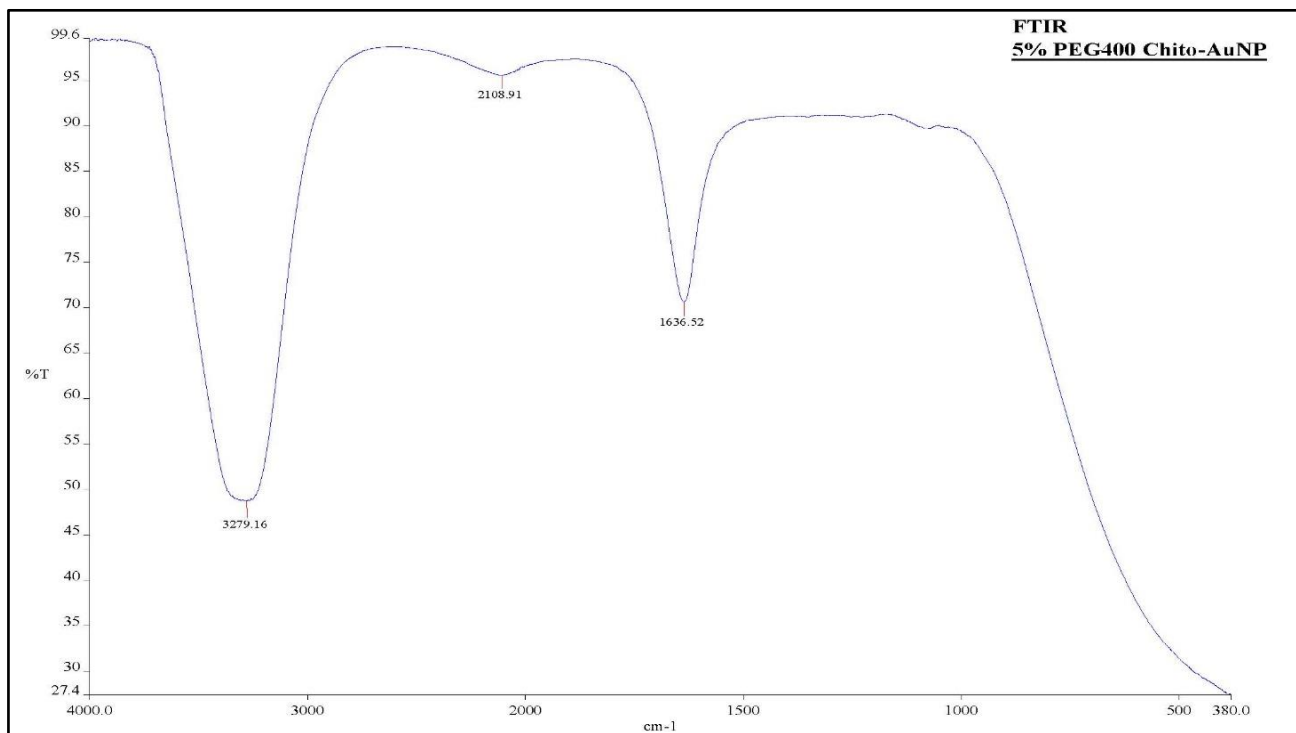
Zhou J., Shum K-T, Burnett J.C., and Rossi J.J. (2013). *Nanoparticle-Based Delivery of RNAi Therapeutics: Progress and Challenges*. Pharmaceuticals. **6**: 85-107.

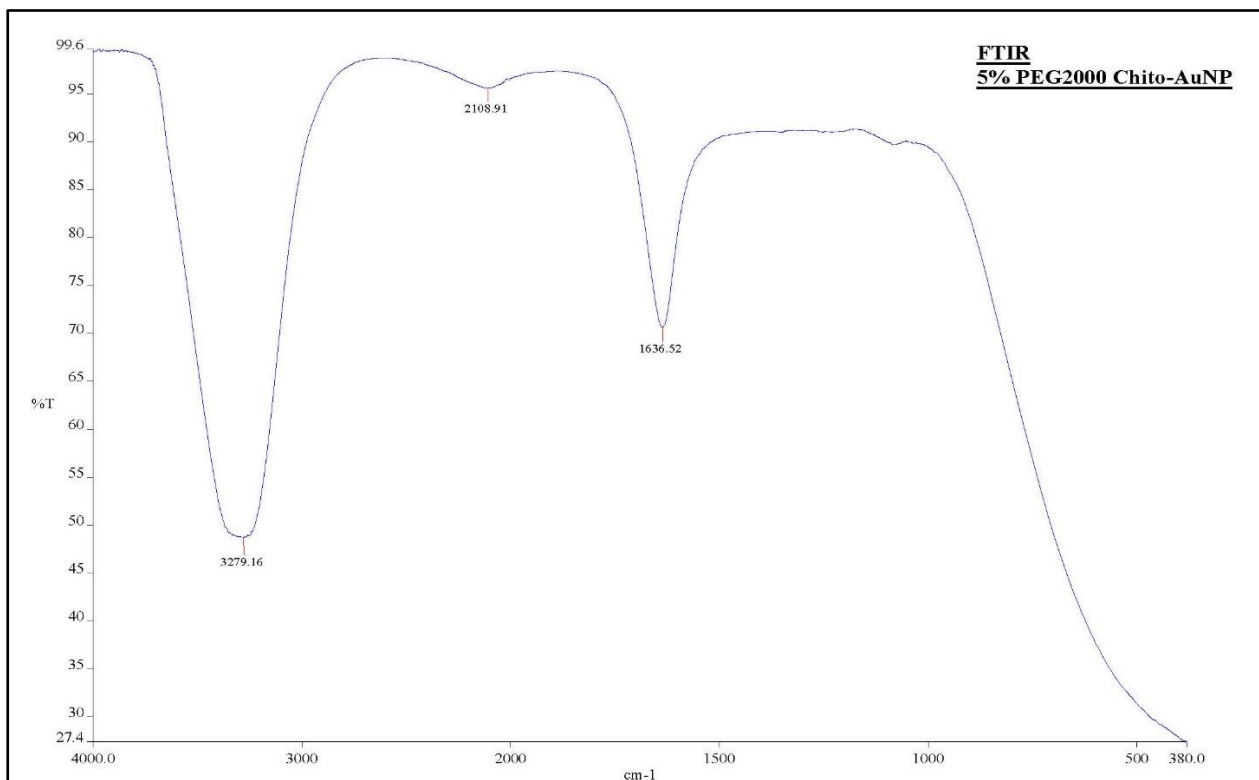
Zolnik B.S., and Sadrieh N. (2009). *Regulatory perspective on the importance of ADME assessment of nanoscale material containing drugs*. Advanced Drug Delivery Reviews. **61(6)**: 422-427.

Zuhorn I.S., Visser H., Bakowsky U., Engberts J.B.F.N., and Hoekstra D. (2002). *Interference of serum with lipoplex-cell interaction: Modulation of intracellular processing*. Biochimica et Biophysica Acta. **1560**: 25-36.

APPENDIX A2



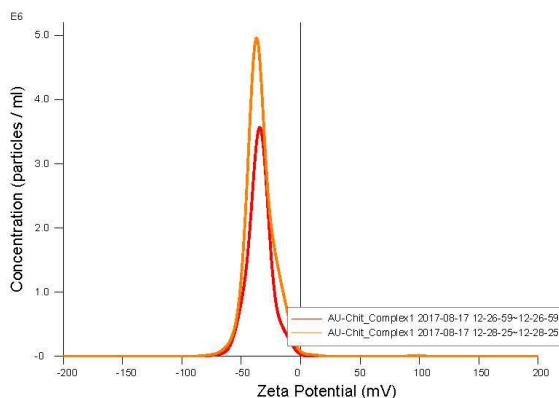




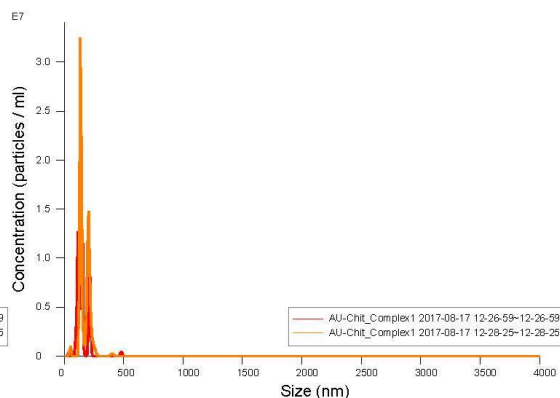
APPENDIX A3

NANOSIGHT

AU-Chit Complex1 2017-08-17 12-24-42

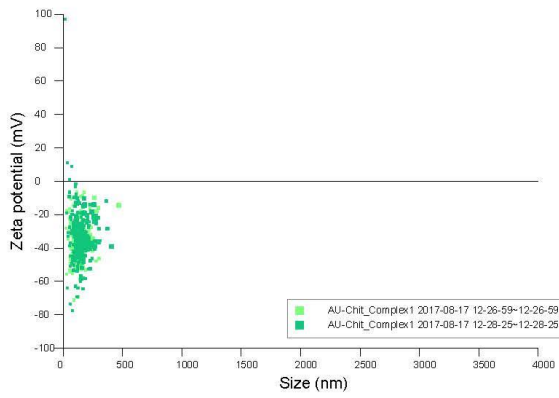


Concentration / Zeta Potential graph for Experiment:
 AU-Chit_Complex1 2017-08-17 12-24-42

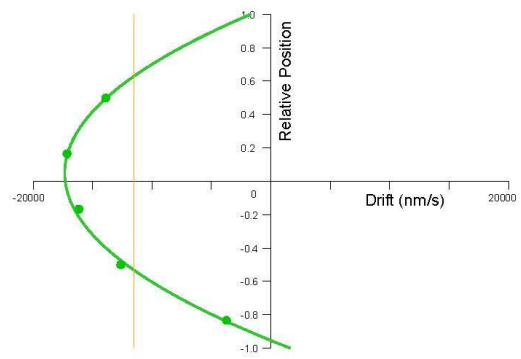


FTLA Concentration / Size graph for Experiment:
 AU-Chit_Complex1 2017-08-17 12-24-42

Included Files	Results
AU-Chit_Complex1 2017-08-17 12-26-59	Stats: Mean +/- Standard Error
AU-Chit_Complex1 2017-08-17 12-28-25	Mean: 160.7 +/- 7.4 nm
	Mode: 144.3 +/- 7.3 nm
	SD: 48.5 +/- 4.9 nm
	D10: 111.0 +/- 10.2 nm
	D50: 135.4 +/- 2.7 nm
	D90: 206.8 +/- 0.8 nm
	Concentration: 9.60e+007 +/- 1.90e+007 particles/ml
	4.9 +/- 1.0 particles/frame
	6.6 +/- 1.2 centres/frame
Details	Zeta Settings and Results
NTA Version: NTA 3.2 Dev Build 3.2.16	Parabola fit complete
Script Used: SOP Zeta Measurement 12-24-42PM 17Aug2~	Adjusted r-square: 0.99
Time Captured: 12:24:42 17/08/2017	
Operator: Alicia	Applied Voltage: 24.0 V
Pre-treatment:	Dielectric Constant: 80.00
Sample Name: AU-Chit_Complex1	Average Current: 0.90 - 0.94 μ A
Diluent: Water	
Remarks:	Stats: Mean +/- Standard Error
	Mean: -34.4 +/- 0.2 mV
	Mode: -35.8 +/- 1.3 mV
	SD: 11.3 +/- 0.9 mV
	D10: -48.3 +/- 0.1 mV
	D50: -36.0 +/- 0.4 mV
	D90: -21.3 +/- 1.7 mV
Capture Settings	
Camera Type: sCMOS	
Laser Type: Blue405	
Camera Level: 13	
Slider Shutter: 1232	
Slider Gain: 219	
FPS: 25.0	
Number of Frames: 1498	
Temperature: 25.0 - 25.0 $^{\circ}$ C	
Viscosity: (Water) 0.9 cP	
Dilution factor: Dilution not recorded	
Analysis Settings	
Detect Threshold: 7	
Blur Size: Auto	
Max Jump Distance: Auto: 14.0 - 15.6 pix	



Zeta Potential / Size graph for Experiment:
AU-Chit_Complex1 2017-08-17 12-24-42



Flow profile for Experiment:
AU-Chit_Complex1 2017-08-17 12-24-42

Script Used: (Full Text):

SOP Zeta Measurement 12-24-42PM 17Aug2017.txt

APPENDIX B

PI62

**Pegylated-chitosan functionalized gold nanoparticles
for siRNA delivery *in vitro***

A N Daniels¹ M Singh¹

*1: Non-viral Gene Delivery Laboratory, Discipline
of Biochemistry, University of KwaZulu-Natal, Private Bag
X54001, Durban 4000, South Africa*

The rapidly developing field of nanotechnology has provided a strong support for the development of nanoparticle mediated gene delivery systems. Amongst these, gold nanoparticles (AuNPs) have attracted much attention as gene and drug delivery vehicles due to their low toxicity, ease of synthesis, small size and the ability to be functionalized with suitable polymers or targeting molecules. In this study, AuNPs were functionalized with chitosan which has a high positive charge density. These AuNPs were further modified by the addition of the steric stabilizing polymer, polyethylene glycol (PEG). Physicochemical characterization using TEM, UV spectroscopy and NTA revealed that surface modification of the AuNPs with chitosan and PEG influenced the size, colloidal stability, polydispersity and zeta potential. The ability of these nanoparticles to bind and afford protection to siRNA was determined using the band shift, dye displacement and RNase A protection assays. The cytotoxicity of the modified AuNPs and their respective nanocomplexes with siRNA, evaluated using the MTT and Alamar Blue assays in the HEK 293, Caco-2 and MCF-7 cell lines, showed minimal toxicity with cell survival over 75%. Cellular uptake studies utilizing fluorescently labelled siRNA, confirmed that there was a good correlation between pegylation/non-pegylation, and internalization and eventual transfection ability of these nanocomplexes. Ideal physicochemical properties, low cytotoxicity and the relative ease of cellular uptake for transfection, make these pegylated-chitosan functionalized AuNPs promising delivery vehicles for siRNA and other therapeutic molecules. Further research into their optimization and modification may be required before they can be extended to *in vivo* studies.

Research Article

Enhanced *c-MYC* oncogene silencing mediated by siRNA associated with sterically stabilised chitosan functionalised gold nanoparticles in a breast cancer cell model

Aliscia Nicole Daniels and Moganavelli Singh

Department of Biochemistry, Non-viral Drug and Gene Delivery Laboratory, School of Life Sciences, College of Agriculture, Engineering and Science, University of KwaZulu-Natal (Westville Campus), Private Bag X54001, Durban 4000, South Africa. E-mails: alisciadaniels@gmail.com (A.D.), singhm1@ukzn.ac.za (M.S.).

Abstract

Elevated *c-MYC* expression is a genetic aberration present in breast cancers. The use of RNA interference (RNAi), mediated by siRNA molecules, for the silencing of the *c-MYC* oncogene is an attractive option for inhibiting and controlling breast cancer progression. The delivery of these therapeutic siRNA molecules is crucial and thus, a suitable carrier is important and needed for their cellular delivery. Accordingly, this study investigates the efficiency of three gold nanoparticle (AuNP) based delivery systems to deliver intact *c-MYC* targeted siRNA to the MCF-7 cell line, *in vitro*.

AuNPs were prepared using the citrate reduction method, functionalised with chitosan and further modified using 0-5 mass percentage of poly(ethylene glycol)-400 (PEG₄₀₀) to afford sterically stabilised Chitosan- AuNPs. TEM and NTA analysis revealed that the AuNPs were spherical in shape with favourable sizes in the nanometre size range. The AuNP formulations were capable of successfully binding, condensing and protecting the siRNA against degradation following the band shift, dye displacement and RNase A protection assays, respectively. Cytotoxicity studies showed that all the AuNP preparations were well tolerated by the MCF-7 cell line with cell survival exceeding 75%. Gene knockdown studies following qRT-PCR revealed that the PEGylated and non-PEGylated AuNPs showed comparable levels of gene knockdown with the PEGylated Chitosan-AuNPs inducing > 84% of *c-MYC* gene silencing, exceeding that achieved by Lipofectamine® 3000 (80% gene knockdown). This trend was confirmed by the ELISA assay which showed a reduction of MYC protein levels greater than 90% by the PEGylated Chitosan-AuNPs as compared to the untreated MCF-7

cells. The results obtained suggest that these AuNP formulations have great potential as vectors for siRNA mediated gene silencing in breast cancer cells.

Key words: siRNA, *c-MYC*, gold nanoparticles, PEGylation, gene silencing

Functionalised Gold Nanoparticle Delivery for c-MYC siRNA in Cancer Gene Therapy

ORIGINALITY REPORT

13%	7%	8%	6%
SIMILARITY INDEX	INTERNET SOURCES	PUBLICATIONS	STUDENT PAPERS

PRIMARY SOURCES

1	Submitted to University of KwaZulu-Natal Student Paper	3%
2	146.230.128.141 Internet Source	<1%
3	Lee, So Jin, Min Ju Kim, Ick Chan Kwon, and Thomas M. Roberts. "Delivery strategies and potential targets for siRNA in major cancer types", Advanced Drug Delivery Reviews, 2016. Publication	<1%
4	D. M. Miller, S. D. Thomas, A. Islam, D. Muench, K. Sedoris. "c-Myc and Cancer Metabolism", Clinical Cancer Research, 2012 Publication	<1%
5	Koh, Cheryl M., Arianna Sabò, and Ernesto Guccione. "Targeting MYC in cancer therapy: RNA processing offers new opportunities", BioEssays, 2016. Publication	<1%
	Fundamental Biomedical Technologies, 2011.	